



**UNIVERSITY OF NAIROBI**

**SIMULATION MODEL FOR PREDICTION OF THE  
SERVICE LIFE OF WATER CONVEYANCING  
REINFORCED CONCRETE STRUCTURES**

**BY**

**MOGIRE, PHILIP OSIEMO**

**F80/51086/2016**

**A Thesis Submitted in Fulfillment of the Requirements for the Award of Doctor of  
Philosophy in Civil Engineering of the University of Nairobi**

**2021**

## DECLARATION AND APPROVAL

I declare that this thesis is my original work and has not been submitted elsewhere for examination, award of a degree or publication. Where other people's work or my own work has been used, this has properly been acknowledged and referenced in accordance with the University of Nairobi's requirements.

Signature: 

Date: 24.11.2021

**Mogire, Philip Osiemo**

**F80/51086/2016**

Department of Civil and Construction Engineering

Faculty of Engineering

University of Nairobi

This thesis is submitted for examination with our approval as research supervisors:

**Signature**

**Date**

Dr. John Mwero



25/11/2021

Department of Civil and Construction Engineering

University of Nairobi

P.O Box 30197-00100

Nairobi Kenya

Johnmwero1@uonbi.ac.ke

Prof. Silvester Abuodha



26/11/2021

Department of Civil and Construction Engineering

University of Nairobi

P.O Box 30197-00100

Nairobi Kenya

sochieng@yahoo.com

Prof. Geoffrey Mang'uriu



25/11/2021

Department of Civil, Construction and Environmental Engineering

Jomo Kenyatta University of Agriculture and Technology

P.O Box 30197-00100

Nairobi Kenya

gnmanguriu@yahoo.co.uk

## **DEDICATION**

To my Family and  
Best Friends

## **ACKNOWLEDGEMENT**

I would like to express my sincere gratitude to my supervisors Dr. John N. Mwero, Professor Silvester O. Abuodha and Professor Geoffrey N. Mang'uriu for their continuous interest and guidance during the course of this work. I am grateful to them for being part of this research, which has proven to be enormously interesting and challenging at times. It has been a pleasure being their student.

I would also like to thank the Teaching and non-Teaching staff of the University of Nairobi for their helpful and valuable comments of the research in general and of this thesis in particular.

Finally, I would like to acknowledge the unconditional love and support so generously given to me by my family.



## **ABSTRACT**

With increased competing demands of sustainable structures to support the United Nations sustainable development goals, new technologies are evolving for efficient design, manufacture and construction of civil and environmental engineering projects. Researchers have upscaled their effort to develop techniques that can monitor the performance of civil engineering structures within their service life for optimum return from investment. Reinforced concrete structures constitute a good percentage of components of civil engineering structures in water conveyancing structures. The service life of these structures affect sustainable systems including hydropower generation, water supply for consumption and for irrigation. Existing service life models of reinforced concrete structures are structure specific and each of them have inherent limitations resulting from the specific use.

Most codes of practice define the design life of reinforced concrete water conveyancing structures as 50 years. The performance of a structure at any reference age within the service life of a structure should be able to be defined. Deterioration due to reinforcement corrosion affects the performance of reinforced concrete water structures and hence their service life. Because of the high investments involved and risk associated with water structures, there is need to create a service life model to predict their performance. The main objective of this research was to create a corrosion model to predict the service life of water conveyancing structures.

To realize the main objective an accelerated corrosion experiment to monitor evolution and propagation of crack width to 0.2mm maximum. There was a variation of concrete characteristic strength and reinforcement cover. In order to extend the service life of reinforced concrete, corrosion inhibitors are often used. Corrosion inhibitors prevent corrosion or lowers the rate of corrosion. Test samples from four selected corrosion inhibitors; a calcium nitrite and

nitrate based, a dimethylathanolamine based organic inhibitor and fly ash in combination with a selected brand of cement X, Y or Z were used. From the results, the rate of corrosion decreases with increase in concrete cover and strength. The results were used in derivation of a corrosion model for the service life of reinforced concrete water conveyancing structures.

A corrosion model for prediction of the service of reinforced concrete water conveyancing structures was formulated by dividing the service life into the initiation period and propagation period. The initiation period was found by dividing the critical penetration depth by the rate of corrosion. Models for calculating the critical penetration depth were evaluated from which the Xu and Shayan model was selected as applicable for this work. A model for the propagation period was derived by calculating the period from corrosion initiation to appearance of 0.05mm crack and adding up to propagation of the crack width from 0.05mm to 0. 2mm. The results of the proposed corrosion propagation period model were compared with the experimental results and models of other researchers and found that it has a strong correlation with the laboratory output.

From the experiments, it was noted that due to variation in chemical composition of cement, the choice of cement brand affects the rate of corrosion of steel embedded in concrete. It was also noted that all the selected corrosion inhibitors increased the bond strength of reinforced concrete. A corrosion current density model was formulated for corrosion propagation period. A corrosion model for prediction of the service life of reinforced concrete water conveyancing structures was proposed and compared with experimental work and models of other researchers. The proposed service life model compares well with the experimental work. Further research has been recommended to improve the model.

**Keywords:** Corrosion, Hydropower, Service life model, Water conveyancing structures.

## TABLE OF CONTENTS

<b>DECLARATION.....</b>	<b>ii</b>
<b>DEDICATION.....</b>	<b>iii</b>
<b>ACKNOWLEDGEMENT.....</b>	<b>iv</b>
<b>ABSTRACT.....</b>	<b>v</b>
<b>TABLE OF CONTENTS .....</b>	<b>vii</b>
<b>CHAPTER 1.....</b>	<b>1</b>
<b>1.0 INTRODUCTION.....</b>	<b>1</b>
<b>1.1 Background .....</b>	<b>1</b>
1.1.1 Deterioration mechanisms of Reinforced Concrete.....	4
1.1.2 Alkali silica reactivity (ASR) .....	5
1.1.3 Corrosion of reinforcing steel.....	6
<b>1.2 Problem Statement.....</b>	<b>10</b>
<b>1.3 Objectives.....</b>	<b>11</b>
1.3.1 Main objective .....	11
1.3.2 Specific Objectives .....	12
<b>1.4 Research Significance .....</b>	<b>12</b>
<b>1.5 Scope of the Study.....</b>	<b>13</b>
<b>1.6 Limitations.....</b>	<b>14</b>
<b>1.7 Assumptions.....</b>	<b>14</b>
<b>1.8 Thesis Organization.....</b>	<b>14</b>
<b>CHAPTER 2.....</b>	<b>16</b>
<b>2.0 LITERATURE REVIEW .....</b>	<b>16</b>
<b>2.1 Introduction.....</b>	<b>16</b>

<b>2.2 Properties of rust and Corrosion in Reinforced concrete water structures .....</b>	<b>24</b>
2.2.1 Properties of Rust .....	24
2.2.2 Corrosion in Reinforced concrete water conveyancing structures. ....	25
<b>2.3 Critical penetration depth of rust and its influence on the service life of reinforced concrete. ....</b>	<b>28</b>
<b>2.4 Use of corrosion inhibitors and anticorrosion coatings as methods of preventing corrosion. ....</b>	<b>35</b>
2.4.1 Design consideration .....	36
2.4.2 Use of alternative materials .....	36
2.4.3 Use of corrosion inhibitors .....	36
2.4.3 Corrosion inhibitors in the Kenyan market .....	42
2.4.4 Efficiency of corrosion inhibitors.....	47
2.4.5 Factors influencing inhibitor choice .....	47
<b>2.5 Coating of ribbed bars as a method of corrosion prevention .....</b>	<b>48</b>
<b>2.6 Modelling of corrosion in reinforced concrete .....</b>	<b>52</b>
<b>2.7 Corrosion Kinematics.....</b>	<b>56</b>
2.7.1 Introduction to Corrosion kinematics .....	56
2.7.2 Reinforcement corrosion .....	57
<b>2.8 Deterioration Models .....</b>	<b>61</b>
2.8.1 Introduction to Chloride ingress models .....	61
2.8.2 Chloride ingress models .....	62
<b>2.9 Service life models.....</b>	<b>74</b>
<b>2.10 Relationship between accelerated test results to real reinforced concrete in determination of the service life of structures.....</b>	<b>82</b>
<b>CHAPTER 3.....</b>	<b>84</b>

<b>3.0 METHODOLOGY .....</b>	<b>84</b>
<b>3.1 General introduction .....</b>	<b>84</b>
<b>3.2 Part 1: Investigation of material properties .....</b>	<b>86</b>
<b>3.3 Part 2: Corrosion tests.....</b>	<b>90</b>
3.3.1 Introduction to corrosion tests .....	90
3.3.2 Accelerated corrosion tests and tests program to ASTM G109 07.....	90
3.3.3 Detection of the onset of corrosion-induced Cracking.....	93
3.3.4 Estimation of critical penetration depth ( $X_{crit}$ ) .....	93
<b>3.4 Part 3: To investigate the effect of corrosion inhibitors on the bond strength of reinforced concrete in water conveyance structures. ....</b>	<b>95</b>
3.4.1 General Introduction.....	95
3.4.4 Bond stress calculation .....	99
<b>3.6 Proposed Service Life Model .....</b>	<b>101</b>
3.6.1 Introduction to service life modelling. ....	101
3.6.2 Model development from corrosion product evolution.....	102
3.6.3 The Corrosion initiation period and Current density ( $\mu\text{A}/\text{cm}^2$ ).....	107
3.6.4 Proposed Service Life Model .....	109
<b>CHAPTER 4.....</b>	<b>111</b>
<b>4.0 RESULTS AND DISCUSSION .....</b>	<b>111</b>
<b>4.0 Introduction.....</b>	<b>111</b>
<b>4.1 Results of the properties of materials.....</b>	<b>111</b>
4.1.1 Results of fresh concrete tests .....	111
4.1.2 Aggregates .....	115
4.1.3 Tensile strength and mechanical properties of ribbed bars .....	119

4.1.4 Chemical Composition of Ordinary Portland cement brands used in the research	122
4.1.5 Corrosion Inhibitors.....	125
4.1.6 Concrete strength.....	126
<b>4.2 Accelerated corrosion Results.....</b>	<b>129</b>
4.2.1 Results of accelerated corrosion test .....	129
4.2.2 Critical Penetration depth of rust.....	132
<b>4.3 Effect of corrosion inhibitors on bond strength.....</b>	<b>135</b>
4.3.1 Results of hardened concrete with corrosion inhibitors .....	135
4.3.3 Parametric study of the results.....	139
4.3.4 Proposed Bond strength Model .....	146
<b>4.4 Service Life model.....</b>	<b>148</b>
4.4.1 Corrosion Current density .....	148
4.4.2 Proposed service life model.....	154
4.4.3 Application and limitation of the proposed model.....	159
<b>CHAPTER 5.....</b>	<b>161</b>
<b>5.0 CONCLUSION AND RECOMMENDATIONS.....</b>	<b>161</b>
<b>REFERENCES.....</b>	<b>163</b>
<b>APPENDICES</b>	
Appendix A1 Properties of materials used in the research.....	185
Appendix A2 Concrete mix design.....	192
Appendix A3 Results from experimental work.....	195
Appendix A4 Pictures during experimentation.....	203
Appendix A5 Published papers from this research.....	210

## List of Tables

<b>Table 2.1</b> Existing small hydro power projects with salient features of conveyance structures inhibitor .....	27
<b>Table 2.2</b> Properties of the dimethylathanolamine based organic inhibitor .....	45
<b>Table 2.3</b> Constants in Bolomey's formula.....	60
<b>Table 2.4</b> Summary of Service Life models, their strengths and weaknesses.....	81
<b>Table 3.1</b> Summary of concrete constituents used in this study.....	89
<b>Table 3.2</b> Matrix of experimental sample size.....	89
<b>Table 3.3</b> Parametric study of predicted and observed times to cracking of the research and the model.....	107
<b>Table 3.4</b> Adopted values for determination of equilibrium potential( $E_{corr}$ ).....	108
<b>Table 4.1</b> Results of fresh concrete test.....	112
<b>Table 4.2</b> Physical properties of aggregates used in the study.....	115
<b>Table 4.3</b> Result of Mechanical Properties of Coarse aggregates.....	117
<b>Table 4.4</b> Chemical analysis of the 10mm rebar used in the study and their effect.....	120
<b>Table 4.5</b> Result of Chemical composition the brands of cement tested.....	122
<b>Table 4.6</b> Chemical analysis of the fly ash used in the research.....	125
<b>Table 4.7</b> Comparative study of concrete strength results used in this research.....	126
<b>Table 4.8</b> Statistical analysis of the results of tensile strength of this work and the output of other models for Tensile strength.....	128
<b>Table 4.9</b> Weight loss and duration of accelerated corrosion samples.....	129
<b>Table 4.10</b> Critical penetration depth for the samples.....	133
<b>Table 4.11</b> Comparative study of results of hardened concrete.....	139

<b>Table 4.12</b> Pearson Correlation of the measured split tensile strength of this study and with the output of other researchers.....	143
<b>Table 4.13</b> Parametric study of bond strength of this work with other authors.....	144
<b>Table 4.14</b> Correlations of results of this work with results of other researchers.....	145
<b>Table 4.15</b> Tests of Between-Subjects Effects of this research and those of Orangun et al and Stanish et al.....	146
<b>Table 4.16</b> Correlations of bond strength results of this work with the proposed model and Stanish et al bond strength model.....	146
<b>Table 4.17</b> The rate of corrosion of rebar from samples from different diameter samples and strengths.....	148
<b>Table 4.18</b> Correlations of the results of this work and those of Vu and Stewart.....	152
<b>Table 4.19</b> Statistical relationship between the results of this work, the Vu model and the proposed model for corrosion current density during propagation period.....	154
<b>Table 4.20</b> Parametric study of the service life models for a steady corrosion current of 1 g /m <sup>2</sup> /day.....	155
<b>Table 4.21</b> Parametric study of correlations of the propagation period.....	158



## List of figures

<b>Figure 1.1</b> Installed electricity capacity by source in Kenya.....	3
<b>Figure 1.2</b> Corrosion-induced cracking of concrete .....	6
<b>Figure 1.3</b> Mechanism of corrosion of steel in concrete .....	7
<b>Figure 1.4</b> The relative volumes of iron and its corrosion reaction products.....	9
<b>Figure 2.1</b> Partial collapse of the Berlin Congress Hall on May 21 <sup>st</sup> , 1980.....	16
<b>Figure 2.2</b> Collapsed Ynys-y-Gwas bridge .....	17
<b>Figure 2.3</b> Iron-water system, without chloride, at 25°C Pourbaix diagram .....	19
<b>Figure 2.4</b> Iron-water system with the presence of chloride, at 25°C Pourbaix diagram.....	23
<b>Figure 2.5</b> Various stages in the development of reinforcement corrosion in concrete .....	28
<b>Figure 2.6</b> A conceptual diagram for corrosion-induced cracking.....	32
<b>Figure 2.7</b> Corrosion threshold of uncoated and galvanized steel.....	52
<b>Figure 2.8</b> Evans diagram for the anodic and cathodic processes taking place on the reinforcing steel surface .....	57
<b>Figure 2.9</b> Graph of Chloride concentration VS depth from surface.....	65
<b>Figure 2.10</b> A schematic sketch of steel corrosion sequence in concrete.....	74
<b>Figure 2.11</b> Cady-Weyers' corrosion-deterioration model for concrete bridge .....	76
<b>Figure 3.1(a) and (b)</b> 120mm zinc sprayed coat length of 400mm long ribbed bars.....	87
<b>Figure 3.2</b> Detail of embedded bar in concrete sample.....	91
<b>Figure 3.3(a)</b> Schematic view of accelerated corrosion experimental set up.....	91
(b) Schematic experimental circuit set up of accelerated corrosion test.....	92
(c) Accelerated corrosion set up during experimentation.....	92
<b>Figure 3.4</b> Pictorial view of: a) Samples during experimentation) b) sample with 0.2mm longitudinal crack width c) crack width measurement.....	93

<b>Figure 3.5</b> (a) recovering the corroded steel, (b) cleaned rebar's for gravimetric weight loss.....	93
<b>Figure 3.6</b> Digital compression machine for testing cubes.....	97
<b>Figure 3.7</b> (a) Pictorial detail of the UTM used during the study.....	97
(b) Schematic detail of the UTM used during the study.....	98
<b>Figure 3.8</b> Schematic view of the pull out testing equipment used during the study.....	99
<b>Figure 3.9</b> (a)- (b) Pull out Testing equipment during sample testing.....	99
<b>Figure 3.10</b> Schematic deformations of expansive pressure on surrounding concrete due to accumulation of rust products (Source: Author).....	102
<b>Figure 4.1</b> Relationship between a selected brand of cement with corrosion inhibitor and the achieved slump.....	113
<b>Figure 4.2</b> Relationship between a selected brand of cement with corrosion inhibitor and the achieved compaction factor.....	113
<b>Figure 4.3</b> Relationship between slump and compaction factor .....	114
<b>Figure 4.4</b> Grading curve of Coarse aggregates.....	118
<b>Figure 4.5</b> Grading curve of fine aggregates.....	118
<b>Figure 4.6</b> Stress Vs strain graph of 10mm rebars used in the research. ....	119
<b>Figure 4.7</b> Relationship between tensile and compressive strength for concrete used in the study.....	127
<b>Figure 4.8</b> Graph of a relationship between corrosion period in days and concrete cover in mm for concrete of characteristic strength a) 25N/mm <sup>2</sup> b) 25N/mm <sup>2</sup> c) 25N/mm <sup>2</sup> .....	130

<b>Figure 4.9</b> Graph of a relationship between loss in mass of rebars in grams after corrosion and concrete cover in mm for concrete of characteristic strength a) 25N/mm <sup>2</sup> b) 25N/mm <sup>2</sup> c) 25N/mm <sup>2</sup> .....	131
<b>Figure 4.10</b> Relationship between the critical penetration depth and concrete cover thickness for (a)M25, (b) M30 and M35 by various authors.....	134
<b>Figure 4.11</b> Compressive strength in N/mm <sup>2</sup> of samples with a selected brand of cement and a corrosion inhibitor at 7,14 and 28 days.....	136
<b>Figure 4.12</b> Failure mode of the samples during split tensile test.....	137
<b>Figure 4.13</b> Relationship of Split tensile strength in N/mm <sup>2</sup> for samples with a brand of cement and a selected corrosion inhibitor.....	137
<b>Figure 4.14</b> Relationship of bond strength in N/mm <sup>2</sup> for samples with a brand of cement and a selected corrosion inhibitor.....	138
<b>Figure 4.15</b> Relationship between the bond strength and a selected brand of cement with a corrosion inhibitor.....	140
<b>Figure 4.16</b> Relationship between the tensile strength and bond strength form Table 4.11....	141
<b>Figure 4.17</b> Correlations of Result of Split tensile strength of this work with results of other authors.....	142
<b>Figure 4.18</b> Relationship of measured bond strength with the output of other authors for a selected brand of cement and a corrosion inhibitor.....	145
<b>Figure 4.19</b> a)-c) Graph of Current density vs reinforcement cover for 25N/mm <sup>2</sup> ,30N/mm <sup>2</sup> and 35N/mm <sup>2</sup> and d) propagation period.....	149
<b>Figure 4.20</b> Relationship between the critical penetration depth and the corrosion current density of this work and selected models.....	150

<b>Figure 4.21</b> Relationship between corrosion current density and reinforcement mass loss for a crack width of 0.2mm.....	151
<b>Figure 4.22</b> Graph of the result of this work against and Vu and Stewart Model for corrosion current density in $\mu\text{A}/\text{cm}^2$ .....	153
<b>Figure 4.23</b> Graph a)-c) Relationship between the reinforcement cover and the propagation period results of this work, the proposed model and the results of other models.....	156
<b>Figure 4.25</b> Relationship between the measured and proposed model propagation period...	157
<b>Figure 4.26</b> Corrosion initiation and propagation points.....	160

## Notations and Abbreviations

$C$  = concentration of oxygen dissolved in the pore solution ( $\text{kg/m}^3$  of pore solution);

$C_o$  = oxygen concentration at the external concrete surface ( $\text{kg/m}^3$  of solution);

$C_s$  = chloride surface concentration ( $\text{kg/m}^3$ );

$c$  = concrete cover (m);

$d$  = reinforcing steel diameter (mm);

$E_a$  = electrical potential (V);

$E_c$  = equilibrium potential of the anodic reaction (V);

$E_{oa}$  = elastic modulus of concrete (MPa);

$E_{oc}$  = equilibrium potential of the cathodic reaction (V);

$F$  = Faraday's constant (= 96,486.7 C/mol of electrons);

$f'_c$  = cylinder compressive strength of concrete (MPa);

$f'_t$  = tensile splitting strength of concrete (MPa);

$i$  = current density vector ( $\text{A/m}^2$ );

$i_a$  = current density of the anodic reaction ( $\text{A/m}^2$ );

$i_c$  = current density of the cathodic reaction ( $\text{A/m}^2$ );

$i_{corr}$  = corrosion rate ( $\text{A/m}^2$ );

$i_{oa}$  = exchange current density for the anodic reaction ( $\text{A/m}^2$ );

$i_{oc}$  = exchange current density for the cathodic reaction ( $\text{A/m}^2$ );

OPC = ordinary Portland cement;

$\rho_{corr}$  = Combined density factor for steel and rust (kg/m<sup>3</sup>)

$\Delta d$  = increase in diameter of rebar due to rust formation(cm)

$j_r$  = instantaneous corrosion rate of rust (g/m<sup>2</sup>s)

P = perimeter of rebar(mm)

W=equivalent weight of steel(g)

## **CHAPTER 1**

### **1.0 INTRODUCTION**

#### **1.1 Background**

The opportunities and challenges to invest in hydropower infrastructure are complex, and ultimately dependent on the resources, skills, and will to invest responsibly, with due regard to all aspects of sustainable development. Hydropower as a renewable energy also plays a unique dual role in climate change: as an adaptation strategy for growing weather variability and as a renewable resource to move economies to a lower-carbon future.

Currently, there is a growing demand for clean, reliable, and affordable energy in Kenya and to a large extent the global arena. Hydropower and water infrastructure projects offers important opportunities for poverty alleviation, clean water, sanitation and clean energy. It is also part of the first United Nations sustainable development goals which are geared towards creating a framework for respective sustainable development of third and middle level economies and is expanding. Beyond the principal role of providing electricity access, which remains critical, hydropower as a blue economy generation resource, has a powerful contribution to make to regional cooperation and development where it is utilized. Water as a resource is shared and is increasingly becoming scarce due to changing climatic trends. This underscores the importance of sustainable exploitation of any available flows.

Concrete is among the oldest and most durable building materials. Its earliest known use was for a floor of small hut along the Danube River in the area of former Yugoslavia, dating from 5600BC. Other notable structures where concrete was used include the Great Pyramid at Giza and the Parthenon in Rome. Although the Romans experimented with bronze reinforcement, reinforced concrete as we know it today dates from the mid-19<sup>th</sup> century following the

introduction of Portland cement concrete in 1824 when it was patented by Joseph Aspeden in Wakefield.

Reinforced concrete is a composite material constituting concrete and reinforcements (steel bar). Concrete is strong in compressive strength but weak in tension. Steel has the advantage of having the tensile strength that concrete lacks, and is highly compatible in its chemical and physical characteristics. The term reinforced is used because the steel reinforces the concrete and makes it a stronger construction material. The matching of thermal expansion coefficients is critical to the versatility of reinforced concrete as a composite material, but corrosion becomes a major drawback as a corroded member exhibits different properties along its length.

Hydropower accounts for 16% of the world's electricity supply and accounts for 9% of the energy demand in Kenya [1]. It has helped shape and promote economic growth in developed and developing countries. Environmental, social and economic constraints, resulted in a period of stagnant global investment in the 1990s and critical assessment of the role of hydropower in development. Past lessons, present challenges together with emerging global technologies and dynamics, are recasting the role of hydropower as a contributor to the blue economy thus stimulating a renaissance in new investment and rehabilitation. Fig.1.1[2] shows the current electricity generation in Kenya, amounting to a combined installed capacity of 2,351MW for the period ending 2018 against 6,000MW estimated in 1991[3].

In 2008, the Kenya government developed a Feed In Tariff (FIT) policy (revised in January 2010) to attract investment and development of small and mini hydropower plants. Through this policy and with licensing from the Ministry of Energy, private investors can develop hydropower infrastructure and connect their generation to the national grid through a power purchase agreement with the Kenya Power and Lightning.



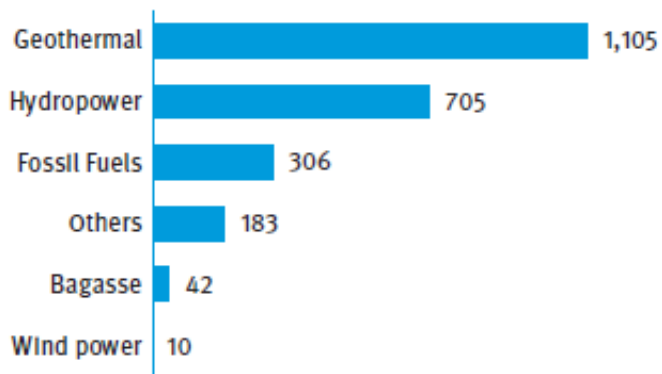


**Figure 1.1: Installed electricity capacity by source in Kenya(MW) [2]**

Kenya's economic growth, which has been growing at approximately 5.1% per year over the last 10 years is constrained by an insufficient supply of electricity [3]. Private investors have taken advantage of the FIT policy to develop small hydropower projects to meet their electric power supply and connect excess to the national grid through power purchase agreements. These investors include the Kenya Tea Development Authority, Tana River Development Authority, Green power, James Finlay (Kenya) Limited, Unilever Tea Kenya among others. A similar trend has followed in many third world economies.

Majority of small hydropower projects are a run of the river comprising of a diversion weir, a desilting tank, a low pressure canal or pipe, a forebay tank, a high pressure pipe and a turbine for generation of electric power. The focus of this study was on corrosion prediction of the reinforced concrete canal under free flow-a water conveyance structure between the desilt and forebay tanks.

The world's reserves of fossil fuels are getting depleted, studies have projected crude oil reserves will near an end between 2050 and 2075 [4]. Hydropower is a renewable source of energy and will serve to be a reliable source if we project its future sustainability. Many developing economies are giving incentives to use of machinery that rely less on fossil fuel eg solar power and clean cars.

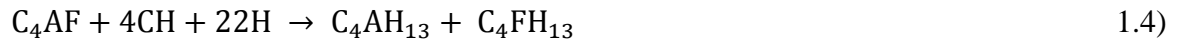
### 1.1.1 Deterioration mechanisms of Reinforced Concrete.

Reinforced concrete structures deteriorate under attack from external elements such as carbon dioxide, chloride ions, freeze-thaw damage and erosion. In concrete there are additional mechanisms caused by the greater complexity of its composition. Of particular concern is the alkali silica reaction in the concrete and the corrosion of the reinforcing steel, both of which are affected by the alkalinity of Portland cement concrete.

Portland cement is made by proportioning constituents which include Calcium Oxide (CaO), Silica (SiO<sub>2</sub>), Alumina (Al<sub>2</sub>O<sub>3</sub>), and Iron Oxide (Fe<sub>2</sub>O<sub>3</sub>) to produce a mixture with the desired chemical composition and then ground and blended by a dry process or wet process. The materials are then fed through a kiln at 2,600° F to form clinker. The alumina and iron act as fluxing agents which lower the melting point of silica from 3,000 to 2600° F. The clinker is cooled, pulverized and gypsum added to regulate setting time. It is then ground to particle size in the range of 0.007-0.2mm [5].

Portland cement is a highly alkaline material which reacts with water and hardens. When added to coarse and fine aggregates and mixed with water, the cement forms chemical bonds with water molecules and becomes hydrated. Hydration of Portland cement is not linear through time, it progresses very slowly at first, allowing the mixture to be properly placed before hardening. The main clinker phases present in Portland cements are tricalcium silicate (C<sub>3</sub>S), dicalcium silicate (C<sub>2</sub>S), tricalcium aluminate (C<sub>3</sub>A), and tetra calcium aluminoferrate (C<sub>4</sub>AF). The hydration of these phases in OPC is simplified in Equations 1.1-1.4[6].





Hydration of  $\text{C}_3\text{S}$  and  $\text{C}_2\text{S}$  results in the formation of CH and CSH. CSH is a cementitious material that imparts strength to cement based materials [6]. The hydration products of  $\text{C}_3\text{A}$  and  $\text{C}_4\text{AF}$  are not of significance to the strength of hardened cement [6]. At the early ages of mortar/concrete curing, CH is useful since it provides the necessary alkalinity to the hardened cement [6].

The chemical reactions that cause the delay in hardening are critical to developing a rational methodology for the control of cement setting. Each of the compounds in cement has a role to play in the hydration process. By changing the proportion of each of the constituent compounds in the cement (and other factors such as grain size), it is possible to make different types of cement to suit several construction needs and environment. The hardening process (hydration reaction) is complex and continues over many years, depending on the amount of water in the mix. There must be excess water for workability and a pore network therefore develops as it dries out. Excess calcium hydroxide and other alkaline hydroxides are present in the pores and a solution of pH 12.0 to 14.0[6] develops. It is this pore network and the solutions it contains that are critical to the durability of the concrete.

### **1.1.2 Alkali silica reactivity (ASR)**

Aggregates are becoming increasingly scarce as old quarries get depleted of quality materials leading to pressure to use aggregates from new sources which are of marginal quality. As demand for aggregate use increases, the probability of using marginal quality aggregates increases. ASR occurs when some siliceous minerals, such as quartzes and opals contained in aggregates react with water in a high alkaline environment to form silica gel, a material that absorbs moisture. As silica gel swells when it absorbs moisture, the material can cause concrete

to crack, and white, weeping deposits of silica appear on the surface of the concrete. In many cases ASR is superficial and harmless, but it is unattractive and difficult to treat. The most effective remedy is to dry out the affected areas.

Most types of concrete incorporate aggregates some which are susceptible to ASR. However very few structures show signs of significant ASR damage, as the reactive aggregate components which cause the problem are consumed in the process.

### 1.1.3 Corrosion of reinforcing steel

Although the alkalinity within the concrete pore structure can lead to ASR, the high pH value also provides a protective coating of oxides and hydroxides on the surface of the steel reinforcement. This is the main reason why reinforced concrete is a durable construction material. Without this layer, which is known as a 'passive' film, the steel can be exposed to the air and moisture in the pores, leading to rapid corrosion (Fig. 1.2) [7]. The layer is durable and self-repairing, and it can last for hundreds of years if the alkalinity is maintained [8]. However, the passive layer itself can be attacked by chlorides and the alkalinity of the concrete can be reduced by reaction with atmospheric carbon dioxide.

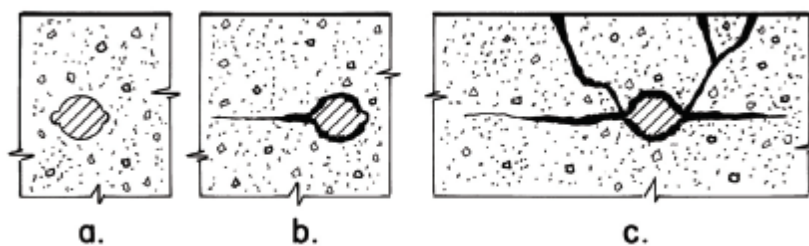


**Figure 1.2 Corrosion-induced cracking of concrete [7].**

a) Steel rebar in the passive state, b) Delamination within the concrete caused by rust growth and c) Spalling of concrete by expansive rust products.

For corrosion to occur, four elements must be present; there must be at least two metals (or two locations on a single metal) at different energy levels, an electrolyte, and a metallic connection. In reinforced concrete, the rebar may have many separate areas at different energy levels. Concrete acts as the electrolyte, and the metallic connection is provided by wire ties, chair supports, or the rebar itself [9].

Corrosion is an electrochemical process involving the flow of charges (electrons and ions). Fig.1.3[10] shows a corroding steel bar embedded in concrete. At the anodes, iron atoms lose electrons and move into the surrounding concrete as ferrous ions. This process is called a half-cell oxidation reaction, or the anodic reaction, and is represented as Equation 1.5:

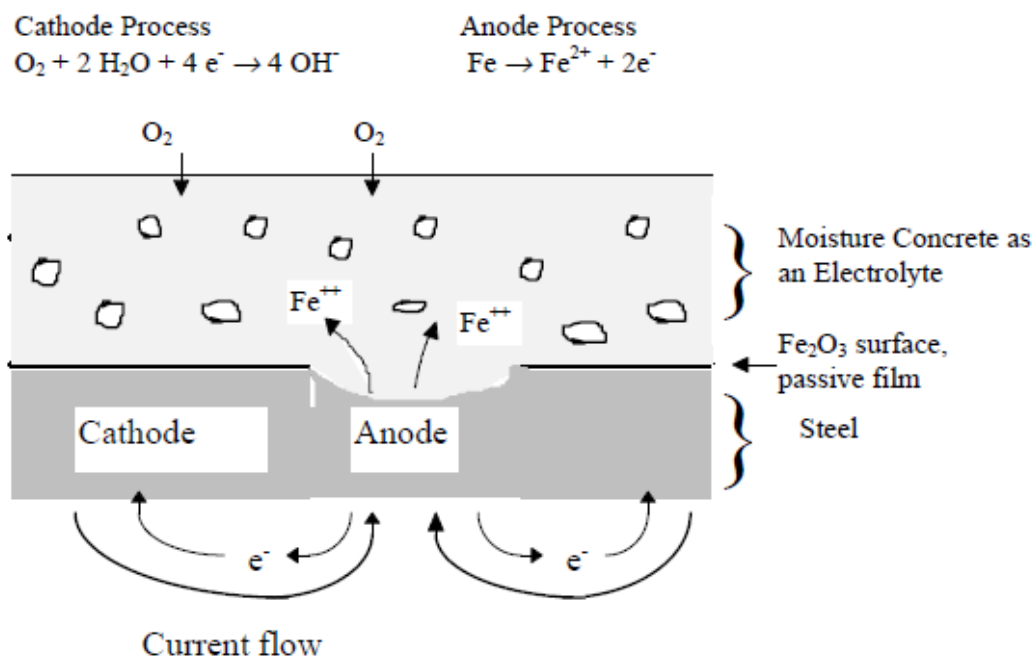


**Figure 1.3: Mechanism of corrosion of steel in concrete [10].**

The electrons remain in the bar and flow to sites called cathodes, where they combine with water and oxygen in the concrete. The reaction at the cathode is called a reduction reaction and is represented by Equation 1.6;



It should be noted that water is not only required for the cathodic reaction but also as a carrier for the cations produced in the anodic reaction. To maintain electrical neutrality, the ferrous ions migrate through the concrete pore water to these cathode sites where they combine to form iron hydroxides, or rust shown in Equation 1.7;



This initial precipitated hydroxide tends to react further with oxygen to form higher oxides. The increases in volume as the reaction products react further with dissolved oxygen leads to internal stress within the concrete that may be sufficient to cause cracking and spalling of the concrete cover. The corrosion of steel reinforcement inside a concrete structure is undesirable in the following ways:

- (i) The presence of rust impairs the bond strength of deformed reinforcement because corrosion occurs at the raised ribs and fills the gap between ribs, thus evening out the original deformed shape. In essence, the bond between concrete and deformed bars originates from the mechanical lock between the raised ribs and concrete. The reduction of mechanical locks by corrosion results in the decline in bond strength with concrete.
- (ii) The presence of corrosion reduces the effective cross sectional area of the steel reinforcement. Hence, the available tensile capacity of steel reinforcement is reduced by a considerable reduction in the cross sectional area.
- (iii) The corrosion products occupy about 3-6 times the original volume of steel [11, 12] from which it is formed. Since the volume of rust products is much higher (about 3 to 6 times) than

that of the iron as shown in Fig.1.4 [13], Such drastic increase in volume generates significant bursting forces in the vicinity of steel reinforcement. Consequently, cracks are formed along the steel reinforcement when the tensile strength of concrete is exceeded.

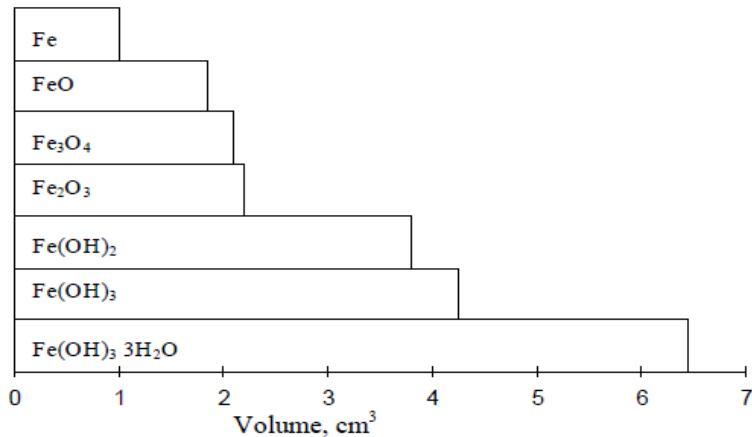


**Figure 1.4: The relative volumes of iron and its corrosion reaction products [13].**

Corrosion problems in concrete have led researchers to investigate the viability of new corrosion-free reinforcement, such as fiber-reinforced polymer (FRP) bars. Those bars are expensive, but if long-term costs are taken into account, the economic picture changes dramatically [13].

Various methods of limiting rust have been suggested, among them use of vapour phase corrosion inhibitors and rust convertors. Inhibitors are chemical substances which will reduce the intensity of the anodic or cathodic reactions. The most important class of chemical agents used function by changing the electrochemical processes occurring at the metallic surfaces, e.g. chromates, nitrites and phosphates. The vapor phase corrosion inhibitors (VpCI) including epoxy, polyurethane and acrylic, minimizes corrosion to metals and their alloy by producing vapors with sufficient vapor pressure due to their volatile nature. They also prevent the metal or alloys from corrosion by adsorption of their vapors onto the metal surface. VpCIs function by forming a bond with the metal surface and creating a barrier layer that helps prevent contact

of aggressive ions such as chloride with the protective barrier in place, the corrosion cell cannot form and corrosion is halted. That barrier self-replenishes through further condensation of the vapor [14]. The effective use of surfactants for VpCI depends upon environment and properties of metals as well as surface- active agents (surfactants) [15-19].

This study aims at establishing a corrosion model to predict the service life of reinforced concrete water conveyancing structures.

## **1.2 Problem Statement**

Hydropower and other water infrastructure projects require a lot of money to develop which is borrowed from multinational financial institutions in most instances. Repayment of the borrowed money is from the sale of power to the national grid or consumers depending on the power purchase agreement during the operational phase of the project. Interests accrue for non-repayment which may result from underperforming of the structures or stoppage due to unscheduled structural maintenance. This source of repayment demands that the structures support a continuous operation of the project hence a need to predict a scheduled time for rehabilitation. The number of scheduled rehabilitations within the service life have a cost implication and their reduction increases the projects sustainability.

Corrosion inhibitors reduce the rate of corrosion and subsequently the number of rehabilitations required for a defined design life. There is a need to evaluate the effect of selected corrosion inhibitors on properties that influence the service life.

Structural concrete is designed to meet specific criteria for workability, strength and durability. Current specifications are largely prescriptive, laying down values for limiting parameters such as minimum binder content, maximum w/b ratio, minimum compressive strength, amount of entrained air. Prescriptive specifications work on a ‘deemed-to-satisfy’ basis, where if the



requirements are met (which is frequently not verifiable in practice), the structure is ‘deemed-to-satisfy’ the durability requirements. Their main drawback is that they specify parameters that are often unverifiable in practice, more particularly on the as-built structure, and thus cannot be verified objectively. Usually, once the concrete has been mixed and placed, only the compressive strength is measured to ensure compliance with the design requirements and specifications, using specially prepared samples made, cured and tested under conditions that bear little resemblance to those in the actual structure.

One of the challenges of infrastructure owners and contractors is the ability to predict time to maintenance and rehabilitation. To address this, predictive models have been developed, especially related to time to corrosion of reinforced concrete exposed to marine environment. Service life modelling and prediction Service life modelling for reinforced concrete structures involves quantitative calculations or estimates to predict the time to unacceptable damage (e.g. cracking, corrosion, loss of section, etc.) for a given environment. Service life models are semi-empirical in nature, based on laboratory and site data that are necessary for calibration.

Existing service life prediction of concrete structures are structure and environment specific and each of them have inherent disadvantages when applied to unintended infrastructure projects. There is need to develop a simulation model to predict the service life of reinforced concrete water conveyancing structures. This study attempted to address these needs.

### **1.3 Objectives**

#### **1.3.1 Main objective**

The main objective is to develop a simulation model to predict the service life of reinforced concrete water conveyancing structures.

### **1.3.2 Specific Objectives**

- i. To investigate the critical penetration depth of rust in reinforced concrete water conveyancing structures.
- ii. To investigate the effect of corrosion inhibitors on the bond strength of reinforced concrete in water conveyance structures.
- iii. To develop a corrosion current density model for reinforced concrete water conveyancing structures.
- iv. To develop a simulation model to predict the service life of reinforced concrete water conveyancing structures.

### **1.4 Research Significance**

Cracking of the concrete cover caused by corrosion can seriously affect the serviceability and durability of reinforced concrete structures [20]. Corrosion can also reduce the cross-sectional area of reinforcing steel, thus reducing its tensile strength. The level to which the performance of a structure is degraded depends on the nature, severity and the location of occurrence of corrosion. Considering the importance of reinforced concrete water conveyancing structures in hydropower, irrigation and domestic water infrastructure projects there was a considerable need for reliable techniques to assess and reduce the effects of corrosion on continued performance of the existing projects. It is also necessary to monitor the behavior of the structures during the design life and schedule necessary rehabilitation works for the structures to continue to be in-service.

Incorporating corrosion inhibitors in reinforced concrete structures reduces the rate of corrosion and subsequently the number of rehabilitations required. The study of the effect of

the corrosion inhibitors on the properties that affect the service life of structures is advantageous in making an informed decision in their selection.

Monitoring tools for structures include corrosion service life models which forms the basis of this study. Considerable research has been devoted to the development of structural deterioration models, but few are specific to reinforced concrete water structures.

The central focus in structural modelling of corrosion is the consideration of its physical effects on the materials and structural behavior. The following aspects should be considered [20]:

- i) Steel area reduction in the main bars due to corrosion.
- ii) Changes in the ductility of reinforcing steel bars due to pitting corrosion.
- iii) Reduction of concrete cover due to cracking or spalling.
- iv) Changes in strength and ductility of concrete in compression, because of micro-cracking induced by corrosion of the reinforcing bars.
- v) Changes in tension stiffening because of cover cracking and bond deterioration
- vi) Changes in the bond between the reinforcing bars and concrete.

The service life model developed took into account the strength of concrete, the concrete cover and steel area reduction due to corrosion with time to enable a focused schedule for the rehabilitation of reinforced concrete water conveyancing structures to continue performing their service function.

### **1.5 Scope of the Study**

The study covers corrosion degradation in reinforced concrete water conveyancing structures subjected to chloride ingress.

## **1.6 Limitations**

Reinforced concrete degradation due to corrosion is caused by chloride and carbon dioxide ingress. For run of the river small hydropower projects, the predominant corrosion agent in reinforced concrete conveyancing structures is chloride ingress. Validity of the model developed is for chloride ingress only.

## **1.7 Assumptions.**

The study assumed that the concrete is homogeneous and crack free.

## **1.8 Thesis Organization**

This thesis is organized into five chapters. Chapter one gives a brief background of reinforcement corrosion, its effect on steel in concrete water conveyancing structures, methods of corrosion prevention and the objectives of the study.

The second chapter reviews the literature relevant to the study. It begins with the outline of the corrosion process and discusses factors influencing corrosion behavior of reinforcing steel embedded in concrete. A review covering passivity and pitting of corrosion in an alkaline media is also presented. The examination of corrosion protection and prevention strategies for concrete is discussed. The effect of corrosion on bond strength between steel and concrete is reviewed. The use of corrosion inhibitors and their application is discussed. A review of corrosion current density and service life models are discussed. The literature review ends with some concluding remarks on the grey areas and a specific focus for this study.

Chapter three of this thesis comprises of the methodology and experimental study divided into three parts. In part one the properties of material for reinforced concrete were investigated. In part two corrosion tests were investigated. The experimental methods including specimen design and preparation followed by corrosion rate measurement is presented. The modelling

methodology for the service life of reinforced concrete water conveyancing structures is also presented.

In part three, a comparative study of the effect of selected four corrosion inhibitors on the bond strength on reinforced concrete is described and how the pull out test was performed to evaluate the bond strength between steel and concrete.

The fourth chapter of this thesis presents and discusses results from experimental work including the proposed corrosion model for predicting the service life of reinforced concrete water conveyancing structures.

The Fifth chapter gives a brief summary of the work, major conclusions resulting from the present investigation and recommendations for future work.

## CHAPTER 2

### 2.0 LITERATURE REVIEW

#### 2.1 Introduction

Corrosion of steel reinforcement has been recognized as a primary factor contributing to the deterioration of concrete structures [21-23]. The economic damage caused by corrosion of reinforcing steel in concrete water conveyancing structures is one of the largest infrastructure problems in both developing and developed countries. Public safety can be jeopardized and the escalating repair cost could directly burden the future economies [24]. In Berlin the southern external roof overhang of the Berlin Congress Hall partially collapsed (Fig.2.1) on 21 May 1980, 23 years after its construction due to hydrogen-induced stress corrosion [25], one person died and another was critically injured.

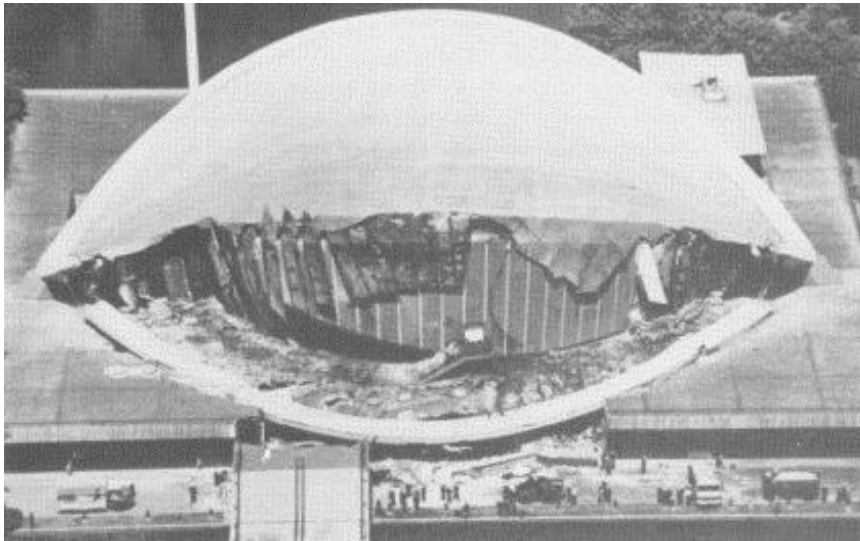


**Figure 2.1: Partial collapse of the Berlin Congress Hall on May 21st, 1980[25]**

Ynys-y-Gwas, a post tensioned concrete bridge in the neighborhood of Port Talbot in Wales in the United Kingdom collapsed (Fig.2.2) collapsed on December 4<sup>th</sup>, 1985 at 7 o'clock in the morning [26,27]. This concrete bridge was an 18m single span segmental post-tensioned structure which carried a minor road and was constructed in 1953. When its deck collapsed

there was no traffic on the bridge. The cause of the collapse was serious corrosion of the post-tensioned tendons. The corrosion took place at the transverse joints in which chloride-containing water could penetrate.



**Figure 2.2: Collapsed Ynys-y-Gwas bridge [27]**

Owing to its significant economic impact, an increase in demand for studies on corrosion has arisen. Corrosion as a subject stands out once it was found out that water structures suffered corrosion damages at a premature age. Today many civil infrastructure developers require service lives of 80, 100 or even 200 years for important reinforced concrete structures. In the south-western part of the Netherlands, the Eastern Scheldt Storm Surge Barrier is designed for a service life of 200 years. Although there was lack of practical experience with respect to such a long service life for structures continuously exposed to an aggressive marine environment, an attempt was made to meet this requirement by analyzing the process of corrosion initiation by chlorides. Most present design codes do not give quantified guidance for designing for such long service lives. Usually a service life of 50 years is only implicitly assumed [27].

In 1970-71, a bridge was built over the Muckbachtal river as part of the motorway connecting Würzburg and Heilbronn, Germany. The bridge sustained short winter periods followed by longer dry periods necessitating high concentrations of chlorides in the concrete coverings of reinforcing and prestressing steel components of the bridge. The chlorides were able to penetrate the concrete cover and corrosion was exacerbated because low quality concrete containing porous aggregates had been used. No fatalities were reported, as the defects were reported during the bridge inspection as a damage due to errors in planning and execution.

Corrosion of embedded steel in reinforced concrete results from carbonation or chloride attack. Carbonation reduces the alkalinity of concrete to a pH value of about 9 and once the pH of the concrete surrounding the steel drops to below 10, the steel will become de-passivated and if water and oxygen are available the steel will start to corrode.

Carbonation takes place even at small CO<sub>2</sub> concentrations and occurs progressively from the outside of concrete exposed to CO<sub>2</sub> but does so at a decreasing rate because CO<sub>2</sub> has to diffuse through the pore system, including the already carbonated surface zone of concrete. Such diffusion is a slow process if the pores in hydrated cement paste are filled with water because diffusion of CO<sub>2</sub> in water is 4 orders of magnitude slower than in air. In the presence of insufficient water, CO<sub>2</sub> and calcium hydroxide do not ionize fully. Conversely, in presence of sufficient water, carbonation process takes place leading to the formation of pore filling solid CaCO<sub>3</sub> in the hydrated cement pore network as the diffusivity of CO<sub>2</sub> is lower in water than in air [28].

Highly porous concrete materials allow greater penetration of CO<sub>2</sub> in the bulk of hydrated cementitious materials. Porosity in combination with factors such as relative humidity has a significant impact on CO<sub>2</sub> diffusion, i.e., the pore sizes. When mortars are exposed to a 57%



relative humidity environment, a calculated Kelvin radius would be 4 nm. When the cement matrix has a larger fraction of pores below this pore size, CO<sub>2</sub> diffusion will be very slow since pores with sizes below 4 nm will be filled by condensed water [29].

Chloride attack does not harm the concrete but can lead to corrosion of steel inside concrete and it is the corrosion that causes deterioration of reinforced concrete structures. When cement is mixed with water in the concrete, it produces hydration products with a pH ranging from 12.5 to 13.5. This state of pH environment helps in the development of a thin passivity layer. The steel reinforcement in the concrete is protected by this passivation layer [28] and the oxide layer is maintained by the high alkalinity in the concrete. The dependence of the state of the steel on the corrosion potential and the pH in the concrete is demonstrated in Pourbaix diagram for iron as shown in Fig.2.3 [29]. This diagram shows that under normal conditions, the pH of the concrete supports passivity of the steel.

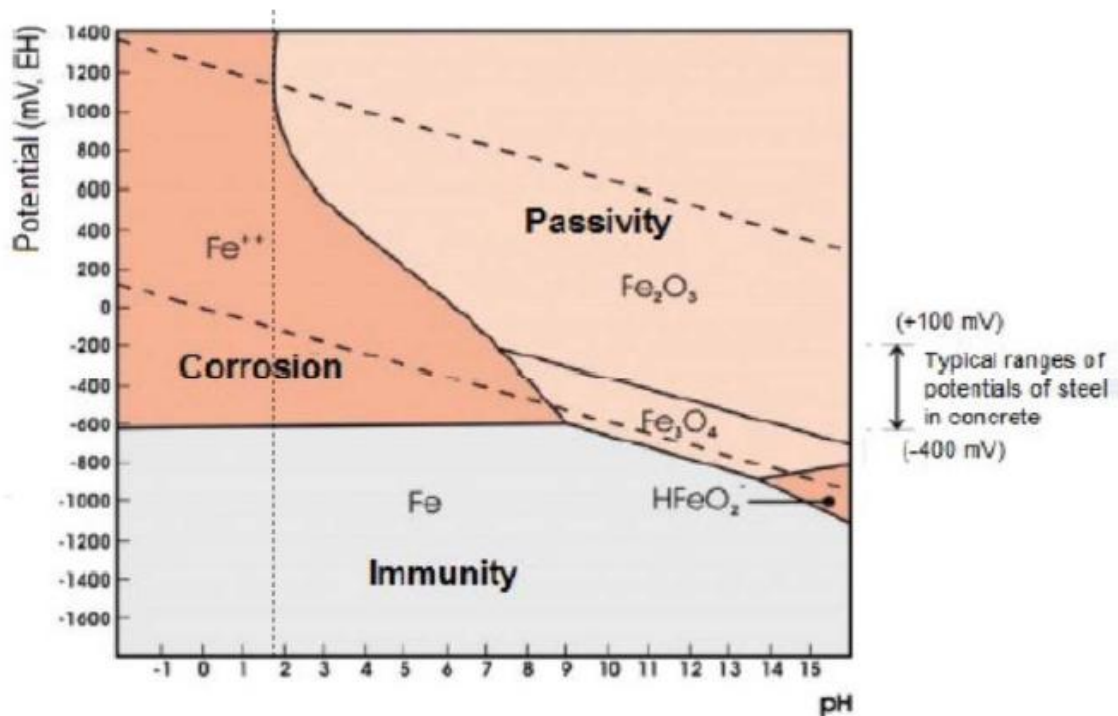


Figure 2.3 Iron-water system, without chloride, at 25°C Pourbaix diagram [29].

Each line of the diagram in Fig.2.3 represents conditions of thermodynamic equilibrium for some reaction. A horizontal line represents a reaction that does not involve pH; that is, neither H<sup>+</sup> nor OH<sup>-</sup> is involved, as in the reaction of Equation 2.1,



For this equilibrium, using the Nernst equation [30], we obtain Equation 2.2;

$$E = E^0 - 2.303 \frac{RT}{zF} \log \frac{1}{[\text{Fe}^{+2}]} \quad (2.2)$$

If (Fe<sup>+2</sup>) is taken as 10<sup>-6</sup>M, then E= 0.617 V, a horizontal line on the Pourbaix diagram.

A vertical line involves H<sup>+</sup> or OH<sup>-</sup> but not electrons; for example, Equation 2.3;



In Fig.2.3 the vertical line separating Fe<sup>+3</sup> from Fe<sub>2</sub>O<sub>3</sub> corresponds to this reaction. For this equilibrium we have Equations 2.4 and 2.5;

$$K = \frac{(\text{H}^+)^6}{(\text{Fe}^{+3})^2} \quad (2.4)$$

$$\begin{aligned} \log K &= 6 \log(\text{H}^+) - 2 \log(\text{Fe}^{+3}) \\ &= -6\text{pH} - 2 \log(\text{Fe}^{+3}) \end{aligned}$$

Since  $\Delta G^0 = -RT \ln K$  and  $\Delta G^0 = -8240 \frac{\text{J}}{\text{mole}}$  we obtain

$$\log K = 1.43$$

$$\log(\text{Fe}^{+3}) = -0.72 - 3\text{pH} \quad (2.5)$$

Taking (Fe<sup>+3</sup>) = 10<sup>-6</sup> M, then pH = 1.76, and this line at pH= 1.76 represents the equilibrium reaction to the right of this line Fe<sup>+3</sup> + 3H<sub>2</sub>O → Fe<sub>2</sub>O<sub>3</sub> + 6H<sup>+</sup> is stable phase; and this oxide as a protective film would be expected to provide some protection against corrosion. To the left of this line (pH<1.76) ferric ions in solution are stable, and corrosion is expected to take place without any protection afforded by a surface oxide film.

A sloping line involves  $H^+$ ,  $OH^-$ , and electrons. For example, the sloping line separating  $Fe^{2+}$  from  $Fe_2O_3$  represents the reaction of Equation 2.6;



From Equation 2.6;

$$E = E^0 - 2.303 \frac{RT}{zF} \log \frac{[Fe^{+2}]^2}{[H^+]^6}$$

Since  $E^0 = 0.728V$  and  $z=2$

$$E = 0.78 - 0.0592(Fe^{+2}) - 0.1776pH,$$

Taking  $(Fe^{+2}) = 10^{-6}M$  we obtain Equation 2.7;

$$E = 1.082 - 0.1776pH \quad (2.7)$$

This line represents the equilibrium,  $Fe_2O_3 + 6H^+ + 2e^- \rightarrow 2Fe^{2+} + 3H_2O$

To the right of this line,  $Fe_2O_3$  is stable phase that is expected to form a surface oxide film that protects the underlying metal from corrosion. To the left of this line  $Fe^{+2}$  is a stable species in solution.

The fields marked  $Fe_2O_3$  and  $Fe_3O_4$  are sometimes labeled "passivation" on the assumption that iron reacts in these regions to form protective oxide films. This is correct only insofar as passivity is accounted for by diffusion-barrier oxide layer. [29,31].

When the concentration of chloride in reinforced concrete is low, it is ineffective in denuding the protection layer as the hydroxyl ions formed in the pore solution replenish the oxide film [32]. When a high chloride concentration develops in the vicinity of the rebar, the oxide layer can be destroyed [33]. This critical concentration triggers the onset of corrosion and is referred to as the threshold value expressed as a concentration ratio between the chloride and hydroxyl ions and ranges from 0.35 to 1% of the mass of the cement [34,35] but it is generally accepted that the value is 0.6 [36].

Chlorides originate from internal ingredients of the concrete mix and externally from the environment. Chlorides penetrate concrete by transport of water containing the chlorides, as well as by diffusion of the chloride ions in the pore water and by absorption. Most small hydropower structures are located in mountainous and partly forested areas where carbon dioxide concentration is less than 0.03% [37]. Sources of chlorides in these regions are natural which include precipitation, rock-water interactions and background concentration; and /or anthropogenic sources which include road runoff, human sewage, livestock waste, water conditioning salts, synthetic fertilizer, municipal landfills [38]. Under these conditions chloride-induced rebar corrosion is likely to be the dominant mechanism determining the service life of reinforced concrete structures, whereas carbonation-induced corrosion can be neglected [38].

Several aspects influence the probability of occurrence of corrosion due to chloride ions. The decrease in the concrete water/cement ratio and concrete relative humidity, resistivity and increasing concrete cover thickness, the use of mineral additions, and the use of inhibitors tend to hinder the occurrence of corrosion.

The influence of the chloride ions on the depassivation of reinforcement can be observed by the alteration in the Pourbaix diagram for the iron-water system in the presence of chlorides (Fig.2.4). In this diagram, a decrease in the passivity region is observed in comparison to the Pourbaix diagram without the presence of chlorides (Fig.2.4). This reduction is due to the presence of pitting corrosion and imperfect passivity regions occurring due to the presence of these ions. From this diagram, it is possible to observe that corrosion can occur for all pH values, including values between 8.5 and 14, the zone of passivity or immunity for the iron water system without chloride ions.

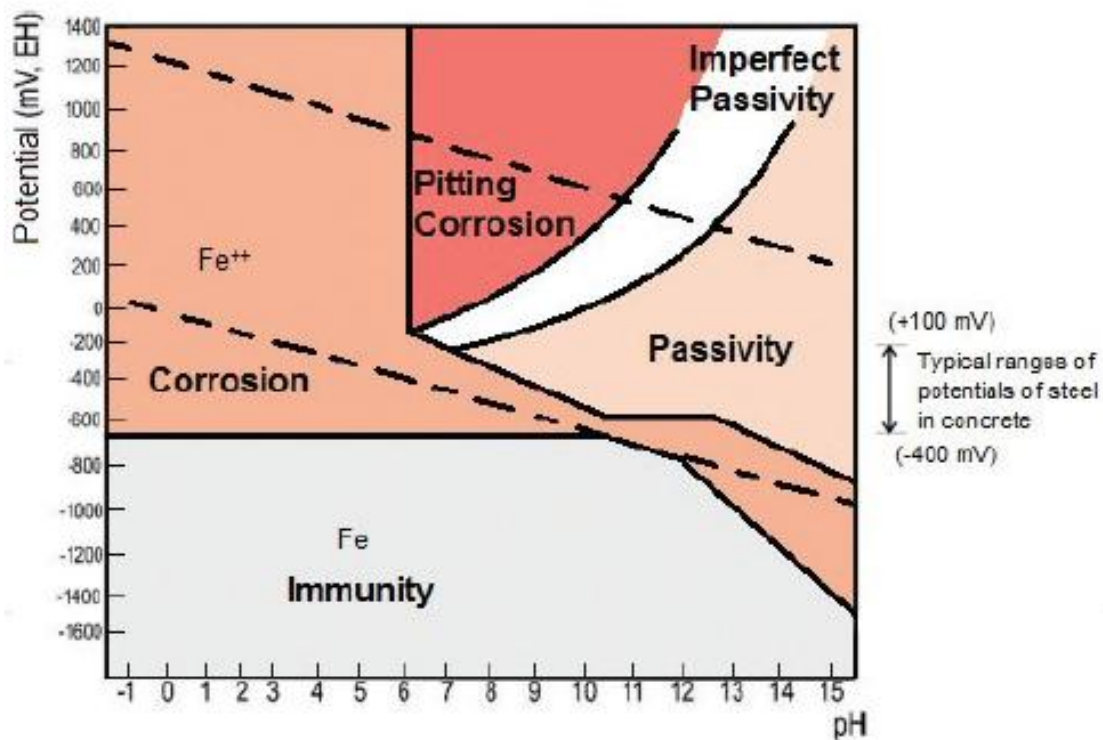
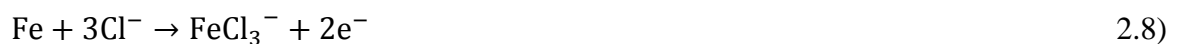


**Figure 2.4. Iron-water system with the presence of chloride, at 25°C Pourbaix diagram [29].**

The most accepted theory suggests that the presence of ions causes a destabilization of the passivating layer, reacting with iron to form iron hydroxide (Equations 2.8 and 2.9). In this process, the chloride ions are not consumed and are thus available to continue to react.



This chapter provides relevant literature review on development of corrosion in reinforced concrete water structures, methods of overcoming corrosion and their shortcomings, existing models to predict service life and the need to develop a simulation model to predict the service life of water conveyancing structures.

## 2.2 Properties of rust and Corrosion in Reinforced concrete water structures

### 2.2.1 Properties of Rust

The properties of rust are not clearly defined, although recent work has indicated that rust properties differ significantly from those used by current cover-cracking models. Konopka [39,40] obtained rust samples from iron filings produced from a steel reinforcing bar. The process was accelerated by bubbling air through water containing a mild acid while impressing an electrical current. The resulting rust flakes were dried with as little handling as possible and then tested in small versions of standard soil mechanics triaxial and oedometer cells. The range of values measured for the elastic modulus was in the range 40–87 MPa, and 0.48–0.54 GPa for the bulk modulus.

Rust production rate is assumed to follow a rule that combines two earlier predictions. It is postulated that the rate of production for low rust thicknesses is linear and follows Faraday's law, but when the rust thickness increases the rate reduces, as ions have to diffuse through an increasing rust thickness for rust production to proceed. This phenomenon is introduced by considering a formula proposed by Liu and Weyers [41]. That formula gives unrealistic corrosion rates at the start of corrosion, hence the introduction of the combined rule [42]. Recent tests on rust layers have revealed that the inner layers are denser than outer layers [43]. To include the preceding, the following formula in Equation 2.10 is included [42];

$$\frac{dM_r}{dt} = \frac{k_p}{M_r^{n_1}} \rightarrow M_r = (n_1 \int k_p dt)^{1/n_1} \quad (\text{kg/m}) \quad 2.10)$$

Where:

$n_1 = 2$ , a coefficient for rust with uniform density across the thickness but increases towards 3 as the nonlinearity of the rust production versus time increases.

$k_p$  = the rate of metal loss, which may be expressed in terms of corrosion rate.

$M_r$  = the mass of rust products per unit length of anode (kg/m),

$t$  = the corrosion time in seconds

$k_p$  is dependent on  $n_1$ ; they decrease while  $n_1$  increases from 2 to 3. Values of  $k_p$  were back-calculated to reach agreement with published experimental data.

### **2.2.2 Corrosion in Reinforced concrete water conveyancing structures.**

Corrosion is the chemical or electrochemical reaction between a material, usually a metal, and its environment that produces a deterioration of the material and its properties. For corrosion of steel, oxygen and moisture are required for the electrochemical reaction to occur. Eliminating any one of these will prevent the chemical reactions and damage incurred due to corrosion.

Switching to expensive high-alloy steel is one way to prevent corrosion damage entirely. Although, high-alloy steel costs nearly ten times more than the hot rolled deformed reinforcing steel bars, it would increase initial production costs of a project. However, the costs associated with regular inspection and repairs in the long run are reduced, making it a cheaper and more durable alternative. Comparable to high-alloy steel, common reinforcing steel is more realistic for budgets and is already present in the majority of today's reinforced concrete water conveyancing structures. For this reason, rehabilitation of the structures has been the focus. As reinforced concrete water conveyancing structures age and concrete corrodes, engineers keep searching for cheaper, more effective ways to test progression corrosion and schedule rehabilitation.

In 2017, two corrosion detection systems were introduced to the market, one of which is mounted on a small skid-steer robot, the other of which is mounted in a cart that can be towed along a roadway. Both of these corrosion detection systems make use of machine learning

technology and do not require any sort of destructive intervention to gather results. The robot-mounted system utilizes ground penetrating radar and electrical resistivity sensors to locate any corrosion of steel or deteriorating concrete in bridges and structures. It is also fully autonomous and has proved to be faster and more accurate than human inspectors but has not been modelled for water conveyancing structures.

Zhu et al [44], designed a system to detect defects in concrete bridge decks. Her approach is an early-warning system for bridges based on acoustics. It has proven to be a more accurate alternative to other methods of identifying delamination, a gradual separation of concrete layers that can affect the structural integrity of a bridge or structure and can be caused by rebar corrosion. Her system also delivers much faster results than conventional testing methods allowing people to find delamination in a timelier manner and make the necessary repairs before the damage becomes too significant. This system has not been modelled for application in water conveyancing structures.

Corrosion results in the formation of rust that has two to six times the volume of the original steel [13] and none of the corrosion products has good mechanical properties. The great majority of reinforced concrete structures are built to guidelines given in international codes of practice and are in situations where they survive very long maintenance-free lives. However, concrete cannot be expected to give the desired, almost indefinite, protection to the steel reinforcement. This is because of the following circumstances:

- a) Where, because of error of construction, poor mix proportions, poor compaction among other errors, the full thickness of concrete cover is not given to the reinforcement.



(b) Where the concrete contains damaging amounts of chloride, either present in high concentration in the materials from which the concrete is made or added deliberately to accelerate setting.

(c) Where the concrete is exposed to sea water, to de-icing salts or to acid.

Table 2.1 shows salient features of some run of the river water infrastructure projects within the East African region.

**Table 2.1: Existing Small Hydro Power projects with salient features of conveyance structures (Source: Author)**

Project	Discharge	Low pressure section	High pressure flow
2.5MW Chemosit SHPP In Kericho County, Kenya	15m <sup>3</sup> /s	622m long RC canal 4m wide x 2.1 m high	9mm thick steel x 2.4m diameter x 92m long
2.6MW Kipsonoi SHPP in Bomet County, Kenya	5.4m <sup>3</sup> /s	6597m long RC canal, 3.6m x 2m (width x height)	9mm thick x 1.7m, 1.5m, 1m diameter Total length=460m
5.0 MW Gura SHPP in Nyeri County, Kenya	4.5m <sup>3</sup> /s	6828m long RC canal, 2.5m x 1.4 (width x height)	12mm thick x 1.9m diameter. Total length=376m
5.0MW Siti 1 SHPP in Chesower, Bukwo, Uganda.	2.86m <sup>3</sup> /s	240m long RC Canal 1.6m wide x 0.9m high. 1200mm diameter GRP, Length =2980m	688mm diameter GRP Penstock, Length 1900m
16.5MW Siti 2 SHPP in Tulel, Bukwo District, Uganda	4.3m <sup>3</sup> /s	2000 m long RC canal, 2.2m x 1.1m (width x height)	14mm thick x 80mm diameter steel Penstock, Length 1760 m

From Table 2.1, it can be noted that low pressure water conveyance structures are reinforced concrete structures for discharges over 3m<sup>3</sup>/s. This is because the technology to construct reinforced concrete canals is readily available while the alternative materials Glass Reinforced Plastics (GRP) pipes have to be imported. This makes reinforced concrete a preferred material for water conveyancing structures for discharges greater than 3.0m<sup>3</sup>/s.

### 2.3 Critical penetration depth of rust and its influence on the service life of reinforced concrete.

The development of corrosion in concrete over time is generally seen as a multi-stage process as shown in Fig.2.5[45]. The passage from passive corrosion state to an active state is known as the “depassivation” of the reinforcements. In the first period, aggressive substances such as chloride ions or carbon dioxide penetrate the cover and ultimately reach the steel, which causes the onset of corrosion (mark 1), called depassivation or corrosion initiation.

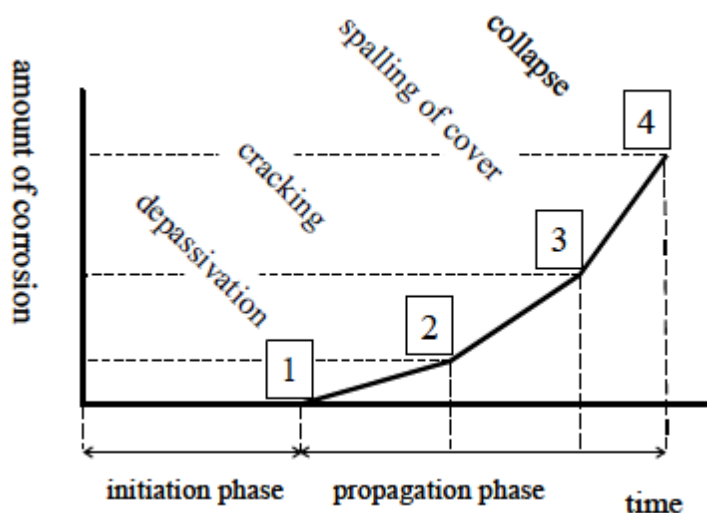


**Figure 2.5: Various stages in the development of reinforcement corrosion in concrete [45]**

Two main depassivation mechanisms are identified for reinforcements of concrete structures: the decrease in pH of the concrete interstitial solution linked to the penetration of atmospheric

CO<sub>2</sub> into the porosity of the concrete, and local damage to the passive layer in the presence of chlorides. While the action of carbon dioxide leads to global depassivation as there is indeed a destabilization of the passive layer due to the decrease in pH, the mechanism is not the same for the chloride action as the oxides and hydroxides present in the passive layer are not dissolved in the presence of chlorides [46]; here there are local failures in the passive film, which can nevertheless be referred to as local depassivation.

In the second stage, actual corrosion takes place (its rate depends on moisture and oxygen availability) and the expansion due to corrosion products being formed builds up tensile stresses in the concrete cover until it cracks (mark 2). This cracking produces the first visible signs of corrosion, although in some cases, rust stains at the concrete surface may show before cracking. In the next stage, expansion due to corrosion proceeds until parts of the concrete cover completely detach and spall off (mark3), constituting a potential danger for users of the structure or the general public. In the fourth and final stage, reinforcing bar diameter loss becomes so severe as to approach the minimum required for structural stability; eventually, collapse cannot be ruled out (mark 4). The period from  $t = 0$  until mark 1 is called the initiation stage. The period from mark 1 until mark 4 is generally called the propagation stage. Each of the marks can be seen as a limit state.

Corrosion of steel in concrete causes cracking of the concrete cover when the metal loss reaches a critical penetration depth [47]. The value of the critical penetration depth is important to formulate reliable models of the corrosion propagation stage. Knowledge of the critical rebar corrosion penetration needed for cracking along with a reliable estimate of the projected corrosion rate is crucial for the overall service life prediction for a corroding reinforced

concrete structure. Corrosion of steel in concrete is commonly localized in nature especially in high quality concrete structures.

Due to the harmful nature of corrosion, its development has been studied by many researchers. Chen and Leung [48], studied non uniform corrosion due to chloride penetration. In their study, the time-varying corrosion penetration around the rebar was first obtained by solving a diffusion equation numerically by Matlab. In their calculation, corrosion was assumed to initiate at a point when a specified chloride threshold value is reached at that position. They studied the effects of reinforcement cover thickness and the rate of corrosion on the non-uniformity of corrosion penetration.

Most current research work is focused on developing models for determining the critical penetration depth by assuming an approximately uniform distribution of corrosion along the length of rebar. Localized corrosion is commonly encountered in practice in high quality concrete structures due to the presence of preexisting narrow cracks in cover concrete, concrete joints or coating defects in epoxy-coated steel. Torres-Acosta and Sagüés [49], proposed a relationship whereby when corrosion is localized to a short length there is a greater amount of critical penetration depth compared to the case of more uniform corrosion. In their relationship of uniform corrosion based on experiments, Equation 2.11;

$$X_{crit}/mm \approx 0.011 \left( \frac{C}{d} \right) \left( \frac{C}{L} + 1 \right)^2 \quad 2.11)$$

Where;

C is the concrete cover depth(mm),

d is the rebar diameter(mm), and

L is the length of the uniformly corroding segment(mm).

For cases approximating uniform corrosion, Equation 2.12 can be simplified to:

$$X_{\text{crit}} = 11.0 \frac{C}{d} \quad 2.12)$$

For cover-bar diameter ratios between 2 and 3 the critical corrosion losses obtained from equation (2.12) are 22-33  $\mu\text{m}$  and 26-35  $\mu\text{m}$ , respectively. However, that investigation did not extend to small enough corroding lengths to ensure reasonable extrapolation to conditions representative of those typically encountered at the intersection of rebar with a preexisting narrow crack. Equation 2.11 is less conservative based on the both finite element and experimental results for corrosion loss greater than 50  $\mu\text{m}$  [50].

Darwin et al [51], proposed Equation 2.13, an alternative relationship based on experiments on damage results calculated by Faradaic conversion and not gravimetric measurements of epoxy-coated rebars with controlled areas of coating damage.

$$\frac{X_{\text{crit}}}{\mu\text{m}} = 45 \left( \frac{(C/25.4)^{2-A_f}}{d^{0.38} L_f^{0.1} A_f^{0.6}} + 0.2 \right) \cdot 3^{A_f-1} \quad 2.13)$$

Where;

$x_{\text{crit}}$  = Corrosion loss at crack initiation( $\mu\text{m}$ )

C= Concrete cover (mm)

d= bar diameter(mm)

$L_f$  = fractional corroding length relative to the entire bar

$A_f$  = fractional corroding area relative to that of the entire rebar.

The experimental findings however were based on corrosion damage results calculated solely by Faradaic conversion, and not confirmed by gravimetric measurements. Other factors including the tensile strength that may contribute to the critical penetration depth were not taken into account in Equation 2.13.

Concrete cover cracking is caused by accumulation of corrosion products at the steel concrete interface. As corrosion progresses, the corrosion products continue to accumulate and once it

fills up the concrete pores, radial and hoop stresses start to develop thereby generating expansive pressures on the surrounding concrete. The pressure builds up to levels that cause internal cracking around the bar and eventually leads to through cracking of the cover and spalling. Fig.2.6[52] shows the critical penetration depth indicating the amount of rebar radius loss needed to initiate cracking.

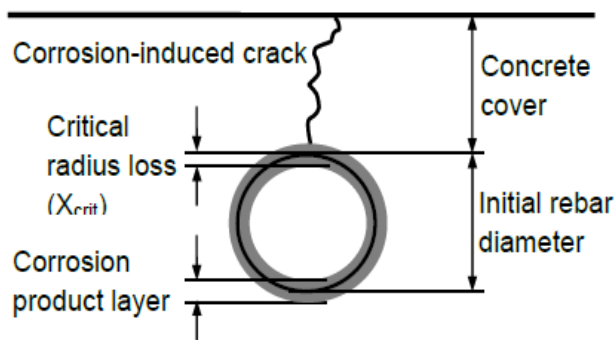


**Figure 2.6 A conceptual diagram for corrosion-induced cracking [52]**

Alonso et al. showed that the corrosion loss required to generate the first visible crack is linearly proportional to the cover-rebar diameter ratio ( $c/d$ ) in Equation 2.14:

$$x_{crit} = 7.53 + 9.32 \frac{c}{d} \quad (2.14)$$

where

$x_{crit}$  = corrosion loss at crack initiation in  $\mu\text{m}$

$c$  = concrete cover in mm

$d$  = bar diameter in mm

In Alonso's study, specimens with cover-bar diameter ratios ranging between 2 and 3 were used. Equation 2.14 is derived based on the assumption that general corrosion in steel will cause the concrete to crack, and in cases when corrosion is limited to small locations, such as

when corrosion occurs at damaged sites of epoxy-coated bars, cannot predict the critical corrosion loss.

Based on experimental studies, Rodriguez et al., [53] and Duracrete [54] evaluated the attack penetration  $x_o$  corresponding to crack initiation as shown in Equation 2.15;

$$x_{crit} = 83.8 + 7.4 \frac{c}{d} - 22.6 f'_t \quad (2.15)$$

Where

$x_{crit}$  = the attack penetration or the decrease in the reinforcing bar radius ( $\mu\text{m}$ ),

$c/d$  = the cover/diameter ratio and

$f'_t$  = the concrete tensile strength ( $\text{N}/\text{mm}^2$ )

The surface crack width evolution with increasing corrosion level was examined for both non-uniform and uniform corrosion cases with different cover thicknesses. It was found that cover cracking is more severe for non-uniform corrosion than uniform corrosion under similar percentage of steel loss and for larger cover thickness, the initiation of surface cracking is delayed, but its width becomes larger for the same amount of steel loss after surface cracking [55].

Xu and Shayan [56] considered the combination of concrete cover and its embedded steel as a thick-wall concrete cylinder which surrounds the embedded steel, and the expansion of corroded steel exerting an internal pressure to the concrete cylinder. They derived Equation 2.16 for the attack penetration depth  $x_{crit}$ ;

$$x_{crit} = \frac{f_t(c+d)(1+\nu)}{E_{eff}d\beta} \quad (2.16)$$

Where,

$x_{crit}$  = Corrosion loss at crack initiation ( $\mu\text{m}$ )

C = Concrete cover (mm)

$d$  = bar diameter(mm)

$f_t$  = Concrete tensile strength (N/mm<sup>2</sup>)

$\nu$  =concrete poisson's ratio

$\beta$  = Relative volume change due to conversion of steel to rust =  $(\Delta V/V)$

$E_{\text{eff}}$  =effective elastic modulus= $E/(1+\phi)$  (N/mm<sup>2</sup>)

$E$  =Elastic modulus (N/mm<sup>2</sup>)

$\phi$  = concrete creep coefficient

From their model, the predicted critical corrosion loss was found to be four times or greater as much as the calculated values based on the measured corrosion rates from Linear Polarization Resistance (LPR) test in their research. This is because in calculating corrosion loss from the LPR test, it is assumed that the whole surface area subjected to corrosion is corroding. This is not true for non-uniform corrosion and therefore the calculated corrosion loss from LPR tests should be modified based on the actual corroded area of the embedded steel to present the real values.

Chen et al [57] studied pitting and weight loss of carbon steel due to corrosion caused by a sulfate reducing bacteria culture. The study was done in reactors with constant bubbling of nitrogen to ensure the anoxic condition, over a 40-day period after the organic substrate had been exhausted. The extents of pitting corrosion on the polished and unpolished sides of the carbon steel were also compared to investigate the effect of roughness. It was found that the sulfate reducing bacteria surviving through the 40-day starvation of an organic energy source, caused severe pitting corrosion with a maximum pit depth of 46  $\mu\text{m}$ . On the rougher surface the pitting initiated earlier and reached a much higher pit density. This finding is helpful in understanding of sulfate reducing bacteria activities in corrosion environments.



Andrade et al. [58,59], Troconis De Rincón et al. [60] and Castro-Borges et al. [61-63] reported cumulative corrosion rate as a useful tool to know details of initiation and propagation periods. The information reported by these authors contains useful information of cumulative corrosion and its interpretation in both natural and accelerated tests.

Concrete resistivity is an important parameter for describing the rate of corrosion of reinforced concrete structures. Alonso et al. [64] monitored the corrosion rate and simultaneous electrical resistance values of reinforcing bars embedded in mortars made with six different types of cements, and exposed to varying moisture conditions. They noted that electrical resistivity appeared to be the factor controlling the maximum corrosion rate in aerated specimens. Morris et al. [65] aimed at establishing a corrosion evaluation criterion based on concrete electrical resistivity measurements. They noted that the concrete resistivity can be used as a parameter to evaluate the risk of rebar corrosion regardless of the mix design and environmental exposure conditions. The volumetric development of corrosion on reinforcing bars affects the service life of reinforced concrete, hence the need to establish the rate of corrosion.

#### **2.4 Use of corrosion inhibitors and anticorrosion coatings as methods of preventing corrosion.**

The adequate performance of reinforced concrete structures is a function of its durability against the aggressive elements in the environment. A thorough knowledge of these aggressive elements and their mechanism of attack of concrete structures are very important [66]. Corrosion protection methods focus on delaying the initiation period as it is easier to control than propagation of corrosion. A lot of research has been done on various techniques towards corrosion control.

#### **2.4.1 Design consideration**

Design plays a major role in controlling deterioration of concrete structures and this is done in reference to updated international codes of practice. Improper design can accelerate the rate of corrosion. Design for corrosion control in rebar can be achieved by appropriate applications of mix designs, curing, concrete thickness cover and incorporation of corrosion inhibitors. [67,68].

#### **2.4.2 Use of alternative materials**

Many researchers have investigated corrosion problems in reinforcement with the aim of its complete eradication. One of the materials that favorably resists corrosion is stainless steel, which has a greater corrosion resistance than the hot rolled deformed steel bars [69], as alternative to carbon steel. Stainless steel is a corrosion resistance iron alloy that contains about 10.5% chromium. Its corrosion resistance is attributed to the presence of chromium which form passive film layer when exposed to oxygen which aids corrosion resistance. The high cost of stainless steel makes it the last alternative.

#### **2.4.3 Use of corrosion inhibitors**

A corrosion inhibitor is a chemical substance added to Ordinary Portland Cement concrete mixes during batching in a required amount to supplement the concrete's natural ability to protect the embedded steel by preventing or reducing the corrosion rate. Corrosion inhibitors are often used in low permeability concrete and they have the effect of increasing the chloride threshold needed to initiate corrosion. Corrosion inhibitors, organic or inorganic, work as either anodic, cathodic or mixed inhibitors [70,71] by adsorbing themselves on the metallic surface by forming a film layer on the surface. The use of corrosion inhibitors for corrosion control for improvement of concrete performance has increased in the recent years.

Some of the common anodic, inorganic inhibitors that have been used in concrete structures include calcium nitrite, sodium nitrite and Sodium tungstate. These inhibitors have the capacity to inhibit initiate pitting corrosion and their efficiencies increase considerably with increase in dosage [72-77]. Some inorganic inhibitors delay pitting initiation without any detrimental effect on the concrete [78-83]. Monte et al [84] revealed that calcium nitrite is detrimental to concrete properties. The inhibiting effect of calcium nitrite from reinforcement corrosion is not obvious and sometimes speeds up the macro-cell corrosion when critical value of  $n(\text{NO}_2^-)/n(\text{Cl}^-)$  in reinforced concrete is less than 0.4[85].

The organic acid inhibitor that contains oxygen, nitrogen and/or sulfur is adsorbed on the metallic surface blocking the active corrosion sites. Although the most effective and efficient organic inhibitors are compounds that have pi-bonds (bonds from the side-side overlap between two dumbbell-shaped electron cloud with the nucleus between the two lobes), it presents biological toxicity and environmental harmful characteristics. [86]. The metal surface covered by an inhibitor is proportional to the inhibitor concentrates, the concentrations of the inhibitor in the medium is critical. [87,88]. Some examples are amines, urea, Mercaptobenzothiazole (MBT), benzotriazole etoliotriazol, aldehydes, heterocyclic nitrogen compounds, sulfur-containing compounds and acetylenic compounds and also ascorbic acid, succinic acid, tryptamine, caffeine and extracts of natural substances [89,90]. There are still some inhibitors that act in vapor phase (volatile corrosion inhibitor). Some examples are: dicioexilamônio benzoate, diisopropylammonium nitrite or benzoate, etha- nolamine benzoate or carbonate and also the combination of urea and sodium nitrite [91-95]. The total chemical composition of a majority of commercial inhibitors is not unveiled to the public, the only revelation is the inhibiting chemical [96].

Samiento-Bustos et al. [97] investigated the effect of Lithium Nitrate ( $\text{LiNO}_3$ ), Lithium Chromate ( $\text{Li}_2\text{CrO}_4$ ) and Lithium Molybdate ( $\text{Li}_2\text{MoO}_4$ ) inorganic inhibitors on the corrosion performance of 1018 carbon steel in the Lithium bromide + ethylene glycol + water. It was found that the inhibitor efficiency increases with the inhibitor concentration except for chromates where the highest efficiency was reached with 20 ppm of inhibitor. According to Skotinck [98] and Slater [99], under long-term accelerated testing, calcium nitrite is of a better quality in terms of strength of concrete.

De Schutter and Luo [100], reported that calcium nitrite inhibitor increases the early age compressive strength of concrete. They concluded that the effect on the ultimate strength seems to depend on the amount of inhibitor added to the concrete. A calcium nitrite-based corrosion inhibitor increases somewhat the air content as well as the workability of the fresh concrete.

According to Kondratova et al. [101], the addition of calcium nitrite influences the hydration process of cement paste, but calcium nitrite accelerates and stabilizes the formation of the crystal phase of calcium hydroxide which leads to an increase in the micropore diameter in the hardened cement paste increasing chloride permeability compared to concrete without inhibitor. Calcium nitrite can also decrease the resistivity of concrete and also tends to increase concrete chloride permeability values.

According to Tritthart and Banfill [102], all the sources of chloride must be analyzed for the concrete in question and a threshold free nitrite concentration needs to be achieved such that the chloride/nitrite ratio remains below 1.5. Organic corrosion inhibitors assume a great significance due to their application in preventing corrosion under various corrosive environments. The organic corrosion inhibitor development is based on organic compounds containing nitrogen, oxygen, sulfur atoms and multiple bonds in the molecules that facilitate

adsorption on the metal surface [103]. Further, corrosion inhibition efficiency of organic compounds is related to their adsorption properties and the nature and the state of the metal surface on the type of corrosive medium and on the chemical structure of the inhibitor.

Ormellese et al. [104] researched 80 organic substances to be used as inhibitors. He grouped the inhibitors as primary and tertiary amines and alkanolamines, aminoacids, mono and polycarboxylates. Amines and alkanolamines are used as constituents in commercial products due to their high water solubility and their negligible influence on properties of both fresh and hardened concrete.

El- Azhar et al. [105]; Tritthart, [106]; Gaidis, [107]; Baddini et al. [108]; Ali et al., [109]; Gece, [110]; Hong, [111]; Noor and Al-Moubaraki, [112]; Saliyan et al., [113]; Yildirim and Çetin, [114] Obot et al., [115] researched on N-heterocyclic organic compounds and their derivatives. The organic compounds used were confirmed satisfactorily good for corrosion inhibition of mild steel in acids and chloride media based on the adsorption of the molecules on the metallic surface and follows Langmuir isotherm adsorption model. But they were unable to investigate their effects on concrete properties.

Benzina et al. [116] investigated the use of benzotrazole as corrosion inhibitor for carbon steel in simulated pore solution. They concluded that the addition of benzotrazole into a simulated chloride-contaminated pore solution caused a significant increase in the corrosion resistance of the carbon steel. The improvement of corrosion resistance by benzotrazole (1.5 % by weight) addition was superior to that associated to the addition of nitrite (1.5% by weight) to the electrolyte suggesting that benzotrazole is a potentially attractive alternative to nitrites for inhibiting corrosion of steel reinforcement in concrete.

Sawada et al. [117] and Kubo et al. [118] electrochemically injected ethanolamine and guanidine organic inhibitors into saturated specimens of carbonated and non-carbonated concrete from external electrolytes under the influence of an electrical field applied between embedded steel cathodes and external anodes. From their research;

- i) Ethanolamine and guanidine were both capable of being effectively injected into carbonated reinforced concrete of the sort investigated by means of relatively short-term electrochemical treatments of the type applied.
- ii) The cathodic current densities and electrochemical treatment durations required to cause substantial penetration of the aforementioned corrosion inhibitors through carbonated concrete cover of w/c of 0.86 and thickness 35 mm were of similar magnitudes to those typically employed for electrochemical realkalisation of carbonated concrete. Accumulation of high concentrations of the two corrosion inhibitors in carbonated concrete at the level of the embedded steel (in the case of guanidine) and in the cover zone a few millimeters from the embedded steel (in the case of ethanolamine), occurred as a result of electrochemical treatments of the type applied.
- iii) The inhibitor penetration profiles observed in carbonated concrete were explicable in terms of the degrees of ionization of ethanolamine (pKa 9.5) and guanidine (pKa 13.6) in carbonated concrete which has a pore solution pH value  $< 9.5$  except in the vicinity of the steel cathode where much higher pH values are expected to occur
- iv) Electrochemical treatments applied to non-carbonated concrete of the type studied which had a w/c of 0.65 and a pore solution pH value  $> 13$  were far less effective in causing injection of the corrosion inhibitors than those applied to carbonated concrete
- v) In the case of ethanolamine, it is thought that the low degree of ionization of the inhibitor in the alkaline pore solution phase of non-carbonated concrete prevented significant

migration of the inhibitor under an applied field. Similar considerations would presumably apply also to other organic base inhibitors with pKa values = 13.

- vi) In the case of guanidine, although penetration of the inhibitor was significantly enhanced by an applied field indicating that the higher pKa value allowed migration to occur, the application of a cathodic current density of  $5\text{A/m}^2$  for 2 weeks did not prove sufficient to cause the inhibitor to reach the steel cathode at a cover depth of 35 mm. Further work is therefore needed to assess whether the electrochemical injection of guanidine, or similar relatively strong organic base inhibitors, into noncarbonated concrete can be induced over conveniently short timescales for practical applications

The effect of alkanolamine and water based inorganic inhibitors on the corrosion of steel reinforcements in concrete was evaluated by using anodic polarization, electron spectroscopy for chemical analysis and Auger electron spectroscopy by Servicemen et al. [119]. Their results indicated that the time-to-cracking in uncontaminated concrete specimens incorporating inhibitors alkanolamine and water based inorganic was higher than that in the control concrete specimens.

The long-term stability and performance, the effect on corrosion propagation after initiation and the effect on the physical properties of concrete over the service life of the structure of corrosion inhibitors are a major concern. For a corrosion inhibitor to be effective as a long-term corrosion protective strategy, it must be intact and physically present. The amount of dosage of a corrosion inhibitor has an effect on corrosion progression, an insufficient amount will have an effect on chloride transport and can reduce the rate of chloride ion migration. An effective corrosion inhibitor should not have any negative effect on the properties of concrete.

### **2.4.3 Corrosion inhibitors in the Kenyan market**

Majority of corrosion inhibitor producers withhold the chemical composition details of their products and give only general information.

#### **a) MasterLife CNI**

This is a calcium nitrite or nitrate based corrosion inhibitor admixture that contains 30% active ingredients by mass for the nitrite and 3-7% nitrate. Calcium nitrite was pioneered in Japan and became available in the 1970s as a stable solution and found immediate use as an accelerator. Calcium nitrite chemically reacts with the reinforcing steel by repassivating the steel surface, which continues to provide a corrosion barrier against chloride ion attacks. The chemical reaction that occurs between the nitrite ions and ferrous ions creates a more stable form of ferric ions that are less susceptible to corrosion [120].

The ferric ions enhance the passivation layer around the steel surface so much so that calcium nitrite type admixtures are also called anodic inhibitors [121]. However, the nitrite ions must compete with the amount of chloride ions present within the concrete in reaction with the ferrous ions in order to be effective as a corrosion inhibitor [122]. Sufficient quantities of the calcium nitrite based admixtures must be added in comparison with the anticipated chloride ion content that may exist in order to maintain control of the corrosion process within the concrete matrix.

Calcium nitrite will prevent pitting corrosion of steel reinforcement in concrete where the  $\text{Cl}^-/\text{NO}_2^-$  concentration ratio in the pore fluid is up to 0.9 and  $\text{Cl}^-/\text{OH}^-$  ratios are in the range 0.27–0.57[123,124]. According to studies carried out by Hausmann [125], for  $\text{Cl}/\text{OH}$  molar ratios higher than 0.6, the passivating film becomes permeable or unstable, thus leaving the steel reinforcement unprotected against corrosion. There is also evidence to show that



the admixture is effective in protecting the steel in carbonated or cracked concrete where crack widths are  $< 0.2$  mm at the surface but other studies [126] have shown that calcium nitrite does not perform well in cracked concrete.

According to Ryu et al. [123], greater care is needed in estimating the quantity of calcium nitrite based inhibitors to be used, because if the amount is less than necessary, it will have a negative impact on both the concrete and steel. Thus, it is of utmost importance to define the optimal amount to be added for the inhibitor work properly.

Despite their efficiency in reducing the corrosion rate of concrete structure reinforcement, nitrites are carcinogenic and toxic [124] and banned in several European countries, such as Germany and Switzerland [123]. Because of this, alternative inhibitors are being studied. Among other inorganic inhibitors are sodium monofluorophosphate ( $\text{Na}_2\text{PO}_3\text{F}$ ) and red mud.

Calcium nitrate,  $\text{Ca}(\text{NO}_3)_2$ , works as a retarder against chloride induced corrosion of concrete reinforcement just like calcium nitrite,  $\text{Ca}(\text{NO}_2)_2$ . The kinetics for the nitrate reaction is slower for nitrite, but this is only relevant for rapid tests since rebar corrosion in practice is a rather slow process. Calcium nitrate offers a larger buffer than does calcium nitrite. It is also cheaper, less harmful and more available. Between 2 - 4 % calcium nitrate of cement weight is sufficient to protect the rebar against chloride-induced corrosion.

#### **b) MasterLife CI 222**

This organic corrosion-inhibiting admixture is a product of BASF Construction Chemicals that provides two different mechanisms of corrosion protection. It contains 10-30% by weight of Monoethanolamine as the main ingredient. The first mechanism of protection that is provided by this admixture is a waterproofing type inhibition within the concrete matrix.

The rate of chloride and moisture penetration into the concrete is reduced due to the admixture lining the pores of the concrete matrix creating a barrier against these components needed for the corrosion process.

The second mechanism of corrosion protection that organic based corrosion inhibiting admixtures offer is that of creating a protective film around the reinforcing steel. Unlike other admixtures that simply repassivates the concrete matrix around the reinforcing steel, MasterLife CI 222 provides a secondary corrosion protection by adsorbing onto the steel. This adsorption onto the steel creates a protective film and further slows the penetrations of chlorides, moisture, and oxygen that would react with the steel in the corrosion process.

MasterLife CI 222, being an organic based corrosion inhibitor, does not have to compete against chloride ion concentrations within the concrete as other corrosion inhibiting admixtures such as calcium nitrite based admixtures [126].

### **c) Ferrogard 901**

Ferrogard 901 is a blend of surfactants and amine salts in a water medium produced by Sika Corporation and is recommended for use in corrosive environments. It contains 5-10% by weight of 2-dimethylaminoethanol (DMEA) as the main active ingredient. This inhibitor has a dual action corrosion inhibitor. Firstly, a physical formation of a barrier against chloride ions and other similar substances. The second active mechanism is by the adsorption of Ferrogard 901 onto the reinforcing steel surface due to the high vapor pressure of the product. Due to this bond between Ferrogard 901 and the reinforcing steel, the chloride ions are displaced from the metal surface, which in turn provides protection against chloride induced corrosion.

#### **d) Dimethylathanolamine organic inhibitor**

This inhibitor has 90% dimethylathanolamine (DMEA) [127] while the rest is composed of carboxylic acids (mainly benzoic acid). DMEA provides protection on steel by forming an adsorption layer on the steel surface, hindering steel dissolution [128]. DMEA inhibits corrosion through mechanism whereby DMEA displaces chloride ions and forms a durable passivating film. Table 2.2 shows the properties of the Dimethylathanolamine based organic inhibitor as shown in the manufacturers data sheet.

**Table 2.2: Properties of the Dimethylathanolamine based organic inhibitor**

Property	Value
pH Value	10 ± 1
Chloride Content	> 0.1 %
Specific Gravity	1.06 kg/L
VOC Content	21.2 g/L

#### **e) Fly Ash**

Fly ash is a coal combustion product and third as the most abundant nonfuel mineral resources [129]. It is created from the by-products of the combustion of ground or powdered coal removed from electric power generating plant exhaust gases. Fly ash is primarily silicate glass containing silica, alumina, iron, calcium and other minor ingredients including magnesium, sulfur, sodium, potassium, and carbon [130]. Fly ash admixtures improves workability, reduced segregation, bleeding, heat evolution and permeability, inhibits alkali-aggregate reaction, and enhanced sulfate resistance [131].

The use of fly ash (Class C and Class F) in concrete offers several significant advantages. These include:

- i. Reduced permeability

- ii. Reduced water/cement ratio
- iii. Reduced concrete segregation
- iv. Reduced bleeding
- v. Increased workability/ plasticity
- vi. Increased flexural and compressive strength
- vii. Increases pumpability
- viii. Reduced heat of hydration
- ix. Cost savings to the user
- x. Increased sulfate resistance
- xi. Improved freeze-thaw durability
- xii. Reduced volume changes: dry shrinkage
- xiii. Better finishability
- xiv. Reduced expansion due to ASR
- xv. Improved hot weather handling characteristics
- xvi. Reduced corrosion damage

In a well-hydrated concrete mix, the Portland cement may contain up to 15 – 40 percent calcium hydroxide by weight of cement. This is usually adequate to maintain the pH at 12 – 13. Because fly ash improves the density of concrete along with other beneficial factors, it more than compensates for the slightly lower pH.

During the cement hydration process, 15 to 40 percent of the cement does not hydrate. This unhydrated cement or calcium hydroxide (CH) is detrimental to concrete because it aides in the premature deterioration of concrete. Chemically, calcium hydroxide will react with sulfates, alkali silica and CO<sub>2</sub> to deteriorate concrete. Thus, the goal of the designer of the concrete mix is to chemically change this calcium hydroxide and maximize CSH (Calcium Silicate

Hydroxide) while maintaining the pH. If we examine a simple 25% replacement, one would be removing a very small portion of the calcium hydroxide. The pozzolanic reaction in fly ash converts the CH into more of the CSH<sup>-</sup> thus leading to reduced permeability. With the use of fly ash, the ingress of moisture, oxygen, chlorides, and aggressive chemicals are slowed significantly - thus improving durability and serviceability. It should be noted that after twenty years of curing, it is not uncommon to see fly ash concrete have a chloride diffusion coefficient 100 times less than a control Portland cement concrete [132]. Thus, fly ash can improve durability against alkali attack, sulfate attack, chloride ingress, CO<sub>2</sub> and corrosion.

#### **2.4.4 Efficiency of corrosion inhibitors**

The efficiency of organic corrosion inhibitors is related to the presence of polar functional groups with S, O or N atoms in the molecule, heterocyclic compounds ( $\sigma$ ) and pi ( $\pi$ ) electrons and generally have hydrophilic or hydrophobic parts ionizable [132,133].

The efficiency of an organic inhibitor depends of the following factors:

- i) chemical structure, like the size of the organic molecule;
- ii) aromaticity and/or conjugated bonding, as the carbon chain length type and number of bonding atoms or groups in the molecule (either  $\pi$  or  $\sigma$ );
- iii) nature and the charges of the metal surface of adsorption mode like bonding strength to metal substrate;
- iv) ability for a layer to become compact or cross-linked,
- v) capability to form a complex with the atom as a solid within the metal lattice;
- vi) type of the electrolyte solution like adequate solubility in the environment.

#### **2.4.5 Factors influencing inhibitor choice**

Given the variety of available inhibitors, choosing the appropriate inhibitor should be based on

the physical-chemical properties of the inhibitor, as well as the nature and conditions of the metal surface and the aggressive environment in which the concrete structure is situated.

This research used a calcium nitrite and nitrate based inhibitor, a dimethylathanolamine based organic inhibitor and fly ash and compared their effect on bond strength of reinforced concrete.

## **2.5 Coating of ribbed bars as a method of corrosion prevention**

Reinforcing steel bars are subjected to various severe environments before being placed in concrete and in service while embedded in concrete. Coated bars are subjected to damage or abrasion during fabrication, transportation, handling, installation and concrete placement. The coated bars are exposed to condensation temperatures from rain during placement and a variation with time of the pH after placement of concrete. At all these times the coating must be stable and defect free. Various coating strategies have been employed in ribbed bars, including epoxy coating, zinc coating and galvanizing.

### **a) Epoxy Coating**

Epoxy coating of reinforcing steel is adapted from the method used by utility companies for coating pipes in the petroleum industry and is one of the most widely used method of corrosion prevention. It was first used in the USA and Japan as protection of decks of highway structures from deicing salts but has now spread to other structures and countries. Currently there are updated international standards that can be referred to in application of epoxy coating to steel.

#### **i) Methods of epoxy coating**

Epoxy can be applied in liquid or powder form. The powder form of application is done by electrostatic spraying of the whole length of the bar and has a better efficiency in corrosion protection and accounts for majority of coated bars in the market. In its application the bar is first cleaned by blasting with grit to a near-white finish to remove millscale, rust and contaminates. The bar is then heated to the temperature required for the application of the epoxy

powder, typically 230°C, and passed through an electrostatic spray that applies charged, dry epoxy powder to the steel. The epoxy melts, flows and cures on the bars, which then are quenched, usually with a water spray bath.

**ii) Mode of action of epoxy coating**

Epoxy coating act as a barrier against the corrosive environment. The thickness should be between 130 microns-300 microns to fulfill the requirement of flexibility, bonding and corrosion protection [134]. The coating must be free of pores, cracks and damage to prevent aggressive agents from penetrating.

**iii) Epoxy Properties of coating**

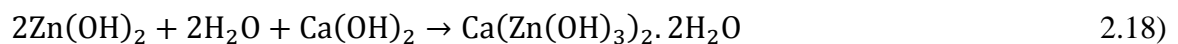
Epoxy resins have a high ductility, good abrasion resistance, good heat resistance, small shrinkage in polymerization and if a metal surface is sufficiently preheated an outstanding adhesion. They also exhibit good durability to solvents, chemicals and water.

**b) Zinc coating**

Zinc coatings can protect the underlying steel by acting as a barrier against oxygen, moisture, and chloride ions. Zinc provides protection by serving as a sacrificial anode. For concrete with pH between 11 and 12.3 isolated crystals of ZnO and  $\epsilon$ -Zn(OH)<sub>2</sub> will form due to localized corrosion of zinc [135]. In concrete with pH between 12.2 and 13.3, zinc reacts with water of alkaline pore solution to form zinc hydroxide and hydrogen gas as shown in Equation 2.17;



Zinc hydroxide then reacts with calcium ions in the pore solution to form calcium hydroxyzincate in Equation 2.18 [130];



For environments with pH above 12.2 calcium hydroxyzincate produces small compact crystals, which in turn, forms a stable passive layer on the surface of the bar. With increase of

pH, crystals become larger and due to the formation of tiny gaps in between, they are not able to seal the surface completely. For environments with pH above 13.3, calcium hydroxyzincate produces large isolated crystals that cannot seal the surface at all, and are not able to protect the underlying layer against corrosion [136]. Hydrogen gas produced in equation 7 can increase the permeability of the surrounding concrete. ASTM A767 requires galvanized bars to be submerged in a chromate bath after coating to passivate the zinc surface and prevent reaction of hydroxide ions in fresh concrete with zinc [137]. This passive layer can be broken down with the presence of chlorides in a manner similar to that of iron. Concrete carbonation also can destroy the passive layer of calcium hydroxyzincate and form amorphous products of  $ZnCO_3$  and  $Zn_5(CO_3)_2(OH)_6$ , which have limited passivating properties [138]. This carbonation process, however, lowers the critical chloride threshold of the galvanized bar in concrete [138].

A zinc layer is flexible and compressible, will not crack or be damaged by bending the rebars and offers a good adhesion to the concrete. The drying time of zinc coat before the contact with the concrete is very short (approx. 1 hour). As soon as the zinc coat is touch dry, the concrete can be cast. From the moment that the fresh concrete encapsulates the reinforcing steel protected by a zinc layer, some oxidation of the zinc layer will occur (due to the pH of the fresh concrete), which will have the following consequences [139]:

- i. Zinc salts are formed on the surface of the coating. These will seal off the zinc layer completely, thus providing an additional barrier protection.
- ii. The zinc salts will roughen the zinc coat surface. This will provide an even better adhesion for the concrete.

In 2006 the Steel Authority of India made a comparison between uncoated steel rebars, fusion bonded epoxy coated rebars (FBEC), hot-dip galvanized rebars (HDG) and zinc coated rebars.



The corrosion rate per year was measured after immersion and salt spray. This test demonstrated several advantages of zinc coating; the greater degree of galvanic protection, the lower sacrificial zinc consumption due to the dispersion of zinc dust in the binder and the additional barrier protection created by the binder [140].

In 2006 at Jadavpur University a comparison was made between uncoated steel (Mild steel and Stainless steel) rebars, fusion bonded epoxy coated rebars (FBEC), hot-dip galvanized rebars (HDG) and zinc coated rebars. The salt spray test pointed out that the zinc sprayed rebars have a corrosion resistance that is about 2 times higher than that of hot dip galvanized rebars. Zinc coating is also least susceptible for stress corrosion cracking [140].

### **c) Galvanized Rebars**

This is protecting the rebar itself by hot dip galvanizing. Hot dip galvanized coatings form an impervious metallic zinc and zinc alloy barrier around the steel that isolates the steel surface from the surrounding concrete. Galvanized rebar offers many advantages over conventional unprotected rebar. The corrosion protection afforded by galvanized rebar in concrete is due to a combination of beneficial effects. Of primary importance is the substantially higher chloride threshold 2-4 times (Fig.2.7) [141] for zinc coatings to start corroding compared to uncoated steel. In addition, zinc has a much greater pH passivation range than steel, making galvanized rebar resistant to the pH lowering effects of carbonation as the concrete ages. Even when the zinc coating does start to corrode, its corrosion rate is considerably less than that of uncoated steel.

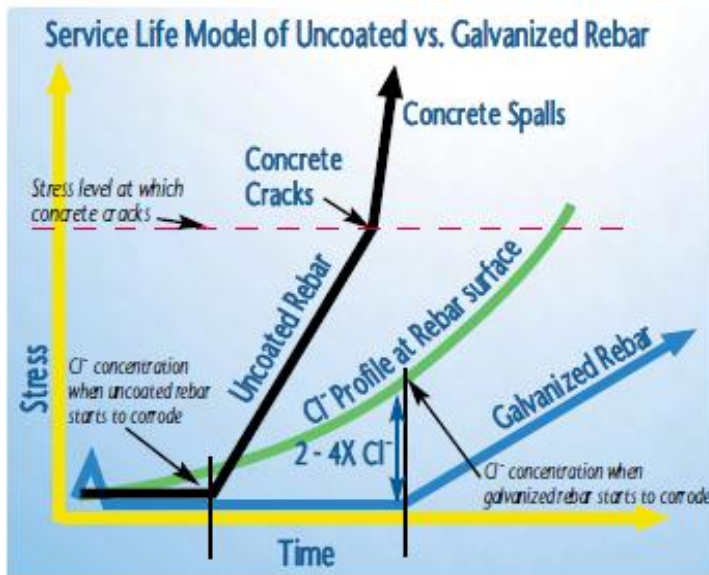


**Figure 2.7 corrosion threshold of uncoated and galvanized steel [141]**

Once corrosion of the zinc coating does occur, the properties of the corrosion products and their ability to migrate into the concrete matrix reduces stress generation in the surrounding concrete, further extending the life of the reinforced concrete structure.

### 2.6 Modelling of corrosion in reinforced concrete

Although most of the research on chloride-induced corrosion has been on chloride ingress into concrete, there has been an increasing effort in recent years to quantify the progressive damage in reinforced concrete due to the advancement of steel reinforcement corrosion [142]. The new effort is of great relevance in the structural assessment of deteriorated reinforced concrete water conveyancing structures with corroded reinforcement. The quantified damage due to reinforcement corrosion must be included in estimations of the service life.

Employing Faraday's law, the rate of corrosion can be expressed (Equation 2.19) as the loss of metal per unit of surface area per unit of time;

$$\text{Corrosion rate (V}_{\text{corr}}) = \frac{dr_t}{dt} = \frac{i_{\text{corr}}}{nF} \quad (2.19)$$

Where:

$$i_{\text{corr}} = \text{corrosion current density } \left( \frac{\text{A}}{\text{m}^2} \right)$$

$$F = \text{Faraday constant } \left( 96494 \frac{\text{C}}{\text{mol.e}^-} \text{ or } \frac{\text{A.s}}{\text{mol.e}^-} \right)$$

$n =$  electrons per mole of iron

$$\frac{dr_t}{dt} = \text{reinforcement radius loss with time } \left( \frac{\text{mm}}{\text{year}} \right)$$

$$\begin{aligned} \frac{dr_t}{dt} &= \frac{1.10^{-6} \left( \frac{\text{A}}{\text{cm}^2} \right) \cdot 55.85 \left( \frac{\text{g}}{\text{mol Fe}} \right) \cdot 86400 \left( \frac{\text{s}}{\text{day}} \right) \cdot \frac{1}{7.86} \left( \frac{\text{cm}^3}{\text{g}} \right) \cdot 365 \left( \frac{\text{day}}{\text{year}} \right)}{2 \cdot \left( \frac{\text{mol.e}^-}{\text{mol Fe}} \right) \cdot 96494 \left( \frac{\text{A.s}}{\text{mol e}^-} \right)} \\ &= 0.0116 \left( \frac{\text{mm}}{\text{year}} \right) \end{aligned}$$

Thus

$$\frac{dr_t}{dt} = 0.0116 i_{\text{corr}} \left( \frac{\text{mm}}{\text{year}} \right) \quad 2.20)$$

The corrosion current density,  $i_{\text{corr}}$ , should be expressed with the unit  $\mu\text{A}/\text{cm}^2$  which is the typical unit used in accelerated corrosion tests. Assuming that the corrosion rate (or corrosion current density) is time invariant, Equation 2.21 can be used to evaluate the remaining diameter of a rebar after  $t$  years of uniform corrosion.

$$d_t(t) = d_{\text{bo}} - 0.0116 \cdot i_{\text{corr}} \cdot t \quad 2.21)$$

Where  $d_t(t)$  = remaining bar diameter in mm and  $d_{\text{bo}}$  is the original bar diameter in mm.

The rate of corrosion ( $V_{\text{corr}}$ ) in reinforced concrete can be represented by the volumetric loss of the reinforcement bars by unit of area and unit of time and can be obtained from Equation 2.22 or 2.23[20].

$$V_{\text{corr}} (\text{mm/y}) = 0.0116 i_{\text{corr}} (\mu\text{A}/\text{cm}^2) \text{ for uniform corrosion current} \quad 2.22)$$

or

$$V_{\text{corr}} (\text{mm/y}) = 0.0116 I_{\text{corr}} (\mu\text{A}/\text{cm}^2) \text{ for non-uniform corrosion current} \quad 2.23)$$

Where:

$i_{\text{corr}}$  = the uniform corrosion current density

$I_{\text{corr}}$  = the non-uniform corrosion current density

Taking pitting or non-uniform corrosion into account Duracrete 2000[143] introduced a pitting factor,  $\alpha$  to Equation 2.23 and obtained Equation 2.24;

$$V_{\text{corr}} (\text{mm/y}) = 0.0116\alpha i_{\text{corr}} (\mu\text{A}/\text{cm}^2) \quad 2.24)$$

The formulation suggested by Stewart and Al-Harthy [144], expressed in Equation 2.25, was employed to calculate the reduced steel cross-sectional area. A pitting factor  $\alpha$ , defined as the ratio of the maximum pit depth to the corrosion penetration calculated based on uniform corrosion, is used to define the degree of pitting.

$$\alpha = P/P_{\text{avg}} \quad 2.25)$$

Where:

$\alpha$  = pitting factor

$P_{\text{avg}}$  = corrosion penetration calculated based on uniform corrosion

$P$  = Maximum pit depth

Due to the impossibility of direct visual observation of the morphology of corrosion,  $I_{\text{corr}}$  is the most feasible expression of the corrosion current when measuring in concrete [145] and therefore Equation 2.23 is preferred. For getting accurate corrosion rate, it is essential that the values of the corrosion current density are obtained in order to accurately predict the service lifespan of the reinforced concrete structures [146]. It is also necessary to accurately predict the corrosion rate if the damage prediction models are to be reliably used [147].  $I_{\text{corr}}$  is usually obtained through electrochemical measurement in an experiment [148]. The shortcomings of the electromechanical determination of  $I_{\text{corr}}$  include;

- i.  $I_{\text{corr}}$  is measured on the whole exposed area of the steel reinforcement; however, the corrosion is localized in a small zone.
- ii. The measured  $I_{\text{corr}}$  value is significantly affected by the galvanic current flowing

between the corroding and passive zones on the steel surface [149].

Due to the shortcomings of the electromechanical technique to measure  $I_{\text{corr}}$ , there is need to develop an accurate criterion for its measurement. The rate of reinforcement corrosion can also be calculated from the weight loss method in Equation 2.26[150].

$$V_{\text{corr}} (\text{mm/y}) = 87.6 \times (W / DAT) \quad 2.26)$$

Where W = weight loss of the reinforcement bar in milligrams

D = Reinforcement bar density in  $\text{g/cm}^3$

A = Surface area of the sample exposed to corrosion in  $\text{cm}^2$

T = time of exposure of the reinforcement bar in hours

The theoretical mass loss of steel resulting from the applied current was calculated based on Faraday's first law of electrolysis shown in Equation 2.27[151].

$$\Delta m_F = (M/n \times F) \times I \times t \quad 2.27)$$

Where:

$(M/n \times F)$  = the electrochemical equivalence of the iron substance

M = the molar mass of iron ( $M=55.847 \text{ g/mol}$ ),

n = the effective valence of the iron ions dissolving ( $n=2$ ) and

F = Faraday's constant which is made up of the product of the electron charge by the Avogadro's number ( $F=96485 \text{ C/equivalent}$ ).

$(I.t)$  = the electric charge,

I = the applied anodic current in amperes

t = the time in seconds during which the current has been passed through the circuit.

$$\text{Current Efficiency} = \Delta m_F / W \quad 2.28)$$

Equation 2.28 is useful in checking the efficiency of the rate of corrosion by the weight loss method.

## 2.7 Corrosion Kinematics

### 2.7.1 Introduction to Corrosion kinematics

The electrochemical process that underlies corrosion of steel reinforcement in concrete involves two chemical reactions. The anodic reaction which is iron oxidation, described by Equation 2.29. Iron ions ( $\text{Fe}^{2+}$ ) dissolve into the pore solution with electrons left inside the steel bar. These electrons are consumed by a cathodic reaction, i.e., an oxygen reduction producing hydroxides according to Equation 2.30.

Anodic reaction:



Cathodic reaction



Both the anodic and cathodic reactions occur along the surface of the steel electrode. Additionally, an ionic current of hydroxide ions flows through the surrounding electrolyte from the cathodic to the anodic areas, balanced by an electric current through the steel, as shown in Fig. 2.8[152]. The anode hydroxide ions and  $\text{Fe}^{2+}$  ions form ferrous hydroxide, the primary corrosion product, which undergoes further oxidation, becoming black rust or brown rust depending on the amount of oxygen available.

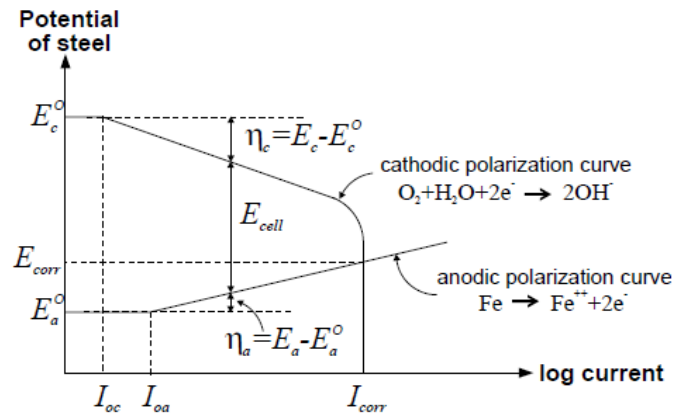


**Figure 2.8: Evans diagram for the anodic and cathodic processes taking place on the reinforcing steel surface. [152]**

### 2.7.2 Reinforcement corrosion

Assuming an electric charge and isotropic conductivity, the electric potential distribution is described by Laplace's Equation 2.31 whose solution can only be derived with prescribed geometries and boundary conditions.;

$$\nabla^2 E = 0 \tag{2.31}$$

Where  $\nabla^2$  is the Hamilton operator

E is the Electric potential

The current density at any location of the steel surface can also be determined by Ohm's law from Equation 2.31.

$$i_{corr.} = \frac{1}{\rho_{el}} \frac{\partial E}{\partial n} \tag{2.31}$$

Where

$\rho_{el}$  is the concrete resistivity

n is the direction normal to the steel surface.

Taking into account the effects of activation and concentration polarization according to Butler-Volmer kinetics, the surface boundaries can be described by the Tafel Equations 2.32 and 2.33.

The kinetics of oxidation of iron are given by:

$$i_a = i_{oa} 10^{(E_a - E_{oa})/\beta_a} \quad 2.32)$$

The kinetics of oxygen reduction are given by:

$$i_c = \frac{C}{C_o} i_{oc} 10^{(E_{oc} - E_c)/\beta_c} \quad 2.33)$$

Where

$i_a$  = Current density of the iron oxidation reaction ( $\mu\text{A}/\text{cm}^2$ )

$i_{oa}$  = Exchange current density for iron dissolution ( $\mu\text{A}/\text{cm}^2$ )

$E_a$  = Potential at the concrete pore solution immediately next to the steel surface (V)

$E_{oa}$  = Equilibrium potential of the anodic reaction (V)

$\beta_a$  = Activation tafel slope for the anodic reaction (V)

$i_c$  = Current density of the oxygen reduction reaction ( $\mu\text{A}/\text{cm}^2$ )

$i_{oc}$  = Exchange current density for cathodic reaction ( $\mu\text{A}/\text{cm}^2$ )

$E_{oc}$  = equilibrium potential of the cathodic half-cell reaction, taken as the standard electrode potential, i.e., 0.160 V vs. SCE

$E_c$  = potential at the concrete pore solution immediately next to the steel surface (V)

$\beta_c$  = Activation tafel slope for the Cathodic reaction (V)

$C_o$  = dissolved oxygen concentration at the external concrete surface ( $\text{kg}/\text{m}^3$  of solution)

$C$  = dissolved oxygen concentration at the steel surface ( $\text{kg}/\text{m}^3$  of solution)

It has been observed that  $\beta_a$  increases over time when chloride ions are present in the concrete, from 0.338 V at 1 day to 0.480 V at 90 days while  $\beta_c$  decreases over time from 0.309–0.394 V. to value of 0.350 V [153].



The reinforcing steel is freely corroding when the polarization taking place at the anode and the cathode is enough to make their polarization curves meet as illustrated in Fig.2.5. At this point, the corrosion system develops a new equilibrium corrosion potential  $E_{corr}$  and corrosion current  $I_{corr}$ . The intersection of the two electrode polarization curves represents conditions at which the anodic and cathodic currents are equal (but opposite in polarity) and no net current flows across the steel/concrete interface, Equation 2.34:

$$I_{corr} = i_a \times A_a = i_c \times A_c \quad (2.34)$$

where  $A_a$  and  $A_c$  denote the surface areas where the anodic and cathodic reactions take place, respectively. By substituting Equations 2.32 and 2.33 into Equation 2.34 an estimate of the equilibrium corrosion potential can be obtained from Equation 2.35:

$$E_{corr} = \frac{1}{\beta_a + \beta_c} \left[ \frac{\beta_a \beta_c}{2.3} \ln \left( \frac{i_{oc}}{i_{oa}} \frac{C}{C_o} \frac{A_c}{A_a} \right) + \beta_c E_{oa} + \beta_a E_{oc} \right] \quad (2.35)$$

Taking into account the effects of resistivity and oxygen diffusion, and assuming a relative humidity of 75 % and temperature of 20°C, Vu and Stewart [153] developed an empirical model which gives the corrosion current density at the start of the propagation period (at time  $t_0$ ) as a function of water cement ratio and cover thickness shown in Equation 2.36:

$$i_{corr}(t_1) = 37.8(1 - w/c)^{-1.64}/d \quad (\mu A/cm^2) \quad (2.36)$$

Where

$w/c$  = the water cement ratio obtained from the Bolomey's formula (Equation 2.37)

$d$  = the cover thickness (mm).

$$\left. \begin{aligned} f_{cm} &= A_1 \left( \frac{1}{w/c} - 0.5 \right) \text{ if } w/c > 0.4 \\ f_{cm} &= A_2 \left( \frac{1}{w/c} + 0.5 \right) \text{ if } w/c \leq 0.4 \end{aligned} \right\} \quad (2.37)$$

Where:

$f_{cm}$  = the average compressive strength of the concrete at 28 days (MPa).

w/c = water and cement ratio of the concrete

A<sub>1</sub> and A<sub>2</sub> = constants from Table 2.3 that depend on the way aggregates are produced and on the strength class of cement.

**Table 2.3 Constants in Bolomey's formula [153]**

Aggregate	w/c	Constants <sup>a</sup>	Strength class of cement					
			25	35	40	45	52.5	55
Natural(rounded)	>0.4	A <sub>1</sub>	13.73	17.65	19.61	20.59	22.0675	22.56
Natural(rounded)	≤ 0.4	A <sub>2</sub>	9.32	11.7	12.75	14.22	14.5875	14.71
Natural(crushed)	> 0.4	A <sub>1</sub>	15.2	19.61	21.57	23.54	25.01	25.5
Natural(crushed)	≤0.4	A <sub>2</sub>	10.3	13.24	14.22	15.69	16.7925	17.16

<sup>a</sup> The constant between the presented strength class was determined by interpolation and the average value of the rounded and crushed aggregates was considered if information on the way the aggregates were produced was not provided.

For t < 1 year, Equation 2.38 applies:

$$i_{\text{corr}}(t) = \left[ i_{\text{corr}}(t_1)(1 + t_2)^{-\frac{1}{3}} \right] / d \text{ (}\mu\text{A/cm}^2\text{)} \quad 2.38$$

Inserting Equation 2.36 into Equation 2.38 gives Equation 2.39:

$$i_{\text{corr}}(t) = \left[ 37.8 (1 - w/c)^{-1.64} (1 + t_2)^{-\frac{1}{3}} \right] / d \text{ (}\mu\text{A/cm}^2\text{)} \quad 2.39$$

The rate of corrosion in reinforced concrete is indicated by the corrosion current density ( $I_{\text{corr}}$ ). It is crucial to obtain accurate values of the corrosion rate and  $I_{\text{corr}}$  so as to assess the corrosion of the steel reinforcement and predict the service lifespan of the reinforced concrete structure [147]. Presently, the corrosion current density is obtained through electrochemical measurement in an experiment [149]. The electrochemical measurement is disadvantageous in accuracy measurement.

$I_{\text{corr}}$  which is significantly affected by the galvanic current flowing between the corroding and passive zones on the steel surface [154], is measured on the whole exposed area of the steel reinforcement; however, the corrosion is localized in a small zone. It is therefore necessary to develop a more accurate method to validate the corrosion current density.

## **2.8 Deterioration Models**

### **2.8.1 Introduction to Chloride ingress models**

A number of models for predicting the service life of concrete structures exposed to chloride environments of different corrosion protection strategies have been developed recently and some of these are available on a commercial basis. The approaches adopted by the different models vary considerably and consequently there can be significant variances between the solutions produced by individual models. Several proposals exist based in modelling the mechanisms of attack or in the “performance” concepts or in the use of durability indicators [155]. Nevertheless, their effective incorporation into the standards seem to be slow and a worldwide controversy exists on which is the best approach, due to the lack of enough tradition and experience of these new proposals. This situation demands the calibration of the new proposals and the need to make coherent the new models with long term experience. It is after calibration that the best proposal can be considered.

Several approaches exist for description of the time-dependent process of chloride ingress in concrete. Many models utilize the widely-used Crank’s solution to Fick’s 2nd law of diffusion probably first applied by Collepardi et al. [156]. This approach is based on the fact that observations indicate that the transport of chlorides in concrete is mainly diffusion-controlled, and thus the convection zone is relatively small [157].

## 2.8.2 Chloride ingress models

### a) Clinconc (Cl in concrete) Model

It was first presented in the 1990's and it focusses on the mechanisms occurring within the concrete, namely diffusion and chemical interactions [158]. It is essentially based on the knowledge of physical and chemical processes involved in the chloride transport and binding in concrete. This is a physical model which uses a flux equation based on the principle of Fick's law [158,159]. A numerical solution is obtained using the mass balance equation combined with a non-linear chloride binding isotherm, with both free- and bound-chlorides considered in chloride transport.

The model consists of two main procedures:

- i. Simulation of free chloride penetration through the pore solution in concrete using a genuine flux equation based on the principle of Fick's law with the free chloride concentration as the driving potential, and
- ii. Calculation of the distribution of the total chloride content in concrete using the mass balance equation combined with non-linear chloride binding.

The model can be summarized in Equation 2.39 and 2.40:

$$\frac{\partial q_{cl}}{\partial x} = -\frac{\partial}{\partial x} \left( D_0 \frac{\partial C_f}{\partial x} \right) \quad 2.40)$$

$$\frac{\partial q_t}{\partial t} = \frac{\partial C_f}{\partial t} + \frac{\partial C_b}{\partial t} \quad 2.41)$$

Where:

$C_t$  = the total chloride contents;

$C_f$  = free chloride contents;

$C_b$  = bound chloride contents;

$q_{cl}$  = the net flux of free chloride per unit area;

$D_0$  = the intrinsic diffusion coefficient.

The model input parameters include concrete mix proportions, binder components, curing temperature, environmental temperature and the chloride concentration in the solution to which the concrete is exposed. In this model chloride diffusivity is considered as a material property. It changes only when concrete is young, like many other material properties, such as porosity and strength. After an age of a half of year, this diffusion coefficient becomes more or less constant according to the experiments. The climatic parameters, such as chloride concentration and temperature, are used in both the flux and the mass balance equations. Thus, the model can well describe the effects of exposure conditions on chloride penetration. This model is suitable for different dry-and-wet environments, such as splash zone and road environment.

**b) The Hetek Model,**

The Hetek Model is based directly on measured chloride profiles whose results may be satisfactory from an engineering point of view. The model allows the owner, the designer, or the contractor to estimate the chloride ingress into a given concrete in a given environment and at the same time to define the requirements to be met in a relatively fast laboratory test [160].

The applied model is based upon Fick's 2<sup>nd</sup> law of diffusion i.e. the flow of chloride in concrete is proportional to the gradient of the chloride concentration in the medium. Fick's 2<sup>nd</sup> law of diffusion is a partial differential equation, which cannot be solved without specifying the material parameters, i.e. the chloride diffusion coefficient, and the initial and boundary conditions. We choose the average diffusion coefficient in Equation 2.42( $D_{av}(t)$ ) such that:

$$D_{av}(t) = \frac{1}{t-t_{ex}} \int_{t_{ex}}^t D(\tau) d\tau = D_{aex} \left\{ \frac{t_{ex}}{t} \right\}^{\alpha}, t > t_{ex} \quad 2.42$$

$D_{aex} > 0$  and  $\alpha \in [0,1]$  are constants. When we multiply by  $t - t_{ex}$  and then differentiate the result, it follows that the instantaneous diffusion coefficient is given by Equation 2.43,

$$D(t) = D_{aex} \left\{ \frac{t_{ex}}{t} \right\}^{\alpha} \left( 1 - \alpha + \alpha \frac{t_{ex}}{t} \right) \quad 2.43$$

Since

$$\int_{t_{ex}}^t D(\tau) d\tau = D_{aex}(t - t_{ex}) \left\{ \frac{t_{ex}}{t} \right\}^\alpha$$

It follows that the Hetek Model is best formulated as shown in Equation 2.44:

$$\begin{cases} \frac{\partial y}{\partial x} = D_{aex} \left\{ \frac{t_{ex}}{t} \right\}^\alpha \left( 1 - \alpha + \alpha \frac{t_{ex}}{t} \right) \frac{\partial y}{\partial x}, & x > 0, t > t_{ex}, & \text{diff. Equation} \\ C(0, t) = C_i + S \left( D_{aex}(t - t_{ex}) \left\{ \frac{t_{ex}}{t} \right\}^\alpha \right)^p, & x = 0, t > t_{ex}, & \text{bd cond.,} \\ C(x, t_{ex}) = C_i & x \geq 0, t = t_{ex}, & \text{initial condition} \end{cases} \quad 2.44)$$

The solution to the above Equation is

$$C(x, t) = C_i + S \left( D_{aex}(t - t_{ex}) \left\{ \frac{t_{ex}}{t} \right\}^\alpha \right)^p \Psi_p \left( \frac{x}{2 \sqrt{D_{aex}(t - t_{ex}) \left\{ \frac{t_{ex}}{t} \right\}^\alpha}} \right) \quad 2.45)$$

For  $x \geq 0, t > t_{ex}$ , the introduction of the exponent  $\alpha$  more or less compensates for the fact that the flow is non Fickian close to the boundary. The Hetek Model contains only five unknown parameters,  $D_{aex}$ ,  $\alpha$ ,  $p$ ,  $S$  and  $C_i$ .

### c) Selmer model

The Selmer model was introduced by Collepardi in the 1980s, but its application gave an unrealistic rapid transport of chloride ions when long-term predictions were based on short-term characterization of the material's diffusion coefficient. In the late 1980s Selmer started work to improve the model [161]. In the Selmer model (Equation 2.46) and shown on Fig.2.9, it is assumed that chloride ingress into concrete obeys Fick's second law of diffusion for a semi-finite medium with constant exposure, and that there is a critical value of the chloride content in the concrete leading to the corrosion of steel.

$$C(x, t) = C_i + (C_s - C_i) \operatorname{erf} \left( \frac{x}{\sqrt{4tD}} \right) \quad 2.46)$$

where:

$C(x, t)$  = Chloride content at depth  $x$  at time  $t$ .

$C_i$  = Initial chloride content.

$C_s$  = Chloride content on the exposed surface.

$t$  = Exposure time.

$x$  = Depth in mm

erf = Error function.

$D$  = Chloride diffusion coefficient.

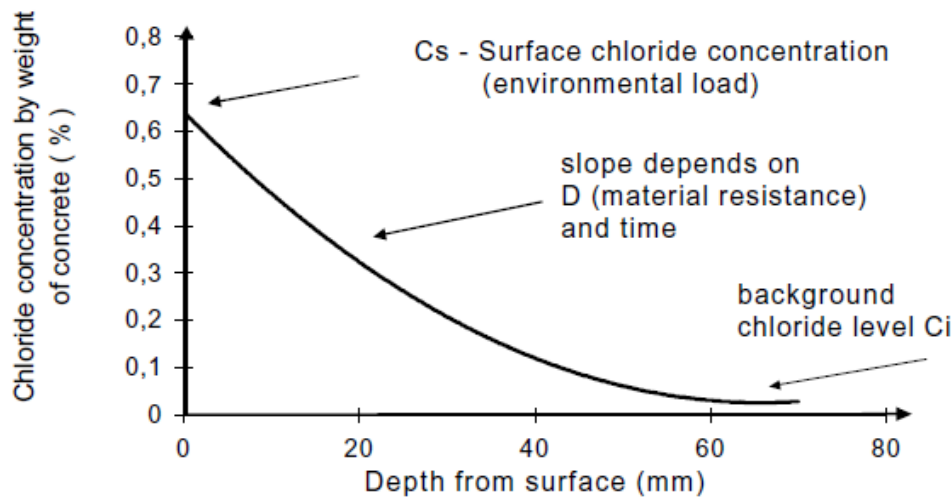


**Figure 2.9 Graph of Chloride concentration VS depth from surface [161].**

The chloride diffusion coefficient,  $D$  shown in Fig.2.9 is an important material parameter that has been considered as a time independent parameter. However, laboratory testing [162,163] and results from existing structures [163] show that the concrete age dependency of the coefficient obeys a straight line in a double logarithmic coordination system. This means that a general mathematical model may be expressed as Equation 2.47:

$$D(t) = D_R \left( \frac{t_R}{t} \right)^k \quad (2.47)$$

where:

$D(t)$  = Time dependent chloride diffusion coefficient.

$t$  = Time when  $D(t)$  is valid.

$t_R$  = Time when reference diffusion coefficient  $D_R$  was measured.

$D_R$  = Reference diffusion coefficient at time  $t_R$ .

$k$  = Parameter to be determined by regression analysis of test results.

The basis of the Selmer Model was the characteristics measured on a number of Norwegian coastal bridges and cast and exposed concrete specimens subject to various laboratory and field conditions. Due to these experimental data the Selmer model was derived as an empirical curve-fitting to the observations. This Selmer model does not state whether the chloride transport is due to a diffusion process or a combination of different phenomena, it just considers this equation as a convenient one for curve-fitting.

#### **d) DuraCrete Model**

This model, applicable for the prediction of chloride ingress was developed in the Brite EuRam project DuraCrete [164] and updated by Gehlen [165]. In this model given in Equation 2.48;

$$C(x, t) = (C_{s,\Delta x} - C_i) \cdot \left[ 1 - \operatorname{erf} \left( \frac{x - \Delta x}{2\sqrt{t \cdot D_{\text{eff}}(t)}} \right) \right] + C_i \quad 2.48)$$

Where

$$D_{\text{eff}}(t) = K_{RH} \cdot D_{RCM,0} \cdot K_t \cdot K_T \cdot \left( \frac{t_0}{t} \right)^n \quad 2.49)$$

$C(x, t)$  = chloride concentration in depth  $x$  in percentage by mass of cement at time  $t$ ;

$C_s, \Delta x$  = chloride concentration in depth  $\Delta x$  at time of inspection in percentage by mass of cement;

$C_i$  = initial chloride concentration in percentage by mass of cement;

$\operatorname{erf}$  = error function;

$x$  = depth with corresponding chloride concentration  $C(x, t)$  in m;



$\Delta_x$  = depth of the "convection" zone in which the chloride profile deviates from behavior according to the 2<sup>nd</sup> law of diffusion in m;

$t$  = age of concrete in s;

$D_{\text{eff}(t)}$  = effective diffusion coefficient of concrete at time  $t$  in  $\text{m}^2/\text{s}$ ;

$K_{\text{RH}}$  = environmental parameter accounting for the influence of the degree of saturation;

$D_{\text{RCM},0}$  = chloride migration coefficient of water saturated concrete prepared and stored under predefined conditions, determined at the reference time  $t_0$  in  $\text{m}^2/\text{s}$ ;

$k_t$  = test parameter to account for deviations of the chloride migration coefficient, determined under accelerated condition with the Rapid Chloride Migration method (RCM), and a diffusion coefficient determined under natural conditions

$K_T$  = temperature parameter in Kelvin with

$$K_T = \exp \left[ b_T \left( \frac{1}{T_{\text{ref}}} - \frac{1}{T} \right) \right] \quad 2.50)$$

Where,

$b_T$  = regression parameter in Kelvin;

$T_{\text{ref}}$  = reference temperature in Kelvin;

$T$  = temperature of the environment (micro climate) in Kelvin and

$n$  = exponent regarding the time-dependence of  $D_{\text{eff}}$ ;

$t_0$  = reference time in s.

The applied model is probabilistic, i.e. each parameter is inserted in terms of a mean value, standard deviation and distribution type. Depassivation of the reinforcement will start when the critical corrosion inducing chloride content  $C_{\text{crit}}$  will be exceeded in the depth of the concrete cover  $d_c$ , expressed by the limit state function.

$$p_f = p\{C_{crit} - C_i - (C_{s,\Delta x} - C_i) \cdot \left[ 1 - \operatorname{erf}\left(\frac{d_c - \Delta x}{2\sqrt{K_{RH} \cdot K_t \cdot K_T \cdot D_{RCM,0} \cdot t \cdot \left(\frac{t_0}{t}\right)^n}}\right)\right] < 0\} \quad 2.51)$$

Where,

$p_f$  = failure probability;

$p$  = probability of a certain event to occur;

$C_{crit}$  = critical chloride concentration in percentage by mass of cement;

$d_c$  = cover depth in mm.

#### e) Mangat and Molloy Diffusion Model

They derived a diffusion coefficient a time-dependent parameter used to quantify the expected service life extension. According to Mangat and Molloy [166] the concentration of chloride ingress into concrete reduces with time (Equation 2.52).

$$D_c = D_i t^{-m} \quad 2.52)$$

Where:

$D_c$  = Effective diffusion coefficient at time  $t$  ( $\text{cm}^2/\text{s}$ )

$D_i$  = Effective diffusion coefficient at time  $t = 1.0$  sec

$t$  = Time (s)

$m$  = Empirical coefficient that varies with mixture proportions

The chloride contents were measured from Equation 2.53:

$$C_{(x,t)} = C_0 \left( 1 - \operatorname{erf}\left(\frac{x}{2\sqrt{\frac{D_i}{1-m} t^{(1-m)}}}\right)\right) \quad 2.53)$$

$m$  is the parameter depending on the ratio of water to cement (w/c) given in Equation 2.54:

$$m = 2.5 \left(\frac{w}{c}\right) - 0.6 \quad 2.55)$$

Equation 2.53 is valid if the initial diffusion coefficient and the age at the time of first exposure to chlorides are taken at time  $t = 1$  second [167]. The requirement of the diffusion coefficient at time equal to 1 second results in the overestimation of chloride concentrations. Measuring the parameter of  $D_c$  is not feasible and equally estimating the value of  $m$  is probably inaccurate [168].

**f) Maheswaran and Sanjayan Diffusion Model**

Maheswaran and Sanjayan [168] developed a solution to Mangat and Molloy Equation (Equation 2.52) using the different times of chloride application and  $D_c$  measurement. They presented Equation 2.56 for chloride content estimation:

$$C_{(x,t)} = C_o \left[ 1 - \operatorname{erf} \left( \frac{x}{2 \sqrt{\frac{D_{\text{ref}}(t_{\text{ref}})^m}{1-m} [(t)^{1-m} - (t_i)^{1-m}]}} \right) \right] \quad (2.56)$$

where:

$D_{\text{ref}}$  = Diffusion coefficient measured at time  $t_{\text{ref}}$ ;

$t_i$  = Age at first exposure to chloride;

$m$  = Empirical coefficient varying with mixture proportions, determined as Mangat and Molloy Model.

Although the Maheswaran and Sanjayan model overcomes the limitations of the Mangat and Molloy's model, estimating an appropriate value for  $m$  still remains difficult [168].

**g) Bamforth Diffusion Model**

Thomas and Bamforth [169] used Equation 2.57 to predict chloride concentration at depth  $x$  at time  $t$ .

$$C_{(x,t)} = C_o \left[ 1 - \operatorname{erf} \left( \frac{x}{2 \sqrt{D_{\text{ca}}(t_m) \left( \frac{t}{t_m} \right)^n t}} \right) \right] \quad (2.57)$$

Where:

$D_{ca}(t_m)$  = Apparent diffusion coefficient measured at time  $t_m$ , shown in Equation 2.58:

$$D_{ca} = at^n \quad (2.58)$$

Where:

$D_{ca}$  = Apparent diffusion coefficient

$a = D_{ca}$  at  $t = 1$  year

$n$  = Empirical constant

For this model the empirical constant  $n$  is assumed to be constant for a particular mix type and unaffected by w/cement ratio. This assumption has been found to be incorrect for silica fume concrete [170].

#### **h) The Fib model**

The fib model is based on Fick's 2<sup>nd</sup> law of diffusion [170]. The convection zone is referred to as being the surface of a concrete that is exposed to a frequent wetting and drying. In the convection zone, diffusion is no longer the main method of transportation for chloride, resulting in Fick's 2<sup>nd</sup> law no longer being a satisfactory approximation to model the chloride ingress. For Fick's 2<sup>nd</sup> law to still give a good approximation of the chloride ingress, the data of the convection zone is neglected and Fick's 2<sup>nd</sup> law of diffusion is applied starting at a depth  $\Delta_x$ , with a substitute surface concentration  $C_{s,\Delta_x}$ . With this simplification, Fick's 2<sup>nd</sup> law of diffusion gives a good approximation of the chloride ingress at a depth  $x \geq \Delta_x$  [170].

The fib model is described by Equation 2.59:

$$C_{crit} = C(x = \alpha, t) = \left( C_0 + (C_{s,\Delta_x} - C_0) \cdot \left[ 1 - \operatorname{erf} \left( \frac{\alpha - \Delta_x}{2\sqrt{D_{app,c}t}} \right) \right] \right) \quad (2.59)$$

Where:

$C_{crit}$  = critical chloride content in % by mass of cement;

$C(x, t)$  = chloride concentration in depth  $x$  in percentage by mass of cement at time  $t$   
and depth  $x$  (structural surface  $x=0m$ );

$x$  = depth in mm;

$\alpha$  = concrete cover in mm;

$t$  = concrete age in years;

$C_o$  = initial chloride concentration in percentage by mass of cement;

$C_s, \Delta_x$  = chloride concentration in depth  $\Delta x$  and a certain point in time  $t$  in % by mass  
of cement;

$\Delta_x$  = depth of the "convection" zone in which the chloride profile deviates from behavior  
according to the 2<sup>nd</sup> law of diffusion in m;

$D_{app,c}$  = the apparent chloride diffusion coefficient in concrete in mm<sup>2</sup>/years;

$C_i$  = initial chloride concentration in percentage by mass of cement;

erf = error function;

With:

$$D_{app,c}(t) = K_e \cdot D_{RCM,0} \cdot K_t \cdot A(t) \quad 2.60)$$

Where:

$D_{RCM,0}$  = the chloride migration coefficient in mm<sup>2</sup>/years

$K_e$  = the environmental transfer factor (-);

$K_t$  = the test method variable (transfer variable) (-);

$A(t)$  = the aging function (-);

With:

$$A(t) = \left(\frac{t_0}{t}\right)^\alpha$$

Where:

$t$  = concrete age in years;

$t_0$  = the reference concrete age in years (reference point of time);

$\alpha$  = the age exponent (-);

With;

$$K_e = \exp \left[ b_e \left( \frac{1}{T_{ref}} - \frac{1}{T_{real}} \right) \right] \quad 2.61)$$

Where,

$b_e$  = regression parameter in Kelvin;

$T_{ref}$  = reference temperature in Kelvin;

$T_{real}$  = temperature of the environment (micro climate) in Kelvin.

The fib model has various sources of uncertainty associated with the parameters which include, model uncertainty, statistical uncertainty and physical uncertainty. Model uncertainty arises from the use of a simplified mathematical relationship between the variables and the true values of the actual physical mechanism of chloride ingress. The statistical uncertainty emerges from estimating the mean and standard value of the parameters from a limited set of data and the physical uncertainty is associated with the uncertainties in the concrete cover depth, the diffusion coefficient and surface chloride concentration. Looking at the uncertainties mentioned above it is clear that a significant error can be associated with the fib model [170].

#### **i) Finite Element Model (FEM)**

FEM is a numerical technique for finding the solution to a set of partial differential equations. Williamson [167] claimed that there are more details and parameters in the use of FEM to estimate the diffusion of chlorides into concrete than those investigated in Fickian models. Saetta et al. [171] applied the Finite Element Method to solve a set of nonlinear equations of

the chloride penetrating partially saturated concrete. The effects of many factors in diffusion of chloride including a time-dependent chloride diffusion coefficient, degree of cement hydration, temperature, humidity, and moisture flux, are solved in this model.

Boddy et al. [172-174] determined diffusion and convection of chloride transport by Equation 2.62:

$$\frac{\partial C}{\partial t} = D \cdot \frac{\partial^2 y}{\partial x^2} - v \cdot \frac{\partial C}{\partial x} + \frac{\rho}{n} \frac{\partial s}{\partial t} \quad 2.62)$$

where:

C = free chloride in solution at depth x after time t

D = diffusion coefficient

$\rho$  = concrete density

n = porosity

S = bound chloride

v = average linear velocity

$$v = \frac{Q}{nA} = -\frac{k}{n} \frac{dh}{dx} \quad 2.63)$$

Where:

Q = flow rate

A = cross-sectional area

k = hydraulic conductivity

h = hydraulic head

Equation 2.63 solves the rate of change in chloride concentration, account for the effects of chloride diffusion, convective flow, and chloride binding. The FEM is able to predict the time to diffusion and corrosion. According to Williamson [167], the FEM is difficult to handle because of the complexity of the calculations required.

## 2.8.2 Limitations of Diffusion Models

The rate at which the chloride diffusion coefficient reduces is dependent upon concrete mix proportions. The rate is affected by the w/c ratio, pozzolan content, and curing conditions. Due to the high variability in mixture proportioning and curing conditions, estimating the appropriate parameters used in calculating a time-dependent chloride diffusion coefficient accurately remains a difficult task [167].

## 2.9 Service life models

### i) Tuutti's model

Tuutti [175] suggested a model (Fig.2.10) for predicting the service lives of reinforced concrete structures. The maximum acceptable corrosion level is related to the appearance of cracks. The deterioration process consists of two periods: initiation and propagation. The length of the initiation period can be estimated from the time required for aggressive ions to reach reinforcement surfaces and trigger active corrosion, while that of the propagation period can be taken as the time elapse until repair becomes mandatory.

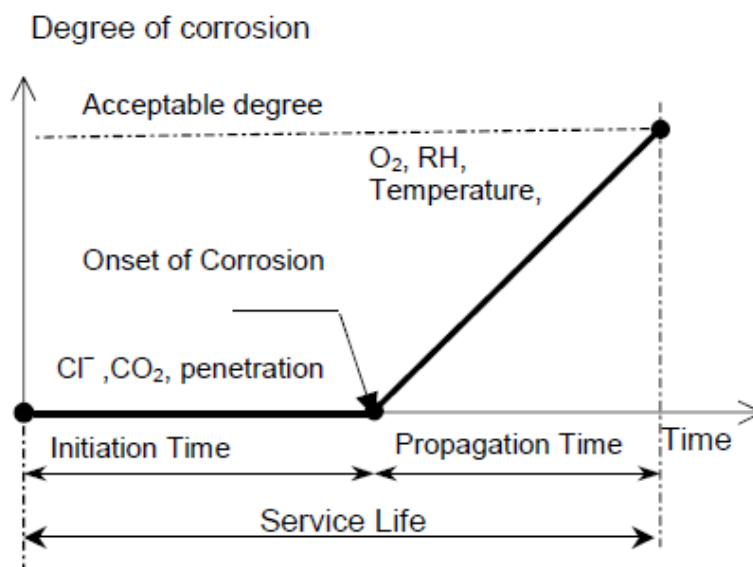


Figure 2.10: A schematic sketch of steel corrosion sequence in concrete [175].



Tuutti's model underestimates the time to corrosion cracking compared with times obtained from field and laboratory observations because it includes the same assumption as Bezan's model in section 2.8.2(iv), that all corrosion products create expansive pressure on the concrete.

## **ii) Life 365 Service life prediction model**

This model estimates the service life and the life-cycle costs associated with different corrosion protection strategies. The analyses carried out within Life-365 can be split into four separate steps [176]:

- a) Predicting the time to the onset of corrosion, commonly called the initiation period,  $T_1$ ;
- b) Predicting the time for corrosion to reach an unacceptable level, commonly called the propagation period,  $T_2$ . The time to first repair,  $t_r$ , is the sum of these two periods (Equation 2.64):

$$T_1 = T_1 + T_2 \quad 2.64)$$

- c) Determining the repair schedule after first repair; and
- d) Estimating life-cycle costs based on the initial concrete (and other protection) costs and future repair costs.

### **Limitation**

According to the Life-365 user's manual [176], the solutions found in Life 365 program model are only intended to be approximations and to be used as simply a guideline in designing reinforced concrete structures. The Life -365 documentation informs the user that the program is limited due to the fact that the transport process, loss of passivity on embedded steel, corrosion of steel and subsequent damage of concrete surrounding the corroded steel are highly complex and not understood in entirety. The model assumes that concrete is saturated with water and it does not account for corrosion induced by carbonation.

### iii) Cady-Weyers' Deterioration Model

Based on the premise that salt-induced corrosion of the steel is the main cause of deck deterioration, a deterioration model developed by Cady and Weyers has been used to estimate the remaining life of concrete bridge components in corrosive environments [177]. The model (Fig. 2.11) predicts deck deterioration as measured in an area percentage of the entire deck. The total area of spalls, delamination, asphalt patches, and crack lengths multiplied by a tributary width combine to produce the total damage. According to Cady-Weyers' model, the corrosion rate is the key to predicting the time to cracking.

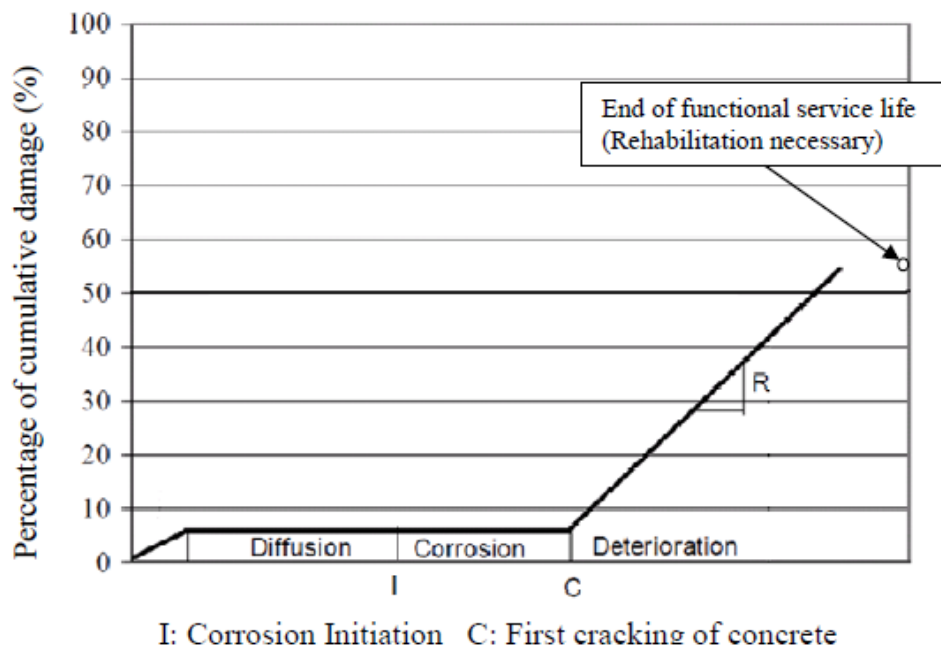


**Figure 2.11: Cady-Weyers' corrosion-deterioration model for concrete bridge [177]**

The corrosion rate is the key to predicting the time to cracking. The corrosion rate is mainly controlled by the rate of oxygen diffusion to the cathode, resistivity of the pore solution, and temperature [178]. The prediction of the time to cracking using corrosion rate of reinforced concrete water conveyancing structures is the task of this study.

#### iv) Baezant's Mathematical Models for Time to Cracking

Based on theoretical physical models for corrosion of steel in concrete exposed to seawater, Bazant et al. [179], [180] proposed a numerical model shown in Equation 2.65 for reinforcement corrosion in concrete, to assess the time to corrosion that may lead to splitting of cover concrete.

$$T_2 = \rho_{\text{corr}} \frac{d\Delta d}{pj_r} \quad 2.65)$$

Where:

$T_2$  = propagation period (years);

$\rho_{\text{corr}}$  = Combined density factor for steel and rust ( $\text{kg}/\text{m}^3$ );

$d$  = diameter of rebar (mm);

$\Delta d$  = increase in diameter of rebar due to rust formation (cm);

$P$  = perimeter of rebar (mm);

$j_r$  = instantaneous corrosion rate of rust ( $\text{g}/\text{m}^2\text{-s}$ );

The instantaneous corrosion rate of rust can be calculated from Equation 2.66;

$$j_r = \frac{W}{F} i_{\text{corr}} \quad 2.66)$$

Where:

$W$  = equivalent weight of steel;

$F$  = Faradays constant (C);

$i_{\text{corr}}$  = Corrosion current density ( $\mu\text{A}/\text{cm}^2$ ).

The damage of corrosion considers the volume of expansion because of the arrangement of hydrated rust over the remaining rebar center. This hydrated rust is expansive in nature and involves four times the volume of guardian steel. Subsequently a uniform radial weight is applied on to the encompassing concrete bringing about outward radial pressure exerted on

concrete. This radial pressure is same as the increment in distance across the rebar, and increments with an increase in the volume of rust till the cover concrete splits.

According to Bazant's model, the time to cracking is a function of corrosion rate, cover depth, spacing, and certain mechanical properties of concrete such as tensile strength, modulus of elasticity, Poisson's ratio and creep coefficient. A sensitivity analysis of Bazant's theoretical equations demonstrates that for these parameters, corrosion rate is the most significant parameter in determining the time to cracking of the cover concrete. Unfortunately, Bazant's model has never been validated experimentally.

#### v) Morinaga's Empirical Model

Based on field and laboratory data, the empirical Equation 2.67 suggested by Morinaga [180] can be used for predicting the time to cracking. It is assumed that cracking of concrete will first occur when there is a certain quantity of corrosion products forming on the reinforcement.

Morinaga's empirical equation does not consider the mechanical properties of concrete which would be influential.

$$T_2 = \frac{Q_{cr}}{j_r} \quad 2.67)$$

$$Q_{cr} = 0.602d \left(1 + \frac{2c}{d}\right)^{0.85} \quad 2.68)$$

Where:

$j_r$  = instantaneous corrosion rate of rust (g/m<sup>2</sup>s);

$Q_{cr}$  = amount of corrosion in concrete cracks(g/cm<sup>2</sup>);

$c$  = concrete cover thickness(mm);

$d$  = diameter of reinforcement (mm).

### vii) Wang and Zhao's Model

Wang and Zhao [181] recommended a stage technique for utilizing limited component examination to focus the thickness of the corrosion product comparing to the time term when the surface concrete cracks. Further by breaking down an extensive number of rebar corrosion information gathered from research and contrasting them and the after effects of limited component examination, the researchers established an exact expression to focus the proportion of thickness of corrosion product to the penetration depth of the rebar H, comparing to the crack in spread concrete. Their model is defined in Equations 2.69-2.71:

$$T_2 = \frac{H}{p_r} \quad 2.69)$$

and

$$\frac{\Delta}{H} = 0.33 \left(\frac{d}{c}\right)^{0.565} f_{cu}^{1.436} \quad 2.70)$$

$$p_r = \frac{W}{F\rho_{st}} i_{corr} \quad 2.71)$$

Where:

$F_{cu}$  = cube strength of concrete(kN/cm<sup>2</sup>);

$\Delta$  = thickness of corrosion product (cm);

H= no of cracks in the cover;

$\rho_{st}$  =density of steel(kg/m<sup>2</sup>).

### vii) Indian Roads Congress (IRC) model

In this model, corrosion propagation time is evaluated due to falling pH. The reason for the falling pH as a consequence of chloride substance transcending the limit near to the reinforcement. If there should arise an occurrence of generalized corrosion, the basic loss of bar span is in view of the cover cracking. The permeation of chloride ions is modelled by the

Fick's second law of diffusion. The corrosion initiation time in years ( $t_1$ ) can be obtained by Equation 2.72, an approximate solution to the Fick's law [182]:

$$t_1 = \frac{C_0 c^2}{12D_C(\sqrt{C_0} - \sqrt{C_{th}})^2} \quad (2.72)$$

Where:

$C_0$  = equilibrium chloride concentration ( $\text{kg}/\text{m}^3$ ) on the exposed surface of concrete;

$C_{th}$  = threshold value of chloride concentration ( $\text{kg}/\text{m}^3$ );

$c$  = concrete cover thickness (mm), and

$D_C$  = coefficient of chloride diffusion through concrete ( $\text{mm}^2/\text{year}$ ).

There are uncertainties in all these variables, thus affecting the initiation time.

After initiation of corrosion, there is reduction in the net section of a bar. Although chloride-induced corrosion causes pitting on the surface of a bar, the pitting is randomly distributed on the surface in absence of major cracks or in the presence of distributed cracks of small width.

A uniform reduction in the diameter of the bar can be assumed for modelling the reduction in the net section. The total cross-sectional area of the bars in a layer ( $A_{st}$ ) is given as a function of time ( $t$ ) in Equation 2.73:

$$A_{st} = \begin{cases} \frac{n\pi\phi^2}{4}, & t \leq t_0 \\ \frac{n\pi}{4} [\phi - 2r(t - t_0)], & t > t_0 \end{cases} \quad (2.73)$$

Where:

$n$  = number of bars in a layer;

$\phi$  = initial nominal diameter of a bar, and

$r$  = corrosion rate for the bars in uncracked concrete.

The steady state of corrosion in years can be found from Equation 2.74:

$$t_r = \frac{80C}{Dr} \quad (2.74)$$

where

C= the thickness of the concrete cover (mm);

d = the diameter of the reinforcing bar (mm);

r= rate of corrosion ( $\mu\text{m}/\text{year}$ );

**viii) Strength, weaknesses and general comments on existing service life models**

Table 2.4 shows a summary of existing models, their strengths and weaknesses and general comments.

**Table 2.4: Summary of Service Life models, their strengths and weaknesses.**

Model	Strength	Weaknesses	Comment
Tuuti Model	- practicality and simplicity in its approach -agrees that the corrosion rate is the most significant parameter	-Underestimates the time to corrosion cracking - does not show the different stages of corrosion induced damage in the propagation phase.	Is a general criterion for service life estimation and does not define a criterion for different limit states during propagation period.
Selmer model	-Simplicity in its approach -agrees that the corrosion rate is the most significant parameter	-Does not state whether the chloride transport is due to a diffusion process or a combination of different phenomena. - uniform corrosion was assumed irrespective of their corrosion type	Cannot be reliable in determining the service life of water conveyancing structures.
Life 365 model	-Informs the user of its limitations -agrees that the corrosion rate is the most significant parameter	-intended to give approximate results only. -assumes that concrete is saturated with water.	Cannot be reliable in determining the service life of water conveyancing structures.
Cady-Weyers's Model	-agrees that the corrosion rate is the most significant parameter	-Is specific in its application-bridge decks -it is assumed that the chloride content at the concrete surface is uniform	Cannot be reliable in determining the service life of water conveyancing structures as its specific to bridge decks
Baezant's Models	-agrees that the corrosion rate is the most significant parameter. -Takes into account the mechanical properties of concrete	-the influence of concrete exposure environment, -has never been validated experimentally. -only effect of nominal perimeter of bar for calculating the steady state corrosion period.	Cannot be reliable in determining the service life of water conveyancing structures
Morinaga's Model	-Applicable o	-ignores the time-varying process of corrosion rate	-Will not give accurate service life for water conveyancing structures.

	-agrees that the corrosion rate is the most significant parameter	-does not take into the mechanical properties effect on corrosion. - uniform corrosion was assumed irrespective of their corrosion type	
Wang and Zhao's Model	-agrees that the corrosion rate is the most significant parameter	-uniform corrosion was assumed irrespective of their corrosion type	Not reliable in determining the service life of water conveyancing structures
IRC model	agrees that the corrosion rate is the most significant parameter	-Is a generalized model.	Not reliable in determining the service life of water conveyancing structures

From table 2.4, it can be noted that there is need to formulate a service life model specific for reinforced concrete water conveyancing structures.

## **2.10 Relationship between accelerated test results to real reinforced concrete in determination of the service life of structures.**

Its erroneous to undertake a direct linear extrapolation of accelerated test results to real reinforced concrete water conveyancing structures in predicting the service life of structures. The test results must be calibrated against test-data representative of actual conditions in practice. To minimize the error in predicting the time to cracking when extrapolating accelerated corrosion test results to the behavior of real reinforced concrete structures with low corrosion rates, Equation 2.75 can be applied [183];

$$T_{2(\text{real})} = k_R \times \frac{i_{\text{corr}(\text{exp})}}{i_{\text{corr}(\text{real})}} T_{2(\text{exp})} \quad (2.75)$$

Where:

$T_{2(\text{real})}$  = Corrosion propagation time for real structures;

$k_R$  = Rate of loading correction factor;

$i_{\text{corr}(\text{exp})}$  =accelerated corrosion rate;

$i_{\text{corr}(\text{real})}$  = any value of selected corrosion rate;



$T_{2(\text{exp})}$  = is the propagation period from accelerated corrosion experiment and can be obtained from the proposed model.

If the rate of loading does not affect crack propagation, then  $k_R = 1$ . Empirically (Equation 2.76) [166,183].

$$k_r \approx 0.95 \left[ \exp\left(\frac{-0.3i_{\text{corr}(\text{exp})}}{i_{\text{corr}(\text{real})}}\right) - \frac{i_{\text{corr}(\text{exp})}}{i_{\text{corr}(\text{real})}} + 0.3 \right] \quad k_R \geq 0.25 \quad 2.76)$$

### **2.11 Need to develop a simulation model for prediction of the service life of water conveyancing reinforced concrete structures.**

A lot of investments are incurred in developing concrete water conveyancing structures and financial institution have the first interest in recovering their investment. In the long term, the users including governmental organizations and private developers are left with the challenge of maintenance and improvement of the structures. From the details shown in Table 2.3, none of the models for prediction of service life specifically addresses corrosion in reinforced concrete water conveyancing structures. There is need to develop a performance based model to simulate the service life of reinforced concrete for water conveyancing structures to account for the shortcomings of the discussed models.

This research presents a service life model for reinforced concrete water conveyancing structures. The validity, accuracy, and efficiency of the proposed model is established by comparing the model results with experimental work and works of other researchers.

## CHAPTER 3

### 3.0 METHODOLOGY

#### 3.1 General introduction

The purpose of this research was to develop a model to simulate the service life of reinforced concrete water conveyancing structures. It was also necessary to determine experimentally the critical penetration of rust (a function of service life) in concrete of characteristic strength  $25\text{N/mm}^2$ ,  $30\text{N/mm}^2$  and  $35\text{N/mm}^2$  used in water retaining and conveyancing structures. The minimum characteristic strength was informed by industry practice in terms of economy and functionality while the subsequent strengths are incremental in cost and strength. Higher flow velocities greater than  $2\text{m/s}$  require strengths greater than  $25\text{N/mm}^2$  to reduce the rate of erosion by water flow [184]. Alternatively, an increase in member thickness may be introduced to account for erosion thickness within the service life of the structure. The effect on bond strength of corrosion inhibitors in the Kenyan market was also experimentally determined.

This study was conducted at the University of Nairobi Concrete and Materials Laboratory where the physical properties of the materials, sample preparation and testing were done. The chemical properties of the ordinary Portland cement and chloride content was done at the State Department of Infrastructure in the Ministry of Transport, Infrastructure, Housing and Urban Development of the Government of Kenya. This chapter gives the details of experiments and the procedures followed. The investigations were carried out in three parts.

In part one, the properties of materials used in concrete for casting the experiment samples were investigated. These materials were coarse aggregates, fine aggregates, 10mm ribbed bars, and ordinary Portland cement. The properties of selected corrosion inhibitors were obtained from the literature. In part two, accelerated corrosion tests were carried out to determine the critical penetration depth of rust in reinforced concrete water conveyancing structures, the first

objective in this study. As characteristic strength of  $25\text{N/mm}^2$  is most common in the industrial practice for water conveyancing structures, three cement brands were used to determine if a selected brand of cement affects the corrosion rate. These accelerated corrosion test procedures were done to ASTM G901 procedures.

In part three, the effect of four selected corrosion inhibitors on the compressive, tensile and bond strength of concrete with ribbed bars were investigated in order to address the second objective. The choice of the inhibitors was by ease of availability and frequency of use in the Kenyan market. Test samples from four selected corrosion inhibitors; a calcium nitrite and nitrate based, a dimethylathanolamine based organic inhibitor and fly ash in combination with a selected brand of cement A, B and C were prepared. A control experiment without any inhibitor was performed to compare the results. The dosage of corrosion inhibitors was done to the manufacture's specification. The results obtained for the critical penetration test and the rate of corrosion were used to propose a corrosion current density and a service life model for water conveyancing structures in chapter four to address the third and fourth objectives.

To develop the current density model, the rate of corrosion( $\text{mm/year}$ ) was calculated from the weight loss method and compared with the result from the Vu and Stewart model and Li 2004a [185] model. From the results, it was noted that the proposed corrosion current density model correlates with the Vu and Stewart [154] results. A statistical relationship between the result from the weight loss method and the Vu and Stewart model was established to propose a current density model for this work.

A corrosion service life model of reinforced concrete structures constitutes two periods; initiation( $T_1$ ) and propagation ( $T_2$ ). The initiation period was evaluated by the ratio of the critical penetration depth( $\text{mm}$ ) to the rate of corrosion( $\text{mm/year}$ ). The propagation period was

evaluated by subtracting  $T_1$  from the measured experimental period and this was indicated as the measured period model for the expansion of corrosion products during propagation period for this study for evaluation of  $T_2$ . The resulting service life  $T_1 + T_2$  was compared with the works of other authors.

### **3.2 Part 1: Investigation of material properties**

#### **3.2.1 Aggregates**

##### **Physical and mechanical Properties**

Physical properties of aggregates play a vital role in strength and durability of aggregates [186]. Granite crushed stone coarse aggregates were procured from Kenya Builders quarry in Embakasi, Nairobi while the fine aggregates were procured from a stockpile sourced from Machakos River. The coarse aggregates were tested for;

- a) Crushing value to BS EN 1097-2 standard
- b) Impact value to BS EN 1097-2 standard
- c) Flakiness index to BS/EN 933-3 standard
- d) Loss Angeles abrasion value to BS/EN 1097-2 standard.

The fine and coarse aggregates were graded to the respective standards shown in the results.

Further the physical properties of the aggregates were investigated for;

- a) Specific gravity to ASTM C128 standard
- b) Water absorption to BS 812-2:1995 standard
- c) Silt content to ASTM C142-97 standard

#### **3.2.2 Ribbed bars**

##### **a) Tensile strength test**

The tensile properties and chemical composition of the ribbed bars for this study were done at the manufacturer's laboratory. Before tensile testing of the ribbed bars, on the bar surface marks

with an initial distance of ten times the nominal diameter of bars, i.e.,  $10d_{nom} = 160 \text{ mm}$ , were made to determine the original gauge length. The Tensile test was controlled by displacement with  $2 \text{ mm/min}$ . During the tensile test, the applied load was recorded using a computerized data acquisition system, and the deformation values were obtained with an extensometer with a  $50 \text{ mm}$  base. The data obtained were utilized to plot load-displacement curve, determine the yield load and ultimate load, and calculate the elongation for each tested bar. The stress strain curve was obtained from the load displacement curve.

**b) Preparation of the ribbed bars for experiments.**

The reinforcing ribbed steel bars were 108 pieces of  $10 \text{ mm}$  diameter,  $400 \text{ mm}$  total length with a  $120 \text{ mm}$  section, wire brushed to remove the mill scale and spray coated with a zinc coat in the Lab as shown in Fig.3.1 for the accelerated corrosion experiment to ASTM G901 test procedures. 135 pieces of  $10 \text{ mm}$  diameter and  $1010 \text{ mm}$  long were for the pullout test. The deformed uncoated ribbed steel bars, sourced from a local manufacturer, were cut to length and zinc sprayed as shown in Fig.3.1. The bars were kept in the lab covered with a dry cloth and kept free of moisture until just before concrete placement. Any visible corrosion product was removed by wire brushing prior to placing the bars in the molds during casting.

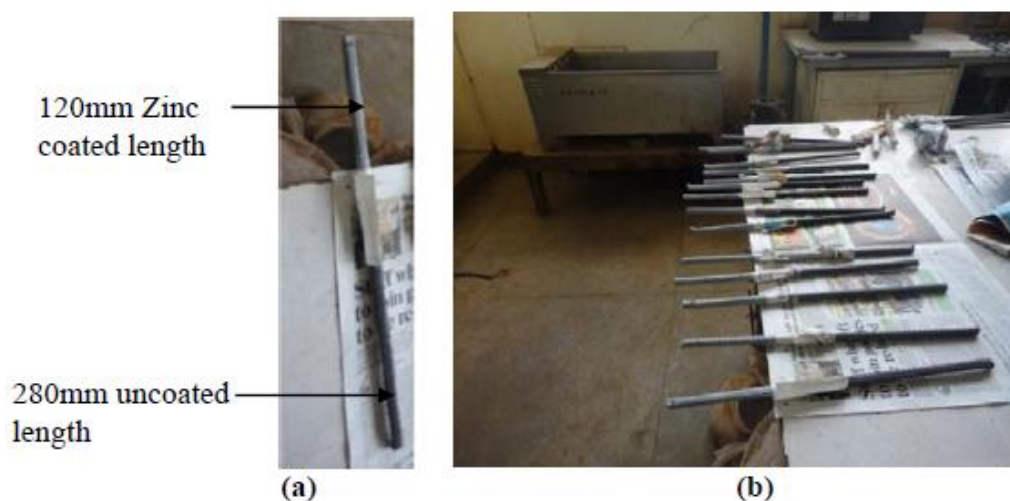


**Figure 3.1(a) and (b) 120mm zinc sprayed coat length of 400mm long ribbed bars**

The essence of coating the exposed surface of the rebar was to limit corrosion to the embedded length only.

### **3.2.3 Ordinary Portland Cement**

To determine the effect of local cement brands on corrosion, three brands of ordinary Portland cement (OPC 42.5 N), KS EAS 18-1:2001, (Sample A, Sample B and Sample C), sourced from a wholesale supplier were used in the study. The chemical composition to KS EAS 148-4:2017 of each brand of cement was analyzed in the State Department of Infrastructure in the Ministry of Transport, Infrastructure, Housing and Urban Development of the Government of Kenya laboratory.

### **3.2.4 Water for the study**

Potable water was used for mixing and curing of concrete samples.

### **3.2.5 Selected corrosion inhibitors**

The properties of a dimethylathanolamine based organic (inhibitor Z), calcium nitrate (inhibitor X) and calcium nitrite based (inhibitor Y), were obtained from the literature while the chemical composition of fly ash used was analyzed at the State Department of Infrastructure in the Ministry of Transport, Infrastructure, Housing and Urban Development of the Government of Kenya laboratory.

### **3.2.6 Mix Design**

The concrete was batched by weights while the mix design was by the building research establishment (BRE). The mix design is shown in Appendix A2. Table 3.1 gives a summary of the concrete constituents.

**Table 3.1: Summary of concrete constituents used in this study.**

Characteristic strength(N/mm <sup>2</sup> )	Coarse aggregates (kg/ m <sup>3</sup> )	Fine aggregates (kg/ m <sup>3</sup> )	Cement (kg/ m <sup>3</sup> )	Water(kg/m <sup>3</sup> )
25	1190	650	450	225
30	1069	638	450	225
35	1075	631	469	225

**3.2.7 Experimental matrix of the sample size adopted**

Table 3.2 gives a summary of the sample size of the respective experimental study.

**Table 3.2: Matrix of experimental sample size**

Identification	Characteristic strength of concrete	Samples for accelerated corrosion	Cubes for compression test	Cylinders for split tensile test	Cylinders for bond strength
25N/mm <sup>2</sup>	150mm dia	27	27	27	
	130mm dia	9			
	100mm dia	9			
30 N/mm <sup>2</sup>	150mm dia	9	27	27	
	130mm dia	9			
	100mmdia	9			
35N/mm <sup>2</sup>	150mm dia	9	27	27	
	130mm dia	9			
	10mm dia	9			
25N/mm <sup>2</sup>	Fly ash concrete		27	27	27
	Concrete with Inhibitor X		27	27	27
	Concrete with Inhibitor Y		27	27	27
	Concrete with Inhibitor Z		27	27	27
	Control samples		27	27	27

From table 3.2, after testing, the average of the results was used in the analysis of the effects of parameters that affect corrosion. For the characteristic strength of 25N/mm<sup>2</sup> and sample size 300mm high x 150mm diameter, 27 samples were cast for accelerated corrosion test to evaluate the effect of selected cement brands on the rate of corrosion.

### **3.3 Part 2: Corrosion tests**

#### **3.3.1 Introduction to corrosion tests**

The following corrosion tests were performed with outlined procedures:

- i) Accelerated corrosion;
- ii) Weight loss measurement.

#### **3.3.2 Accelerated corrosion tests and tests program to ASTM G109 07[184].**

##### **a) Specimen Preparation**

- i) The 10mm diameter, 400mm long ribbed bars were polished with abrasive papers.
- ii) 120 mm of the surface length of each bar were zinc sprayed and left to dry as shown in Fig.3.1.
- iii) The mixed concrete (in two batches) was poured into cylindrical moulds (150 mm in diameter and 300 mm high) where the reinforcement was placed along its longitudinal axis as shown in Fig.3.2.
- iv) The specimens were mechanically vibrated for 60s and demoulded after 24 hours. The cylindrical concrete specimens were then cured for 27 days in a water bath.
- v) The test specimens were removed from the water bath and dried for 24 hours and then subjected to accelerated corrosion. This was achieved by storing them in a tank containing 3.5 % NaCl at room temperature. The experiment was run until a longitudinal crack of 0.2mm width was achieved.



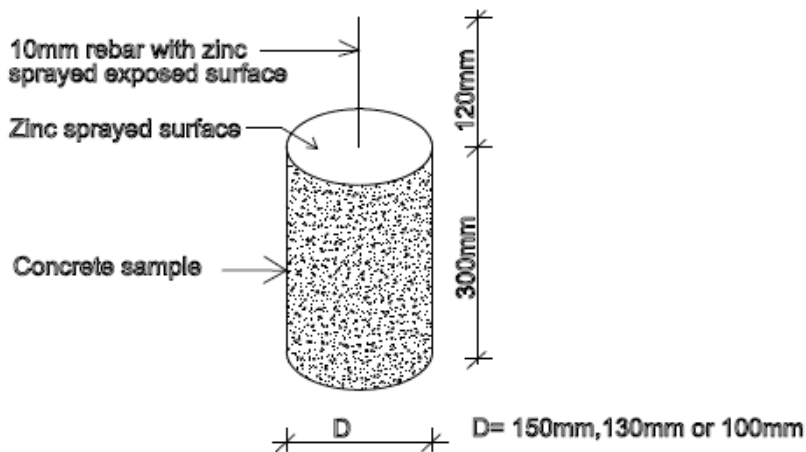


**Figure 3.2: Detail of embedded bar in concrete sample**

**b) Tests program to ASTM G109 07[187]**

The accelerated corrosion tests consist of impressing an anodic current to the rebar in order to enhance its corrosion. Figure 3.3 presents a schematic set up of the experiment.

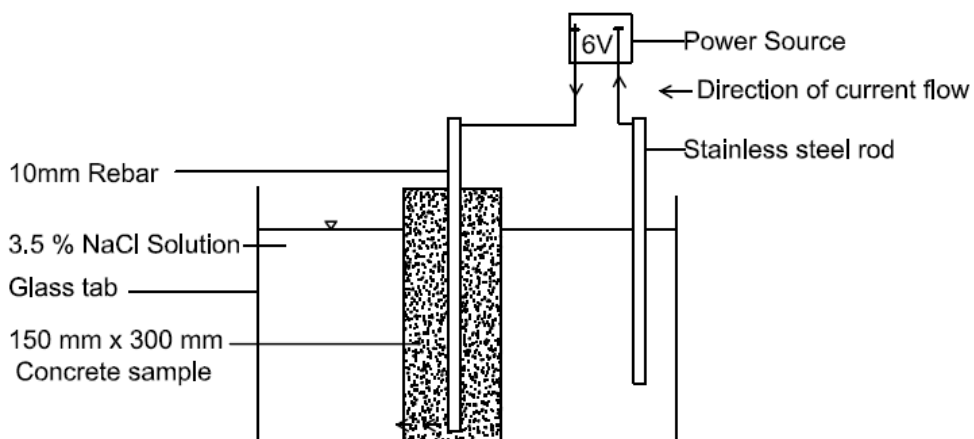


**Figure 3.3(a): Schematic view of accelerated corrosion experimental set up**

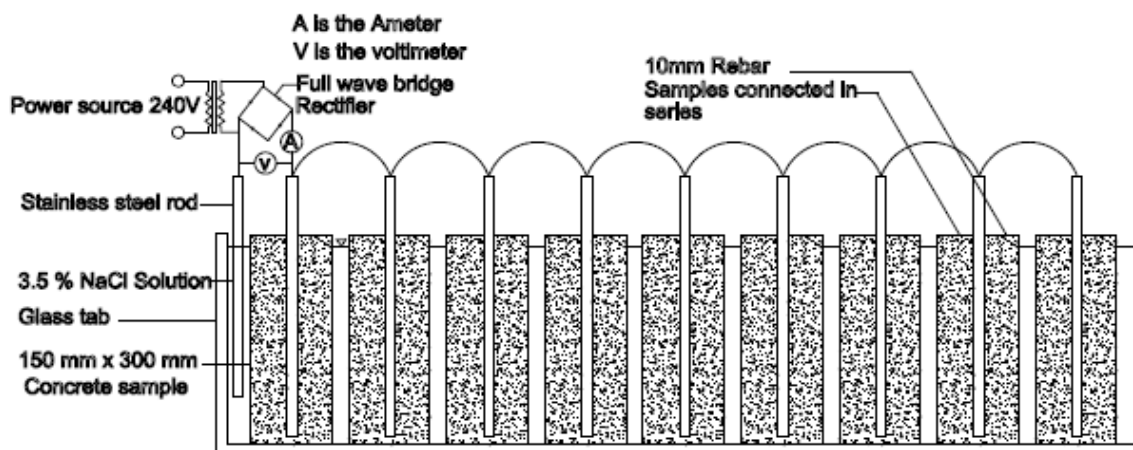


**Figure 3.3:(b) Schematic experimental circuit set up of accelerated corrosion test.**



**Figure 3.3:(c) Accelerated corrosion set up during experimentation.**

Each specimen was immersed in 3.5% sodium chloride solution. A power supply was used to apply a constant direct current of 6Volts between the reinforcement and a counter electrode, made of stainless steel rod. The current applied was assumed to be only possible to flow through the carbon steel-concrete interface. The applied voltage was kept constant continuously and the current response was monitored with respect to time. The variation of current was recorded with time. For each specimen, the time taken for initial crack and the corresponding maximum anodic current flow was recorded.

At the end of the accelerated corrosion test, the embedded steel specimens were recovered by breaking the concrete specimens longitudinaly. They were cleaned, dried and weighed as per ASTM G1-03 [188].

### 3.3.3 Detection of the onset of corrosion-induced Cracking

Once the specimens were subjected to anodic polarization, the applied current and voltage was monitored on a daily, then weekly basis until corrosion induced cracking appeared on the concrete surface. A digital veneer caliper and a magnifying glass of 1000X-magnification were used to monitor the growth of the crack width as shown in Fig. 3.4.a-c.

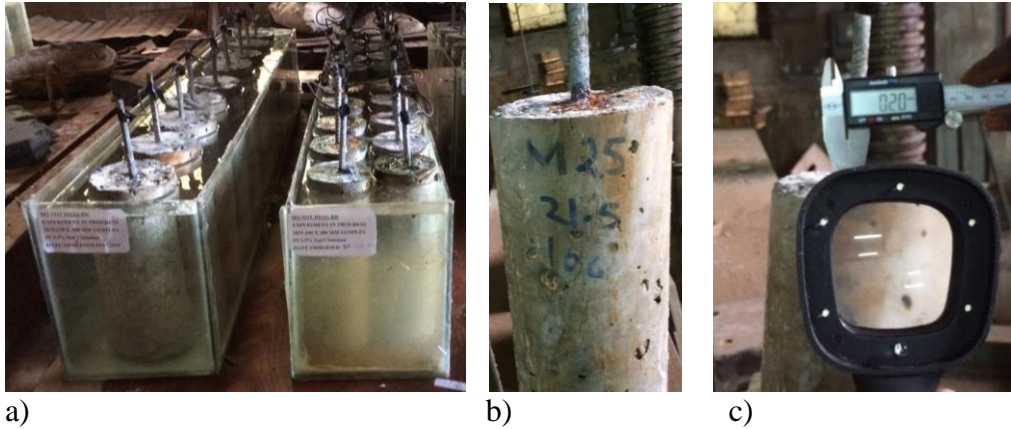


**Figure 3.4: Pictorial view of: a) Samples during experimentation) b) sample with 0.2mm longitudinal crack width c) crack width measurement.**

### 3.3.4 Estimation of critical penetration depth ( $X_{crit}$ )

The cracked specimens were demolished to retrieve the carbon steel segments for inspection of corrosion morphology and for gravimetric evaluation of mass loss as shown in Fig.3.5



**Figure 3.5:(a) recovering the corroded steel, (b) cleaned rebar's for gravimetric weight loss**

The extent to which the steel corrosion product was radially transported into surrounding concrete was visually examined. The surface area of corroded steel regions was estimated by the area covered by the steel corrosion product which was confirmed after rust removal.

The steel corrosion product was removed off the surface of steel segments in accordance with the procedure of ASTM G1-03 [189]. The measured amount of lost steel mass in grams was estimated by subtracting the final weight measured after cleaning from the initial weight. The theoretical mass loss of steel resulting from the applied current was calculated based on Faraday's first law of electrolysis shown in Equation 2.27.

$$\Delta m_F = (M/n \times F) \times I \times t$$

Where:

$(M/n \times F)$  is the electrochemical equivalence of the iron substance

$M$  = the molar mass of iron ( $M=55.847$  g/mol),

$n$  = the effective valence of the iron ions dissolving ( $n=2$ ) and

$F$  = Faraday's constant which is made up of the product of the electron charge by the Avogadro's number ( $F=96485$  C/equivalent).

$(I \times t)$  = the electric charge,

$I$  = the applied anodic current in amperes

$t$  = the time in seconds during which the current has been passed through the circuit.

The distribution of corrosion along and around the surface of steel segments was examined for determination of the type of corrosion (uniform or pitting). The critical penetration depth was determined from Equation 2.16 while the rate of corrosion was determined from the mass loss technique and compared with the current density criteria.

### **3.4 Part 3: To investigate the effect of corrosion inhibitors on the bond strength of reinforced concrete in water conveyance structures.**

#### **3.4.1 General Introduction**

To investigate the bond strength, other properties affected were investigated. This include the compressive and split tensile strength of concrete. The concrete was batched by weights using the building research establishment (BRE) mix design. The mix design is shown in appendix 3. Concrete mixes tested included an ordinary Portland cement concrete control samples, which contained no admixtures. Other specimens included the following inhibitors applied at the respective concentrations of the active ingredient by composition:

- 1) 30% calcium nitrite based inhibitor,
- 2) 30% calcium nitrate based inhibitor,
- 3) fly ash (25% cement replacement),
- 4) 90% dimethylathanolamine based organic inhibitor.

The corrosion inhibitors in combination with the mineral admixtures should provide dual protection, combining the reduced permeability from the mineral admixtures with the passivating mechanism of protection from the inhibitors. It was of interest to determine if effects were cumulative, or if they were diminishing. Calcium nitrite and nitrate based inhibitors were added to mix water at a dosage of 5L/m<sup>3</sup> of concrete while the dimethylathanolamine based organic inhibitor was added at a dosage of 10L/m<sup>3</sup>.

#### **3.4.2 Procedure**

A minimum of three specimens were cast for testing at a time for any test and the average value obtained by testing the specimens considered. A total number of 135 cubes of size 150mm x 150mm x 150mm for compressive strength test, 135 cylinders of 150mm diameter and 300mm long for split tensile strength test, 135 numbers of 150mm diameter and 300mm long concrete

cylinders with centrally placed steel rod of diameter 10 mm and length 1010mm for bond strength

Before pouring the concrete in the moulds of pull out test, the internal surfaces of these moulds were oiled and the sides tightly secured by a binding wire. The length of reinforcing steel bars was about 1010 mm. Fresh concrete was prepared by using an electric mixing pan and poured into the mould in five layers and vibrated by a vibrating table for 60 seconds. After 24 hours, the moulds were removed and the concrete specimens cured in a water tank for 27 days.

Specimens were cured in the curing tanks for a period of 27 days. Concrete cubes and cylinders for each type of cement were cast in 9 samples, and the compressive strength, split tensile strength and pull out strength was tested at 7, 14 and 28 days. All the tests listed below were conducted;

**a) Tests on fresh concrete**

- i) Slump test to BS EN 12350-2:2019 standard
- ii) Compacting Factor test to BS EN 12350-1:2000 standard

**b) Strength tests**

- i) Compressive strength test to BS EN 12390-3:2019 standards
- ii) Split tensile strength test to BS EN 12390-6:2009 standard
- iv) Bond strength test to BS EN 12504-3:2005 standard

**3.4.3 Testing of samples**

**a) Compression test**

The digital compression machine shown in figure 3.6 was used to test concrete cubes at age 7, 14 and 28 days



**Figure 3.6: Digital compression machine for testing cubes**

**b) Split tensile test**

A Universal testing machine(UTM) maximum load of 2000 kN was used to test the cylinders for tensile strength. Fig.3.7 shows a picture and schematic detail of the UTM used during the study for split tensile test. A load was continuously applied without shock at a rate of 1.4 MPa/min.



**Figure 3.7:(a): Pictorial detail of the UTM used during the study**



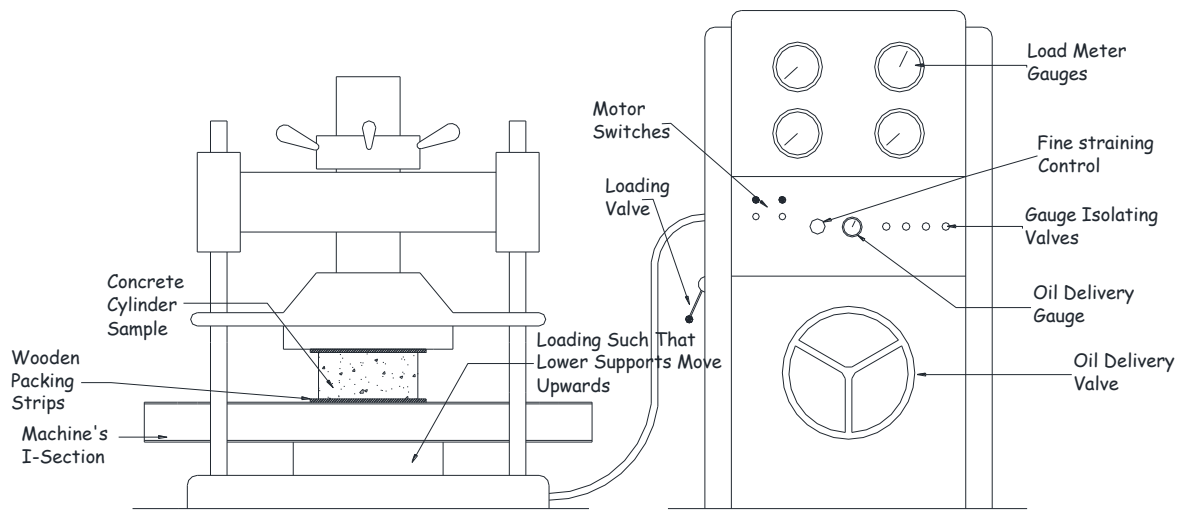


**Figure 3.7:(b): Schematic detail of the UTM used during the study**

### Calculations

The splitting tensile strength(T) of the samples was expressed as shown in Equation 3.1;

$$T = \frac{P_{\max}}{\pi LD} \quad (3.1)$$

Where:

T = splitting tensile strength (MPa)

P = maximum applied load indicated by the testing machine (N)

D = diameter of the specimen(mm)

L = length of the specimen (mm)

### c) Pull-out testing

A hydraulic machine with a loadcell of 100 kN was used to perform the bond tests. The load was applied at a rate of 2 kN/sec and distributed on the specimen surface by a square steel plate with size of 20 cm and a hole at the center. All the specimens were tested at age of 28 days. Fig 3.8 shows the schematic view of the equipment used while Fig.3.9 shows samples during testing.



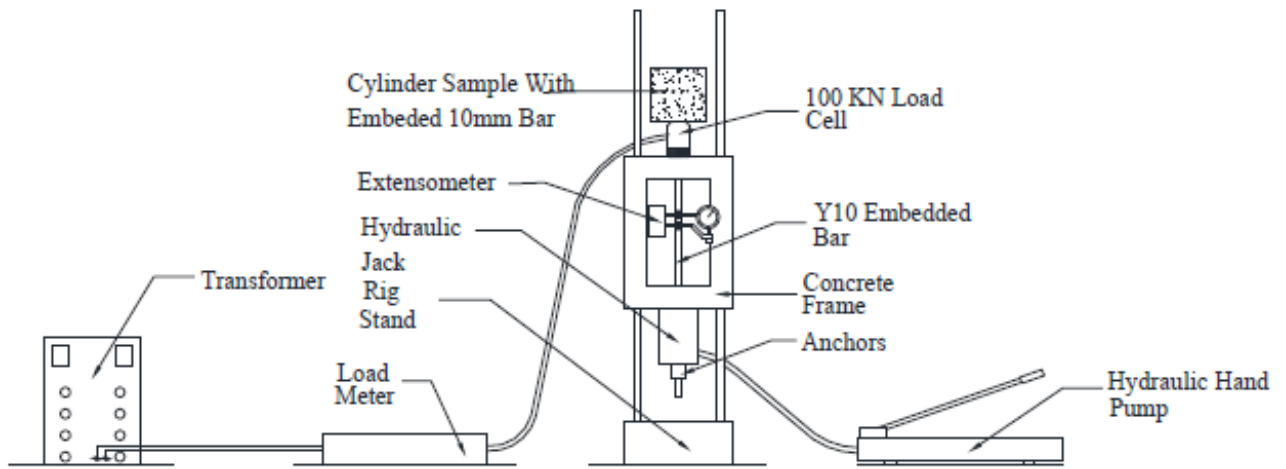


**Figure 3.8: Schematic view of the pull out testing equipment used during the study**



**(a) Sample confining apparatus (b) Tensile load detection equipment**

**Figure 3.9: (a)- (b) Pull out Testing equipment during sample testing**

### **3.4.4 Bond stress calculation**

Bond stress was calculated as average stress between the reinforcing bar and the surrounding concrete along the embedded length of the bar. In general, the bond stress corresponding to the maximum pull out load can be regarded as the bond strength or the ultimate bond. The criterion of ultimate bond strength is characterized by its clear definition and simplicity in bond strength interpretation. For uniform bond, the bond stress  $S$  was calculated from Equation 3.2[190]:

$$S = \frac{P_{\max}}{\pi d_b L_d} \quad (3.2)$$

Where:

$P_{max}$  = maximum pullout load(kN),

$d_b$  = diameter of the bar(mm)

$L_d$  = the embedded bar length(mm).

### 3.5 Corrosion density and Service Life modelling.

#### a) Corrosion current density( $\mu\text{A}/\text{cm}^2$ ) and the rate of corrosion(mm/year)

Corrosion current density is an important input parameter during initiation and propagation period in service life modelling for calculating the rate of corrosion. During initiation period, the corrosion current density was calculated from the following procedure;

- i) The equilibrium corrosion potential was calculated from Equation 2.35 shown below;

$$E_{corr} = \frac{1}{\beta_a + \beta_c} \left[ \frac{\beta_a \beta_c}{2.3} \ln \left( \frac{i_{oc}}{i_{oa}} \frac{C}{C_o} \frac{A_c}{A_a} \right) + \beta_c E_{oa} + \beta_a E_{oc} \right]$$

- ii) With the electric potential as an input parameter, the anodic current during initiation period was calculated from Equation 2.32

$$i_a = i_{oa} 10^{(E_a - E_{oa})/\beta_a}$$

- iii) Having identified the type of corrosion as pitting, the corrosion current density was calculated from Equation 2.34.

$$I_{corr} = i_a \times A_a$$

- iv) The rate of corrosion during initiation period was calculated from Equation 2.24;

$V_{corr}$  (mm/y) =  $0.0116 \alpha I_{corr}$  ( $\mu\text{A}/\text{cm}^2$ ) and compared with the rate of corrosion from the mass loss method from Equation 2.26.

## **b) Service Life modelling**

### **i) Initiation Period**

The initiation period was calculated by dividing the critical penetration depth by the rate of corrosion from Equation

$$T_1(\text{years}) = \frac{x_{\text{crit}}(\text{mm})}{V_{\text{corr}}\left(\frac{\text{mm}}{\text{year}}\right)} \quad 3.3)$$

Where:

$x_{\text{crit}}$  = the critical penetration depth in mm from Equation 2.16,

$V_{\text{corr}}$  = the rate of corrosion in mm/year from Equation 2.24.

### **ii) Propagation period.**

The period from corrosion initiation to 0.2mm cover cracking was calculated from the model developed in section 3.6.

## **3.6 Proposed Service Life Model**

### **3.6.1 Introduction to service life modelling.**

When corrosion of reinforcement develops significantly, the corrosive products expand continuously and generate internal pressure to the concrete surface around the steel bar. The continuous process of reinforcement corrosion affects structural serviceability by cracking, spalling the concrete cover and also decreases the load-carrying capacity thus endangering the structural safety. The physical effects of corrosion include loss of steel area, loss of bond strength between steel reinforcing bars and concrete and reduction of concrete strength due to cracking. In this section, the development of the model due to corrosion cracks was developed.

### 3.6.2 Model development from corrosion product evolution

Based on the material mechanics and elasticity theory of concrete [19,20], consider the embedded steel bars to be a thick wall cylinder as shown in Fig.3.10(a)-(c);

Where:

$c$  = concrete cover in mm;

$d$  = rebar nominal diameter in mm;

$P$ = expansive pressure induced at the steel concrete interface;

Layer 1( $t_2$ ) and layer 2 ( $t_1$ ) are the radial deformation thicknesses in mm of the concrete and the corrosion products at concrete/corrosion products interface, respectively.

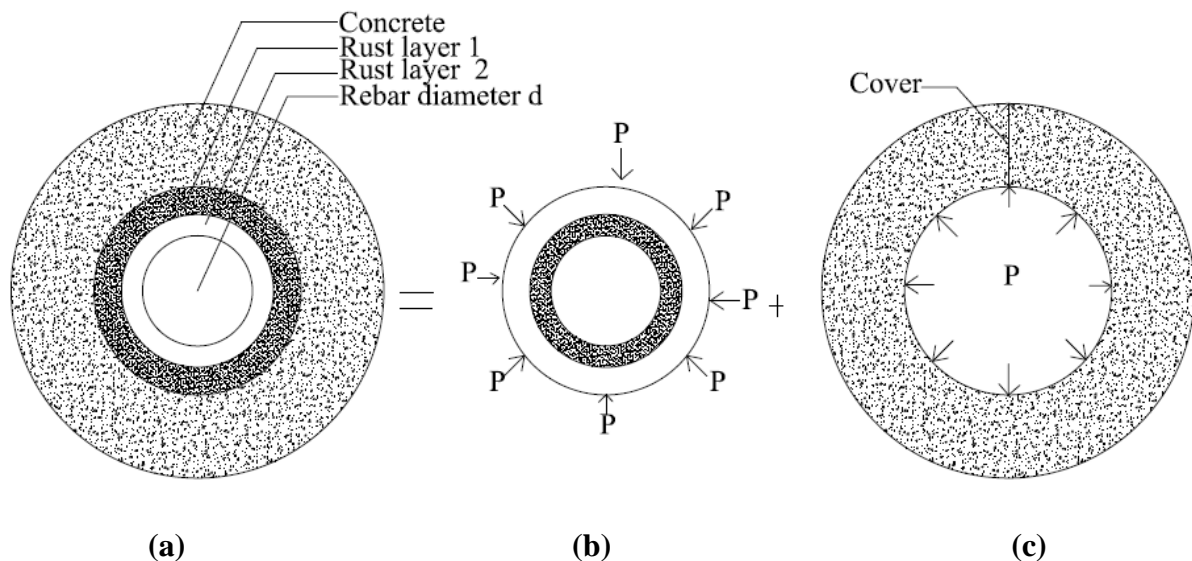


**Figure 3.10 Schematic deformations of expansive pressure on surrounding concrete due to accumulation of rust products (Source: Author)**

The rust layer 2 ( $t_1$ ) is a transition zone between cement paste and aggregate and is influenced by the water/cement ratio, degree of consolidation and hydration, aggregate sizes and steel reinforcement. The mass of corrosion products in this zone denoted as  $M_p$  can be expressed as Equation 3.4,

$$M_p = \rho_{\text{rust}} V_p \quad (3.4)$$

Where:

$\rho_{\text{rust}}$  = the density of corrosion products and

$V_p$  = the total volume of interconnected pores around layer 2 of thickness  $t_1$ .

A steel bar having diameter  $d$  will increase its diameter to  $d+2t_1$ , when the mass of the amount of corrosion products reaches  $M_p$ . For a 290mm length of steel bar, since  $t_1 \ll d$ ,  $M_p$  can be estimated from Equation 3.5,

$$M_p = 0.29\pi\rho_{\text{rust}}dt_1 \quad (3.5)$$

It can be seen that  $M_p$  is related to the size of the reinforcement, density of rust products and property of steel/concrete interface.

**a) Estimation of the critical mass of corrosion products ( $M_{\text{crit}}$ )**

The critical amount of rust products ( $M_{\text{crit.}}$ ) consists of two parts,  $M_p$ , the amount of corrosion products to fill the total interconnected pores around the steel/concrete interface (layer 2), and the amount of corrosion products that generate the critical tensile stresses (layer 1), for of 290mm embedded length of steel bar, the value  $M_{\text{crit.}}$  can be estimated from Equation 3.5,

Let  $t_1 + t_2 = \delta$ , neglecting the deformations of the corrosion products and the remaining steel then,

$$\frac{0.29\pi}{4} [(d + \delta)^2 - d^2] = \frac{M_{\text{rust}}}{\rho_{\text{rust}}} - \frac{M_{\text{st}}}{\rho_{\text{st}}} \quad (3.6)$$

Neglecting  $(\delta)^2$  (since  $\delta \ll d$ ) and rearranging

$$\frac{M_{\text{rust}}}{\rho_{\text{rust}}} = \frac{0.29\pi}{4} [(d + \delta)^2 - d^2] + \frac{M_{\text{st}}}{\rho_{\text{st}}}$$

$$M_{\text{rust}} = \rho_{\text{rust}} \left[ \frac{0.29\pi}{4} 2d\delta + \frac{M_{\text{st}}}{\rho_{\text{st}}} \right]$$

but  $\delta = t_1 + t_2$ , then;

$$M_{\text{crit}} = \rho_{\text{rust}} \left[ \frac{0.29\pi}{2} d(t_1 + t_2) + \frac{M_{\text{st}}}{\rho_{\text{st}}} \right] \quad (3.7)$$

Where:

$\rho_{\text{rust}}$  = the density of corrosion products  $\text{g/cm}^3$ ;

$\rho_{\text{st}}$  = the density of steel in  $\text{g/cm}^3$ ;

$M_{\text{st}}$  = mass loss of the rebar in grams;

$M_{\text{rust}} = M_{\text{crit}}$  = mass of the corrosion product in grams;

$t_1$  = the thickness of the area around the steel/concrete interface and is the radial displacement under pressure in cm;

$t_2$  = the thickness of the corrosion products to generate the tensile stresses in mm;

$d$  = the diameter of the steel reinforcement in cm.

Based on the theory of elasticity Timoshenko and Goodier [209] modelling the reinforced concrete as a thick wall cylinder under internal pressure  $P$ . The pressure  $P$  at concrete/rust products interface can be expressed as Equation 3.8:

$$P = \frac{2E_{\text{ef}}t_2}{(d+2t_1)\left(\frac{b^2+a^2}{b^2-a^2}+v_c\right)} \quad 3.8)$$

Where:

$v_c$  = Poisson's ratio of the concrete;

$E_{\text{ef}}$  = an effective elastic modulus of the concrete;

$a$  = the inner radius =  $(d+2t_1)/2$  in cm;

$b$  = the outer radius =  $C+(d+2t_1)/2$  in cm,  $C$  is the cover in cm in which

$E_{\text{ef}} = E_c/(1+jcr)$ ;

$E_c$  = elastic modulus of the concrete and

$jcr$  = the creep coefficient of the concrete;

$t_2$  = the thickness of the concrete under pressure in cm;

The thickness subjecting concrete under pressure is the thickness of corrosion products generating the pressure on the concrete( $t_2$ ).

At failure and considering that cracking occurred over the reinforcement (the observed corrosion cracks were located above the steel rebars and then longitudinally), the minimum stress required to cause cracking of the cover concrete equals the tensile strength of concrete in Equation 3.9,

$$P = \frac{2Cf_t}{d+2t_1} \quad (3.9)$$

where:

$C$  =the cover depth of concrete;

$f_t$  =the tensile strength of concrete;

From equations 3.8 and 3.9,  $t_2$  may be expressed as Equation 3.10,

$$t_2 = \frac{Cf_t}{E_{ef}} \left( \frac{a^2+b^2}{b^2-a^2} + \nu_c \right) \quad (3.10)$$

Therefore, the critical amount of corrosion products needed to induce cracking of the cover concrete can be estimated from Equation 3.11 by substituting for  $t_1$  and  $t_2$  in Equation 3.7;

$$M_{crit} = \rho_{rust} \left( \frac{0.29\pi}{2} \left[ \frac{Cf_t}{E_{ef}} \left( \frac{a^2+b^2}{b^2-a^2} + \nu_c \right) + t_1 \right] d + \frac{M_{st}}{\rho_{st}} \right) \quad (3.11)$$

From Equation 4.10, the critical amount of corrosion products needed to induce cracking of the cover concrete is dependent on the tensile strength of concrete, cover depth, elastic modulus of concrete and properties of steel/concrete interface.

### **b) Growth of Rust Products**

As the rust layer grows thicker, the ionic diffusion distance increases, and the rate of rust production decreases because the diffusion is inversely proportional to the oxide thickness [210] similar to the assumption was used for atmospheric corrosion, e.g., Fontana and Greene [211]. The rate of rust production can be written as Equation 3.12;

$$\frac{dM_{crit}}{dt} = \frac{k_p}{M_{crit}} \quad (3.12)$$

Where:

$M_{crit}$  = amount of rust products (kg);

$t$  = corrosion time (days) and

$k_p$  = is a constant.

The solution to the differential equation may be written as Equation 3.13;

$$M_{crit}(t) = \sqrt{2k_p t} \quad 3.13)$$

The constant  $k_p$  may be expressed in terms of corrosion rate as given in Equation 3.14[207];

$$k_p = 2.59 \times 10^{-6} (1/\alpha)\pi d i_{cor} \quad 3.14)$$

Where:

$\alpha$  =the ratio of the molecular weight of rust to that of iron;

$d$  =the steel diameter (cm) and

$i_{cor}$  = the annual mean corrosion rate ( $\mu\text{A}/\text{cm}^2$ ).

After calculating the corrosion rate from experimental data, the amount of rust products for a certain period of corrosion can be estimated.

### c) Time to Cracking

When the amount of corrosion products reaches the critical amount, the internal expansion stress will exceed the tensile strength of concrete and cause the cracking of the cover concrete. According to equation 3.15, for a constant corrosion rate, the time to cracking,  $t_{cr}$  in days can be given as follows:

$$t_{cr} = M_{crit}^2 / 2 [2.59 \times 10^{-6} (1/\alpha)\pi d i_{cor}] \quad 3.15)$$

where  $M_{crit}$  is the critical amount of corrosion products. Since corrosion rate is a function of corrosion time as presented in equation 3.14, using the numerical method, the time to cracking can be also calculated from equation 3.15.



Based on calculated critical amount of rust products is obtained from Equation 3.11 and the times to cracking is obtained from equation 3.15. Table 3.3 shows parametric study of the predicted and observed times to cracking of the research and the proposed model.

**Table 3.3: Parametric study of predicted and observed times to cracking of the research and the model**

Sample series	Rebar diameter(mm)	Cover depth(mm)	Measured corrosion rate mm/year	Time in years Model predicted*	Time in years Measured
100mm diameter x 300mm high	10	70	2.78	0.179-0.212	0.208
130mm diameter x 300mm high	10	65	2.74	0.203-0.241	0.236
150mm diameter x 300mm high	10	45	2.68	0.253-0.300	0.293

\*The model predicted times to cracking were calculated taking a value of 0.523 (Fe(OH)<sub>3</sub>) and 0.622 (Fe(OH)<sub>2</sub>)

As it can be seen from Table 3.3 in columns 5 and 6, the measured times to cracking are comparable to the predicted values by the proposed model and proposed model can be relied in its application.

### 3.6.3 The Corrosion initiation period and Current density ( $\mu\text{A}/\text{cm}^2$ )

#### a) Corrosion initiation period

During initiation period, the corrosion current density can be derived from equation 2.34 in which the parameters shown in Table 3.4 have been adopted for calculating the equilibrium potential.

**Table 3.4: Adopted values for determination of equilibrium potential ( $E_{corr}$ )**

Parameter	Value	Reference source
$C(t = 0)$	$0.005 \text{ kg/m}^3$	Bažant, 1979a[162]
$C_o(t = 0)$	$8.576 \times 10^3 \text{ kg/m}^3$	
$E_{oa}$	-3V	Applied Voltage
$i_{oa}$	$3.75 \times 10^{-4} \mu\text{A/cm}^2$	Kranc, S., and Sag˘u´es, A.
$i_{oc}$	$1.25 \times 10^{-5} \mu\text{A/cm}^2$	[163]
$E_{oc}$	3V	Applied voltage
$\beta_a$	0.57 V	Calculated for an equivalent
$\beta_c$	0.42 V	corrosion period
$E_{corr}$	-1.52 V	From equation 2.35
$i_a$	$14.71 \mu\text{A/cm}^2$	From equation 2.32

Inserting the values in Table 3.3 into Equation 2.35

$$E_{corr} = \frac{1}{0.57+0.42} \left[ \frac{0.57 \times 0.42}{2.3} \ln \left( \frac{1.25 \times 10^{-5}}{3.75 \times 10^{-4}} \frac{0.005}{8576} \frac{100}{290} \right) - 0.42 \times 3 + 0.57 \times 3 \right]$$

$$= -1.52\text{V}$$

$$i_a = i_c$$

Substituting the value of  $E_{corr}$  in equation 2.32 and 2.24

$$i_a = 3.75 \times 10^{-4} \times e^{2.3 \left( \frac{-1.52+3}{0.57} \right)}$$

$$= 0.1471 \text{ (A/m}^2\text{)}$$

$$= 14.71 \mu\text{A/cm}^2$$

$$V_{corr} \text{ (mm/y)} = 0.0116 i_a \alpha \text{ (}\mu\text{A/cm}^2\text{)}$$

$$= 0.1705 \text{ mm/year}$$

**b) Corrosion Current density**

For each sample,  $T_1$  was deducted from the total corrosion period to get the propagation period  $T_2$ . The rate of corrosion was from mass loss method calculated from Equation 2.26. Using Equation 2.34 the corrosion current density was calculated and used in Equation 2.24.

**3.6.4 Proposed Service Life Model**

A service life model constitutes of initiation time and propagation time (Equation 3.16);

$$T_{serv.} = T_1 + T_2 \tag{3.16}$$

Where:

$T_{serv}$  = Service Life in (Years)

$T_1$  = Initiation time (Years)

$T_2$  = Propagation time (Years)

**a) Crack Initiation Period ( $T_1$ )**

This is the time to first visible crack and is obtained from Equation 3.17;

$$T_1 = \left( \frac{f_t(c+d)(1+v)}{E_{eff}d\beta} \right) \times 10^{-3} \times \left( 0.0116I_{corr} \left( \frac{\mu A}{cm^2} \right) \right)^{-1} (\text{years}) \tag{3.17}$$

The propagation period from experimental work was obtained from total period for 0.2mm crack evolution minus crack initiation period ( $T_1$ ).

**a) Crack propagation Period ( $T_2$ )**

Equation 3.18 is proposed for calculation of  $T_2$  in days and compared with the experimental results and models of others researchers.

$$T_2 = \left[ \rho_{rust} \left( L \pi \left[ \frac{Cf_t}{E_{ef}} \left( \frac{a^2+b^2}{b^2-a^2} + v_c \right) + t_1 \right] d + \frac{M_{st}}{\rho_{st}} \right) \right]^2 \frac{4.9691\alpha}{di_{corr}} + \left[ \left( \frac{\omega-0.05}{\beta} + x_{crit} \right) \frac{f_t}{0.07192i_{corr}k} \right] \tag{3.18}$$

$T_2$  can be defined into two levels as shown in Equations 3.19 and 3.20;

$$T_2 = T_{p1} + T_{p2}$$

$$T_{p1} = \left[ \rho_{rust} \left( L \pi \left[ \frac{Cf_t}{E_{ef}} \left( \frac{a^2+b^2}{b^2-a^2} + v_c \right) + t_1 \right] d + \frac{M_{st}}{\rho_{st}} \right) \right]^2 \frac{5.846\alpha}{d_{icorr}} \quad (3.19)$$

$$T_{p2} = \left[ \left( \frac{\omega-0.05}{\beta} + x_{crit} \right) \frac{f_t}{0.07192i_{corr}k} \right] \quad (3.20)$$

Where

$L$  = reinforcement length exposed to corrosion(cm)

$C$  = Concrete cover in cm

$\omega$  = characteristic crack width taken as 0.2mm

$x_{crit}$  = critical penetration depth (mm)

$\beta$  = Coefficient taken as 0.01125

$t_1$  = 0.002 cm

$\rho_{rust}$  = 3.6 g/cm<sup>3</sup>

$v_c$  = Concrete poisson's ratio taken as 0.2

$E_{eff}$  =effective elastic modulus= $E/(1+\phi)$  (N/mm<sup>2</sup>)

$E$  = Elastic modulus (N/mm<sup>2</sup>)

$\phi$  = concrete creep coefficient

$k$  = Current density factor taken as 10.

$f_t$  = Concrete tensile strength (N/mm<sup>2</sup>)

$\alpha$  = relation between atomic weight of iron (55.8) and the molecular weight of the rust product taken as 0.523.

$a$  = the inner radius  $[(d+2t_1)/2]$  (cm)

$b$  = the outer radius  $[C+(d+2t_1)/2]$  (cm)

## **CHAPTER 4**

### **4.0 RESULTS AND DISCUSSION**

#### **4.0 Introduction**

In this chapter the results of the study are presented and discussed with reference to the aim of the study- to develop a simulation model to predict the service life of reinforced concrete water conveyancing structures. The four specific objectives were to investigate the critical penetration depth of rust, to investigate the effect of corrosion inhibitors on the bond strength, to develop a corrosion current density model and to develop a corrosion model to predict the service life of reinforced concrete water conveyancing structures. These aspects were described in the previous chapter that presented the methodology used in the study.

The research specific objectives had to be closely adhered to in order to determine model parameters for the main objective. The physical and chemical properties of the materials used have an influence on corrosion and their results and discussions have been presented in section 4.1. The results of accelerated corrosion have been presented in section 4.2 and were used in calculation of the critical penetration depth to achieve the first objective. In section 4.3 the results of the selected corrosion inhibitors on the bond strength of reinforced concrete have been presented and discussed. Finally, for achieving objective three and four, in section 4.4, by utilizing the experimental results, a corrosion current density and service life model for reinforced concrete water conveyancing structures has been proposed and discussed.

#### **4.1 Results of the properties of materials**

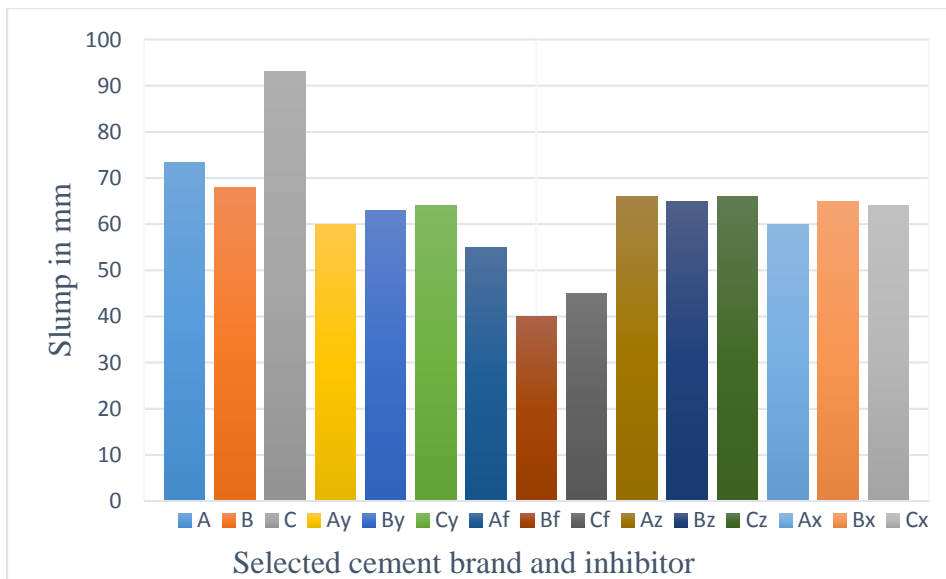
##### **4.1.1 Results of fresh concrete tests**

Table 4.1 shows the result of fresh concrete tests

**Table 4.1: Results(average) of fresh concrete test**

<b>Mix with and without inhibitor</b>	<b>Cement Type</b>	<b>w/c ratio</b>	<b>Slump(mm)</b>	<b>Compaction Factor</b>
Control-No inhibitor	A	0.5	73.3	0.97
	B	0.5	68	0.96
	C	0.5	93	0.95
Inhibitor Y	A	0.5	60	0.95
	B	0.5	63	0.93
	C	0.5	64	0.94
Fly Ash	A	0.5	55	0.93
	B	0.5	40	0.94
	C	0.5	45	0.97
Inhibitor Z	A	0.5	66	0.95
	B	0.5	65	0.95
	C	0.5	66	0.92
Inhibitor X	A	0.5	60	0.96
	B	0.5	65	0.95
	C	0.5	64	0.96

Fig.4.1 shows a relationship between a selected brand of cement with a corrosion inhibitor and the achieved slump as shown in Table 4.1. Similarly, Fig.4.2 shows a relationship between a selected brand of cement with a corrosion inhibitor and the achieved compaction factor.



**Figure 4.1: Relationship between a selected brand of cement with corrosion inhibitor and the achieved slump**

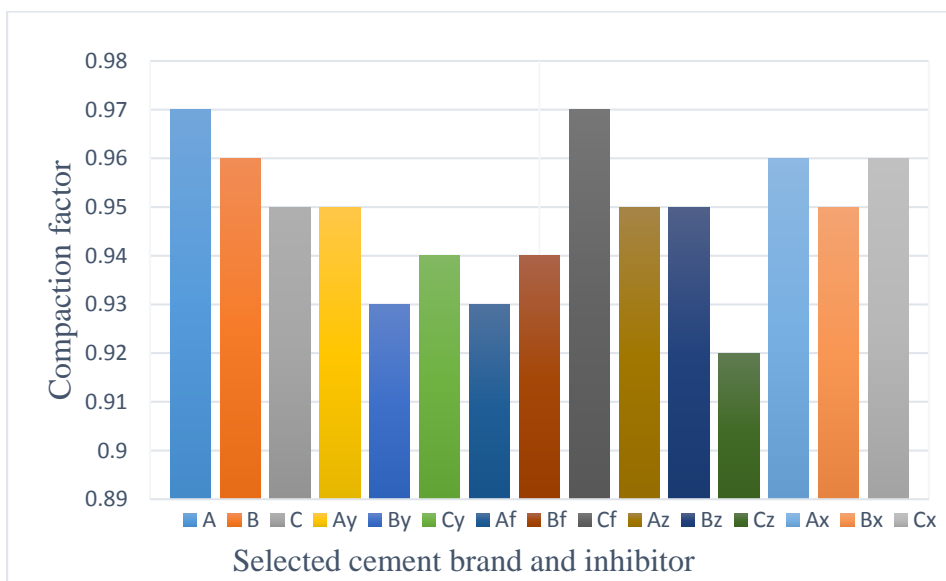


**Figure 4.2: Relationship between a selected brand of cement with corrosion inhibitor and the achieved compaction factor**

From the results of Table 4.1, Fig.4.1 and Fig.4.2, at the same water cement ratio, it can be observed that;

a) all selected cement brands in combination with corrosion inhibitors with exception of fly ash had a plastic workability. Additionally, there was a reduction in workability of all cement

brands in combination with corrosion inhibitors.

b) Fly ash had the lowest slump with all cement brands and on average a stiff plastic workability. Fly ash has spherical shaped particles that act as miniature ball bearings within the concrete mix and require less water for a lubricant effect increasing workability. The strength of concrete is inversely proportional to the workability of concrete. However, it was noted that fly ash concrete gave lowest compressive strength as shown in Section 4.3.2 yet it had the lowest workability. This behavior is due to non-variation of water cement ratio for fly ash concrete. An amount of fly ash in excess of that required to cover the surface of the cement particles would confer no further benefit with respect to water demand. Higher concrete compressive strength slows the percolation of aggressive ions to reinforcement bars to initiate corrosion.

Fig.4.3 shows a relationship between slump and compaction factor achieved in this study.

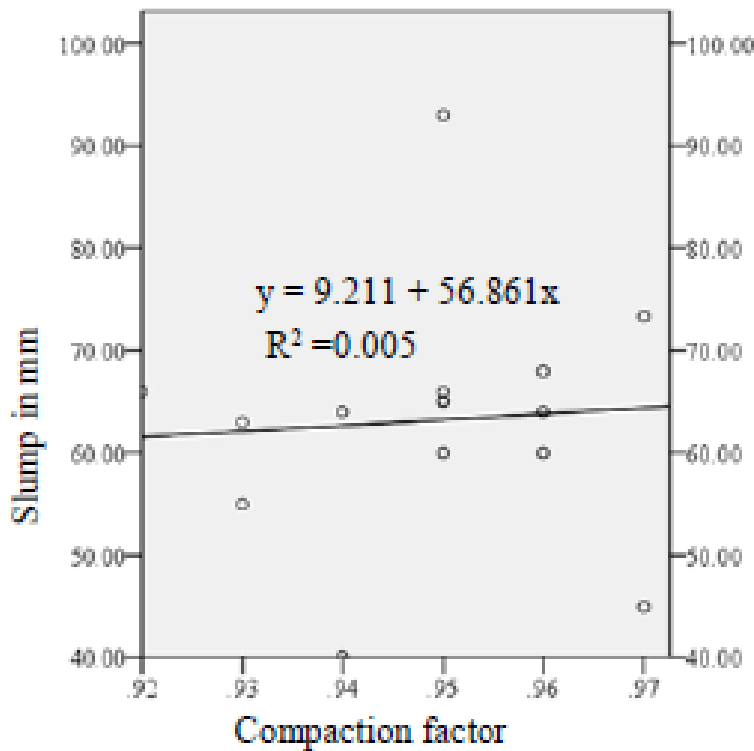


**Figure 4.3: Relationship between slump and compaction factor**



From Fig 4.3, a linear relationship between slump and compaction factor with a regression coefficient of 0.005. By knowing the value of the compaction factor, it is possible to explain 0.5% variance in the slump. The regression coefficient is small due to a smaller quantity of data with a large range. It can be said that for an increase in slump, the compaction factor increases. The linear equation established can be useful if any of the equipment for either the slump test or compaction factor is not available.

#### 4.1.2 Aggregates

##### Physical and mechanical Properties

Table 4.2 shows the physical properties of the aggregates.

**Table 4.2: Physical properties of aggregates used in the study**

Material	Specific gravity	Water Absorption %	Silt content %	Flakiness index %	Max Size
Fine aggregates	2.6	1.8	7.4	-	4.0
Coarse aggregates	2.6	0.3	0	35%	20.0

The specific gravity of all the aggregates are within the limits of 2.4 – 3.0 stated in literature [191-193] and they influence the mix design of the concrete. The water absorption of the fine aggregates is within the limits of 1% – 3% specified in the literature and British Standards [194,195] and therefore a low water absorption hence suitable for concrete works. The very low water absorption in the coarse aggregates need was taken into consideration in the mix design.

ASTM C117[196] give an allowable limit of 10% for silt and clay content in fine aggregates for concrete production while BS 882 give a limit of 4% [197]. As a rule of thumb, the total amount of deleterious materials in aggregates should not exceed 5% [198]. The silt content in

the fine aggregate was more than the allowable percentage of silt content, it was therefore washed and oven dried before use.

The flakiness index for the coarse aggregates was 35% less than the maximum limit allowed by the BS EN 933-3. In flakier aggregates, there is an increased surface area and the density decreases. The compaction of aggregates is less and voids are more and therefore more fines are required to take up this voids. In both cases more cementation material is required from the aggregate cement bond. Voids are filled up with cementitious material and water. The amount of water absorbed by aggregates and cement depends on their surface area. The increase in surface area leads to more friction between the particles and in case of flakiness a locking effect. To counter this more water has to be added for workability. Excess water other than absorbed by aggregates and cement are either used for reaction of cement or evaporates and is lost, both causing voids. The strength of concrete depends on reduction of these voids, bonding between the particles by cement and filling of the voids by cement. More voids in concrete creates more percolation capacity of corrosion agents and this increases the rate of corrosion.

The physical properties of aggregates were within the specified limits and expected to result in reinforced concrete whose rate of corrosion is inversely proportional to their respective characteristic strength.

Gradation as a physical property is one of the most important factors for producing workable concrete, uniform matrix and of sufficient strength. Concrete is viewed as a two phase material, paste phase and aggregate phase. The paste is more permeable than many of the mineral aggregates and is susceptible to deterioration by reacting with aggressive chemicals. Thus, the lesser the quantity of the paste, the better will be the concrete. Well graded aggregates pack

well and reduces the porosity and weak zones in the concrete which limits the percolation routes for ingress of corrosion causing agents.

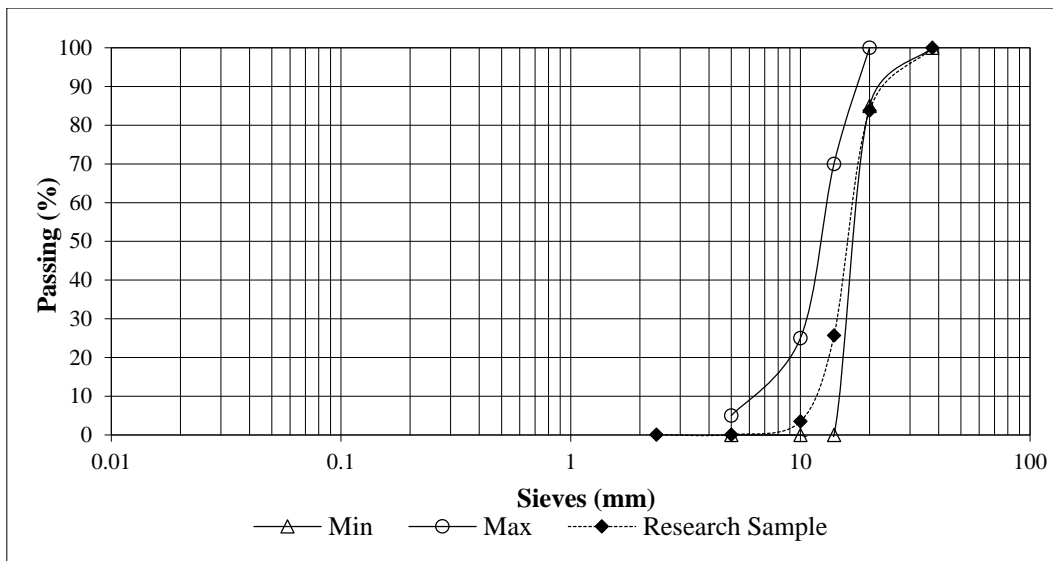
Table 4.3 shows the mechanical properties of the aggregates used in the research.

**Table 4.3: Result of Mechanical Properties of Coarse aggregates**

SN	Property	Test Method	Result	Limit
1.	Loss Angeles Abrasion value	BS/EN 1097-2	20%	30%
2.	Aggregate Crushing Value	BS EN 1097-2	18%	<45%
3.	Aggregate Impact Value	BS EN 1097-2	8%	<45%

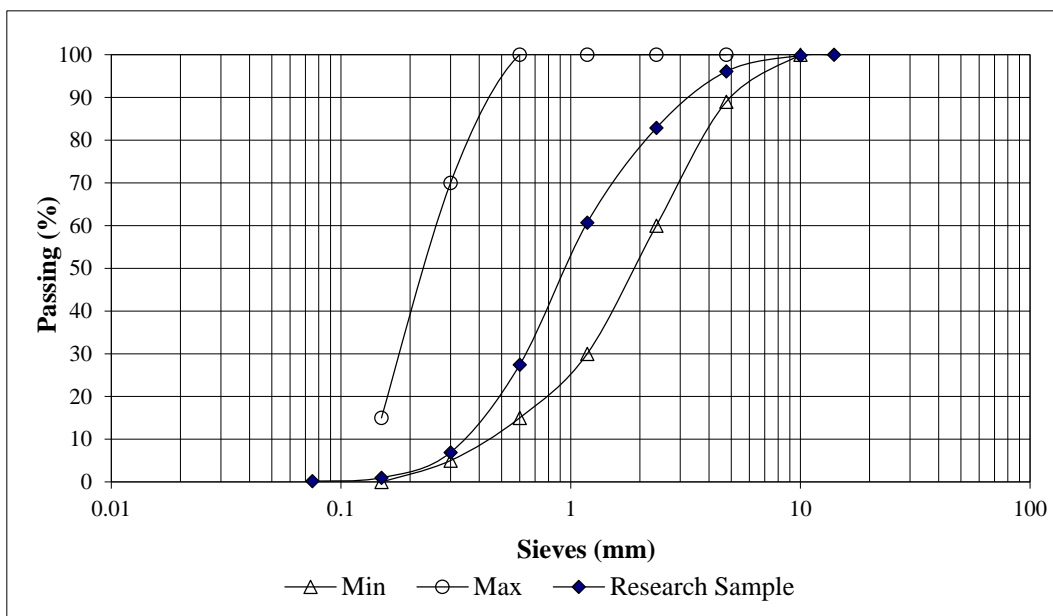
The mechanical properties of aggregates depend on the properties of the parent rock. The Aggregates Impact Value gives a measure of resistance to load 30% as value stated in literature and British Standards [199] and specified in KS EAS 18 [200]. The Aggregate Crushing Value provides resistance of the aggregates to the applied loads and for this research it was within the acceptable limit of 30% for wearing courses. The mechanical properties were suitable for the use in concrete for water conveyancing structures.

Fig. 4.4 and Table (a) in Appendix A1 shows the gradation of the coarse aggregates used in this study.



**Figure 4.4: Grading curve of Coarse aggregates**

The coarse aggregates were of size 5-20mm uniformly graded. Uniformly well graded coarse aggregates give concrete that is well packed and high workability which affects the strength and durability of concrete. The coarse aggregate conforms to BS EN 12620:2002 and suitable for concrete use in water structures. The gradation of the fine aggregates is shown in Fig.4.5 and table b) in Appendix A1.



**Figure 4.5: Grading curve of fine aggregates**

From Fig.4.5, the fines portion that passed the 600micron sieve was used in concrete mix design. This quantity effectively vary the surface contact area exposed to curing and hardening of cement. The fine aggregate conforms to BS EN 12620:2002. The fine aggregates were well graded with 1.7% fines as shown in Fig.4.5 and Table (b) in Appendix A1.

### 4.1.3 Tensile strength and mechanical properties of ribbed bars

#### a) Tensile strength of ribbed bars

Figure 4.6 shows a sample of the Stress strain curve of the 10mm rebar used in the study.

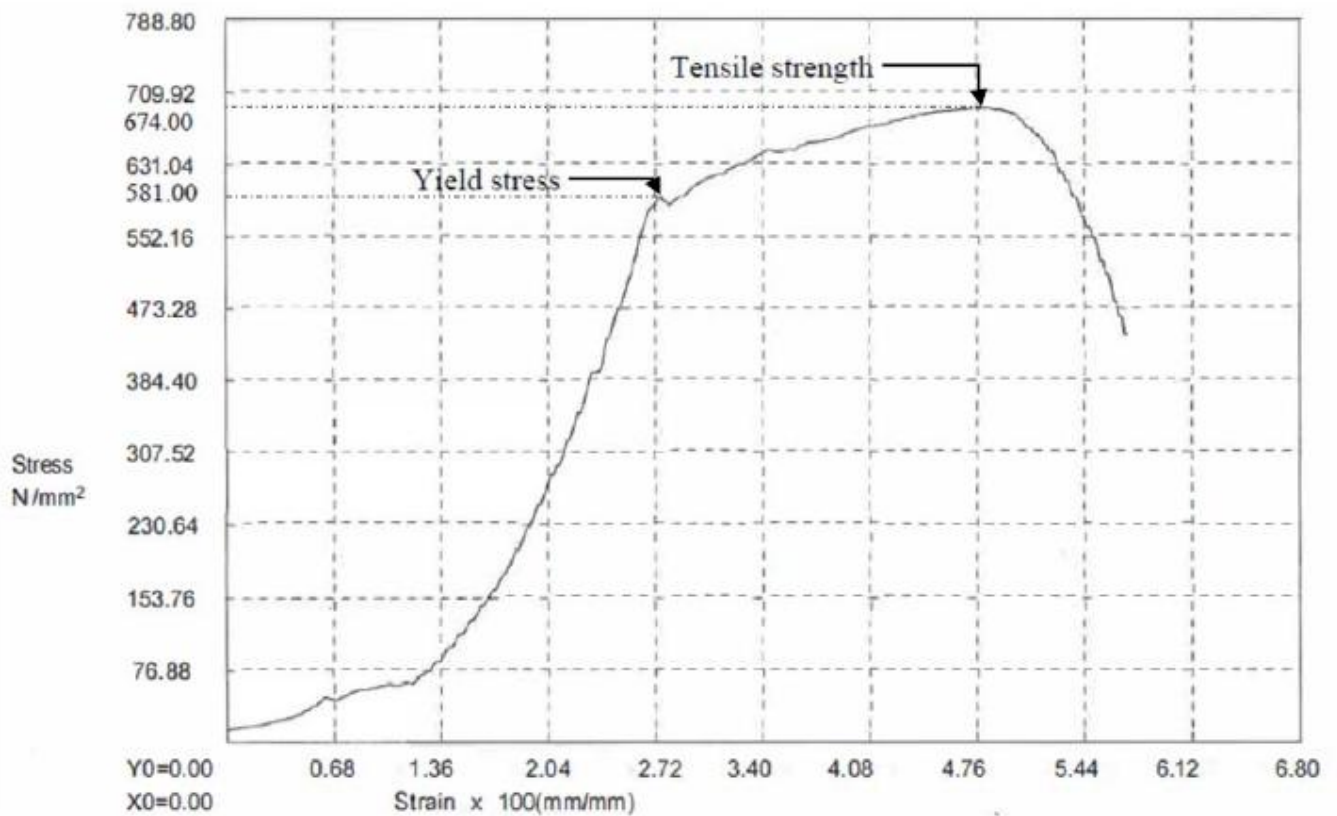


**Figure 4.6: Stress Vs strain graph of 10mm rebars used in the research.**

The graph in Fig. 4.6 reflects a ductile material with a yield strength of 581N/mm<sup>2</sup> which is greater than the 500N/mm<sup>2</sup> acceptance criteria in Table 6 of KS EAS 412-2: 2019. This rebar can withstand large strains as the percentage strain at failure is 101% higher than the yield value.

### b) Chemical properties of ribbed bars used in the study

Reinforcing bar chemistry affects the rate of corrosion by the effect of the constituent alloys.

A summary of the chemical properties is shown in Table 4.4 and Table d in appendix A1

**Table 4.4: Chemical analysis of the 10mm rebar used in the study and their effect**

<b>Element</b>	<b>% Concentration</b>	<b>KS EAS 412-2:2019 Limit</b>	<b>Effect of the on mechanical properties</b>
Carbon (C)	0.209	0.22	Increase hardness and tensile strength but reduces ductility
Silicon(Si)	0.104	0.6	Increases strength, impact strength and toughness, impart corrosion resistance in combination with other elements.
Phosphorus (P)	0.031	0.05	Increases steel embrittlement which reduces the toughness and ductility of the metal.
Manganese (Mn)	0.54	1.6	Improves hardenability, ductility and wear resistance. Mn eliminates formation of harmful iron sulfides, increasing strength at high temperatures
Sulphur (S)	0.025	0.05	Decreases notch impact toughness, reduces weldability and decreases ductility
Chromium (Cr)	0.100	-	Improves hardenability, strength and wear resistance, sharply increases corrosion resistance at high concentrations (> 12%).
Nickel (Ni)	0.071	-	Increases strength, impact strength and toughness, impart corrosion resistance in combination with other elements.
Molybdenum (Mo)	0.013	-	Increases hardenability and strength particularly at high temperatures and under dynamic conditions.
Aluminum (Al)	0.0052	-	Deoxidizer, limits austenite grains growth
Copper(Cu)	0.114	-	Improves corrosion resistance
Titanium(Ti)	0.0008	-	Improves strength and corrosion resistance, limits austenite grain size
Vanadium(V)	0.0047	-	Increases strength, hardness, creep resistance and impact resistance due to formation of hard vanadium carbides, limits grain size
Iron(Fe)	98.78	--	Is the main steel component and is soft in its pure form.
*CEV	0.335		Affects weldability

\*Carbon Equivalent Value

From table 4.4, As per KS EAS 412-2:2019 Limit the carbon equivalent value, CEV,

$$CEV = C + \frac{Mn}{6} + \frac{(Cr+V+Mo)}{5} + \frac{(Cu+Ni)}{15} < 0.50 \quad 4.1)$$

where C, Mn, Cr, V, Mo, Cu and Ni are the mass fractions, expressed as percentages, of the respective chemical elements of the steel.

$$CEV = 0.209 + \frac{0.54}{6} + \frac{(0.1+0.0047+0.013)}{5} + \frac{(0.114+0.071)}{15}$$

= 0.335 < 0.50 therefore acceptable for use as rebar for concrete structures.

Since the CEV and the carbon content are less than 0.50% and 0.25 %, the reinforcement bar is weldable without preheating. From the result of Fig.4.6 and Table 4.4, the steel is acceptable for reinforcement of concrete and confirms the steel density applicable as 7850kg/m<sup>3</sup> applied in modelling in this study. The combination of the chemical constituents in Table 4.4 define the density of steel, and higher steel densities reduce the rate of corrosion during propagation period.

Chromium, Nickel, Copper and Titanium as steel alloys affect corrosion resistance. Chromium as an alloying element in steel helps to increase its corrosion and oxidation resistant properties. From Table 4.4 the percentage of chromium in the steel was 0.1 less than 1.1 required for surface layer formation that helps protect the steel against oxidation. Nickel in combination with other alloys improves the steels corrosion resistance properties. At low concentrations it helps to increase impact strength and hardenability.

In structural steels copper is primarily used as an alloying element to improve atmospheric corrosion resistance and help paint bond the steel. Titanium in steel helps to keep grain size small and also helps manage inclusions by making them rounder.

#### 4.1.4 Chemical Composition of Ordinary Portland cement brands used in the research

Table 4.5 shows the chemical composition of the brands of ordinary Portland cement used in this research.

**Table 4.5: Result of Chemical composition the brands of cement tested.**

SN	Test	Result			KS EAS 18-1: 2001 Requirement
		Sample A	Sample B	Sample C	
1.	CaO%	59.86	59.11	58.82	Sum with SiO <sub>2</sub> ≥ 50
2.	SiO <sub>2</sub> %	16.56	21.56	19.47	Sum with CaO ≥ 50
3.	SO <sub>3</sub> %	2.02	2.78	2.03	≤ 3.5
4.	MgO%	1.76	1.04	0.57	≤ 5
5.	K <sub>2</sub> O%	0.027	0.051	-	
6.	Fe <sub>2</sub> O <sub>3</sub> %	2.32	3.48	1.44	
7.	Al <sub>2</sub> O <sub>3</sub>	7.61	8.09	6.85	3-8
8.	Na <sub>2</sub> O <sub>3</sub> %	0.054	0.018		
9.	LOI%	0.11	0.10	4.75	≤ 5
10.	Cl%	0.012	0.016	0.014	≤ 0.1
11.	IR%	2.20	0.55	1.96	≤ 5

From the results of Table 4.5 all the cements brands selected met the minimum requirement for use and are acceptable for use in Kenya for concrete works. The chemical constituents of the cement affect the strength and durability during construction and in service. As this study is on corrosion chlorides and insoluble residue limitation is critical.

##### **a) Effect of the sum of lime (CaO) and silicon dioxide (SiO<sub>2</sub>) on corrosion**

From Table 4.5 there is a notable variation in the amounts of CaO, SiO<sub>2</sub> and Insoluble Residue. Sample A has the highest amount of CaO (59.86%), Sample B has the highest SiO<sub>2</sub> (21.56%) and Sample A has the highest Insoluble residue (2.20%). The sum of lime (CaO) and silicon dioxide (SiO<sub>2</sub>) obtained in the chemical analysis of ordinary Portland cement should not be less than 50% [199]. All cement samples used for this work satisfied this requirement. Cement



sample B has a CaO + SiO<sub>2</sub> value of 80.67 % and produced the highest compressive strength of 44.89 N/mm<sup>2</sup>. This is consistent with the known fact that both CaO and SiO<sub>2</sub> influence the compressive strength and hence the rate of corrosion of concrete though SiO<sub>2</sub> has to be limited relative to CaO in order not to negatively affect setting time.

**b) Effect of CaO/SiO<sub>2</sub> on corrosion**

The ratio of lime (CaO) to silicon dioxide (SiO<sub>2</sub>) contents in ordinary Portland cement should be greater than 2. The restriction on the ratio of lime to silicon dioxide [201] is to ensure that the quantity of silicon dioxide is considerably lower than that of lime so that the setting of concrete is not inhibited. All the cement samples investigated satisfied this requirement. The lime-silicon dioxide ratio for cement samples A, B, and C were 3.61, 2.71 and 3.0 respectively. Higher the ratios of (CaO/SiO<sub>2</sub>) of cement increases the compressive strength of concrete lowering the rate of corrosion.

**c) Effect of MgO on corrosion.**

The quantity of magnesium oxide (MgO) in ordinary Portland cement should not exceed 5% [201]. All the cement samples satisfied this requirement with 1.76%, 1.04% and 0.57% for cement samples A, B and C respectively. Magnesium oxide contributes to colour of cement and hardness of the resulting concrete. Cement sample A with the highest MgO content of 1.76 % produced concrete with the highest compressive strength as expected since MgO contributes to hardness of concrete and highest bond strength. If the quantity of MgO is in excess of 5 percent, cracks will appear in concrete and which may increase the chloride ingress thus increasing the rate of corrosion.

**d) Effect of SO<sub>3</sub> on Corrosion**

The quantity of Sulphur trioxide (SO<sub>3</sub>) in ordinary Portland cement should be less than 3.5 %. All the samples satisfied this requirement. SO<sub>3</sub> does not have any direct influence on the

strength development or sulfate resistance. The presence of  $\text{SO}_3$  lowers the amount of  $\text{C}_3\text{A}$  and the  $\text{C}_3\text{S}/\text{C}_2\text{S}$  ratio leading to slower strength development and higher the sulfate resistance level lowering the rate of corrosion.

**e) Effect of Chloride Content on corrosion**

The chloride content in ordinary Portland cement should be less than 0.4%. All the cement samples in this work satisfied this requirement. Increased chloride content will increase the rate of corrosion.

**f) Effect of  $\text{Al}_2\text{O}_3$  on corrosion**

Aluminum oxide ( $\text{Al}_2\text{O}_3$ ) aids the quick setting of cement paste. Cement sample B contained the highest quantity of  $\text{Al}_2\text{O}_3$  at 8.09 % resulting in the fastest initial set of the cement paste. Pitting corrosion resistance improves with adding of  $\text{Al}_2\text{O}_3$ , therefore a higher quantity relatively reduces the rate of corrosion.

**g) Effect of  $\text{Fe}_2\text{O}_3$  on corrosion**

Iron oxide ( $\text{Fe}_2\text{O}_3$ ) contributes to cement colour and helps in the fusion of the different ingredients.  $\text{Fe}_2\text{O}_3$  contributes to the tri-layer ( $\text{FeO}/\text{Fe}_3\text{O}_4/\text{Fe}_2\text{O}_3$ ) passive uniform oxide film between 6 and 7 nm that protects the aggressive corrosion agents from the steel surface. The  $\text{Fe}_2\text{O}_3$  contents for the different cement samples are 2.32 %, 3.48 % and 1.4493% for cement samples A, B, and C respectively as shown in Table 3.5.

**h) Effect of Residues on corrosion**

British standards consider  $\text{Na}_2\text{O}$ ,  $\text{K}_2\text{O}$ ,  $\text{TiO}_2$  and  $\text{P}_2\text{O}_5$  in ordinary Portland cement as residues and limit the sum of all of them to 5%. All the cement samples investigated satisfied this requirement with cement samples A, B and C having total residue contents of 0.55, 2.2 and 1.96% respectively. If in excess of 5%, efflorescence and unsightly cracking will occur and increase the rate of corrosion.

#### 4.1.5 Corrosion Inhibitors

##### i) Fly ash

Fly ash acts as an inhibitor by reducing permeability and increasing chloride resistance

Table 4.6 shows the result of the chemical analysis of fly ash that was used in this study.

**Table 4.6: Chemical analysis of the fly ash used in the research**

Parameter	Result	Test Standard
SiO <sub>3</sub>	47.18 %	ASTM C618
Al <sub>2</sub> O <sub>3</sub>	19.87%	
Fe <sub>2</sub> O <sub>3</sub>	10.61%	
UBC	0.99%	
Na <sub>2</sub> O	0.86%	
Fineness(Residue on 45 Micron)	8.69%	
Moisture content	0.07%	
MgO	3.79%	
Cl	0.047%	
Bulk Density	1.03 Gm/cc	
TiO <sub>2</sub>	1.01	
CaO	5.64	
K <sub>2</sub> O	1.17	
P <sub>2</sub> O <sub>5</sub>	0.243	

From result of table 4.6 the % by volume of CaO in the fly ash used is 5.64% which is less than 8% composition by volume and this is fly ash class F as per ASTM C618. Also the sum of SiO<sub>2</sub>, Al<sub>2</sub> O<sub>3</sub> and Fe<sub>2</sub>O<sub>3</sub> by composition in the sample is 71.21% which is greater than 70% as required by ASTM C618 standard for class F fly ash. The fly ash was used in the concrete mix by replacing ordinary Portland cement by 25%. This percentage has the capacity of controlling damaging alkali-silica reaction (ASR) in concrete and the effect has been ascribed to the reduced concentration of alkali hydroxides in the pore solution.

##### iii) **Calcium nitrite and calcium nitrate base inhibitor and dimethylathanolamine based organic inhibitor**

The properties of these inhibitors are contained in the literature review in section 2.4.3.

#### 4.1.6 Concrete strength

Table 4.7 shows a relationship between the compressive and tensile strength of concrete used in this study and how it compares with existing research models. The compressive strength are the averages of the concrete of characteristic strength 25N/mm<sup>2</sup>,30N/mm<sup>3</sup> and 35N/mm<sup>2</sup> respectively. The results for the compressive strengths are attached in Appendix B.

**Table 4.7: Comparative study of concrete strength results used in this research**

Strength Class (N/mm <sup>2</sup> )	Compressive strength (N/mm <sup>2</sup> ) at 28 days	Split tensile strength in N/mm <sup>2</sup>					
		This work $f_i=0.098f_{ck}^{0.999}$	Lavanya & Jegan [202] $f_i=0.249f_{ck}^{0.772}$	ACI Committee 318[203] $f_i=0.56f_{ck}^{0.5}$	Anoglu et al [204] $f_i=0.387f_{ck}^{0.63}$	CEB-FIB [205] $f_i=0.3f_{ck}^{0.66}$	Gardner [206] $f_i=0.33f_{ck}^{0.667}$
25	44.89	4.38	4.70	3.75	4.25	3.70	4.17
30	53.87	5.26	5.41	4.11	4.77	4.17	4.71
35	62.85	6.13	6.09	4.44	5.26	4.61	5.22

From Table 4.7, and using the data obtained from this research, a relationship between the tensile strength and compressive strength is proposed in Fig. 4.4 as Equation 4.2:

$$f_i=0.098f_{ck}^{0.999} \quad 4.2)$$

Where:

$f_i$  =Tensile strength of concrete in N/mm<sup>2</sup>

$f_{ck}$  =Compressive strength of concrete in N/mm<sup>2</sup>.

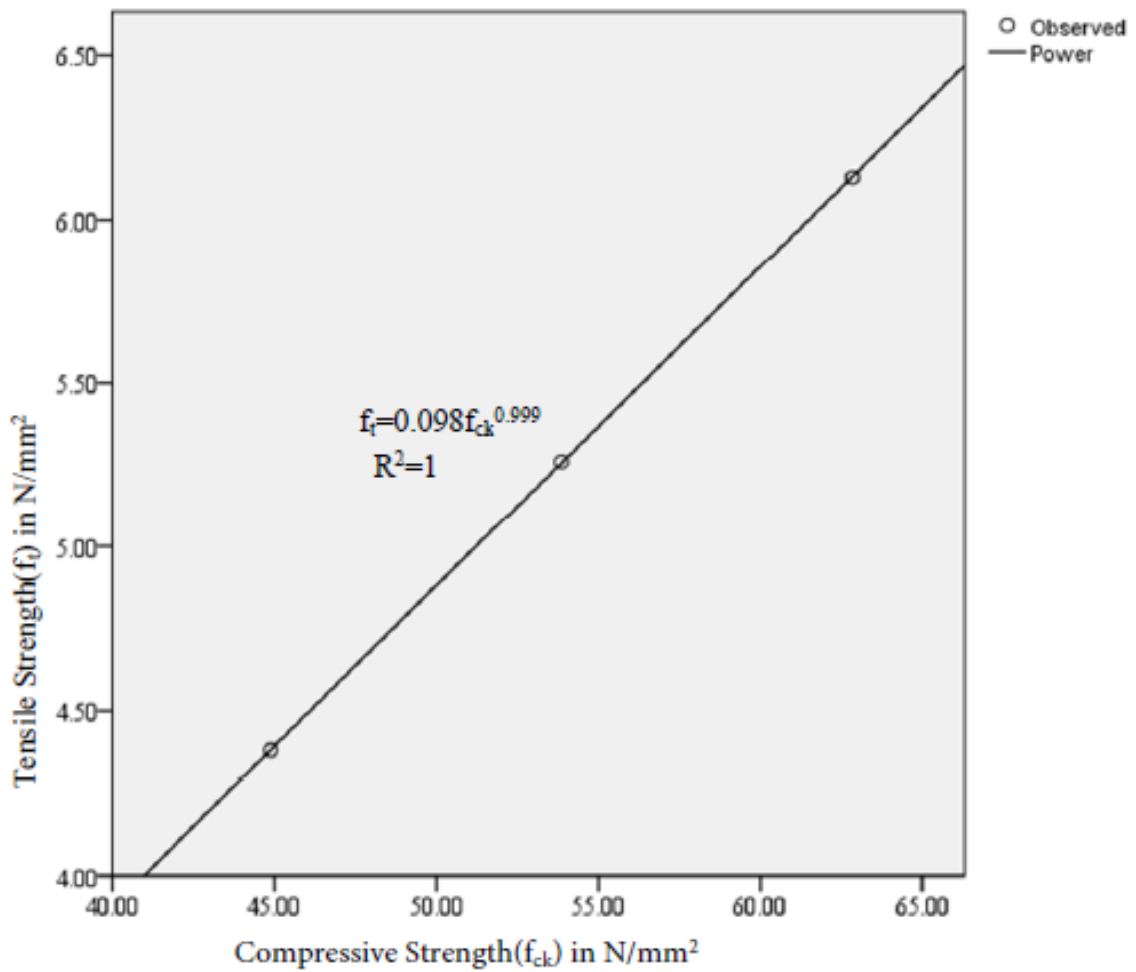


**Figure 4.7: Relationship between tensile and compressive strength for concrete used in the study**

The relationship of the tensile and compressive strength from Fig.4.7 forms a model equation as one of the outputs of this work. Table 4.8 shows a statistical analysis of the output of the proposed model (Equation 4.2) for split tensile strength of this work and results of other researchers.

**Table 4.8: Statistical analysis of the results of tensile strength of this work and the output of other models for Tensile strength.**

	The ratios of split tensile strength of this work and the existing models				
	Mean	Standard deviation	Maximum	Minimum	Maximum-Minimum
This work	5.2567	0.87500	6.13	4.38	1.75
Lavanya & Jegan[202]	5.4000	0.69505	6.09	4.70	1.39
ACI Committee 318[203]	4.1000	0.34511	4.44	3.75	0.69
Anoglu et al [204]	4.7600	0.50507	5.26	4.25	1.01
CEB-FIB [205]	4.1600	0.45508	4.61	3.70	0.91
Gardner[206]	4.7000	0.52507	5.22	4.17	1.05

From Table 4.8, the mean tensile strength of concrete for this study was 5.2567 N/mm<sup>2</sup>, 0.133 N/mm<sup>2</sup> lower than the highest mean, 1.1567 N/mm<sup>2</sup> higher than the lowest mean and hence within the published models. This standard deviation of this study has the highest standard deviation reflecting the spread of the data considered in the difference between the maximum and minimum tensile strength for the characteristic strength of concrete. A bigger sample size could have helped to reduce the standard deviation.

The comparative results of Table 4.7 and 4.8 show that the output of this work is in good agreement with published works of other authors. The split tensile strength is important because it is a function of the initiation time utilized in this work hence its accuracy validation.

## 4.2 Accelerated corrosion Results

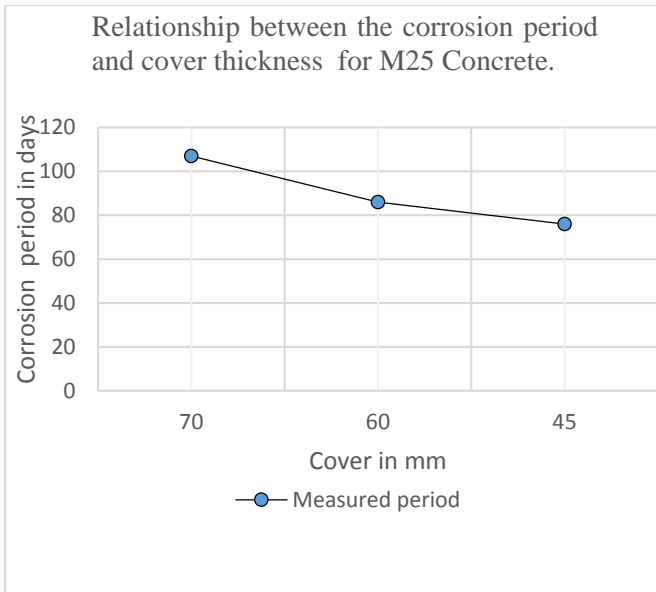
### 4.2.1 Results of accelerated corrosion test

Table 4.9 shows the average duration in days it took the samples to crack to a width of 0.2mm.

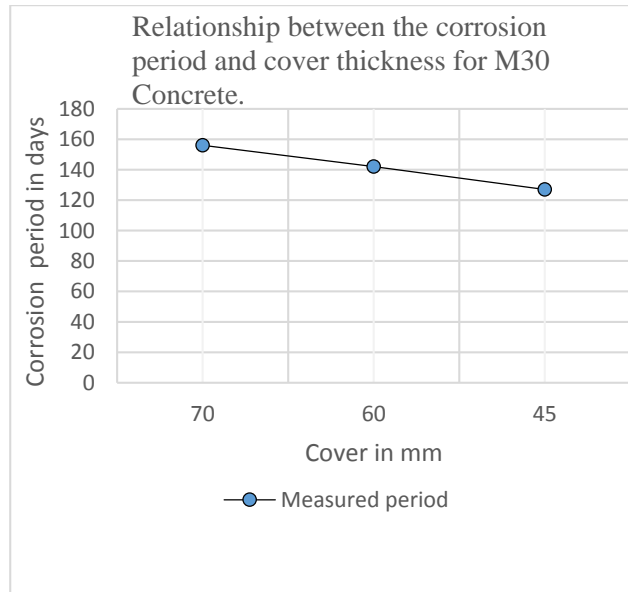
**Table 4.9: Weight loss and duration of accelerated corrosion samples.**

Sample Identity	Characteristic	Strength and Cover	Average mass of steel sample before corrosion (gms)	Average mass of steel sample after corrosion (gms)	Loss in weight (gms) Measured	Loss in weight (gms) Calculated (Eq.2.27)	Duration in days
25	70mm		371	360.4	10.6	10.7	107
N/mm <sup>2</sup>	60mm		371	362.3	8.7	8.7	86
	45mm		371	363.2	7.8	7.6	76
30	70mm		371	361.5	9.5	9.4	156
N/mm <sup>2</sup>	60mm		371	362.4	8.6	8.5	142
	45mm		371	363.4	7.6	7.6	127
35	70mm		371	361.6	9.4	9.3	186
N/mm <sup>2</sup>	60mm		371	362.4	8.6	8.6	172
	45mm		371	363.1	7.9	7.9	158

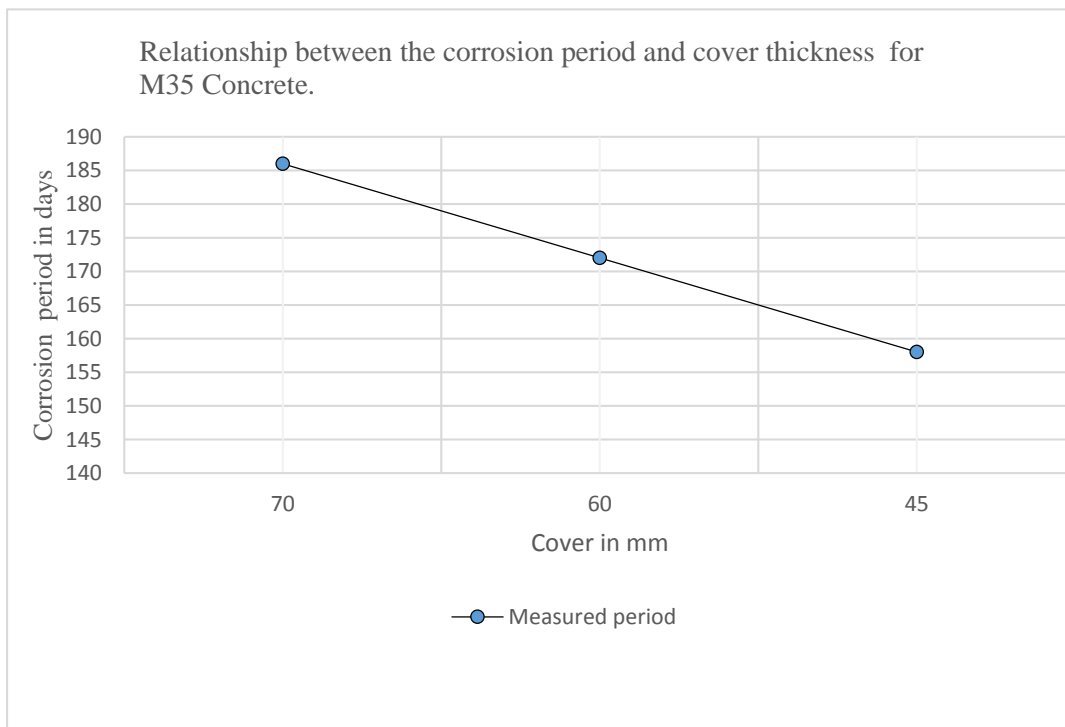
From table 4.9, Fig.4.8(a)-(c) shows the relationship between corrosion period in days and concrete cover in mm while Fig.4.9 (a)-(c) shows the relationship between loss in mass of rebars after corrosion and concrete cover for the concrete classes used in this study.



a)



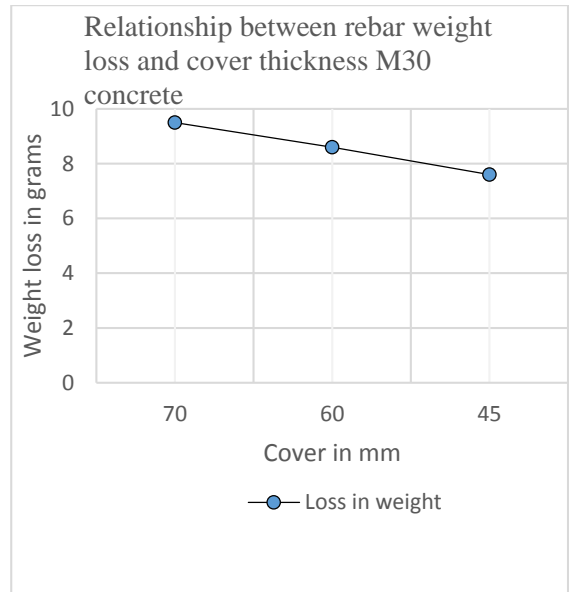
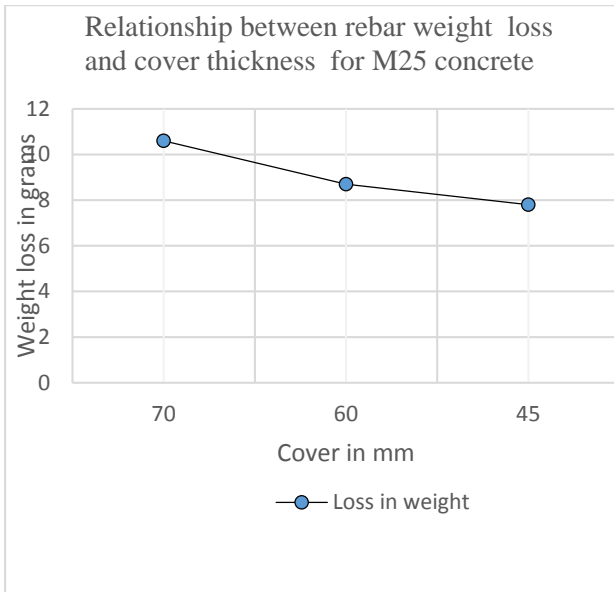
b)



c)

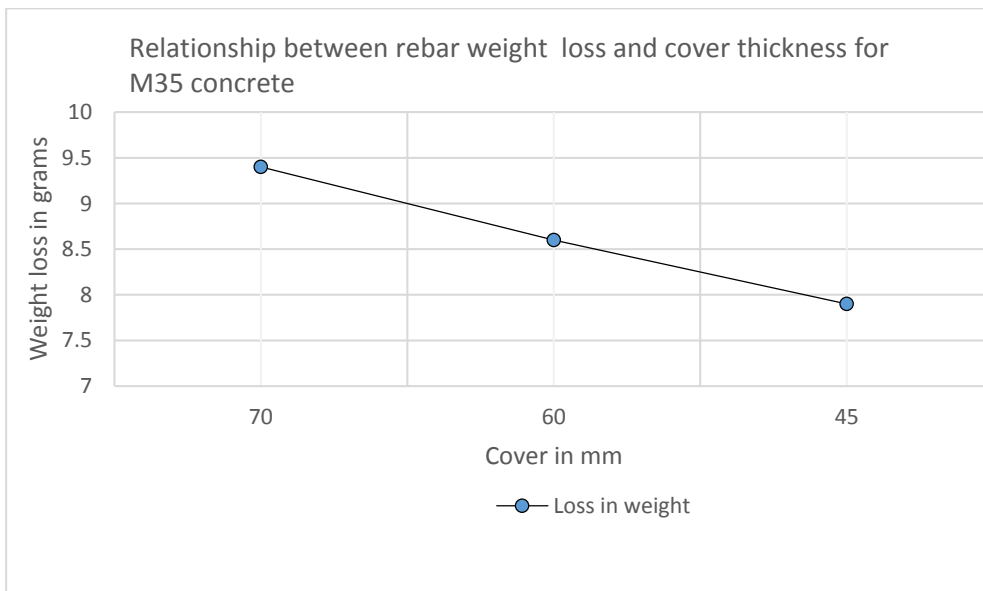
**Figure 4.8: Graph of a relationship between corrosion period in days and concrete cover in mm for concrete of characteristic strength a) 25N/mm<sup>2</sup> b) 25N/mm<sup>2</sup> c) 25N/mm<sup>2</sup>**





a)

b)



c)

**Figure 4.9: Graph of a relationship between loss in mass of rebars in grams after corrosion and concrete cover in mm for concrete of characteristic strength a) 25N/mm<sup>2</sup> b) 25N/mm<sup>2</sup> c) 25N/mm<sup>2</sup>**

From Table 4.9, the measured (an average of 9 bars) and calculated weight loss of the reinforcement bars after accelerated corrosion are very close. This may be attributed to accurate measurement of applied current during the experiment. It can be noted from Fig.4.8(a)-(c) that

the duration to attain the 0.2mm crack increases with increase in concrete cover and strength. This is because in high strength and larger cover, the concrete matrix is more compacted with reduced pore sizes and a longer distance to reinforcement bars for ingress of corrosive aggressive ions. The converse is true for low strength and smaller cover.

From Table 4.9 and Fig.4.9(a)-(c), it can also be noted that there was a reduction in weight loss with a reduction in concrete cover and an increase in strength class. This is because during propagation period, less corrosion products are required to fill the porous surrounding and cause enough expansive pressure for an initiated crack to develop to 0.2mm in samples with smaller covers. The density and volume of cement paste pores tend to be lower in high-strength concrete and, as such, the amount of corrosion product that is absorbed by pores is reduced and the corresponding expansion pressure in the surrounding concrete increases. Therefore, a smaller quantity of corrosion products in higher strength concrete for a crack width to propagate to 0.2mm.

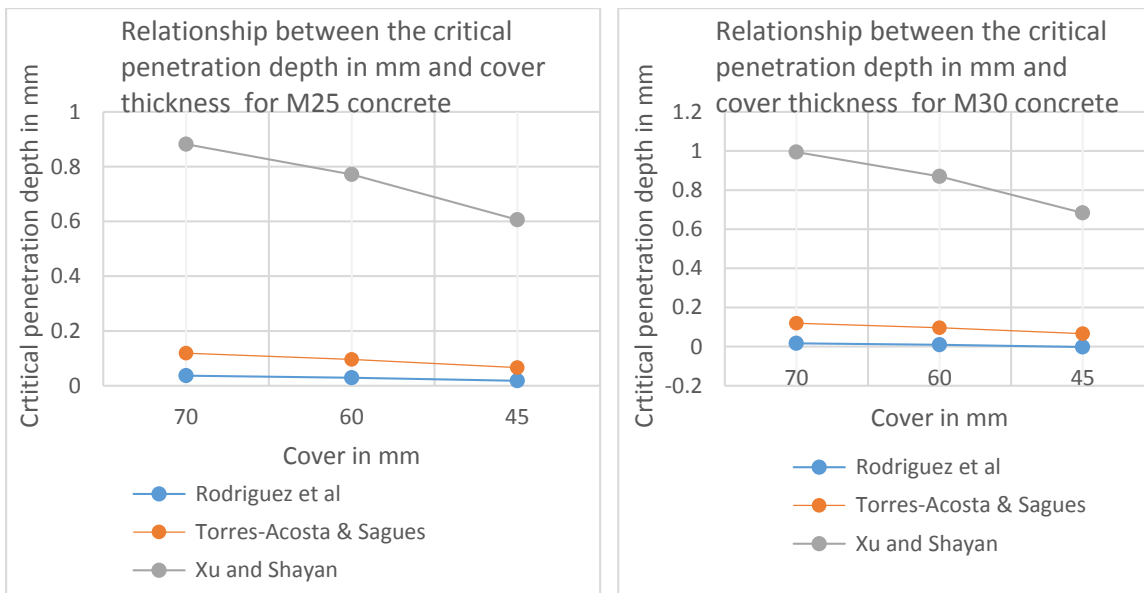
#### **4.2.2 Critical Penetration depth of rust.**

This is the attack penetration depth on reinforcement bar for onset of cracking of cover and the time for this depth to be achieved is the initiation time. From Equation 2.16, the critical penetration depth was calculated and tabulated in Table 4.10 and compared with other models.

**Table 4.10: Critical penetration depth for the samples**

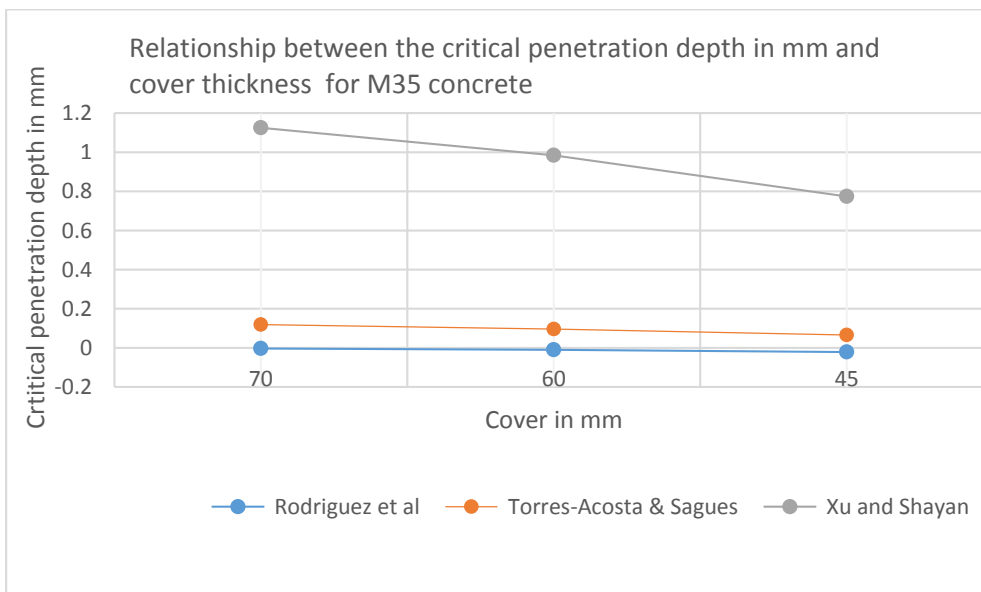
Sample Identity		Compressive strength( $f_{cu}$ ) (N/mm <sup>2</sup> )	Tensile strength( $f_t$ ) (N/mm <sup>2</sup> )	Critical penetration depth mm		
				Rodriguez et al. [53] (Eq.2.15)	Torres-Acosta & Sagues[49] (Eq.2.11)	Xu and Shayan[56] (Eq.2.16)
25	70mm	44.89	4.38	0.0366	0.1190	0.8817
	60mm			0.0292	0.0961	0.7714
	45mm			0.0181	0.0661	0.6061
30	70mm	53.87	5.26	0.0167	0.119	0.9946
	60mm			0.0093	0.0961	0.8703
	45mm			-0.0018	0.0661	0.6838
35	70mm	62.85	6.13	-0.0029	0.1190	1.125
	60mm			-0.010	0.0961	0.9844
	45mm			-0.0214	0.0661	0.7735

From Table 4.10, Fig.4.10 (a)-(c) shows a relationship between the critical penetration depth and concrete cover thickness of selected strength by various authors.



a)

b)



c)

**Figure 4.10: Relationship between the critical penetration depth and concrete cover thickness for (a)M25, (b) M30 and M35 by various authors.**

From the results of Table 4.10 and Fig.4.10, it can be noted that in all the models, the critical penetration depth decreased with decrease in concrete cover. This is due to less quantity of corrosion products to fill the surrounding pores and propagate the initiated crack to 0.2mm in samples with smaller covers in the same strength class. The Torres-Acosta and Sagues model

has no variation in the strength of concrete. It is also noted that in the Rodriguez et al. model, the critical penetration depth tends to below zero for concrete strength of 30N/mm<sup>2</sup> and 35N/mm<sup>2</sup>. This is due to non-consideration of the mechanical properties which affect the resistance of the concrete to cracking. The Xu and Shayan model considers the variants considered in this work and has been adopted in calculation of the initial corrosion period.

The critical penetration depth is essential for determination of the corrosion initiation time from the relation in Equation 3.3 shown below;

$$T_1(\text{years}) = \frac{x_{\text{crit}}(\text{mm})}{V_{\text{corr}}\left(\frac{\text{mm}}{\text{year}}\right)}$$

Where:

$x_{\text{crit}}$  = the critical penetration depth in mm from Equation 2.16,

$V_{\text{corr}}$  = the rate of corrosion in mm/year from Equation 2.24.

### **4.3 Effect of corrosion inhibitors on bond strength.**

#### **4.3.1 Results of hardened concrete with corrosion inhibitors**

##### **a) Compressive strength**

Fig.4.11 shows a relationship of the compressive strength of concrete with selected a selected brand of cement and a corrosion inhibitor at 7,14 and 28 days.

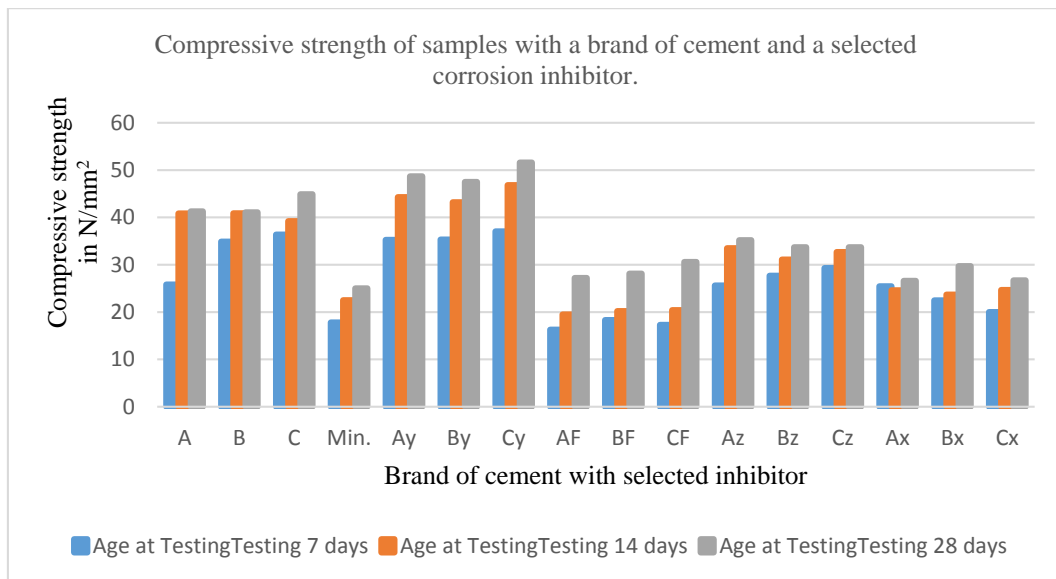


**Figure 4.11: Compressive strength in  $N/mm^2$  of samples with a selected brand of cement and a corrosion inhibitor at 7,14 and 28 days.**

From Fig. 4.10, it can be noted that the corrosion inhibitor with 30% nitrite in combination with selected cement brands had the highest increase in compressive strength as compared to the other inhibitors. The nitrite based corrosion inhibitor increases the degree of hydration of the cement paste. The compressive strength of cement is directly related to the degree of hydration. The hardened cement paste consists of hydrates with various morphologies and densities. The intrinsic strength of the dense, crystalline particles and the bonding properties of well-crystallized material generate bulk strength.

It can also be noted that in all cases, partial replacement of a selected cement brand with fly ash reduced the compressive strength. When replacing part of cement with fly ash, some of  $Ca^{2+}$  was adsorbed on the surfaces of fly ash particles and the decrease of the cement content led to the decrease of  $Ca^{2+}$  concentration in the liquid phase, thus delaying the time of  $Ca^{2+}$  to reach saturation. This leads to an increase of the number of harmful pores consequently reducing compressive strength.

The compressive strength of concrete has an influence on the bond strength and their relationship is critical in bond strength modelling.

**b) Split tensile strength of concrete used in the study**

Fig.4.12 shows the failure mode during split tensile test while Fig.4.13 shows a relationship between the split tensile strength and the corrosion inhibitor in combination with a selected brand of cement.

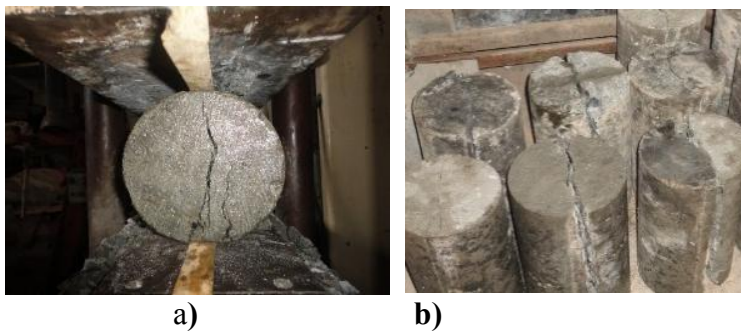


**Figure 4.12: a) and b) Failure mode of the samples during split tensile test.**

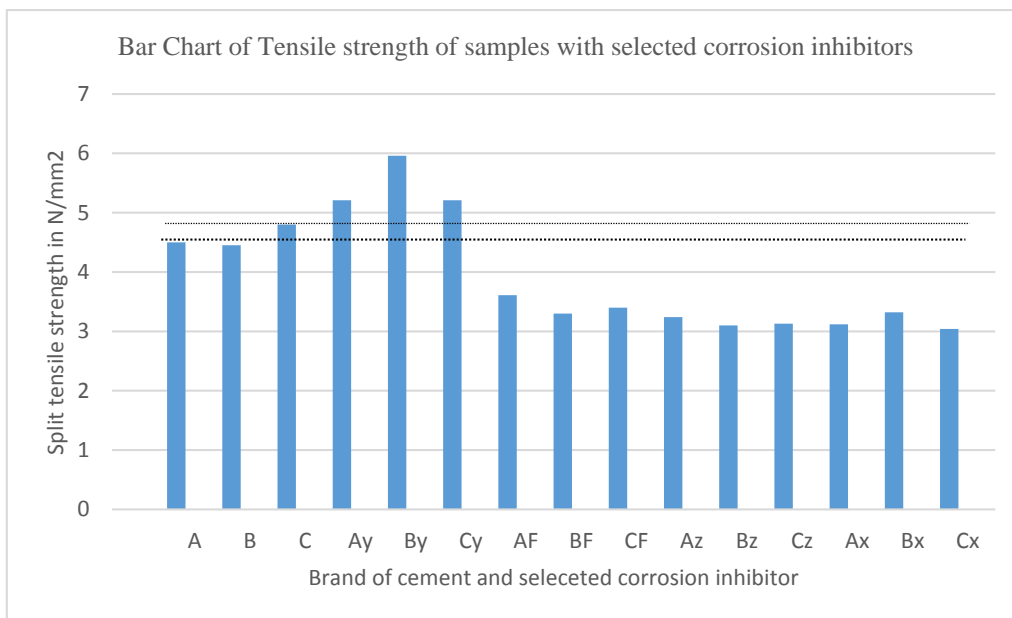


**Figure 4.13: Relationship of Split tensile strength in  $N/mm^2$  for samples with a brand of cement and a selected corrosion inhibitor**

From Figure 2.12 initial cracks were observed near to the top load platens and progressively propagated as wider cracks to the base. This failure pattern is an indication of crack-resisting mechanism nature of concrete as a brittle material.

From Fig.4.13, it can be noted that the corrosion inhibitor with 30% calcium nitrite in combination with selected cement brands had an increased split tensile strength and the converse is true for all the other corrosion inhibitors. The corrosion inhibitors influence in the split tensile strength of concrete is most likely caused by their reaction with water and cement during the hydration process.

Figure 4.14 shows the effect of a choice of a corrosion inhibitor with a selected cement brand on bond strength of reinforced concrete in the study.

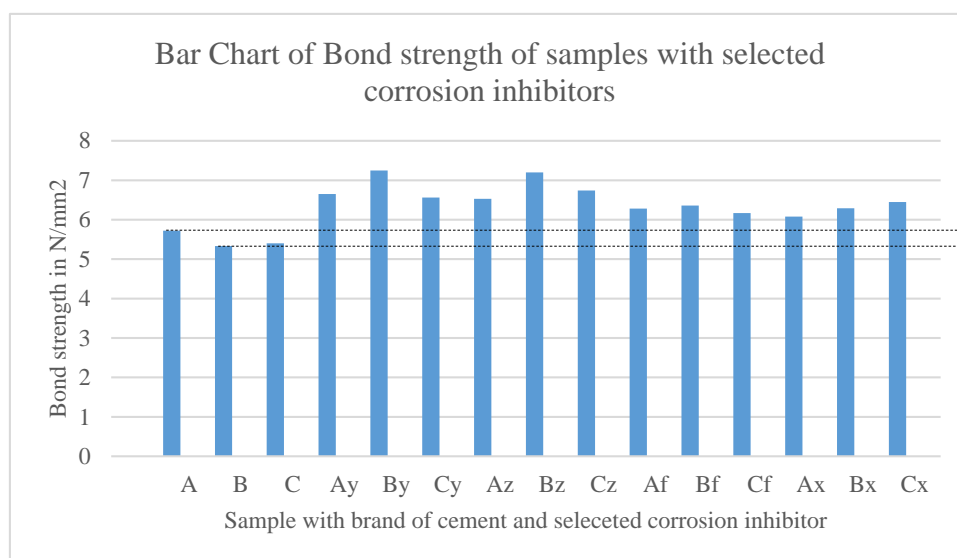


**Figure 4.14: Relationship of bond strength in N/mm<sup>2</sup> for samples with a brand of cement and a selected corrosion inhibitor**

From Fig.4.14, all corrosion inhibitors in combination with the respective cement brand selected increased the bond strength with use of inhibitor x giving the lowest result. The corrosion inhibitors increase in bond strength of concrete is most likely caused by their reaction with water and cement during the reaction of cement hydration thus affecting the compressive



strength. Most bond strength models have based their result on compressive strength and hence the need for a parametric study of the result of this research with the models of other authors.

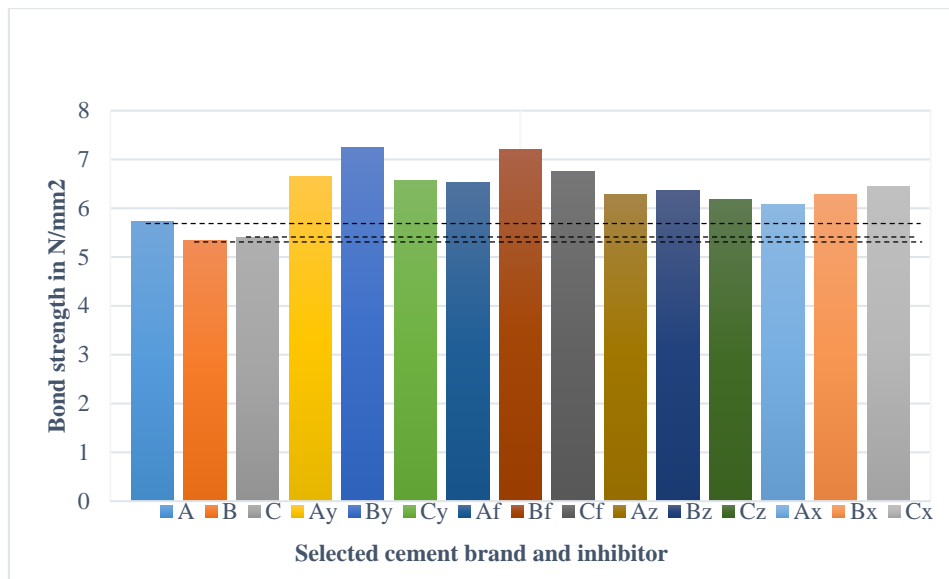
### 4.3.3 Parametric study of the results

Table 4.11 gives a comparative result of the concrete strength of this study and the split tensile strength from works of other authors

**Table 4.11: Comparative study of results of hardened concrete.**

Selected inhibitor	Cement Brand Sample	Bond strength	Compressive strength (N/mm <sup>2</sup> ) at 28 days( $f_{ck}$ )	Split tensile strength in N/mm <sup>2</sup>					
				Measure d Value	Lavanya & Jegan $f_{t1}=0.249f_{ck}^{0.772}$	ACI Committee $318 f_{t2}=0.56f_{ck}^{0.5}$	Anoglu et al $f_{t3}=0.387f_{ck}^{0.63}$	CEB-FIB $f_{t4}=0.3f_{ck}^{0.66}$	Gardner $f_{t5}=0.33f_{ck}^{0.667}$
No Inhibitor	A	5.72	41.29	4.50	4.40	3.60	4.03	3.50	3.95
	B	5.33	41.09	4.45	4.39	3.59	4.02	3.48	3.93
	C	5.40	44.89	4.80	4.70	3.75	4.25	3.69	4.17
Inhibitor Y	A	6.65	48.7	5.21	5.00	3.91	4.48	3.90	4.40
	B	7.25	47.5	5.96	4.90	3.86	4.41	3.83	4.33
	C	6.56	51.6	5.21	5.23	4.02	4.64	4.05	4.58
Inhibitor Z	A	6.53	35.2	3.61	3.89	3.32	3.65	3.15	3.55
	B	7.20	33.7	3.30	3.76	3.25	3.55	3.06	3.45
	C	6.74	33.69	3.40	3.76	3.25	3.55	3.06	3.45
Fly Ash	A	6.28	27.27	3.24	3.20	2.92	6.65	2.66	3.00
	B	6.36	28.13	3.10	3.27	2.97	3.17	2.71	3.06
	C	6.17	30.6	3.13	2.94	3.10	3.34	2.87	3.23
Inhibitor X	A	6.08	26.6	3.12	3.13	2.89	3.06	2.62	2.94
	B	6.29	29.7	3.32	3.41	3.05	3.28	2.81	3.17
	C	6.45	26.7	3.04	3.14	2.89	3.06	2.62	2.95

From Table 4.11, Fig.4.15 show a relationship between the bond strength and a selected brand of cement with a corrosion inhibitor. Similarly, Fig. 4.16 shows a relationship between tensile strength and compressive strength. Further, Fig.4.17 shows a parametric relationship of the split tensile strength output of this work and other researches.



**Figure 4.15: Relationship between the bond strength and a selected brand of cement with a corrosion inhibitor.**

From Figure 4.15, it can be noted that all corrosion inhibitors with selected brand of cement increased the bond strength due to increase in compressive strength. The variation in the increase of bond strength can be partially attributed to the variation of the chemical composition of the interfacing cement paste with the embedded bar. Bond strength between the rebar and the concrete significantly affects the performance of reinforcing steel as it affects the structure's overall strength.

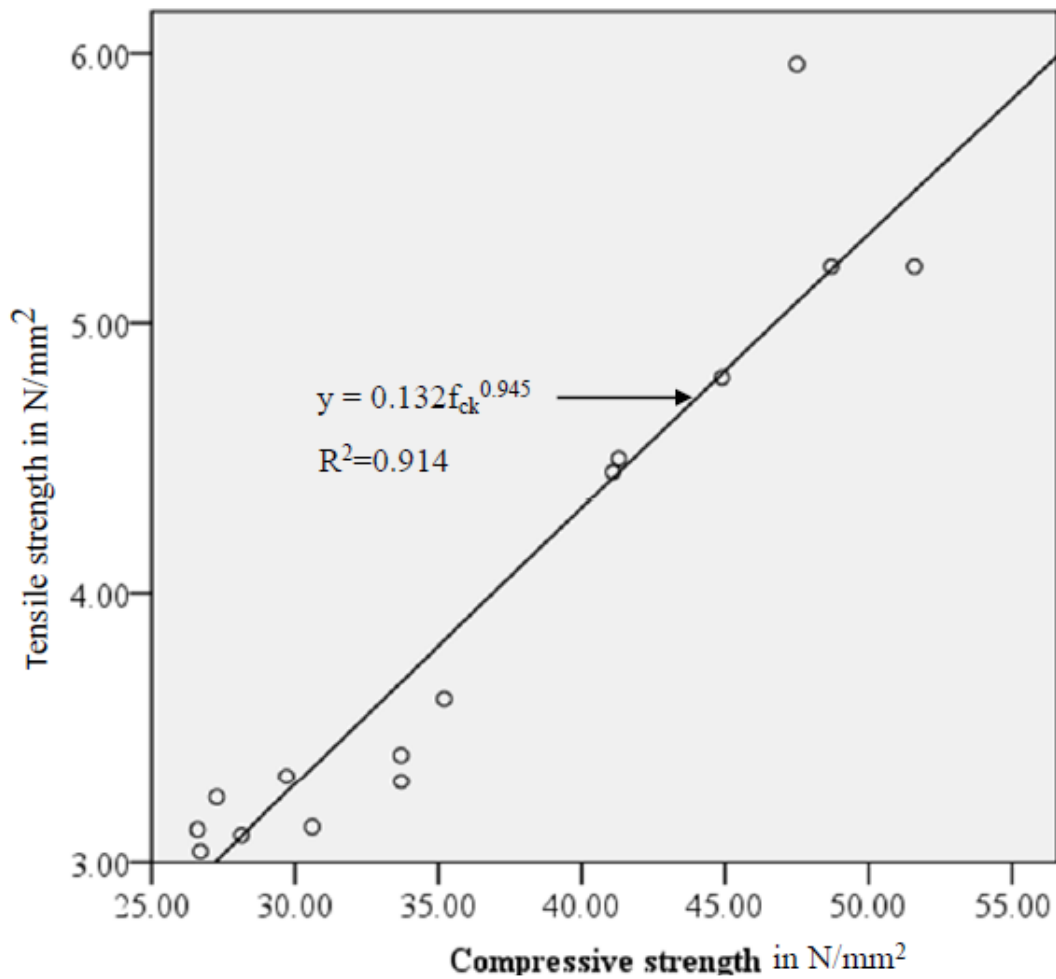


**Figure 4.16: Relationship between the tensile strength and bond strength form Table 4.11.**

From Fig.4.16, the standard deviation is high due to consideration of two variables resulting in a wider range of compressive strength result. A model Equation shown on the graph has been established from the results of this study which can be useful in comparing with other published models. The model equation is also useful in calculating the tensile or compressive strength given any one of them as a known variable.

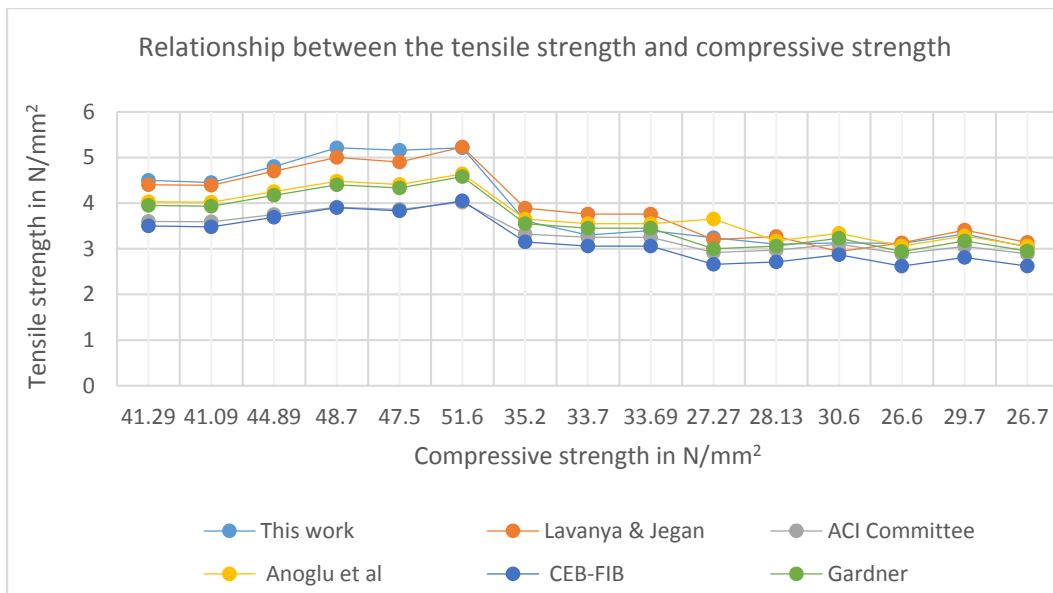


**Figure 4.17: Correlations of Result of Split tensile strength of this work with results of other authors.**

From Fig.4.17, it can be noted that the measured split tensile strength generally compares well with the output of other authors and hence reliable. Table 4.12 shows a Pearson Correlation of the measured split tensile strength of this study and with the output of other researchers.

**Table 4.12 shows a Pearson Correlation of the measured split tensile strength of this study and with the output of other researchers.**

		This work (measured)	Lavanya & Jegan	ACI Committee 318	Anoglu et al	CEB-FIB	Gardner
This work (measured)	Pearson Correlation	1	0.945**	0.947**	0.369	0.948**	0.948**
	Sig. (2-tailed)		0.000	0.000	0.176	0.000	0.000
Lavanya & Jegan	Pearson Correlation	0.945**	1	0.982**	0.330	0.983**	0.983**
	Sig. (2-tailed)	0.000		0.000	0.230	0.000	0.000
ACI Committee 318	Pearson Correlation	0.947**	0.982**	1	0.302	1.000**	1.000**
	Sig. (2-tailed)	0.000	0.000		0.274	0.000	0.000
Anoglu et al	Pearson Correlation	0.369	0.330	0.302	1	0.308	0.310
	Sig. (2-tailed)	0.176	0.230	0.274		0.264	0.261
CEB-FIB	Pearson Correlation	0.948**	0.983**	1.000**	0.308	1	1.000**
	Sig. (2-tailed)	0.000	0.000	0.000	0.264		0.000
Gardner	Pearson Correlation	0.948**	0.983**	1.000**	0.310	1.000**	1
	Sig. (2-tailed)	0.000	0.000	0.000	0.261	0.000	

\*\* . Correlation is significant at the 0.01 level (2-tailed).

From Table 4.11, the measured split tensile strength association with the output of Lavanya and Jegan, ACI Committee, CEB-FIB and Gardener was very high ( $r=0.945$ ,  $r=0.947$ ,  $r=0.948$  and  $r=0.948$ ) and the correlation coefficient is very highly significantly different from zero ( $P < 0.001$ ). The association of the measured of the measured split tensile strength with the output of Anoglu et al is low ( $r=0.369$ ) or 13.69% ( $0.369^2$ ) of the variation in Anoglu et al can be associated with the output of this study. Therefore, except for Anoglu et al, the measured split tensile strength strongly correlates with the output of the other authors considered.

Table 4.13 shows a parametric study of bond stress result of this work with result of other

authors.

**Table 4.13: Parametric study of bond strength of this work with other authors.**

Selected inhibitor	Cement Brand Sample	Bond Strength (N/mm <sup>2</sup> )	Orangun et al* [204]	Bond Strength(N/mm <sup>2</sup> ) Stanish et al [205] $\tau_u=[0.77 - 0.027C_o]\sqrt{0.8f_{cu}}$
No	A	5.72	3.20	4.43
Inhibitor	B	5.33	3.19	4.41
	C	5.40	3.34	4.61
Inhibitor Y	A	6.65	3.45	4.81
	B	7.25	3.43	4.75
	C	6.56	3.56	4.94
Inhibitor Z	A	6.53	2.95	4.09
	B	7.20	2.89	4.00
	C	6.74	2.89	4.00
Fly Ash	A	6.28	2.60	3.60
	B	6.36	2.64	3.65
	C	6.17	2.76	3.81
Inhibitor X	A	6.08	2.66	3.55
	B	6.29	2.72	3.75
	C	6.45	2.57	3.55

$$* \tau_u = 0.083045\sqrt{f_{cu}} \left[ 1.2 + 3 \left( \frac{c}{d_b} \right) + 50 \left( \frac{d_b}{L_d} \right) \right]$$

From Table 4.13, Fig.4.18 shows a relationship of measured bond strength with the output of other authors for a selected brand of cement and a corrosion inhibitor.

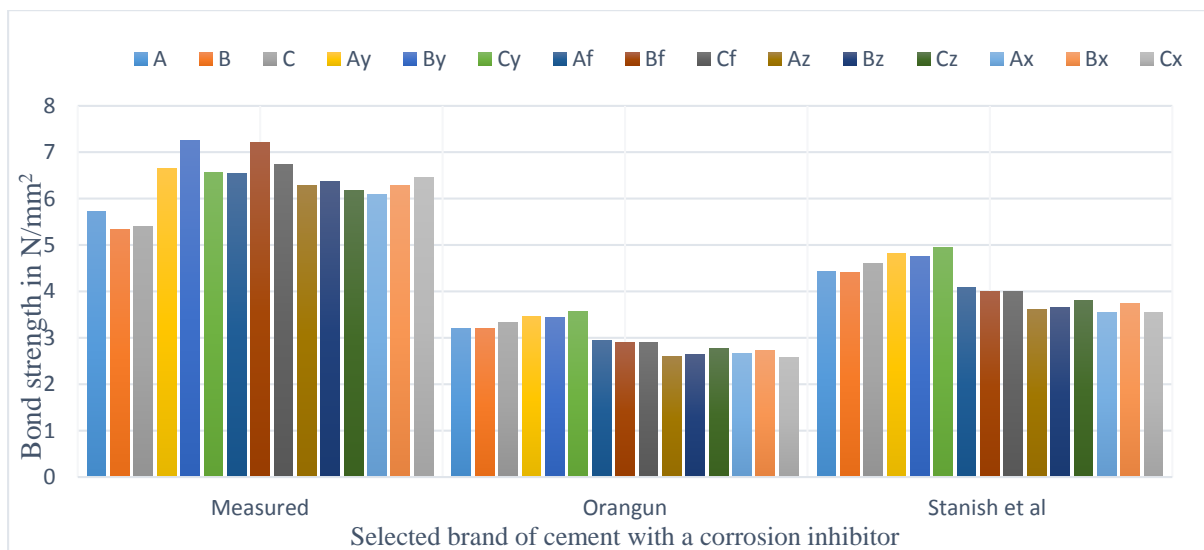


**Figure 4.18: Relationship of measured bond strength with the output of other authors for a selected brand of cement and a corrosion inhibitor.**

From Figure 4.18, it can be observed that all corrosion inhibitors in combination with a selected brand of cement increased the bond strength as explained in Fig.4.15. It can also be observed that the measured bond strength is greater than the output of Orangun and Stanish et al.

Table 4.14 shows statistical correlation of the measured bond strength results and the output of other researchers.

**Table 4.14 Correlations of results of this work with results of other researchers**

		This work	Orangun et al	Stanish et al
This work	Pearson Correlation	1	0.000	0.012
	Sig. (2-tailed)		0.999	0.967
Orangun et al	Pearson Correlation	0.000	1	0.998**
	Sig. (2-tailed)	0.999		0.000
Stanish <i>et al</i>	Pearson Correlation	0.012	0.998**	1
	Sig. (2-tailed)	0.967	0.000	

\*\* . Correlation is significant at the 0.01 level (2-tailed)

From Table 4.14, the results of this work have a very low association with the output of Orangun et al and Stanish et al or their result can only be associated by 0.00% and 0.01%

respectively.

#### 4.3.4 Proposed Bond strength Model

Table 4.15 shows tests between bond stress results of this work and those of Orangun et al and Stanish *et al*

**Table 4.15 :Tests of Between-Subjects Effects of this research and those of Orangun et al and Stanish *et al***

Source	Dependent Variable	Type III Sum of Squares	df	Mean Square	F	Sig.
Corrected Model	This work	.000a	0	.	.	.
	Orangun et al	.000b	0	.	.	.
	Stanish <i>et al</i>	.000a	0	.	.	.
Intercept	This work	601.793	1	601.793	1954.346	.000
	Orangun et al	134.102	1	134.102	1141.984	.000
	Stanish <i>et al</i>	255.854	1	255.854	1063.524	.000
Error	This work	4.311	14	.308		
	Orangun et al	1.644	14	.117		
	Stanish <i>et al</i>	3.368	14	.241		
Total	This work	606.104	15			
	Orangun et al	135.746	15			
	Stanish <i>et al</i>	259.222	15			
Corrected Total	This work	4.311	14			
	Orangun et al	1.644	14			
	Stanish <i>et al</i>	3.368	14			

a R Squared = .000 (Adjusted R Squared = .000)  
b R Squared = .000 (Adjusted R Squared = .000)



From the Table 4.15 and based on the measured bond strength results of this work its, Equation 4.3 is proposed taking into account concrete compressive strength, cover, bar diameter and bonded length.

$$\tau_u = 0.136526\sqrt{f'_c} \left[ 1.2 + 3 \left( \frac{c}{d_b} \right) + 50 \left( \frac{d_b}{L_d} \right) \right] \quad 4.3)$$

Where  $\tau_u$  is the bond strength in N/mm<sup>2</sup>

C is the minimum concrete cover in mm

$f'_c$  is the cylinder compressive strength of concrete in N/mm<sup>2</sup>

$d_b$  is the bar diameter in mm and

$L_d$  is the bonded length in mm

Table 4.16 shows the correlation of the proposed bond strength model from this study and the bond strength model of Orangun et al and Stanish *et al*

**Table 4.16: Correlations of bond strength results of this work with the proposed model and Stanish et al bond strength model**

		This work	Stanish <i>et al</i>	Proposed Model
This work	Pearson	1	.012	.008
	Correlation			
	Sig. (2-tailed)		.967	.979
Stanish <i>et al</i>	Pearson	.012	1	1.000**
	Correlation			
	Sig. (2-tailed)	.967		.000
Proposed Model	Pearson	.008	1.000**	1
	Correlation			
	Sig. (2-tailed)	.979	.000	

\*\* Correlation is significant at the 0.01 level (2-tailed).

From Table 4.16, the proposed model strongly correlates with the results of Stanish et al and it is applicable to the selected corrosion inhibitors for reinforced concrete of characteristic strength 25N/mm<sup>2</sup>.

#### 4.4 Service Life model

In service life modelling of reinforced concrete structures, corrosion current density is a significant parameter and its accurate value is important.

##### 4.4.1 Corrosion Current density

Table 4.17 shows corrosion current density from this work compared with the results of other researchers for different concrete strengths and reinforcement covers.

**Table 4.17: The rate of corrosion of rebar from samples from different diameter samples and strengths**

Sample Identity	Cover (mm)	Mass of steel sample (gms)		Loss in weight (gms) measured	Critical penetrati on depth $X_{crit}$ (mm)	Duration in days		Corrosion current density ( $\mu A/cm^2$ )			
		before corrosion	after corrosion			T <sub>1</sub>	T <sub>2</sub>	This work	Vu and Stewart [154]	Li 2004a [185]	
25 N/mm <sup>2</sup>	150mm diameter	70	371	360.4	10.6	0.8817	19	88	0.691	1.86	0.606
	130mm diameter	60	371	362.3	8.7	0.7714	16	70	0.729	2.204	0.520
	100mm diameter	45	371	363.2	7.8	0.6061	14	62	0.766	2.204	0.473
30 N/mm <sup>2</sup>	150mm diameter	70	371	361.5	9.5	0.9946	21	135	0.388	1.419	0.766
	130mm diameter	60	371	362.4	8.6	0.8703	19	123	0.303	1.674	0.729
	100mm diameter	45	371	363.4	7.6	0.6838	15	112	0.312	2.243	0.691
35	150mm diameter	70	371	361.6	9.4	1.125	24	162	0.237	1.164	0.833

N/mm <sup>2</sup>	130mm diameter	60	371	362.4	8.6	0.9844	21	151	0.237	1.637	0.804
	100mm diameter	45	371	363.1	7.9	0.7735	17	141	0.227	1.836	0.785

From Table 4.17, Fig.4.19 shows the relationship between corrosion current density against reinforcement cover and propagation period from Table 4.18

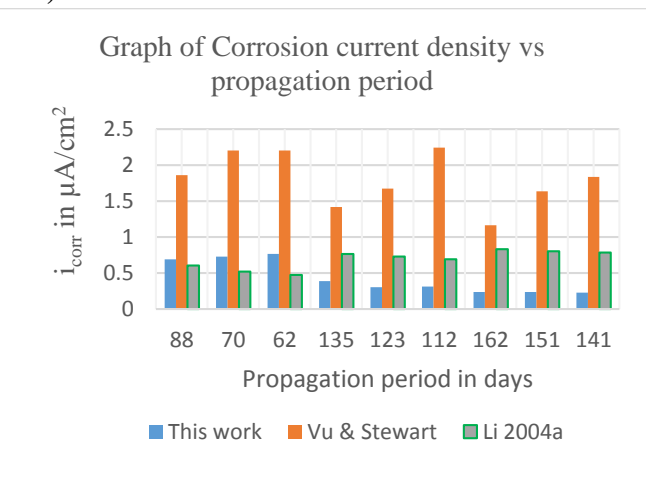
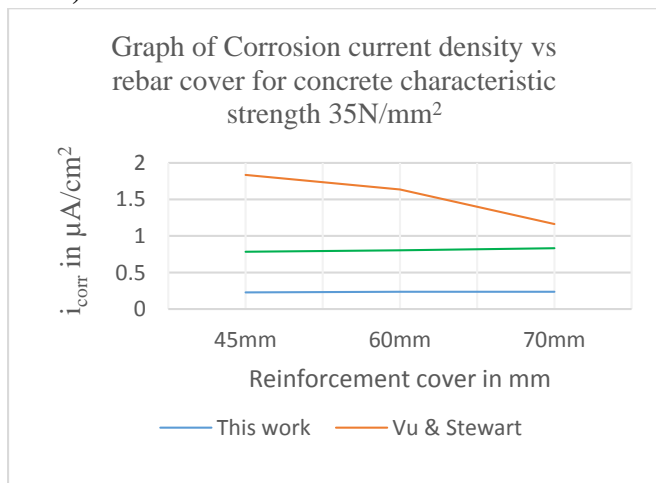
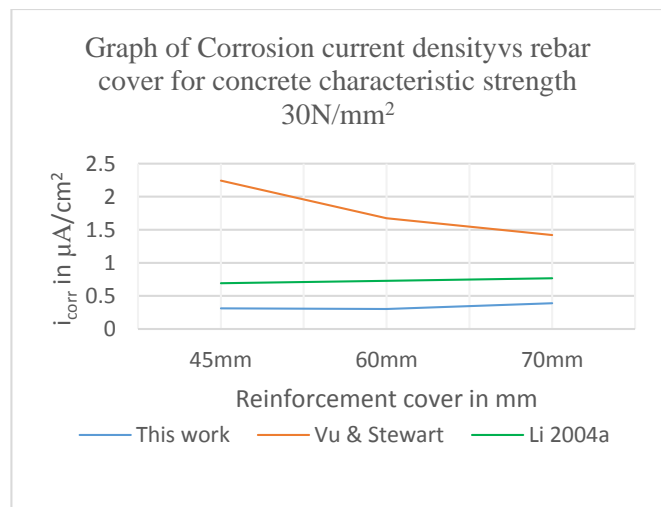
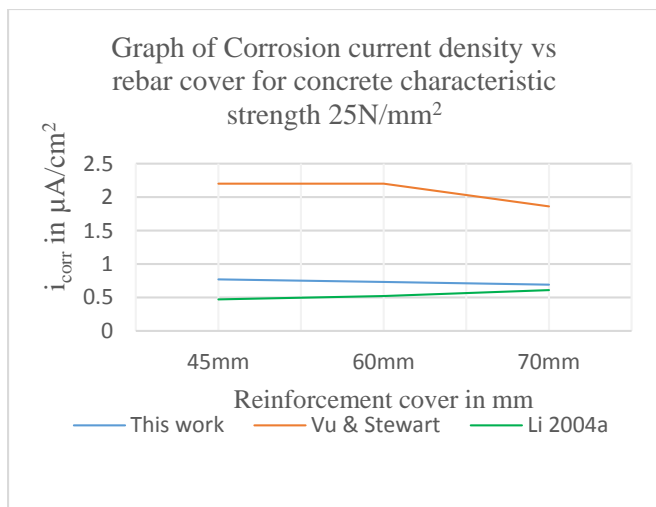


**Figure 4.19: a)-c) Graph of Current density vs reinforcement cover for 25N/mm<sup>2</sup>,30N/mm<sup>2</sup> and 35N/mm<sup>2</sup> and d) propagation period**

From Fig. 4.19 Graph a)-c), its noted that the corrosion current density generally decreased with an increase in reinforcement cover in this work and the Vu and Stewart model in all

concrete strengths considered. Corrosion current density depends on physical, electromechanical and mechanical processes where the cover thickness plays an important role. In the Li 2004a model the corrosion current density increases with an increase in concrete cover within the same concrete strength but remains constant for the same cover in different strengths. The Li 2004a model considers only the corrosion duration and neglects any other factor. From Fig.4.19d), it can be noted that the corrosion current density decreased with increase in propagation period in this study and in the Vu and Stewart. As the current density increases the rust expansion over the bar increases with a decrease in propagation period. Fig.4.20 shows the relationship between the critical penetration depth and the corrosion current density of this work and selected models.

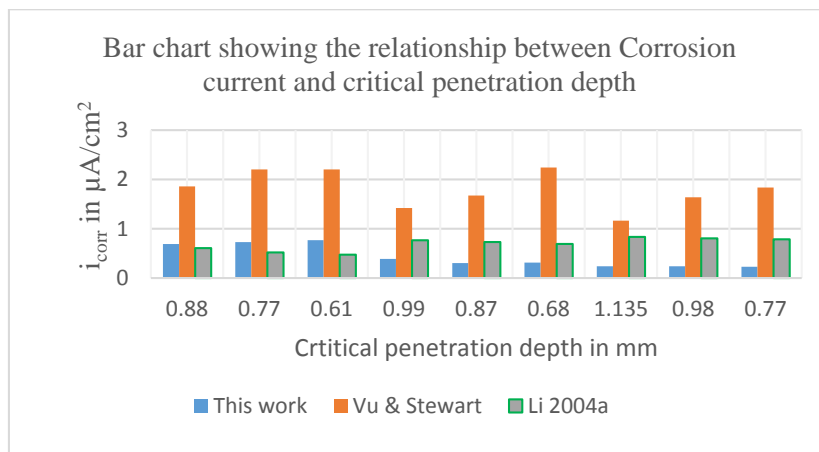


**Figure 4.20: Relationship between the critical penetration depth and the corrosion current density of this work and selected models.**

From Fig.4.20, the corrosion current density by Vu and Stewart is more than twice the results of this work. This is because not all factors affecting the corrosion rate are considered. In the Li 2004a model the corrosion current density decreases with decrease in critical penetration depth contrary to the results of this work. This model considers the corrosion period as the only factor influencing the corrosion current density, the influence of more factors may influence the results.

Fig.4.21 shows the relationship between corrosion current density and reinforcement mass loss for a crack width of 0.2mm

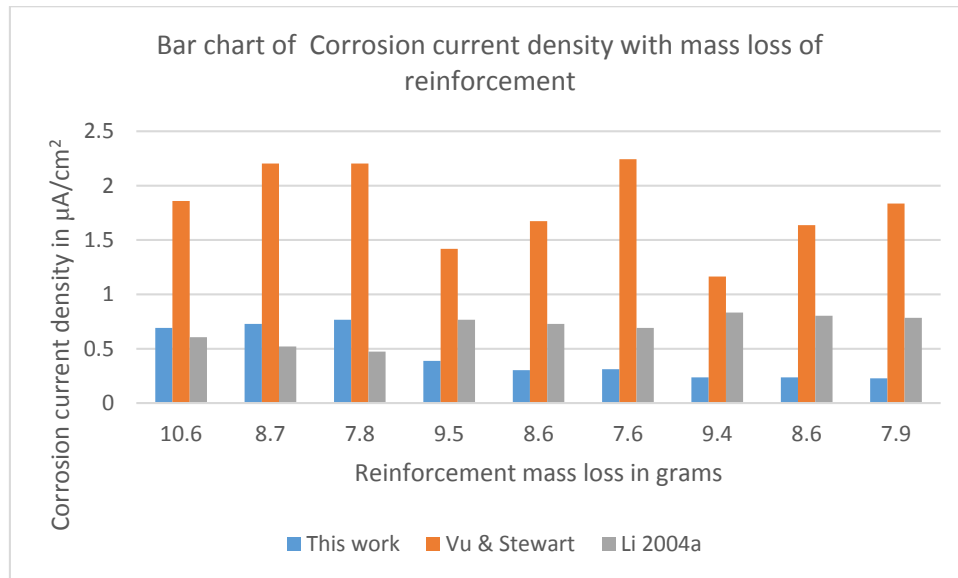


**Figure 4.21: Relationship between corrosion current density and reinforcement mass loss for a crack width of 0.2mm**

From Fig.4.21, the corrosion current density by Vu and Stewart increases with decrease in reinforcement mass loss and is contrary to the results of this work and the Li 2004a model. Other than the corrosion period, the water cement ratio and the concrete cover, the mechanical properties of the concrete may influence the rate of corrosion current density and reinforcement mass loss.

The correlation of the result of this work and those of the Vu and Stewart (2000) model have been used for generation of the proposed current density model for the propagation period for this study and generation of the proposed service life model.

**c) Statistical relationship of the result of this work and those of Vu and Stewart (2000) for corrosion current density.**

Table 4.18 shows the correlation of the result of this work and those of Vu and Stewart (2000)

**Table 4.18: Correlations of the results of this work and those of Vu and Stewart**

		This work	Vu and Stewart
This work	Pearson Correlation	1	0.724*
	Sig. (2-tailed)		0.027
Vu and stewart	Pearson Correlation	0.724*	1
	Sig. (2-tailed)	0.027	

\*. Correlation is significant at the 0.05 level (2-tailed).

From Table 4.18, the result of this work significantly correlate ( $r=0.724$ ) with the results of Vu and Stewart model it was therefore to propose a model to fit this study results.

**d) Proposed corrosion current density model for this work**

Fig. 4.22 shows the relationship between the result of this study and the Vu and Stewart model for corrosion current density.

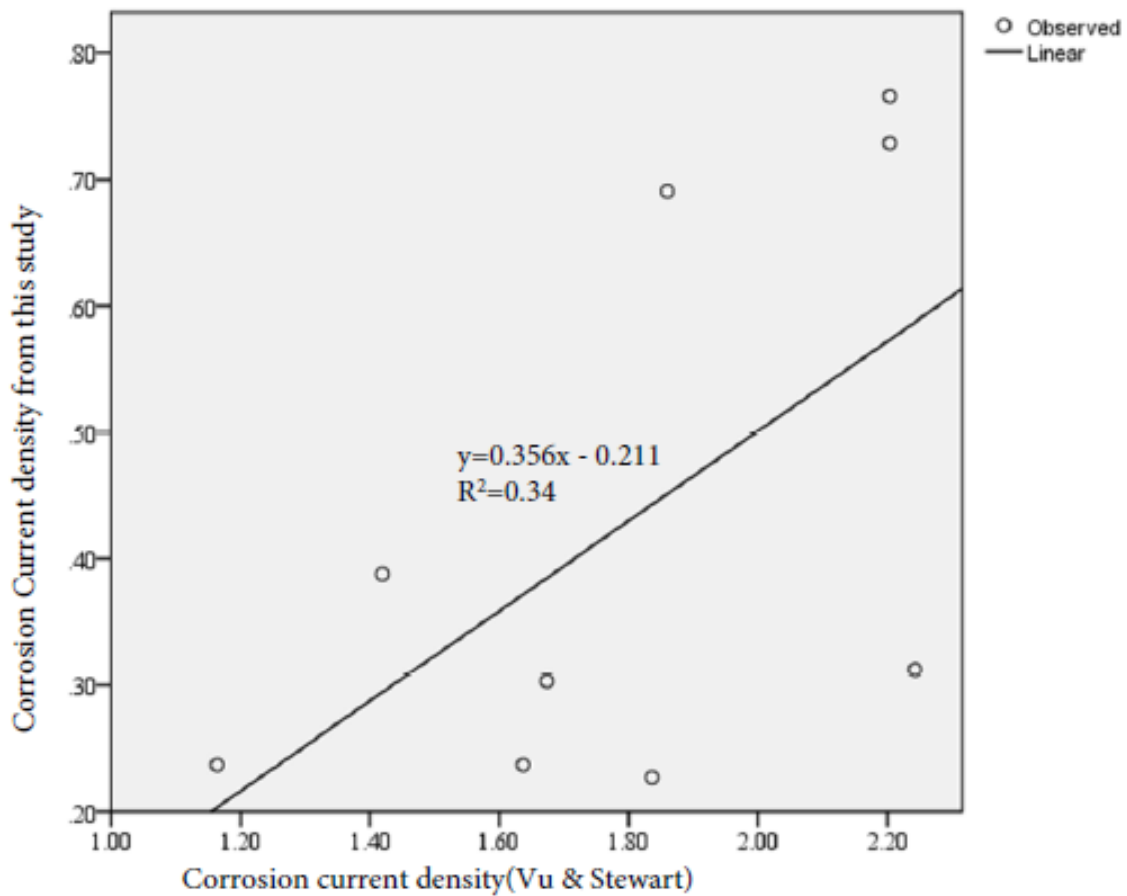


**Figure 4.22: Graph of the result of this work against and Vu and Stewart Model for corrosion current density in  $\mu\text{A}/\text{cm}^2$ .**

From Fig. 4.22, a linear relationship between the results of this study and the Vu and Stewart model has been established. The variance ( $R^2=0.340$ ) is low and hence a corrosion current density model has been proposed which compares well with this work. Table 4.19 shows a statistical relationship between the output of this work, the Vu and Stewart and the proposed model for corrosion current density during propagation period.

**Table 4.19: Statistical relationship between the results of this work, the Vu model and the proposed model for corrosion current density during propagation period.**

	Mean difference	Bias	Std. Error	Sig. (2-tailed)	95% Confidence Interval	
					Lower	Upper
This work	0.36333	0.00012	0.03645	0.010	0.29889	0.44111
Vu and Stewart	0.98000	-0.00058	0.09222	0.001	0.80786	1.17664
Proposed model	0.36333	-0.00017	0.02738	0.001	0.31223	0.42171

From Table 4.19, the proposed model output compares well with the output of this research and therefore the corrosion current density can be obtained from equation 4.4:

$$i_{corr}(t) = -0.211 + \left[ 13.8 (1 - w/c)^{-1.64} (1 + t_2)^{\frac{-1}{3}} \right] / c \quad 4.4)$$

Where:

$i_{corr}(t)$  = Corrosion current density ( $\mu\text{A}/\text{cm}^2$ )

w/c = the water cement ratio obtained from the Bolomey's formula (Equation 2.37)

c = the cover thickness (mm).

#### 4.4.2 Proposed service life model

From Equation 3.18, the corrosion propagation period for the proposed model was calculated and compared with the output of other researches as shown in Table 4.20.

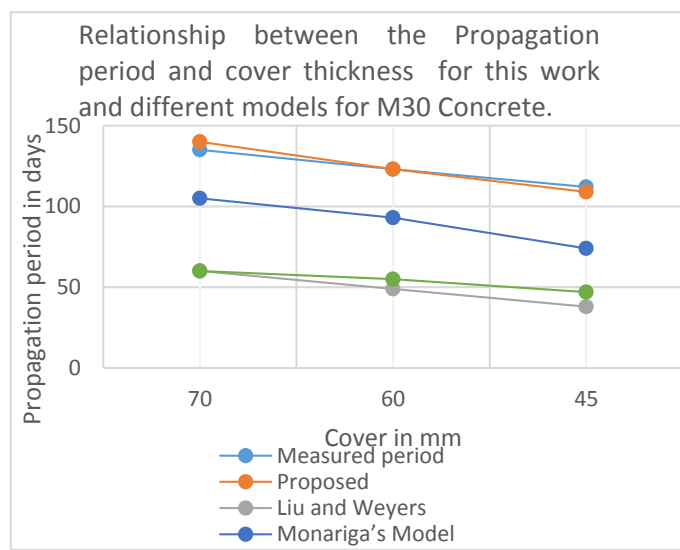
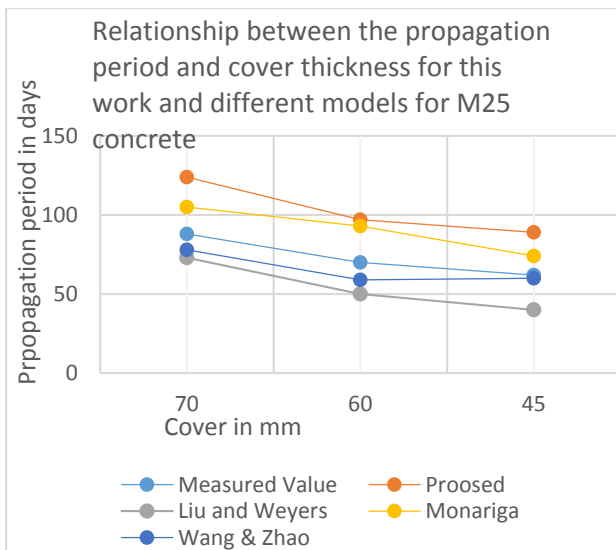


**Table 4.20: Parametric study of the service life models for a steady corrosion current of 1 g/m<sup>2</sup>/day for propagation period.**

Sample Identity		Reinforce ment cover in mm	Mass loss of steel sample after corrosion (gms)	T <sub>2</sub> days				
				Measured period	Proposed Model	Liu and Weyers Model	Monariga' s Model	Wang and Zhao's Model
25 N/mm <sup>2</sup>	150mm diameter	70	10.6	88	124	73	105	78
	130mm diameter	60	8.7	70	97	50	93	59
	100mm diameter	45	7.8	62	89	40	74	60
30 N/mm <sup>2</sup>	150mm diameter	70	9.5	135	140	60	105	60
	130mm diameter	60	8.6	123	123	49	93	55
	100mm diameter	45	7.6	112	109	38	74	47
35 N/mm <sup>2</sup>	150mm diameter	70	9.4	162	169	59	105	48
	130mm diameter	60	8.6	151	147	49	73	44
	100mm diameter	45	7.9	141	122	42	74	37

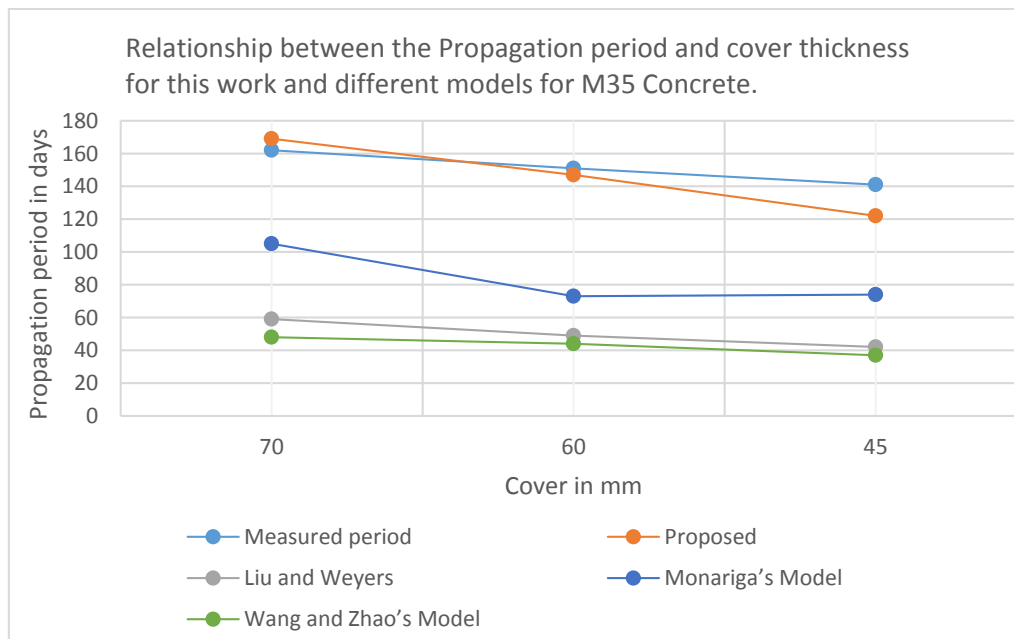
From Table 4.20, it can be noted that in the Monariga model that the propagation period(T<sub>2</sub>) is constant for all concrete compressive strengths considered but varies only with reinforcement cover and this attributed to exclusion of the mechanical properties as a variable. This model can only be applicable where there are changes in reinforcement cover within the same concrete strength.

Fig. 4.23 shows a relationship between the reinforcement cover and the propagation period results of this work, the proposed model and the results of other models as shown in Table 4.20. Similarly, Fig.4.24 shows a relationship between the measured and proposed model propagation period.



a)

b)



c)

**Figure 4.23: Graph (a)-(c) Relationship between the reinforcement cover and the propagation period results of this work, the proposed model and the results of other models as shown in Table 4.20.**

From Fig.4.23, it can be noted that in the measured period and all the models, the propagation period trend is similar and decreases with decrease in cover. This is because a smaller quantity of corrosion products is required to generate enough internal pressure to propagate an initiated crack to 0.2mm is smaller covers.

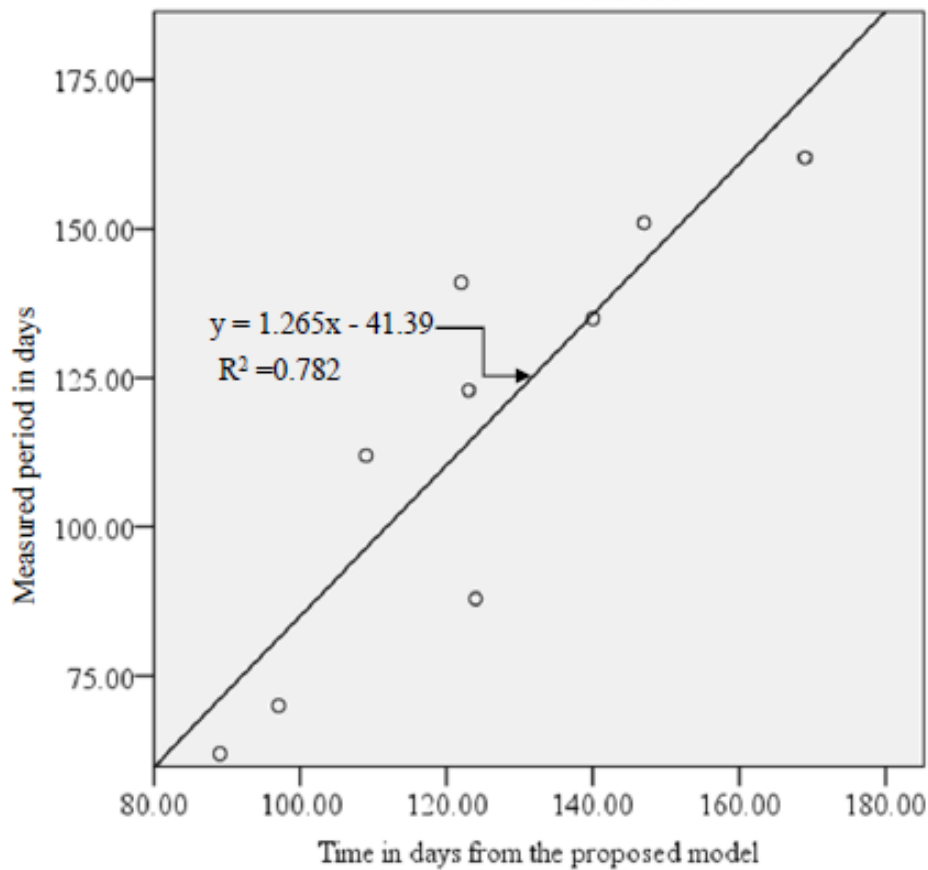


**Figure 4.24: Relationship between the measured and proposed model propagation period.**

A linear model Equation (Fig.4.24) has been established for the relationship between the measured and model proposed propagation period which can be useful in establishing either of the two when one is known. It can be noted that 78.2% ( $R^2=0.782$ ) of the model equation results are strongly associated with the measured propagation period.

Table 4.21 shows a parametric study of correlations of the propagation period.

**Table 4.21: Parametric study of correlations of the propagation period**

		This work (Measured)	Proposed model	Liu and Weyers	Wang and Zhao's
This work (Measured)	Pearson Correlation	1	0.884**	0.088	-0.622
	Sig. (2-tailed)		0.002	0.821	0.074
	N	9	9	9	9
Proposed model	Pearson Correlation	0.884**	1	0.435	-0.256
	Sig. (2-tailed)	0.002		0.242	.507
	N	9	9	9	9
Liu and Weyers	Pearson Correlation	0.088	0.435	1	0.596
	Sig. (2-tailed)	0.821	0.242		0.090
	N	9	9	9	9
Wang and Zhao's	Pearson Correlation	-0.622	-0.256	0.596	1
	Sig. (2-tailed)	0.074	0.507	0.090	
	N	9	9	9	9

\*\* . Correlation is significant at the 0.01 level (2-tailed).

From Table 4.21, it can be noted that comparable to the other models, the proposed model strongly correlates with the measured for the propagation period i.e. 78.1% ( $R^2=0.884$ ) results by the proposed model are associated with the measured output.

From the model proposed in this study and Wang and Zhao's service life model, it can be noted that the propagation period reduces with increase of compressive strength and decreases with decrease in reinforcement cover. This is because the elastic deformation decreases with increase in strength, since the elastic modulus increases with the strength. This is valid only when the same type of aggregate is used and the strength is varied by changing the w/c. The modulus of elasticity of the aggregates dominates the modulus of the concrete. The main influencing factors of the proposed prediction model shows that increasing the cover

thickness, changing the bar diameter and improving the concrete strength can prolong the time to cover cracking, which is beneficial for structural durability.

A comparison of this work's proposed model's predictions to that of Wang and Zhao's Model indicates that the proposed model can give reasonable prediction for the time to cover cracking. It is practical to use the proposed model to predict the chloride corrosion-induced cracking time and analyze the service life of reinforced concrete water conveyancing structures.

The crack initiation and propagation periods are not directly proportional to the corrosion rate so that by increasing the corrosion rate by a given factor, the time to corrosion induced cracking is not shortened by the same factor. A high corrosion rate will affect the corrosion induced cracking phenomena in either of the following ways:

- a) The crack propagation increases at a faster rate with a smaller applied corrosion rate. In other words, cracks may propagate slower as the corrosion rate increases [164].
- b) A higher rate of loading may induce higher deformations and there is less time for corrosion products to dissipate into the pore structure of the concrete, thereby increasing the radial pressure exerted at the steel/concrete interface. This will result in faster crack propagation as corrosion rate increases [165]

#### **4.4.3 Application and limitation of the proposed model.**

Figure 4.25 shows the procedure to estimate the corrosion points of initiation and propagation points for service life prediction.

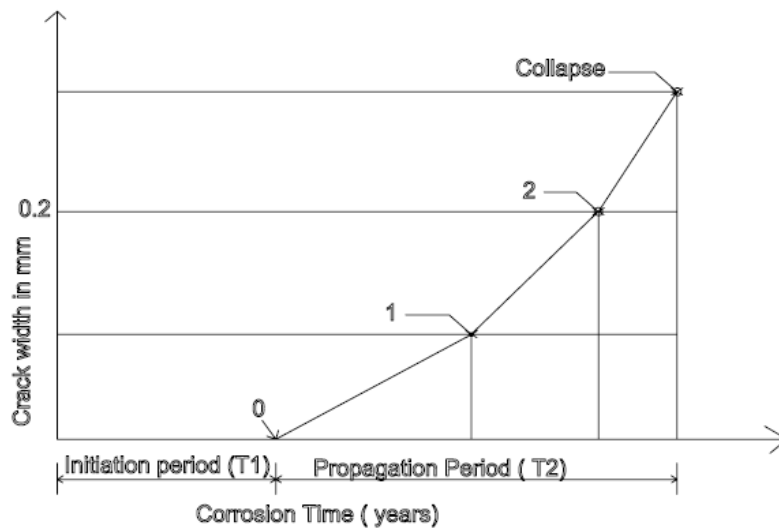


**Figure 4.25: Corrosion initiation and propagation points.**

Point 0: is the initiation period calculated from Equation 3.17 and is associated with lose of the passivation layer.

Point 1: is the propagation period calculated using  $T_{p1}$  and is related to crack with of approximately 0.05mm.

Point 2: is the propagation period calculated using  $T_{p2}$  and is related to crack expansion for maximum acceptable width.

This model is limited for use in water conveyancing structures.

## CHAPTER 5

### 5.0 CONCLUSION AND RECOMMENDATIONS

#### 5.1 Conclusions

The following conclusions can be drawn from this research;

- i) The rate of corrosion is affected by the chemical composition of cement; specifically, lime, silicon dioxide and magnesium oxide.
- ii) Due to their effect on the strength of concrete, the use of a selected brand of cement linearly correlates with the critical penetration depth of rust in reinforced concrete water conveyancing structures.
- iii) The amount of corrosion products to fill the total interconnected pores around the rebar/concrete interface and the amount of corrosion products to generate the critical tensile stress constitute the critical mass of corrosion products to induce cracking of the concrete cover. The critical mass of corrosion products is influenced by the cover to the rebar, the rebar size and the compressive strength of concrete and steel/concrete interface.
- iv) At the selected dosages of the selected corrosion inhibitors in combination with respective brands of cement used, there was an increase of the bond strength of reinforced concrete
- v) A service life model that can predict the initiation and propagation time of reinforced concrete water conveyancing structures has been proposed. The model is a two-stage sequence: an initiation stage, during which chloride ions penetrate the concrete towards the reinforcing steel, and a propagation stage, where the state of damage in concrete resulting from corrosion build-up at the rebar is assessed to determine the propagation period. From the parametric study performed the model proved to be promising as a service life predicting tool for water conveyancing structures subjected to chloride ingress. The

proposed service model is particularly sensitive to cover and reinforcing bar diameter, compressive and tensile strength of concrete.

### **5.3 Recommendations.**

#### **a) Recommendations from this work**

The study model derived is for determining the service life of reinforced concrete water conveyancing structures where the reinforcement bar diameter, cover thickness and compressive strength are variation parameters for chloride induced corrosion.

#### **b) Recommendations for further study**

- i) Research for a model for an accurate rate of loading factor peculiar to reinforced concrete water conveyancing structures.
- ii) Further research for the relationship of the selected corrosion inhibitors on the service life of reinforced concrete water conveyancing structures.



## REFERENCES

- [1] International Hydropower Association (2015). Hydropower Status Report
- [2] Global Legal Insights (2018). Energy in Kenya.
- [3] Liu, H., Masera, D. and Esser, L. (2013). World Small Hydropower Development Report 2013. United Nations Industrial Development Organization; International Center on Small Hydro Power.
- [4] Walsh, J. H. (2000). Projection of Cumulative World Conventional Oil Production, Remaining Resources and Reserves to 2050. In: The Colorado River Commission of Nevada, *World Fossil Fuel Reserves and Projected Depletion*.
- [5] Mohamed.E., Wafa, H., Ezaldin, Ben.,Howell, E.(2019).Quality Assessment of the Various Brands of Portland Cement Available in the Libyan Market.*J. Mater. Environ. Sci.*, 10(12),1324-1331.
- [6] Broomfield, J. P. (1997). Corrosion of Steel in Concrete: Understanding, Investigation, and Repair. *Spon Press Publications, London*.
- [7] Daily, S. F. (2007). Understanding Corrosion and Cathodic Protection of reinforced Concrete Structures. *Corrpro Companies Inc*.
- [8] Ahmed Mohammed Abdelalim,A.M.(2012).Quantitive Assessment of Deteriorated R.C Structures due to Reinforcing Steel Corrosion. *Proceedings of the 9<sup>th</sup> ICCAE-9 Conference*, 29-31.
- [9] Kumar, S. (2018). Innovative Corrosion Control Practices to Provide Long Term Durability of Concrete Structures - A Way Forward. *Indian Roads Congress*,46(7),57-62.
- [10] Page, C. L., and Treadaway K.W.J. (1982). Aspects of Electrochemistry of Steel in Concrete. *Nature*, 297,109-115.

- [11] Kumar V., Ramesh S., M.A Quraishi M.A., (2013). A study on corrosion of reinforcement in Concrete and effect of inhibitors on servive life of reinforced concrete. *J. mater Environment scienc*,4(5),726-731.
- [12] Nielsen A. (1985). Durability in Beton Bogen. *Aalborg Cement Company, Aalborg, Portland*, 200-243
- [13] Balafas, I., and Burgoyne, C. J. (2009). Environmental conditions and corrosion initiation in concrete bridges. *Cem. Concr. Res.*, in press.
- [14] Boyle B.(2004). *Metal Finishing*, 02, 37-41.
- [15] Roberge, P.R., Klassen R.D., Haberecht P.W, (2002). Atmospheric Corrosivity Modeling - A Review. *Materials and Design*, 23,321-330.
- [16] Batis, G., Rakanta E. (2005). Corrosion protection methods of structural steel against atmospheric corrosion. *Cement and Concrete composites*, 27,269-275
- [17] Miksic, B.A. Miller R.H. (1980).*5th European Symposium on Corrosion Inhibitors*, Italy.
- [18] Prenosil, M., (2014). Suppl.Materials Performance.*NACE*.
- [19] Benjamin, R., Marc, Q., Veronique B., Arnaud, D., Lucas, A., (2016). Experimental and numerical analysis of corrosion-induced cover cracking in reinforced concrete sample. *Computers and Concrete*, 18 (3),421-439.
- [20] Jadhav, A.M., Munot, H.K.(2016).Analytical Study of Mechanism of Concrete Cracking and Its Propagation Due to Corrosion of Reinforcement in RCC. *Open Journal of Civil Engineering*, 6(2).
- [21] Bolzoni, F., Coppola, L., Goidanich, S., Lazzari, L., Ormellese, M., and Pedferri, M. P. (2004). Corrosion inhibitors in reinforced concrete structures. Part 1: Preventative technique. *Corrosion Engineering, Science and Technology*, 39(3), 219-228.

- [22] Lee, S. K., Krauss, P. D., and Virmani, Y. P. (2005). Resisting corrosion. *Public Roads*, 68(6), 58-63.
- [23] Bamforth P.B. (2004). Enhancing reinforced concrete durability: guidance on selecting measures for minimizing the risk of corrosion of reinforcement in concrete. *Concrete Society Technical*, 61.
- [24] Tayeh B.A., Abu Bakar B., Johari M, Voo Y.(2012).Mechanical and permeability properties of the interface between normal concrete substrate and ultra-high performance fiber concrete overlay. *Construction Building Materials*, 36,538–48.
- [25] Gert W.,Polder R.B.,Breugel K.(2012).Guideline for service life design of structural concrete -A performance based approach with regard to chloride induced corrosion. *Heronjournal.nl*,57 (3).
- [26]Siemes,T., Polder, R. and de Vries, H.(1998).Design of concrete structures for durability. *Heronjournal.nl*, 43(4).
- [27] Woodward,R.J., Williams,F.W.(1998).Collapse of Yns-Y-Gwas bridge, Glamorgan. *Proceedings of the Institution of Civil Engineers*,84 (4),635-669.
- [28] Neville A.M. (2011). *Properties of Concrete*, (5), Pearson:Harlow, England, UK.
- [29] Ribeiro, D.V., Cunha, M.P.T. (2014).Deterioração das estruturas de concreto armado. In: Ribeiro DV,editor. Corrosão em estruturas de concreto armado: Teoria, Controle e Métodos de Análise.1st ed. Rio de Janeiro: Elsevier, 2014,87-118.
- [30] Dimitrova, V. and Gorkerb,L.(2006).Modified Nernst equation for electroless metal deposition. *Progress in Reaction Kinetics and Mechanism*,31, 45–58.
- [31] Bardal, E. (2004). Corrosion and Protection Engineering Materials and Processes, London. Uk, *Springer*, 1<sup>st</sup> edition,336.

- [32] Ngala, V. T., Page, C. L., Page, M. M. (2002). Corrosion inhibitor systems for remedial treatment of reinforced concrete. Part 1: calcium nitrite. *Corrosion Science*, 44 (9), 2073 - 2087.
- [33] Shah, V. N., Hookham, C. J. (1998). Long-term aging of light water reactor concrete contaminants. *Nuclear Engineering Design*, 185(1), 51 - 81.
- [34] Rhen, F. & Fernandez, D., Hinds, G. and Coey, J. M. D. (2005). Influence of a Magnetic Field on the Electrochemical Rest Potential. *Journal of The Electrochemical Society*, 153,1-7.
- [35] Broomfield, J. P. (2007). Corrosion of Steel in Concrete: Understanding, Investigation and Repair, (2nd ed). London: *Taylor and Francis*, 277.
- [36] Yuan, Q., Shi, C., De Schutter, G., Audenaert, K., Deng, D. (2009). Chloride binding of cement-based materials subjected to external chloride environment. *Journal of Construction and Building Materials*, 23 (2), 1 - 13.
- [37] Wanyama, D. E. Pelster, K. Butterbach-Bahl, L. V. Verchot, C. Martius & Rufino, M.C (2019). Soil carbon dioxide and methane fluxes from forests and other land use types in an African tropical montane region. *Biogeochemistry*, 143, 171–190.
- [38] Panno, S.V., K.C. Hackley, H.H. Hwang, S. Greenberg, I.G. Krapac, S. Landsberger and O’Kelly, D.J. (2006). Characterization and identification of the sources of Na-Cl in ground water. *Ground Water*, 44(2), 176–187.
- [39] Konopka, P. (2005). Structural properties of rust. *4th-year undergraduate project, Univ. of Cambridge*, Cambridge, UK.
- [40] Suda, K., Misra, S., and Motohashi, K. (1993). Corrosion products of reinforcing bars embedded in concrete. *Corros. Sci.*, 35(5-8), 1543–1549.

- [41] Liu, T., and Weyers, R. W. (1998a). Modeling the dynamic corrosion process in chloride contaminated concrete structures. *Cem. Concr. Res.*, 28(3), 365–379.
- [42] Balafas, I., and Burgoyne, C. J. (2009). Environmental conditions and corrosion initiation in concrete bridges. *Cem. Concr. Res.*, in press.
- [43] Melchers, R. E. (2003b). Modeling of marine immersion corrosion for mild and low-alloy steels—Part 1: Phenomenological model. *Corros.Sci.*, 59(4), 319–334.
- [44] Sun,H.,Zhu,J.,Ham,S.(2018).Automated Acoustic Scanning System for Delamination Detection in Concrete Bridge Decks. *Journal of Bridge Engineering*, 23(6).
- [45] Bertolini, L., Elsener, B., Pedferri, P., Polder, R.B., (2004). Corrosion of Steel in Concrete:Prevention, Diagnosis, Repair. *Wiley-VCH Verlag GmbH & Co. KGaA, Weinheim*, 8, 392.
- [46] François,R.,Laurens,S.,Deby, F.(2018). Corrossion and its consequences for reinforced concrete structures, *Esevier*,175-191.
- [47] Ezeddin, B.,and Sagüés, A.(2013).Critical localized corrosion penetration of steel reinforcement for concrete cover cracking. *Corrosion conference and Expo*.
- [48] Chen, G.,Leung, E. andYing, C.K.(2013).Numerical modelling of non-uniform steel corrosion development and its mechanical influences on reinforced concrete structures. *8th International Conference on Fracture Mechanics of Concrete and Concrete Structures - FraMCoS-8, Toledo, Spain*. 1808-1817
- [49] Torres-Acosta, A. and Sagüés, A.(2004).Concrete Cracking by Localized Steel Corrosion - Geometric Effects. *ACI Materials Journal*, 101(6), 501–507.
- [50] O'Reilly, M., Darwin, D., Browning, J.P., and Locke, Jr., C. E. (2011). Evaluation of Multiple Corrosion Protection Systems for Reinforced Concrete Bridge Decks. *SM Report 100, University of Kansas Center for Research, Inc., Lawrence, Kansas*, 535 pp.

- [51] Darwin, D., Browning, J. and O'Reilly, M. (2012). Multiple Corrosion-Protection Systems for Reinforced Concrete Bridge Components. *Federal Highway Administration report no. FHWA-HRT-11-060*.
- [52] Montoya, R., Aperador, W., Bastidas, D.M. (2009). Steel corrosion behaviour in carbonated alkali-activated slag concrete. *Corrosion Science*, 51(2009), 2857.
- [53] Montoya, R., Aperador, W., Bastidas, D.M. (2009). Steel corrosion behaviour in carbonated alkali-activated slag concrete. *Corrosion Science*, 51(2009), 2857.
- [54] Rodriguez, J., Ortega, L., Casal, J., and Diez, J. (1996). Corrosion of reinforcement and service life of concrete structures. In C. Sjöström (Ed.), *Durability of Building Materials and Components*, 7 (1), 117–126.
- [55] Tang F., Chen, G., Brow J., Volz J., Koenigstein M., (2012). Corrosion resistance and mechanism of steel rebar coated with three types of enamel. *Corrosion Science*, 59(2013), 157-168.
- [56] Shayan, A., Xu, A. (2016). Relationship between Reinforcing Bar Corrosion and Concrete Cracking. *Aci Materials Journal*, 113(1).
- [57] Nguyen T.N, Hubbard J.B., (1991). A Mathematical Model for the Cathodic Blistering of organic coatings on steel immersed in electrolytes. *International Journal Coating Technology*, 63, 794.
- [58] Andrade C., Sanchez J., Fulla J., Rebolledo N., and Tavares F., (2012). On-site corrosion rate measurements: 3D simulation and representative values. *Materials and Corrosion*, 63,(12), 1154–1164.
- [59] Chen Y., Howdyshell R., Howdyshell S, Lu-Kwang J., (2014). Characterizing Pitting Corrosion Caused by a Long-Term Starving Sulfate-Reducing Bacterium Surviving on Carbon Steel and Effects of Surface Roughness. *Corrosion Science*, 70(8), 767-780.

- [60] Troconis de Rincón, O., et al. (2007). Effect of the marine environment on reinforced concrete durability in Iberoamerican countries: DURACON project/CYTED. *Corrosion Science*, 49 (7),2832-2843.
- [61] Castro-Borges P., Balancán-Zapata M., López-González A., (2012). Analysis of tools to evaluate chloride threshold for corrosion onset of reinforced concrete in tropical marine environment of Yucatán,México.*Journal of Chemistry*,2013.
- [52] Pedrosa F., Andrade C,(2010).Study of corrosion rate variability in indoor and outdoor specimens.*Proceedings of 4th International RILEM PhD Workshop on Advances in Modeling Concrete Service Life*.
- [63] Busba E.,Sagüés. A. (2013). Localized Corrosion of Embedded Steel in Cracked Reinforced Concrete Pipes. *CORROSION*, 69(4), 403-416.
- [64] Alonso C., Andrade C.,González J.A.,(1988).Relation between resistivity and corrosion rate of reinforcements in carbonated mortar made with several cement types. *Cement and Concrete Research*, 18(5),687–698.
- [65] Morris W., M. Vazquez M., Sanchez S.(2000).Corrosion of reinforcing steel evaluated by means of concrete resistivity measurements. *Corrosion Science*, 44(1),81–99.
- [66] Arup H., Korrosion scentralen .The mechanisms of the protection of steel by concrete, Ellis Horwood Ltd Chichester, 151.
- [67] Bertolini L., Elsener B., Pedeferr P.,Polder R.,(2004).Corrosion of steel in concrete. *Wiley-Vch Verlag GmbH & Co K GaA Weinheim*, 243.
- [68] Arup H., Korrosion scentralen. The mechanisms of the protection of steel by concrete. *Ellis Horwood Ltd Chichester*, 151.
- [69] Lau K., Sagues A., (2011). Impedance of reinforcing steel with disbonded dual polymer-zinc coating. *Electrochimica Acta*.

- [70] Cement Concrete and Aggregate Australia, (2009). Chloride resistance to concrete.
- [71] ASTM Standard practice for making and curing concrete test specimens in the laboratory C192/192M-07
- [72] Nurberger U.(Ed),(1996).Stainless steel in concrete, state of the art report. *Institute of materials London*, 18.
- [73] Gracia-Alonso M.C.,Escdero M.L,Miranda J.M.,Vega M.I., Capilla F.,Correia M.J., Salta M.,Bennani A.,Gonzalez J.A.(2007).Corrosion behaviour of new stainless steels reinforcing bars embedded in concrete. *Cement and concrete research*, 37, 1463-1471.
- [74] Andion L.G.,Garces P.,Cases F.,Andreu C.G.,Vazquez J.L.(2001).Metallic corrosion of steel embedded in calcium aluminate cement mortars. *Cement and concrete research*, 31,431-436.
- [75] Criado M., Bastdas D.M., Fajardo S.,Fernandez-Jimenez A., Batisdas J.M.(2011). Corrosion behaviour of new low-nickelstainless steel embedded in activated fly ash mortars. *Cement and concrete composites*, 22,644-652
- [76] Roberge P.R.(2000). Hand book of corrosion Engineering. *McGraw-Hill*, 834.
- [77] Al-Dulaijan S.U.,Maslehuddin M., Shameen M.,Ibrahim M.,Al-Mehthel (2012). *Construction & building materials*,29, 487-495
- [78] Sastri V.S., Ghali E., Elboudjaini M. (2007). Corrosion prevention & protection practical solution. *John Wiley & sons Ltd*, West Sussex England, 82.
- [79] Soylev T.A.,Richardson M.G.(2006). Corrosion inhibitors for steel in concrete: State of the art report. *Corrosion & building materials*.
- [80] Zhou Y., Zuo Y.,Yan F., (2017). Effect and Mechanism of Inhibitors on Pitting Corrosion of Metals. *Journal of Chinese Society for Corrosion and protection*, 37(6), 487-494.



- [81] Song Q., Qiu X. (2011), "Study on the complex of sodium tungstate and urotropine as inhibitors against stainless steel corrosion in the NaCl Solution. *Materials Science forum*, 698, 450-454.
- [82] Jabeera B., Shibli S.M., Anirudhan T.S. (2006). Synergistic inhibitive effect of tartarate and tungstate in preventing steel corrosion in aqueous media. *Applied surf. Sci*, 252, 3520-3524.
- [83] Ostnor T.A., Justness H. (2011), "Anodic corrosion inhibitors against chloride induced corrosion of concrete rebar. *Advances in applied ceramics*, 3, 131-136.
- [84] Song, Y., Liu, J., Hui Wang, H., Shu, H. (2019). Research Progress of Nitrite Corrosion Inhibitor in Concrete. *International Journal of Corrosion*, 2019.
- [85] Macdonald D. Design Options for Corrosion protection. *8<sup>th</sup> International Symposium, Australia*, 75-83.
- [86] Novokshceov V., Salt penetration & Corrosion in Pre-stressed concrete member. *Federal Highway Administration*, 88-269
- [87] Bashir U., Debi E.G., Idris J., Hamsah E. (2012). Corrosion and Corrosion Mitigation of Rebar in Concrete Exposed to Marine Environment. *Engineering Science and Technology*, 2(5), 2250-3498.
- [88] Montes P., Theodore B.W., Derek L.H. (2004). Influence of Calcium nitrite inhibitor and crack width on corrosion of steel in high performance concrete subjected to a simulated marine environment. *Cem. Concr. Compos*, 26(3), 243-25
- [89] Mahmoud N. (2013). Chitosan as a green inhibitor for copper corrosion in acidic medium. *International Journal of Biological Macromolecules*, 55, 142-149.
- [90] Roberge P.R. (1999). Handbook of corrosion engineering. New York: *Mc Graw Hill Handbook*.

- [91] Sherif M.(2006).Effects of 2-amino-5-(ethylthio)-1,3,4-thiadiazole on copper corrosion as a corrosion inhibitor in 3% NaCl solutions. *Applied Surface Science*,252(24),8615-8623.
- [92] Gentil V.(2003). Corrosion. Rio de Janeiro: *LTC*.
- [93] Dutra A.C., Nunes D.P. (2011). Protection techniques of combating corrosion.Rio de Janeiro: *interscience*.
- [94] Yaro A.S.,Khadom A.,Wael R.K.(2013).Apricot juice as green corrosion inhibitor of mild steel in phosphoric acid. *Alexandria Engineering Journal*, 52(1), 129-135.
- [95] Sastri V. (2001). Corrosion Inhibitor; principles and Applications. *John Willey& sons Inc*.NY, USA .2
- [96] Sanyal B. (1981). Organic compounds as corrosion inhibitors in different environments. *Progress in Organic Coatings*, (9), 165-236.
- [97] Samiento-Bustos E, Rodriguez J.G., Uruchurtu J, Dominguez-Patiño G, Salinas-Bravo VM (2008). Effect of inorganic inhibitors on the corrosion behavior of 1018 carbon steel in the LiBr + ethylene glycol + H<sub>2</sub>O mixture. *Corrosion Sci.*, 50(8),2296-2303.
- [98] Skotinck A (2000). Corrosion of concrete and its prevention. *6<sup>th</sup> International Conference on Corrosion*. Moscow, Russia: 18-25
- [99] Slater J (2001). Corrosion of Metals in Association with Concrete. New Jersey, *Prentice-Hall Inc*.
- [100] De-Schutter G, Luo L (2004). Effect of corrosion inhibiting admixtures on concrete properties. *Constr. Build. Mat.*, 18(7), 483-489
- [101] Kondratova IL, Montes P, Bremner TW (2003). Natural marine exposure results for reinforced concrete slabs with corrosion inhibitors.*Cement Concrete Compos.*, 25(4-5): 483-490.

- [102] Tritthart J, Banfill P.F.G., (2001). Nitrite binding in cement. *Cement Concrete Res.*, 31(7),1093-1100
- [103] Cruz J, Martínez R, Genesca J, García-Ochoa E (2004). Experimental and theoretical study of 1-(2-ethylamino)-2-methylimidazoline as an inhibitor of carbon steel corrosion in acid media. *Journal of Electroanal. Chem.*, 566(1),111-121.
- [104] Ormellese M, Lazzari L, Goidanich S, Fumagalli G, Brenna A. (2009). A study of organic substances as inhibitors for chloride-induced corrosion in concrete. *Corrosion Sci.*, 51(12),2959-2968.
- [105] El Azhar M, Mernari B, Traisnel M, Bentiss F, Lagrenée M, (2001). Corrosion inhibition of mild steel by the new class of inhibitors in acidic media. *Corrosion Sci.*, 43(12),2229-2238.
- [106] Tritthart J (2003). Transport of a surface-applied corrosion inhibitor in cement paste and concrete. *Cement Concrete Res.*, 33(6),829-834
- [107] Gaidis J.M (2004). Chemistry of corrosion inhibitors. *Cement Concrete Compos.* 26(3), 181-189.
- [108] Baddini A., Cardoso S.P, Hollauer E, José-Antonio C. (2007).Statistical analysis of a corrosion inhibitor family on three steel surfaces (duplex, super-13 and carbon) in hydrochloric acid solutions. *Electrochim. Acta*, 53(2),434-446.
- [109] Ali SA, Al-Muallem HA, Rahman SU, Saeed MT (2008).Bisoxazolidines: A new class of corrosion inhibitors of mild steel in acidic media. *Corrosion Sci.*, 50(11),3070-3077.
- [110] Gece G (2008).The use of quantum chemical methods in corrosion inhibitor studies. *Corrosion Sci.*, 50(11),2981-2992.

- [111] Hong J, Kai Z.P, Yan L., (2008).Aminic nitrogen-bearing polydentate Schiff base compounds as corrosion inhibitors for iron in acidic media: A quantum chemical calculation. *Corrosion Sci.*, 50,865– 871.
- [112] Noor E.A, Al-Moubaraki A.H., (2008). Corrosion behaviour of mild steel in Hydrochloric acid solutions. *Int. J. Electrochem. Sci.*, 3,806.
- [113] Saliyan V, Adhikari R, Vasudeva A. (2008). Quinolin-5-ylmethylene-3- {[8-(trifluoromethyl) quinolin-4-yl]thio}propanohydrazide as an effective inhibitor of mild steel corrosion in HCl solution. *Corrosion Sci.*, 50(1),55-61.
- [114] YildIrIm A, Çetin M., (2008), “Synthesis and evaluation of new long alkyl side chain acetamide, isoxazolidine and isoxazoline derivatives as corrosion inhibitors. *Corrosion Sci.*, 50(1),155-165.
- [115] Obot I.B, Obi-Egbedi N.O, and Odozi N.W (2010).Acenaphtho quinoxaline as a novel corrosion inhibitor for mild steel in 0.5 M H<sub>2</sub>SO<sub>4</sub>. *Corrosion Sci.*, 52(3),923-926.
- [116] Benzina M.L, Dhouibi L, Ben M.O, Triki E, Zucchi F. (2008).Investigation of the early effectiveness of an amino-alcohol based corrosion inhibitor using simulated pore solutions and mortar specimens. *Cement and Concrete Compos.*, 30(3),167-173.
- [117] Sawada S, Page CL, Page M.M. (2005). Electrochemical injection of organic corrosion inhibitors into concrete. *Corrosion Sci.*, 47(8),2063-2078.
- [118] BASF Construction Chemicals. (2007). Rheocrete CNI Corrosion Inhibiting Admixture. *Product Data Sheet. BASF Construction Chemicals, LLC.*
- [119] Pham, P.A. and Newton, C.M. (2001). Properties of Concrete Produced with Admixtures Intended to Inhibit Corrosion. *Department of Civil Engineering Research Report, UHM/CE/01-01*

- [120] Uno, J., Robertson, I. N., and Newton, C.M. (2004). Corrosion Susceptibility of Concrete Exposed To A Marine Environment. *Department of Civil and Environmental Engineering, University of Hawaii at Manoa*. Research Report
- [121] Hausmann, D.A. (1967). Steel corrosion in concrete: How does it occur? *Materials Protection*, 6,16-28
- [122] Saaoudi, Abdelkhalek and Assouli, B. and Srhiri, A. (2003). Corrosion Inhibitors in Concrete: A Review. *Chemistry Preprint Archive*, 2003(6),136-157.
- [123] Ryu, H.S., Singh, J.K., Lee, H., Park, W. (2017). An electrochemical study to evaluate the effect of calcium nitrite inhibitor to mitigate the corrosion of reinforcement in sodium chloride contaminated ca(OH)<sub>2</sub> solution. *Advances in Materials Science and Engineering*.
- [124] Bryan, S.N., Alexander, D.D., Coughlin, J.R., Milkowski, A.L., Boffetta, P. (2012). “Ingested nitrate and nitrite and stomach cancer risk: An updated review. *Food and Chemical Toxicology*. 50(10),3646-3665.
- [125] Fei F, Jie H, Wei J, Yu Q, Chen Z. (2014). Corrosion performance of steel reinforcement in simulated concrete pore solutions in the presence of imidazoline quaternary ammonium salt corrosion inhibitor. *Construction and Building Materials*,70(15).
- [126] Master Builders, Inc., (2002). Rheocrete 222+ Organic corrosion inhibitor. *Technical Data Sheet*.
- [127] H Justnes Ravindra K. Dhir , Peter C. Hewlett , and Laszlo J. Csetenyi (2015). Innovations and Developments In Concrete Materials And Construction. *Proceedings of the International Conference held at the University of Dundee, Scotland, UK on 9–11 September 2002*
- [128].Ngala, V. T., Page, C. L. & Page, M. M.(2002).Corrosion inhibitor systems for remedial treatment of reinforced concrete. Part 1: calcium nitrite. *Corros. Sci.* 44, 2073–2087.

- [129] United States Geological Survey, Science for Changing World FY 1999, *Annual Financial Report, Published Dec. 2000.*
- [130] Sika Corporation, (1998). Sika FerroGard 901: Corrosion Inhibiting Admixture. *Technical Data Sheet.*
- [131] Federal Highway Administration. (2011). Fly Ash. U.S. *Department of Transportation Federal Highway Administration.*
- [132] Standard specification for epoxy-coated reinforcing bars, ASTM Designation: A 775-81, *American Society for Testing and Materials*, Philadelphia, 198
- [133] Saricimen H, Mohammad M, Quddus A, Shameem M, Barry MS (2002). Effectiveness of concrete inhibitors in retarding rebar corrosion. *Cement Concrete Compos.*, 24(1): 89-100.
- [134] Andrade, M. C., & Macias, A. (1988). Galvanized Reinforcements in Concrete. Surface Coatings-2, A. D. Wilson, J. W. Nicolson, and H. J. Prosser, eds. *Elsevier Applied Science publications*, 137-182.
- [135] Virmani, Y. P., & Clemeña, G. G. (1998). Corrosion Protection Concrete Bridges. *Federal Highway Administration, Vol. Report No. FHWA-RD-98-099*, 72.
- [136] Roventi, G., Bellezze, T., Giuliani, G., & Conti, C. (2014). Corrosion Resistance of Galvanized Steel Reinforcements in Carbonated Concrete: Effect of Wet–Dry Cycles in Tap Water and in Chloride Solution on the Passivating Layer. *Cement and Concrete Research*, 65, 76-84.
- [137] Xiang-Lin, G., Zheng, D., Qin Y, Wei-Ping, Z. (2020). Corrosion of Stirrups under Different Relative Humidity Conditions in Concrete Exposed to Chloride Environment. *Journal of Materials in Civil Engineering*, 32(1).

- [138] Choe, H., Nishio, Y., Kanematsu, M. (2019). An Investigation on the Usability of Acceleration Test by Impressed Anodic Current for Evaluating Corrosion Behavior of Hot-Dip Galvanized Rebar in Concrete. *Materials*, 12(21), 3566.
- [139] Zhang, J. Baldock, B. 2015. Condition Assessment and Corrosion Mitigation of Galvanized Steel Reinforcement in Concrete Structures, *NRC-CNRC*, Ottawa
- [140] Andrade C., Alonso C. (1996) Durability Design Based on Models for Corrosion Rates. In: Jennings H., Kropp J., Scrivener K. (eds) The Modelling of Microstructure and its Potential for Studying Transport Properties and Durability. NATO ASI Series (Series E: Applied Sciences), *Springer, Dordrecht*,304.
- [141] Andrade, C., and Alonso, C. (1996b). Progress on design and residual life calculation with regard to rebar corrosion of reinforced concrete. In N. Berke, E. Escalante, C. Nmai, and D. Whiting (Eds.), Techniques to Assess the Corrosion Activity of Steel Reinforced Concrete Structures. *ASTM STP 1276*, 23–40.
- [142] Rodriguez, J., Ortega, L., Casal, J., and Diez, J. (1996). Corrosion of reinforcement and service life of concrete structures. In C. Sj ostr om (Ed.), Durability of Building Materials and Components, 7 (1),117–126).
- [143] Duracrete (2000). Probabilistic Performance based Durability Design of Concrete Structures. *The European Union–Brite EuRam III*, BE95-1347/R17, CUR, Gouda, The Netherlands.
- [144] Al-Harthy, A., Stewart, M.G. (2008). Pitting corrosion and structural reliability of corroding RC structures: Experimental data and probabilistic analysis. *Reliability Engineering & System Safety*, 93(3),373-382.

- [145] Muhammad, U.K., Shamsad, A., and Husain, J. A(2017).Chloride-Induced Corrosion of Steel in Concrete: An Overview on Chloride Diffusion and Prediction of Corrosion Initiation Time. *International Journal of Corrosion*,117,1-10.
- [146] RILEM TC 154-EMC (2003). Electrochemical Techniques for Measuring Metallic Corrosion. *Materials and Structures / Matériaux et Constructions*, 37, 623-643.
- [147] Ahmad S. (2003). Reinforcement corrosion in concrete structures, its monitoring and service life prediction: A Review. *Cement and Concrete Composites*, 25(4-5), 459-471.
- [148] Otieno, M., Beushausen, H., Alexander, M. (2011). Prediction of Corrosion Rate in RC Structures - A Critical Review.*RILEM*, 5,15-37
- [149] Montemor, M. F., Simoes, A. M. P., and Salta, M. M. (2000). Effect of fly ash on concrete reinforcement corrosion studied by EIS. *Cement and Concrete Composites*,22(3), 175-185.
- [150] Sathiyarayanan, S., Natarajan, P., Saravanan, K., Srinivasan, S., and Venkatachari, G. (2006). Corrosion monitoring of steel in concrete by galvanostatic pulse technique. *Cement and Concrete Composites*,28(7), 630-637.
- [151] Andrade, C., and Alonso, C. (2004). Test methods for on-site corrosion rate measurement of steel reinforcement in concrete by means of the polarization resistance method. *Materials and Structures*, 37(9), 623-643.
- [152] Des Barker & Frank, C. W. (1991). Applications of Faraday's Laws of Electrolysis in Metal Finishing. *Transactions of the IMF*, 69(4), 158-162.
- [153] RILEM TC 154-EMC (2003). Electrochemical Techniques for Measuring Metallic Corrosion. *Materials and Structures / Matériaux et Constructions*, 36,461-471
- [154] Vu, K.A.T. & Stewart, M.G. (2000). Structural reliability of concrete bridges including improved chloride-induced corrosion models. *Structural Safety*, 22(4), 313-333



- [155] Carmen A, (2010). Types of models of service life of Reinforcement: The case of resistivity. *Institution of construction science*,1(2).
- [156] Markeset, G., Kioumars, M. (2016). Need for further development in service life modelling of concrete structures in chloride environment. *Proceedings of Sustainable Civil Engineering Structures and Construction Materials*,171(2017),549-556.
- [157] Hunkeler,F.(2005).Corrosion in reinforced concrete: processes and mechanisms. *Woodhead Publishing Series in Civil and Structural Engineering*,1-45.
- [158] Tang L. (1996). Chloride Transport in Concrete - Measurement and Prediction. *PhD thesis, Gothenburg, Sweden, Chalmers University of Technology*.
- [159] Tang L. (2008). Engineering expression of the ClinConc model for prediction of free and total chloride ingress in submerged marine concrete. *Cem Concr Res*,38(89),1092-1097.
- [160] Bastidas-Arteaga, E., Chateauneuf, A., Sánchez-Silva, M., Bressolette, P., Schoefs, F. (2011). A comprehensive probabilistic model of chloride ingress in unsaturated concrete. *Engineering Structures. Elsevier*, 33 (3),720-730.
- [161] Maage, M., Poulsen, E., Vennesland, O., Carlsen,J.E.(1994).Service Life Model for Concrete Structures exposed to Marine Environment. Initiation period. *SINTEF report STF70 A94082*. Trondheim, Norway.
- [162] Luping, T., Nilsson, L.O., (1992). Chloride Diffusivity in High Strength Concrete at different Ages. *Nordic Concrete Research, Publication* ,11(1).
- [163] Maage, M., Poulsen, E., Vennesland, O., Carlsen,J.E.(1993).Chloride penetration in High Performance Concrete exposed to Marine Environment. *Symposium on Utilization of High Strength Concrete*. Lillehammer, Norway.
- [164] BE95-1347(1998). *Modelling of Degradation – Report 4-5*.

- [165] Gehlen, C. (2000). Probabilistic life measurement of reinforced concrete structures. Reliability considerations for effective prevention of reinforcement corrosion. *DAfStb*, 510(1).
- [166] Mangat, P.S., Molloy, B.T. (1994). Prediction of long term chloride concentration in concrete. *Materials and Structures*, 27, 338-346.
- [167] Williamson, G. (2007). Service Life Modeling of Virginia Bridge Decks. *Virginia Polytechnic Institute and State University*.
- [168] Maheswaran, T., Sanjayan, J.G. (2004). A semi-closed-form solution for chloride diffusion in concrete with time-varying parameters. *Magazine of Concrete Research*, 56(6):359-366.
- [169] Thomas, M. D. A. and Bamforth, P. B. (1999). Modelling Chloride Diffusion in Concrete: Effect of Fly Ash and Slag. *Cement and Concrete Research*, 29, 487-495.
- [170] Fib (2006), fib Bulletin 34: Model Code for Service Life Design. *Concrete*, 5(4).
- [171] Saetta, A.V., Scotta, R.V., Vitaliani, R. (1993). Analysis of Chloride Diffusion into Partially Saturated Concrete. *ACI Materials Journal*, 90(5).
- [172] Nilsson, L.O., Carcasses. (2004). Models for chloride ingress into concrete – a critical analysis. *Report of Task 4.1 in EU-Project G6RD-CT-2002-00855*, ChlorTest,
- [173] Zhang, J. and Z. Lounis (2006). Sensitivity analysis of simplified diffusion-based corrosion initiation model of concrete structures exposed to chlorides. *Cement and Concrete Research*, 36(7), 1312-1323.
- [174] Boddy, A., Bentz, E., Thomas, M.D.A, Hooton, R.D. (1999). An overview and sensitivity study of a multimechanistic chloride transport model. *Cement and Concrete Research*, 29: 827-837.

- [175] Tuutti, K. (1982). Corrosion of steel in concrete. *Swedish Cement and Concrete Research Institute*, Stockholm.
- [176] Ehlen, M.A. (2012). Life -365 Service life Cost prediction and Computer Program for predicting the Service Life and Life cycle costs of Reinforced Concrete Exposed to Chlorides. Version 2.1. *User's Manual, Life-365 Consortium II*.
- [177] Cady, P. D., and Weyers R. E. (1983). Chloride Penetration and the Deterioration of Concrete Bridge Decks. *Cement, Concrete & Aggregate*, 5(2), 81-87.
- [178] El Hajj, Peter. (2015). Probabilistic Modelling of Multiphasic Degradations for Maintenance Optimization of Infrastructures in Civil Engineering. *Thesis for Doctor of Philosophy in Civil Engineering, University of Nantes*.
- [179] Bazant Z. P. (1979). Physical Model for Steel Corrosion in Sea Structures-Theory. *Journal of the Structural Division*, 105(6) 1137-1153.
- [180] Morinaga S. (1989). Prediction of Service Lives of Reinforced Concrete Buildings Based on Rate of Corrosion of Reinforcing Steel. *Special Report of the Institute of Technology, Skimiza Corporation, Japan*.
- [181] Wang, X.M., Zhao, H.Y., (1993). The residual service life prediction of RC structures In: *Nagataki, S. (Ed.), Durability of Building Materials and Components*, 6, 1107–1114.
- [182] Indian Road Congress, IRC special publication 60-2002. An approach document for assessment of remaining life of concrete bridges. *IRC Publications, Indian Road Congress*.
- [183] Vu, K., Stewart, M.G. and Mullard, J. (2005). Corrosion-Induced Cracking: Experimental Data and Predictive Models. *ACI Structural Journal*, 102(5), 719.
- [184] Amendment No. 1 August 2005 to IS 10430: 2000 Criteria for Design of lined canals and guidance for selection of type of lining.

- [185] Li, C.Q. (2004a). Reliability based service life prediction of corrosion affected concrete structures. *Journal of Structural Engineering*, 130(10), 1570–1577.
- [186] Saraswathy V, Song H. (2007). Corrosion performance of rice husk ash blended concrete. *Construction and Building Materials*, 21, 1779–1784.
- [187] ASTM G109-07(2013). Standard Test Method for Determining Effects of Chemical Admixtures on Corrosion of Embedded Steel Reinforcement in Concrete Exposed to Chloride Environments.
- [188] ASTM G1 – 03 Standard Practice for Preparing, Cleaning, and Evaluating Corrosion Test Specimens.
- [189] Muhammad, N.S. H. (2008). Bond of High Strength Concrete with High Strength Reinforcing Steel. *The Open Civil Engineering Journal*, 2, 143-147.
- [190] Arumugam, B. (2014). Effect of Specific Gravity on Aggregate Varies the Weight of Concrete Cube. *International Journal of Civil Engineering*, 1(3), 1-9.
- [191] BS EN 1097-6 (2000). Tests for mechanical and physical properties of aggregates. Determination of particle density and water absorption. *British Standard Institution, London*.
- [192] BS 882 (1992). Specification for aggregates from natural sources for concrete. *British Standard Institutes*.
- [193] BS 8007 (1987). Code of practice for the design of concrete structures for retaining aqueous liquids. *British Standard Institutes*.
- [194] Zerdi A.T. (2014). Strength Exhibition of M25 Grade Concrete with Limestone Quarry Dust Utilization for Fine Aggregates. *Global Journal of Research Analysis International*, 5(1),2016.

- [195] ASTM C117(1995). Standard Test Method for Materials finer than 75- $\mu$ m (No. 200) sieve in mineral aggregates by washing. *American Society for Testing and Materials*.
- [196] BS 882 (1992). Specification for aggregates from natural sources for concrete. *British Standards Institute, London United Kingdom*.
- [197] ASTM C40, (2004). Standard Test Method for effect of organic impurities in fine aggregates on strength of mortar. *American Society for Testing and Materials ASTM International*.
- [198] Neville A. M. and Brooks J.J. (2010). Concrete Technology, 2nd edition. Prentice Hall.
- [199] BS 12, Specification for Portland cement (BSI Publications, London, 1996).
- [200] KS EAS 18. Cement Standard - Part 1: Composition, Specifications and Conformity Criteria. KEBS, Kenya. 2001.
- [201] Østnor T.A. and Justnes H. (2011). Anodic corrosion inhibitors against chloride induced corrosion of concrete rebars. *Advances in Applied Ceramics*, 110(3), 131-136.
- [202] Lavanya, G., Jegan, J. (2015). ( Evaluation of relationship between split tensile strength and compressive strength for geopolymer concrete of varying grades and molarity. *International Journal of Applied Engineering Research*, 10(15), 35523-35527.
- [203] ACI Standard (2014): Building Code Requirements for Structural Concrete (ACI 318-14)
- [204] Arıoğlu, N., Girgin, Z.C., Arıoğlu, E. (2006). Evaluation of Ratio between Splitting Tensile Strength and Compressive Strength for Concretes up to 120 MPa and its Application in Strength Criterion. *ACI Material Journal*, 18.
- [205] CEB-FIP Model Code for Concrete Structures (1990). Evaluation of the Time Dependent Behaviour of Concrete. *Bulletin d'Information No. 199, Comité Européen du Béton/Fédération Internationale de la Précontrainte, Lausanne, 1991, 201:11.*

- [206] Gardner, N. J. (1990). Effect of Temperature on the Early-Age Properties of Type I, Type III, and Type I/Fly Ash Concretes. *ACI Materials Journal*, 87(1):68-78.
- [207] Orangun C.O., Jirsa I.O., Breen J.E. (1977). A re-evaluation of test data on development length and splices. *ACI J.*, 74(3).
- [208] Stanish K., Hooton R.D. and Pantazopoulou, S.J. (1999). Corrosion effects on bond strength in reinforced concrete. *ACI Structural Journal*, 96(6), 915-21.
- [209] Timoshenko, S.P. and Goodier, J.N. (1982). Theory of elasticity, New York, 1982.
- [210] Liu, Y., and Weyers, R.E. (1998a). Modeling the time-to-corrosion cracking in chloride contaminated reinforced concrete structures. *ACI Materials Journal*, 95(6), 675-681.
- [211] Fontana, M.G. and Greene, N.D. (1978). Corrosion Engineering, New York, 1978.

## APPENDICES

### Appendix A1: Properties of materials used in the research

**Table a: Result of sieve analysis of coarse aggregates**

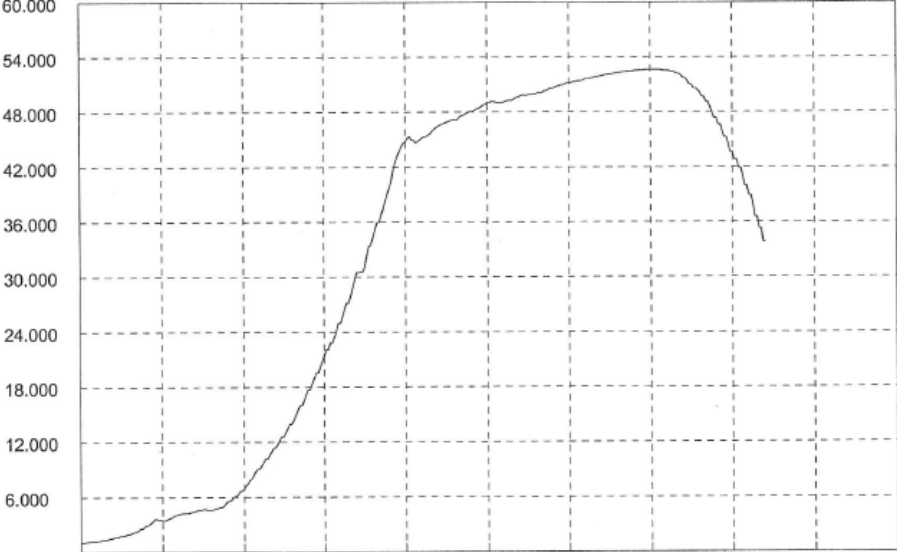

<b>SIEVE ANALYSIS</b>						
Sample Type	COARSE AGGREGATES					
Sample source	Kenya Builders					
Client				Project		
Test date:	22-Sep-17			Corrosion		
Specification	BS EN 12620:2002 Table 3.1					
Dry sample mass		(gm)	5548			
Sieve size (mm)	Retained mass (gm)	% Retained (%)	Cumulative passed percentage (%)	Acceptance Criteria		
				Min(%)	Max (%)	
37.5	0	0.0	100.0	100		
20	801	14.4	85.6	85	100	
14	3126	56.3	29.2	0	70	
10	1231	22.2	7.0	0	25	
5	190	3.4	3.6	0	5	
2.36	0	0.0	3.6			
	5348					

**Table b: Result of sieve analysis of fine aggregates**

<b>SIEVE ANALYSIS</b>					
Sample Type	FINE AGGREGATES-MACHAKOS RIVER SAND				
Sample source	Machakos				
Client			Project		
Test date:	23-Sep-17		Corrosion		
Specification	BS EN 12620:2002 Table 3.2				
Pan mass	(gm)	100			
Initial dry sample mass + pan	(gm)	470			
Initial dry sample mass	(gm)	347	Fine mass	(gm)	6
Washed dry sample mass + pan	(gm)	441	Fine percent	(%)	1.7
Washed dry sample mass	(gm)	341	Acceptance Criteria	(%)	
Sieve size (mm)	Retained mass (gm)	% Retained (%)	Cumulative passed percentage (%)	Acceptance Criteria	
				Min(%)	Max (%)
14	0	0.0	100.0	100	
10	0	0.0	100.0	100	
4.76	4	1.2	98.8	89	100
2.36	9	2.6	96.3	60	100
1.18	28	8.1	88.2	30	100
0.6	76	21.9	66.3	15	100
0.3	125	36.0	30.3	5	70
0.15	92	26.5	3.7	0	15
0.075	30	8.6	-4.9	0	3
	6	1.7			
	370				



**c) Physical and Chemical Analysis of the reinforcement bars used in the research.**

<b>Test Certificate</b>		
Name of Company	: APEX STEEL LIMITED	
Address	: P.O.Box No.18441-00500,NAIROBI	
To	:	
Sample Identification	: 10mm DEFORMED	
Machine	: Universal Testing Machine , 1000 kN	
Input Data	: File Name : 17-08-10mmD-2019 , Record No. : 10 , Date : 17-08-2019	
	: Sample Type -- TMT , Area : 78.042 mm <sup>2</sup>	
	: Length = 586.0 mm , Weight = 0.359 kg , Weight / meter = 0.613 kg/mtr	
	: Gauge Length : 50 mm Final Gauge Length: 59.73 mm	
Results of	: Tension Test	
Maximum Force (Fm)	: 52.600 kN	Yield Stress : 0.581 kN/mm <sup>2</sup>
Disp. at Fm	: 27.700 mm	UTS/YS Ratio : 1.160
Max. Disp.	: 33.600 mm	
Tensile Strength (Rm)	: 0.674 kN/mm <sup>2</sup>	
Elongation	: 19.460 %	
Yield Load	: 45.350 kN	
* Note	: Yield Calculated from graph	
Graph	: Load Vs Displacement	
Load kN		
Y0=0.000 X0=0.000	-----> Displacement mm	
TESTED BY	INSPECTED BY	WITNESSED BY
LEE NYAGA		



Laboratory Test Report

KEBS Sample Ref. No: BS201734664

PRIVATE SAMPLE

Date: 23 November, 2017

1. Description of Sample: Steel Reinforcement Bars

2. Sample Submitted by: Philip

6. Lab Ref: KEBS/TES/MEC-NAR/M/17

3. Customer Contact: Philip.

7. Date of Receipt: 9 November, 2017

4. Customers Ref No:

8. Date Analysis Started: 14 November, 2017

5. Customer's Address P.O. BOX 18070-00100, KENYA

9. Sample Submission Form No: 174895

10. Additional Information provided by the customer:

T10

11. Acceptance criteria-title and number of specification against which it is tested:

ISO 6935-2:2007: Steel for the Reinforcement of Concrete-Part 2: Ribbed Bars

12. Parameters tested and Method(s) of test: as listed in the report below:

LABORATORY TEST REPORT

Table with 4 columns: No., Parameters, Results, Requirements, Test Method No. It contains 4 main test entries: Bend, Mass/metre run, Re-bend, and Tensile strength (with sub-entries I, II, III).

COMMENTS/REMARKS:

The sample performed as shown

[Signature]

Charles Mugaambi - Laboratory Analyst (Mechanical)

FOR: MANAGING DIRECTOR

23 November, 2017

Date of Issue

**d) Chemical analysis of reinforcement used.**

Program: Fe-11-F  
 Comment: Apex Steel (Chemical Analysis) 124973  
 Average (n=0)

16-08-2019 06:05:36 PM

Elements: Concentration

Sample No: VSHYDRO (KENYA) LIMITED.  
 Sample Id: DEFORM 10mm (31524413)

Quality:

	C	Si	Mn	P	S	Cr	Ni	Mo	Al	Cu	Ti	V
	%	%	%	%	%	%	%	%	%	%	%	%
$\bar{x}$	0.209	0.104	0.54	0.031	0.025	0.100	0.071	0.013	0.0052	0.114	0.0008	0.0047
	Fe	C Eq										
	%	%										
$\bar{x}$	98.78	0.335										



**Table e) Chemical analysis of Cement.**

SN	Test	Result			KS EAS 18-1: 2001 Requirement
		Sample	Sample	Sample	
		A	B	C	
1.	CaO%	59.86	59.11	58.82	Sum $\geq$ 50
2.	SiO <sub>2</sub> %	16.56	21.56	19.47	Sum $\geq$ 50
3.	SO <sub>3</sub> %	2.02	2.78	2.03	$\leq$ 3.5
4.	MgO%	1.76	1.04	0.57	$\leq$ 5
5.	K <sub>2</sub> O%	0.027	0.051	-	
6.	Fe <sub>2</sub> O <sub>3</sub> %	2.32	3.48	1.44	
7.	Al <sub>2</sub> O <sub>3</sub>	7.61	8.09	6.85	3-8
8.	Na <sub>2</sub> O <sub>3</sub> %	0.054	0.018		
9.	LOI%	0.11	0.10	4.75	$\leq$ 5
10.	Cl%	0.012	0.016	0.014	$\leq$ 0.1
11.	IR%	2.20	0.55	1.96	$\leq$ 5

## f) Fly Ash

Origin –India

### Chemical Properties to ASTM C618

SN	Chemical Parameter	Unit	Test Method	Result
1.	SiO <sub>2</sub>	%	ASTM C618	47.18
2.	Al <sub>2</sub> O <sub>3</sub>	%	ASTM C618	19.87
3.	Fe <sub>2</sub> O <sub>3</sub>	%	ASTM C618	0.99
4.	UBC	%	ASTM C618	0.80
5.	Na <sub>2</sub> O	%	ASTM C618	2.04
6.	Fineness (Residue on 45	%	ASTM C618	8.69
7.	Moisture Content	%	ASTM C618	0.07
8.	MgO	%	ASTM C618	3.79
9.	Cl	%	ASTM C618	0.047
10.	Bulky Density	Cm/cc	ASTM C618	1.03
11.	TiO <sub>2</sub>	%	ASTM C618	1.01
12.	CaO <sub>2</sub>	%	ASTM C618	5.64
13.	K <sub>2</sub> O	%	ASTM C618	1.17
14.	P <sub>2</sub> O <sub>5</sub>	%	ASTM C618	0.243

## Appendix A2: Concrete Mix design

### Concrete mix design form

Stage	Item	Reference or calculation	Values																								
1	1.1	Characteristic strength	Specified $\left\{ \begin{array}{l} \dots\dots\dots 25 \dots\dots\dots \text{N/mm}^2 \text{ at } \dots\dots\dots 28 \dots\dots\dots \text{days} \\ \text{Proportion defective } \dots\dots\dots 5 \dots\dots\dots \% \end{array} \right.$																								
	1.2	Standard deviation	Fig 3 $\dots\dots\dots \text{N/mm}^2 \text{ or no data } \dots\dots\dots 8 \dots\dots\dots \text{N/mm}^2$																								
	1.3	Margin	C1 or Specified $(k = \dots\dots\dots 1.65 \dots\dots\dots) \dots\dots\dots 1.65 \dots\dots\dots \times \dots\dots\dots 8 \dots\dots\dots = \dots\dots\dots 13.2 \dots\dots\dots \text{N/mm}^2$																								
	1.4	Target mean strength	C2 $\dots\dots\dots 25 \dots\dots\dots + \dots\dots\dots 13.2 \dots\dots\dots = \dots\dots\dots 38.2 \dots\dots\dots \text{N/mm}^2$																								
	1.5	Cement strength class	Specified 42.5/52.5																								
	1.6	Aggregate type: coarse Aggregate type: fine	Crushed/uncrushed Crushed/uncrushed																								
	1.7	Free-water/cement ratio	Table 2, Fig 4 $\dots\dots\dots 0.57 \dots\dots\dots$																								
	1.8	Maximum free-water/cement ratio	Specified $\dots\dots\dots 0.5 \dots\dots\dots$ } Use the lower value <span style="border: 1px solid black; padding: 2px;">0.5</span>																								
2	2.1	Slump or Vebe time	Specified Slump $\dots\dots\dots 60-180 \dots\dots\dots$ mm or Vebe time $\dots\dots\dots 0-3 \dots\dots\dots$ s																								
	2.2	Maximum aggregate size	Specified $\dots\dots\dots$ mm																								
	2.3	Free-water content	Table 3 <span style="border: 1px solid black; padding: 2px;">225</span> kg/m <sup>3</sup>																								
3	3.1	Cement content	C3 $\dots\dots\dots 225 \dots\dots\dots + \dots\dots\dots 0.5 \dots\dots\dots = \dots\dots\dots 450 \dots\dots\dots$ kg/m <sup>3</sup>																								
	3.2	Maximum cement content	Specified $\dots\dots\dots$ kg/m <sup>3</sup>																								
	3.3	Minimum cement content	Specified $\dots\dots\dots 290 \dots\dots\dots$ kg/m <sup>3</sup>																								
	3.4	Modified free-water/cement ratio	$\dots\dots\dots$ } use 3.1 if $\leq 3.2$ use 3.3 if $> 3.1$ <span style="border: 1px solid black; padding: 2px;">450</span> kg/m <sup>3</sup>																								
4	4.1	Relative density of aggregate (SSD)	$\dots\dots\dots$ known/assumed																								
	4.2	Concrete density	Fig 5 $\dots\dots\dots 2400 \dots\dots\dots$ kg/m <sup>3</sup>																								
	4.3	Total aggregate content	C4 $\dots\dots\dots 2400 \dots\dots\dots - \dots\dots\dots 450 \dots\dots\dots - \dots\dots\dots 225 \dots\dots\dots = \dots\dots\dots 1725 \dots\dots\dots$ kg/m <sup>3</sup>																								
5	5.1	Grading of fine aggregate	Percentage passing 600 $\mu\text{m}$ sieve $\dots\dots\dots 66.33 \dots\dots\dots$ %																								
	5.2	Proportion of fine aggregate	Fig 6 $\dots\dots\dots 37.7 \dots\dots\dots$ %																								
	5.3	Fine aggregate content	C5 $\left\{ \begin{array}{l} \dots\dots\dots 1725 \dots\dots\dots \times \dots\dots\dots 0.377 \dots\dots\dots = \dots\dots\dots 650.325 \dots\dots\dots \text{kg/m}^3 \\ \dots\dots\dots 1725 \dots\dots\dots - \dots\dots\dots 650.325 \dots\dots\dots = \dots\dots\dots 1074.675 \dots\dots\dots \text{kg/m}^3 \end{array} \right.$																								
	5.4	Coarse aggregate content		<span style="border: 1px solid black; padding: 2px;">1074.675</span> kg/m <sup>3</sup>																							
<table border="1" style="width: 100%; border-collapse: collapse;"> <thead> <tr> <th rowspan="2">Quantities</th> <th rowspan="2">Cement (kg)</th> <th rowspan="2">Water (kg or litres)</th> <th rowspan="2">Fine aggregate (kg)</th> <th colspan="3">Coarse aggregate (kg) 5-20mm</th> </tr> <tr> <th>10 mm</th> <th>20 mm</th> <th>40 mm</th> </tr> </thead> <tbody> <tr> <td>per m<sup>3</sup> (to nearest 5 kg)</td> <td>450</td> <td>225</td> <td>650</td> <td colspan="3">1074.6</td> </tr> <tr> <td>per trial mix of <math>0.0265 \text{ m}^3</math></td> <td>13.33</td> <td>6.67</td> <td>20</td> <td colspan="3">40</td> </tr> </tbody> </table>				Quantities	Cement (kg)	Water (kg or litres)	Fine aggregate (kg)	Coarse aggregate (kg) 5-20mm			10 mm	20 mm	40 mm	per m <sup>3</sup> (to nearest 5 kg)	450	225	650	1074.6			per trial mix of $0.0265 \text{ m}^3$	13.33	6.67	20	40		
Quantities	Cement (kg)	Water (kg or litres)	Fine aggregate (kg)					Coarse aggregate (kg) 5-20mm																			
				10 mm	20 mm	40 mm																					
per m <sup>3</sup> (to nearest 5 kg)	450	225	650	1074.6																							
per trial mix of $0.0265 \text{ m}^3$	13.33	6.67	20	40																							

## Concrete mix design form

Stage	Item	Reference or calculation	Values				
1	1.1	Characteristic strength	Specified { ..... 30 ..... N/mm <sup>2</sup> at ..... 28 ..... days Proportion defective ..... %				
	1.2	Standard deviation	Fig 3 ..... N/mm <sup>2</sup> or no data ..... N/mm <sup>2</sup>				
	1.3	Margin	C1 or Specified (k = 1.64) 1.64 × 5 = 8.2 N/mm <sup>2</sup>				
	1.4	Target mean strength	C2 ..... 30 ..... + ..... 8.2 ..... = ..... 38.2 ..... N/mm <sup>2</sup>				
	1.5	Cement strength class	Specified 42.5/52.5				
	1.6	Aggregate type: coarse Aggregate type: fine	Crushed/uncrushed Crushed/uncrushed				
	1.7	Free-water/cement ratio	Table 2, Fig 4 ..... 0.54				
	1.8	Maximum free-water/cement ratio	Specified ..... 0.5 } Use the lower value <span style="border: 1px solid black; padding: 2px;">0.5</span>				
2	2.1	Slump or Vebe time	Specified Slump 60-180 ..... mm or Vebe time ..... 0.3 ..... s				
	2.2	Maximum aggregate size	Specified ..... 20 ..... mm				
	2.3	Free-water content	Table 3 ..... <span style="border: 1px solid black; padding: 2px;">225</span> kg/m <sup>3</sup>				
3	3.1	Cement content	C3 ..... 225 ..... + ..... 0.5 ..... = ..... 450 ..... kg/m <sup>3</sup>				
	3.2	Maximum cement content	Specified ..... kg/m <sup>3</sup>				
	3.3	Minimum cement content	Specified ..... 300 ..... kg/m <sup>3</sup> use 3.1 if ≤ 3.2 use 3.3 if > 3.1 <span style="border: 1px solid black; padding: 2px;">450</span> kg/m <sup>3</sup>				
	3.4	Modified free-water/cement ratio	..... <span style="border: 1px solid black; display: inline-block; width: 50px; height: 15px;"></span>				
4	4.1	Relative density of aggregate (SSD)	..... known/assumed				
	4.2	Concrete density	Fig 5 ..... 2400 ..... kg/m <sup>3</sup>				
	4.3	Total aggregate content	C4 ..... 2400 ..... - ..... 450 ..... - ..... 225 ..... = ..... 1725 ..... kg/m <sup>3</sup>				
5	5.1	Grading of fine aggregate	Percentage passing 600 μm sieve ..... 66.3 ..... %				
	5.2	Proportion of fine aggregate	Fig 6 ..... %				
	5.3	Fine aggregate content	C5 { ..... 1725 ..... × ..... 0.37 ..... = <span style="border: 1px solid black; padding: 2px;">638</span> kg/m <sup>3</sup> ..... 1707 ..... - ..... 638 ..... = <span style="border: 1px solid black; padding: 2px;">1069</span> kg/m <sup>3</sup>				
	5.4	Coarse aggregate content					
<b>Quantities</b>		<b>Cement (kg)</b>	<b>Water (kg or litres)</b>	<b>Fine aggregate (kg)</b>	<b>Coarse aggregate (kg)</b>		
					<b>10 mm</b>	<b>20 mm</b>	<b>40 mm</b>
per m <sup>3</sup> (to nearest 5 kg)		450	225	638	1069		
per trial mix of ..... 0.0265 ..... m <sup>3</sup>		12	6	16	28		

Items in *italics* are optional limiting values that may be specified (see Section 7).

Concrete strength is expressed in the units N/mm<sup>2</sup>. 1 N/mm<sup>2</sup> = 1 MN/m<sup>2</sup> = 1 MPa. (N = newton; Pa = pascal.)

The internationally known term 'relative density' used here is synonymous with 'specific gravity' and is the ratio of the mass of a given volume of substance to the mass of an equal volume of water. SSD = based on the saturated surface-dry condition.

(Source: Building Research Establishment)

## Concrete mix design form

Stage	Item	Reference or calculation	Values				
1	1.1	Characteristic strength	Specified { ..... 35 ..... N/mm <sup>2</sup> at ..... 28 ..... days Proportion defective ..... %				
	1.2	Standard deviation	Fig 3 ..... N/mm <sup>2</sup> or no data ..... N/mm <sup>2</sup>				
	1.3	Margin	C1 or Specified (k = 1.64 ) 1.64 × 5 = 8.2 N/mm <sup>2</sup> ..... N/mm <sup>2</sup>				
	1.4	Target mean strength	C2 ..... 35 ..... + ..... 8.2 ..... = ..... 43.2 ..... N/mm <sup>2</sup>				
	1.5	Cement strength class	Specified 42.5/52.5				
	1.6	Aggregate type: coarse Aggregate type: fine	Crushed/uncrushed Crushed/uncrushed				
	1.7	Free-water/cement ratio	Table 2, Fig 4 ..... 0.48 .....				
	1.8	Maximum free-water/cement ratio	Specified ..... 0.5 ..... } Use the lower value <span style="border: 1px solid black; padding: 2px;">0.48</span>				
2	2.1	Slump or Vebe time	Specified Slump ..... 60-180 ..... mm or Vebe time ..... 0.3 ..... s				
	2.2	Maximum aggregate size	Specified ..... 20 ..... mm				
	2.3	Free-water content	Table 3 ..... <span style="border: 1px solid black; padding: 2px;">225</span> kg/m <sup>3</sup>				
3	3.1	Cement content	C3 ..... 225 ..... + ..... 0.48 ..... = ..... 469 ..... kg/m <sup>3</sup>				
	3.2	Maximum cement content	Specified ..... kg/m <sup>3</sup>				
	3.3	Minimum cement content	Specified ..... 300 ..... kg/m <sup>3</sup>				
	3.4	Modified free-water/cement ratio	use 3.1 if ≤ 3.2 use 3.3 if > 3.1 <span style="border: 1px solid black; padding: 2px;">469</span> kg/m <sup>3</sup>				
4	4.1	Relative density of aggregate (SSD)	..... known/assumed				
	4.2	Concrete density	Fig 5 ..... 2400 ..... kg/m <sup>3</sup>				
	4.3	Total aggregate content	C4 ..... 2400 ..... - ..... 469 ..... - ..... 225 ..... = ..... 1706 ..... kg/m <sup>3</sup>				
5	5.1	Grading of fine aggregate	Percentage passing 600 μm sieve ..... 66.3 ..... %				
	5.2	Proportion of fine aggregate	Fig 6 ..... %				
	5.3	Fine aggregate content	C5 { ..... 1706 ..... × ..... 0.37 ..... = <span style="border: 1px solid black; padding: 2px;">631</span> kg/m <sup>3</sup> ..... 1706 ..... - ..... 631 ..... = <span style="border: 1px solid black; padding: 2px;">1075</span> kg/m <sup>3</sup>				
	5.4	Coarse aggregate content					
<b>Quantities</b>		<b>Cement (kg)</b>	<b>Water (kg or litres)</b>	<b>Fine aggregate (kg)</b>	<b>Coarse aggregate (kg)</b>		
					<b>10 mm</b>	<b>20 mm</b>	<b>40 mm</b>
per m <sup>3</sup> (to nearest 5 kg)		469	225	631	1075		
per trial mix of ..... 0.0265 ..... m <sup>3</sup>		12	6	15	25		

Items in italics are optional limiting values that may be specified (see Section 7).

Concrete strength is expressed in the units N/mm<sup>2</sup>. 1 N/mm<sup>2</sup> = 1 MN/m<sup>2</sup> = 1 MPa. (N = newton; Pa = pascal.)

The internationally known term 'relative density' used here is synonymous with 'specific gravity' and is the ratio of the mass of a given volume of substance to the mass of an equal volume of water.

SSD = based on the saturated surface-dry condition.



### Appendix A3: Results of fresh and hardened concrete

**Table a Slump and compacting Factor**

<b>Mix with and without inhibitor</b>	<b>Cement Type</b>	<b>w/c ratio</b>	<b>Slump(mm)</b>	<b>Compacting Factor</b>
Control-No inhibitor	A	0.5	73.3	0.97
	B	0.5	68	0.96
	C	0.5	93	0.95
Inhibitor X	A <sub>X</sub>	0.5	60	0.95
	B <sub>X</sub>	0.5	63	0.93
	C <sub>X</sub>	0.5	64	0.94
Fly Ash	A <sub>F</sub>	0.5	55	0.93
	B <sub>F</sub>	0.5	40	0.94
	C <sub>F</sub>	0.5	45	0.97
Inhibitor Y	A <sub>Y</sub>	0.5	66	0.95
	B <sub>Y</sub>	0.5	65	0.95
	C <sub>Y</sub>	0.5	66	0.92
Inhibitor Z	A <sub>Z</sub>	0.5	60	0.96
	B <sub>Z</sub>	0.5	65	0.95
	C <sub>Z</sub>	0.5	64	0.96

**Table b Result of Compressive Strength N/mm<sup>2</sup>**

Brand of OPC	Age at Testing			Type of inhibitor
	7 days	14 days	28 days	
A	25.81	40.86	41.29	Control –No
B	34.89	40.89	41.09	inhibitor
C	36.37	39.23	44.89	
<b>Min.</b>	<b>17.80</b>	<b>22.5</b>	<b>25</b>	
<b>expected</b>				
A <sub>X</sub>	35.26	44.28	45.34	Calcium nitrite
B <sub>X</sub>	35.32	43.20	44.63	based inhibitor
C <sub>X</sub>	37.06	46.84	47.26	
A <sub>F</sub>	14.149	19.38	28.20	Fly ash
B <sub>F</sub>	15.15	20.25	28.84	
C <sub>F</sub>	16.7	22.73	29.63	
A <sub>Y</sub>	25.63	40.26	44.25	Calcium nitrate
B <sub>Y</sub>	26.83	41.36	43.25	based inhibitor
C <sub>Y</sub>	26.25	43.25	43.0	
A <sub>Z</sub>	25.46	25.33	39.28	Organic
B <sub>Z</sub>	22.46	26.25	38.66	inhibitor
C <sub>Z</sub>	20.01	25.36	40.42	

**Table c Result of Compressive Strength for different characteristic strengths in N/mm<sup>2</sup>**

**i)Compressive strength of concrete with different Brands of cement**

Age and date at Crushing SN(Labels)	Date Cast	Wt. as Measur ed (kg)	Density (kg/m <sup>3</sup> )	Maximum Crushing Load (kN)	Compressive Strength N/mm <sup>2</sup> )		Remarks
					Achieved	Required	
7days 2,3,4	30.9.2017	8.480	2512.59	579.0	25.74	17.8	Cem A
		8.610	2560.00	520.8	23.15		
		8.300	2459.26	642.5	28.55		
		<b>Average</b>	<b>8.46</b>	<b>2510.62</b>	<b>580.77</b>		
14days 5,6 & 7	30.9.2017	8.445	2502.22	880.4	39.13	22.5	
		8.415	2493.33	929.4	41.31		
		8.175	2422.22	919.3	40.86		
		<b>Average</b>			<b>40.43</b>		
28days 1,8 & 9		8.345	2472.59	925.6	41.13	25	
		9.00	2666.67	930.6	41.36		
		9.175	2718.52	931.5	41.4		
		<b>Average</b>	<b>8.840</b>	<b>2619.26</b>	<b>929.2</b>		
7days 11,12,13	01.10.2017	8.775	2600.00	837.3	37.21	17.8	Cem B
		8.805	2608.89	656.7	29.19		
		8.655	2564.44	856	38.04		
		<b>Average</b>			<b>34.81</b>		
7 days	03.10.2017	8.535	2528.89	790.2	35.12	17.8	
		8.205	2431.11	786.3	34.95		
		8.795	2605.93	735.7	32.7		
		<b>Average</b>			<b>34.26</b>		
14days 17.10.2017	14,16 &17 3.10.2017	8.375		895.8	39.81	22.5	
		8.543		916.1	40.7		
		8.287		948.8	42.17		
		<b>Average</b>			<b>40.89</b>		

Age at Crushing	Date Casted	Wt. as Measur ed (kg)	Density (kg/m <sup>3</sup> )	Maximum Crushing Load (kN)	Compressive Strength		Remarks
					Achieved	Required	
28 days	03.10.201 21,22 &20	8.25	2444.44	930.83	41.37	17.8	Cem B
		9.15	2711.11	890.57	39.57		
		8.88	2631.11	952.20	42.32		
		<b>8.76</b>	<b>2595.55</b>	<b>924.53</b>	<b>41.09</b>		
7days	04.10.201	9.25	2740.74	736.4	32.73	17.8	Cem C
		8.63	2557.04	821.6	36.51		
		8.48	2512.59	896.8	39.86		
		Average			<b>36.37</b>		
14days 18.10.20	20,21,22	8.800	2607.41	893.7	39.720	22.5	
		8.987	2660.15	837.20	37.20		
		8.618	2553.48	917.5	40.78		
		Average			<b>39.23</b>		
28days	34,39,40	8.567	2538.37	1026	45.62	25	
			2472.59	985.8	43.81		
		8.745	2591.11	995.2	44.23		
		Average			<b>44.89</b>		

**ii) Compression strength of concrete for different classes for brand Ordinary Portland Cement**

Class of concrete	Compressive strength in N/mm <sup>2</sup> at different ages of Testing					
	7 days		14 days		28 days	
35M	37.48	37.42	52.28	51.26	66.84	65.85
	<hr/>		<hr/>		<hr/>	
	36.84		50.61		63.32	
30M	<hr/>		<hr/>		<hr/>	
	37.94		50.89		67.39	
	35.32	34.35	48.12	47.05	54.83	53.87
25M	<hr/>		<hr/>		<hr/>	
	34.53		47.20		53.18	
	36.2		45.83		53.60	
25M	<hr/>		<hr/>		<hr/>	
	32.73	36.37	39.72	39.23	45.62	44.89
	<hr/>		<hr/>		<hr/>	
	36.51		37.2		43.81	
	<hr/>		<hr/>		<hr/>	
	39.86		40.78		44.23	

**Table d: Compressive strength of concrete with a selected brand of cement and a corrosion inhibitor in N/mm<sup>2</sup>**

Brand of OPC	Compressive strength of concrete in N/mm <sup>2</sup>			Type of inhibitor
	7 days	14 days	28 days	
A	25.81	40.86	41.29	Control –No inhibitor
B	34.89	40.89	41.09	
C	36.37	39.23	44.89	
Min.	17.8	22.5	25	
A <sub>y</sub>	35.26	44.28	48.7	Calcium nitrite based
B <sub>y</sub>	35.32	43.2	47.5	
C <sub>y</sub>	37.06	46.84	51.6	
A <sub>F</sub>	16.3	19.5	27.2	Fly ash
B <sub>F</sub>	18.3	20.2	28.13	
C <sub>F</sub>	17.3	20.4	30.6	
A <sub>Z</sub>	25.63	33.5	35.2	Calcium nitrate based
B <sub>Z</sub>	27.7	31.1	33.7	
C <sub>Z</sub>	29.3	32.7	33.69	
A <sub>x</sub>	25.46	24.6	26.6	Dimethylathanolamine based organic inhibitor
B <sub>x</sub>	22.46	23.7	29.7	
C <sub>x</sub>	20.01	24.68	26.7	

**Table e Split tensile strength of concrete with a selected brand of cement and a corrosion inhibitor in N/mm<sup>2</sup>**

Brand of OPC	Age at Testing			Type of inhibitor
	7 days	14 days	28 days	
A	2.59	3.16	3.25	Control –No inhibitor
B	1.77	2.45	2.88	
C	2.07	2.45	3.13	
A <sub>X</sub>	1.038	1.38	3.15	Calcium nitrite based
B <sub>X</sub>	2.17	2.45	2.45	inhibitor
C <sub>X</sub>	1.86	2.23	3.11	
A <sub>F</sub>	1.038	1.38	2.31	Fly ash
B <sub>F</sub>	2.12	2.50	2.62	
C <sub>F</sub>	1.90	2.20	2.78	
A <sub>Y</sub>	1.56	2.60	3.01	Calcium nitrate based
B <sub>Y</sub>	1.55	2.80	2.89	inhibitor
C <sub>Y</sub>	1.55	3.05	3.11	
A <sub>Z</sub>	1.15	1.93	2.99	Dimethylathanolamine
B <sub>Z</sub>	1.08	1.75	2.94	based organic
C <sub>Z</sub>	1.86	2.19	2.94	inhibitor

**Table f: Result of bond strength of concrete with a selected brand of cement and a corrosion inhibitor**

Brand of OPC	Bond strength of concrete in N/mm <sup>2</sup>			Type of inhibitor
	7 days	14 days	28 days	
A	2.59	3.16	4.42	Control –No inhibitor
B	1.77	2.45	4.33	
C	2.07	2.45	4.40	
A <sub>y</sub>	1.038	1.38	5.65	Calcium nitrite based
B <sub>y</sub>	2.17	2.45	5.25	
C <sub>y</sub>	1.86	2.23	5.56	
A <sub>z</sub>	1.34	1.21	3.28	Calcium nitrite based
B <sub>z</sub>	2.05	2.10	3.36	
C <sub>z</sub>	1.12	2.22	3.17	
A <sub>F</sub>	1.038	1.38	4.53	Fly ash
B <sub>F</sub>	2.12	2.50	4.20	
C <sub>F</sub>	1.90	2.20	4.74	
A <sub>X</sub>	1.15	1.93	3.08	Dimethylathanolamine based
B <sub>X</sub>	1.08	1.75	3.29	
C <sub>X</sub>	1.86	2.19	3.45	



## Appendix A4: Pictures taken during laboratory work

### 1.Reinforcement bar preparation and tests on fresh concrete



a)



b)



c)



d)



e)

- a) Zinc oxide sprayed bars for sections that was not embedded in concrete
- b) Sample during slumps test of concrete
- c) Sample during slump test measurement
- d) Fresh concrete during compaction test
- e) Fresh concrete during compaction test

## 2. Tests on hardened concrete

### i) Compression test



a)



b)







ii) Split tensile test in the lab



a)

b)

a) A picture showing samples ready for split tensile test

b) A picture showing split tensile testing of samples



c) A picture showing a mode of failure during split tensile test

**iii) Accelerated corrosion test**



a) A picture showing samples connected in series during accelerated corrosion experiment





b) A picture showing samples during accelerated corrosion experiment



c) A picture showing samples after accelerated corrosion experiment



d) A picture showing samples with a longitudinal crack



e) A picture showing recovery of embedded steel after accelerated corrosion



**iv) Bond strength Test**



A picture showing a sample during pull out test for bond strength

## **Appendix A5: Papers Published from this research**

**1.Philip Mogire, Silvester Abuodha,John Mwero and Geoffrey Mang'uriu (2018).**The effect of using ordinary cement brands in Kenya on corrosion rate of reinforced concrete water conveyancing structures. *International Journal of Scientific and Research Publications*, 8(4),7664. <http://dx.doi.org/10.29322/IJSRP.8.4.2018.p7664>.

**2.Philip Mogire, Silvester Abuodha,John Mwero and Geoffrey Mang'uriu (2018).**The effect of using selected ordinary cement brands in Kenya on the critical penetration depth of rust of reinforced concrete water conveyancing structures. *International Journal of Scientific and Research Publications*.8(11),8333. <http://dx.doi.org/10.29322/IJSRP.8.11.2018.p8333>.

**3.Philip Mogire, Silvester Abuodha,John Mwero and Geoffrey Mang'uriu,(2020).** Effect of Selected Commercially Available Corrosion Inhibitors in Kenya on Bond Strength of Reinforced Concrete. *International Journal of Scientific and Research Publications, Volume 2*(1),98104. <http://dx.doi.org/10.29322/IJSRP.10.02.2020.p98104>

**4.Philip Mogire, Silvester Abuodha,John Mwero and Geoffrey Mang'uriu,(2020).** A Effect of Selected Commercially Available Corrosion Inhibitors in Kenya on Bond Strength of Reinforced Concrete. *British Journal of Civil and Architecture Engineering (BJCAE)*,2(1),13-152.

**5.Philip Mogire, Silvester Abuodha,John Mwero and Geoffrey Mang'uriu (2020).** A Corrosion Model for Prediction of the Service Life of Reinforced Concrete Water Conveyancing Structures. *British Journal of Civil and Architecture Engineering (BJCAE)*, 2(06),153-181.



**6. Philip Mogire, John Mwero, Silvester Abuodha & Geoffrey Mang'uriu (2021).**

Correlation of tensile strength and corrosion initiation period of reinforced concrete, *Cogent Engineering*, 8:1, 1999039, DOI: 10.1080/23311916.2021.1999039.

**7. Philip Mogire, John Mwero, Silvester Abuodha & Geoffrey Mang'uriu (2021).**The

Relationship between Bond Strength and Critical Penetration Depth of Rust in Reinforced Concrete Structures. *Journal of Materials Science Research*, 10(2), 71-83.

<https://ccsenet.org/journal/index.php/jmsr/issue/view/0/2630>

# The effect of using Ordinary Cement Brands in Kenya on Corrosion Rate of Reinforced Concrete Water Conveyancing Structures

Philip Mogire\*, Silvester Abuodha\*, John Mwero\* and Geoffrey Mang'uriu\*\*

\*Department of Civil and Construction Engineering,  
University of Nairobi, Kenya

\*\*Department of Civil, Construction and Environmental Engineering,  
Jomo Kenyatta University of Agriculture & Technology  
P.O. Box 62000-00200, Nairobi, Kenya

DOI: 10.29322/IJSRP.8.4.2018.p7664  
<http://dx.doi.org/10.29322/IJSRP.8.4.2018.p7664>

**Abstract-** In the past decade Kenya has experienced an increased demand of cement for construction of infrastructure projects including the Mega standard gauge railway and the Lamu Port South Sudan-Ethiopia Transport Corridor. The cement production and consumption increased from 154,781 tonnes per year in January 2005 to 564,000 tonnes per year in January 2017 an average of 22% increment per annum.

Attracted by this growth and to meet the demand, the existing manufacturers have expanded while new cement manufacturers have ventured into the Kenyan market bringing the total number of manufacturers to six. Each of the manufacturers produces his own brand of ordinary Portland cement with specific constituents but meeting the requirements of the Kenya Bureau of Standards. The constituents of the brands of cement react differently when mixed with other constituents of concrete resulting into varying hardened properties that affect corrosion.

In this research three brands of ordinary Portland cement in the Kenyan market: Cem A, Cem B and Cem C were used to investigate their effect on the properties of concrete that affect the rate of corrosion.

The main objective of this research was to investigate the effect of using different Kenyan brands of ordinary Portland cement of the same strength on the rate of corrosion. The physical and chemical properties of the materials were investigated for compliance to applicable British and Kenyan standards. The DOE method was used to derive the mix design for a design strength of 25N/mm<sup>2</sup>. Concrete materials were batched by weight and mixed by using a lab electric pan concrete mixer in batches of 0.009 m<sup>3</sup>. For each brand of cement 9 cubes of 150mm x 150mm x 150mm for compression test, 9 cylinders of 150mm x 300mm for tensile strength and 9 cylinders of 150mm x 300mm for accelerated corrosion test were cast. After 24 hours the cast specimens were demoulded and immersed in curing tanks for 28 days.

Specimens for compression and tensile test were tested at 7, 14 and 28 days while the specimens for impressed corrosion were immersed in a 3.5% industrial sodium chloride solution under a voltage and current of 6V and 2A respectively. The applied current and voltage were monitored on a biweekly basis until corrosion induced cracking appeared on the concrete surface. The impressed corrosion specimens were monitored visually using a 1000x optical magnification glass for onset of cracks and stopped when the crack width were approximately 0.1mm in width. The duration to approximated width of crack were 107days, 115 days and 111 days for Cem A, Cem B and Cem C respectively. From the results in the research, different Kenyan cement brands of the same compressive strength have a significant effect on the rate of corrosion of reinforced concrete structures.

ention the abstract for the article. An abstract is a brief summary of a research article, thesis, review, conference proceeding or any in-depth analysis of a particular subject or discipline, and is often used to help the reader quickly ascertain the paper's purpose. When used, an abstract always appears at the beginning of a manuscript, acting as the point-of-entry for any given scientific paper or patent application.

**Index Terms-** Accelerated corrosion, Cement Brand, Corrosion rate.

- **Introduction**

**T**

he rate of infrastructure development is a key indicator of the behavior of an economy<sup>[1]</sup>. For the last decade, Kenya has experienced a remarkable development of small to mega infrastructure projects attracting investors in producing construction materials including cement and steel. Cement manufacturing has attracted expansion of existing manufacturers and new ones due to existing demand in Kenya which has grown from 154,781 tons in 2005 to 564,000 in 2017 (according to Kenya bureau of statistics records) and is projected to grow steadily until 2026. Currently there are six manufacturers, each producing ordinary Portland cement with different constituent compositions under different brands to Standard Specification KS EAS 18-1<sup>[2]</sup>.

The process of natural steel corrosion is very slow, requiring many years depending on environmental exposure and the properties of concrete materials to cause reasonable structural damage within the service life of the structure. Reinforced concrete has an alkaline environment that protects embedded steel from corrosion. This environment can be destroyed by carbonation or by chloride attack. It takes several years for sufficient chlorides to ingress cover concrete and destroy the passivation layer leading to corrosion of embedded steel.

François & Arliguie (1998), Castel *et al* (2003), Vidal *et al* (2007) and Zhang *et al* (2010), who allowed their laboratory specimens to corrode naturally, had to wait for four years for steel corrosion to start and an additional two years for first cracking to occur. The rate of corrosion is thus accelerated by simulating exposure environment. The objective of this research was to investigate the effect of cement brands on the rate of corrosion.

- **Literature**

Using a sensitivity analysis Li *et al*<sup>[3]</sup> showed that corrosion rate is one of the most important input parameters in the corrosion-induced damage models. There is a clear relationship between corrosion rate and concrete resistivity as exhibited in Alonso *et al.*'s<sup>[4]</sup> experimental results. From the results it was noted that accelerated corrosion tests were used without validation using natural corrosion test results. The use of small specimens (20 x 55 x 80 mm) may have a size effect on the experimental results<sup>[5]</sup>. In addition to concrete resistivity, corrosion rate in concrete can be affected by other factors such as presence of cracks, concrete cover depth, among others<sup>[6]</sup>.

Yalcyn and Ergun<sup>[7]</sup> developed a corrosion model by studying the effect of chloride and acetate ions on the rate of corrosion and evaluated corrosion by measuring half-cell potentials (HCP) and linear polarization potential (LPR). In their model, the rate of corrosion was taken up to a period of 90 days on cylindrical specimens of 150 mm diameter x 150 mm height using Pozzolanic cement.

The rate of Corrosion in reinforced concrete structures is affected by several factors (e.g. concentration of chlorides, concrete penetrability) that vary from time to time in a water conveyance structure. This research attempts to evaluate the effect of different chemical compositions of cement (which are exhibited on cement brands) on the rate of corrosion of reinforced concrete structures.

- **Methodology**

This study was conducted in the University of Nairobi Concrete and Materials lab where the physical properties of the materials, sample preparation and testing were done. The chemical properties of the cement brands and chloride content was done at the State Department of Infrastructure in the Ministry of Transport, Infrastructure, and Housing and Urban Development of the Government of Kenya.

### **3.1 CONCRETE SAMPLES**

The constituent materials for preparing test samples consisted of three brands of cement A, B, C of Ordinary Portland cement (42.5N/mm<sup>2</sup>), clean river sand, and 20mm maximum size coarse aggregate and portable water.

#### **3.1.1 Cement**

Cement is the most commonly used binder material in concrete. It makes concrete impermeable by filling up the voids existing in the aggregates and provides strength to the composite mix upon setting and hardening. The cements properties tested during this research were the chemical composition.

Manufacturing of Cement in Kenya is in accordance to KS EAS 18-1: 2001, an adoption of the European Norm EN 197 cement standards<sup>[8]</sup>. The cements locally available are produced for specific uses<sup>[9]</sup>. Three Brands of Cement

Cem A, Cem B and Cem C of type 42.5N sourced from one wholesaler from three different manufacturers were used during the research.

### 3.1.2. Other concrete materials

Table 1 shows the description and source of other constituents (materials) of concrete used in the research.

**Table 1. Details of materials used in the research**

SN	Description	Source	Remark
1.	Fine aggregates	Stockpile vender sourced from Machakos River	This was washed and oven dried before use
2.	Coarse aggregates	Kenya builders quarry	5-20mm quarry graded
3.	10mm ribbed bars	Local manufacturer	Factory cut to 400mm
4.	Mixing water	Tap water in the Lab	Sourced from Nairobi Water and Sewerage Company

## 3.2. EXPERIMENTATION

### 3.2.1. Constituent Materials Characterization

The cement and aggregates chemical elemental analysis was done in accordance to the EAS 148-2:2001 CS 91.100.10. East African Standard. The physical and mechanical properties tests on aggregates were done at the university of Nairobi Concrete laboratory.

### 3.2.2. Concrete Mix Design

Concrete mix design is the science of correct proportioning of concrete constituent materials based on structure requirements to obtain the desired properties of concrete such as strength and practical workability<sup>[10]</sup>. The effect of the brands of cement on the rate of corrosion was evaluated using the same concrete of design strength of 25N/mm<sup>2</sup> designed in accordance with the DOE method.

### 3.2.3 Test on hardened concrete

#### a) Compressive strength

The compressive strength of concrete was investigated at 7, 14 and 28 days using a digital Universal Testing Machine shown in figure 1b), with a loading capacity of 2000 KN in accordance to BS EN 12390-3:2009.



**Figure 1 Concrete Samples during Compression. a) Sample after curing, b) Digital compression testing machine, c) Concrete Sample after failure.**

#### b) Splitting tensile test

Split Tensile strength of concrete was tested on cylinders cast with Cem A, Cem B and Cem C. The strength of concrete was tested on cylinder at 7, 14 and 28 days curing. 7 days test was conducted to check the gain in initial strength of concrete. 28 days test gives the data of final strength of concrete at 28 days curing. Universal Compression testing machine is used for testing the Split Tensile strength test on concrete along with two wooden strips as shown if figure 2. At the time of testing the cylinder was taken out of water, dried and then tested.



**Figure 2 Samples in splitting tensile test, a) and b) Concrete Sample in the Universal Testing Machine, c) Concrete Samples at failure**

### 3.2.4 Test on the rate of corrosion

This was done through an impressed corrosion test using the procedure below;

- i) 12mm x 400mm long ribbed bars were polished with abrasive papers.
- ii) 120 mm of the surface length of each bar were zinga sprayed and left to naturally dry.
- iii) The mixed concrete (in two batches) was poured into cylindrical moulds (150 mm in diameter and 300 mm high) where the reinforcement was placed along its longitudinal axis.
- iv) The specimens were mechanically vibrated for 60s. After 24 hours, the cylindrical concrete specimens were demoulded and cured for 28 days.
- vi) The test specimens were dried for 24 hours and then subjected to accelerated corrosion and stored in a tank containing 3.5 % NaCl at room temperature. The experiment was run until a crack of 0.1mm was detected..

### 3.2.5 Test preparation and procedure

Concrete materials were batched by weight and mixed by a lab electric pan concrete mixer in batches of 0.009 m<sup>3</sup>. Slump and compacting test were measured for all the batches as a measure of consistency and workability. For each brand of cement 9 cubes of 150mm x 150mm x 150mm and 9 cylinders of 150mm x 300mm were cast. After casting;

- a) The concrete specimens were kept in moulds at room temperature for 24 hours, then demoulded and kept in a curing tank for 28 days before testing.
- b) The concrete cubes and cylinders were tested for compression and tensile strength at 7, 14 and 28 days.

## 4 RESULTS AND DISCUSSION.

### 4.1 Results

#### i) Chemical Properties of Cements in Kenya

Three types of cements were investigated during the research and Tables 2 gives the chemical properties of the different brands Cem A, Cem B and Cem C of the grade 42.5N Cement.

**Table 2 Result of Chemical composition the brands of cement tested.**

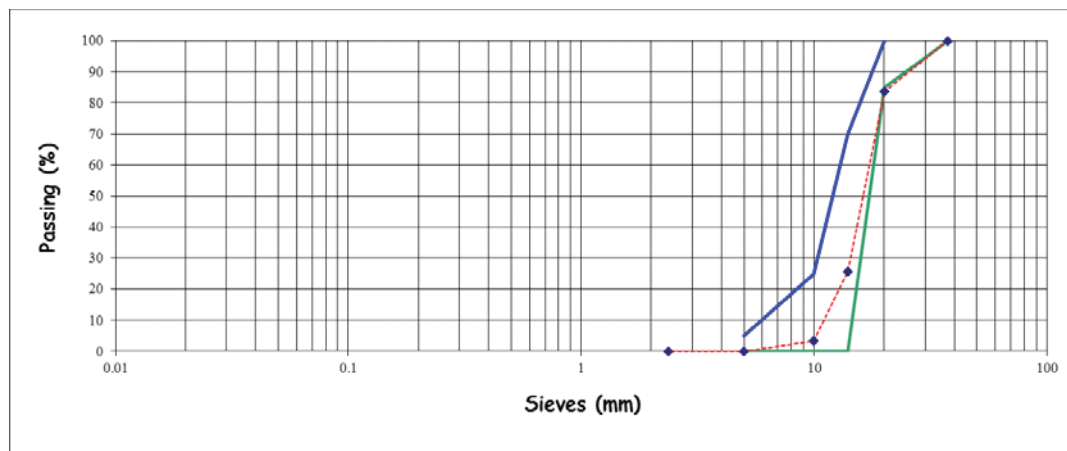
SN	Test	Result Cem A	Cem B	Cem C	KS EAS 18-1: 2001 Requirement
1.	CaO%	59.86	59.11	58.82	Sum ≥ 50
2.	SiO <sub>2</sub> %	16.56	21.56	19.47	
3.	SO <sub>3</sub> %	2.02	2.78	2.03	≤ 3.5
4.	MgO%	1.76	1.04	0.57	≤ 5
5.	K <sub>2</sub> O%	0.027	0.051	-	-
6.	Fe <sub>2</sub> O <sub>3</sub> %	2.32	3.48	1.44	-
7.	Al <sub>2</sub> O <sub>3</sub>	7.61	8.09	6.85	3-8
8.	Na <sub>2</sub> O <sub>3</sub> %	0.054	0.018		-
9.	LOI%	0.11	0.10	4.75	≤ 5
10.	Cl%	0.012	0.016	0.014	≤ 0.1
11.	IR%	2.20	0.55	1.96	≤ 5

**ii) Properties of aggregates**

Various tests were carried out on the aggregates to determine their suitability for the research and the results are shown in table 3 and graphs 1 and 2. Water soluble chlorides ions percent were found to be zero in fine aggregates, 0.002 % in coarse aggregates all less than 0.03% acceptable in compliance with BS EN 12620:2002.

**Table 3: Physical properties of aggregates used in the study**

SN	Property	Test Method	Result	Limit
1.	Loss Angeles Abrasion value	BS/EN 1097-2	20%	30%
2.	Flakiness index	BS/EN 933-3	35%	<35%
3.	Aggregate Crushing Value	BS EN 1097-2	18%	<45%
4.	Aggregate Impact Value	BS EN 1097-2	8%	<45%
5.	Bulk specific gravity	ASTM C128	2.9	
6.	Water absorption capacity	ASTM C127	1.20%	



**Graph 1 Gradation of Coarse aggregates**

**Graph 2: Gradation of fine aggregates**

**iii) Results of compression test**

**Graph 3 Compressive strength of concrete vs testing age**

**iv) Splitting tensile test result**

Tables 4-6 shows the result of the splitting tensile test while Tables 7 and 8 shows a comparison of the result of this research with existing research.

**Table 4.Result of tensile strength ( $f_t$ ) of concrete samples from three cement brands**

brands

SN	Cement Brand	Strength in N/mm <sup>2</sup>		
		7days	14 days	28 days
		$f_t$	$f_t$	$f_t$
1.	Cem A	2.59	2.83	3.25
2.	Cem B	2.07	2.45	3.13
3.	Cem C	1.77	2.45	2.88



**Table 5. Result of relationship of compressive strength ( $f_{ck}$ ) and tensile strength ( $f_t$ ) of concrete samples from three cement brands**

SN	Cement Brand	Strength in N/mm <sup>2</sup>						Rate of Corrosion
		7days		14 days		28 days		
		$f_{ck}$	$f_t$	$f_{ck}$	$f_t$	$f_{ck}$	$f_t$	
1.	Cem A	25.81	3.63	40.28	3.96	41.29	4.55	2.7
2.	Cem B	36.379	2.90	39.23	3.45	44.89	4.38	2.5
3.	Cem C	34.81	2.48	36.26	3.43	41.09	4.03	2.6

**Table 6 predicted splitting tensile strength of concrete from different models.**

Cement brand	Compressive strength (N/mm <sup>2</sup> ) at 28 days	Split tensile strength in N/mm <sup>2</sup>					
		Measured Value	Lavanya & Jegan(2015) $f_{t1}=0.249f_{ck}^{0.772}$	ACI Committee 318(2014) $f_{t2}=0.56f_{ck}^{0.5}$	Anoglu et al(2006) $f_{t3}=0.387f_{ck}^{0.63}$	CEB-FIB(1991) $f_{t4}=0.3f_{ck}^{0.66}$	Gardner (1990) $f_{t5}=0.33f_{ck}^{0.667}$
Cem A	41.29	4.55	4.40	3.60	4.03	3.50	3.95
Cem B	44.89	4.38	4.70	3.75	4.25	3.70	4.17
Cem C	41.09	4.03	4.39	3.59	4.02	3.48	3.93

**Table 7 Checking variance and normality assumptions on the sample datasets.**

SN	Sample	Variance	Test P-value	Decision
1.	Experiment	0.047	0.03	Observations in Sample have normal distribution
2.	$f_{t1}$	0.021	0.01	Observations in Sample have normal distribution
3.	$f_{t2}$	0.005	0.32	Observations in Sample have normal distribution
4.	$f_{t3}$	0.011	0.04	Observations in Sample have normal distribution
5.	$f_{t4}$	0.010	0.41	Observations in Sample have normal distribution
6.	$f_{t5}$	0.008	0.07	Observations in Sample have normal distribution

**Table 8 Welch's 2-sample t-test.**

SN	Data	t-statistics	P-Value	Decision
1.	Experiment and $f_{t1}$	0.40	0.06	On average samples are not significantly different
2.	Experiment and $f_{t2}$	0.05	0.47	On average samples are not significantly different
3.	Experiment and $f_{t3}$	0.29	0.07	On average samples are not significantly different
4.	Experiment and $f_{t4}$	0.01	0.50	On average samples are not significantly different
5.	Experiment and $f_{t5}$	0.18	0.11	On average samples are not significantly different

**v) Rate of corrosion**

Table 9 shows the properties of the rebar used in the research and the rate of corrosion.

**Table 9 Physical property of the reinforcement in impressed corrosion Test**

SN	Cem	Diameter	Area	Length	Initial	Average	Mass	Weght	Duration	Rate	of
----	-----	----------	------	--------	---------	---------	------	-------	----------	------	----

	Type	(mm)	mm <sup>2</sup>	mm	Mass Kg	after corrosion Kg	Loss Kg	in Hours	Corrosion mm/yr
1.	Cem A	12	113.143	400	0.371	0.265	0.106	109 x 24	0.38
2.	Cem B.	12	113.143	400	0.371	0.299	0.072	115 x 24	0.27
3.	Cem C	12	113.143	400	0.371	0.256	0.115	106 x 24	0.43

**Corrosion Rate in mm/yr= 87.6 x [w/(D x A x T)]**

Where W is the weight loss in milligram,

D is the density of the material used, g/cc,

A is the area of the specimen (cm<sup>2</sup>), and

T is the duration of the test period in hours.

**4.2 Discussion of results**

**4.2.1 Properties of aggregates and water**

The fine aggregates were free of silt, clay and any other deleterious material and had a maximum aggregate size of 5 mm. This was achieved using a British standards sieve with 5 mm maximum aperture. Both the fine and coarse aggregates were suitable for concrete production. The water used for the work was potable water from Nairobi water and sewerage Company and suitable for concrete production.

**4.2.2 Chemical Composition of Cement Samples**

The different brands however had varying properties which can be attributed to their manufacturing processes.

The difference in chemical composition of the various brands and types of cements are reflected in the difference in their mechanical properties and in the qualities of concrete produced by the different types of cements and thus it directly affects the compressive strength of concrete.

• **Effect of sum of lime (CaO) and silicon dioxide (SiO<sub>2</sub>)**

From table 2 there is a notable variation in the amounts of CaO, SiO<sub>2</sub> and Insoluble Residue. Cem A has the highest amount of CaO (59.86%), Cem B has the highest SiO<sub>2</sub> (21.56%) and Cem A has the highest Insoluble residue (2.20%). Table 3 shows the chemical composition of the different cement samples used in this research. All the cement samples substantially complied with British Standards requirements for ordinary Portland cement.

The sum of lime (CaO) and silicon dioxide (SiO<sub>2</sub>) obtained in the chemical analysis of ordinary Portland cement should not be less than 50% [11]. All cement samples used for this work satisfied this requirement. Cement sample B has a CaO + SiO<sub>2</sub> value of 80.67 % and produced the highest compressive strength of 44.89 as shown in table 5

This is consistent with the known fact that both CaO and SiO<sub>2</sub> give strength to concrete though SiO<sub>2</sub> has to be limited relative to CaO in order not to negatively affect setting time.

• **Effect of CaO/SiO<sub>2</sub>**

The ratio of lime (CaO) to silicon dioxide (SiO<sub>2</sub>) contents in ordinary Portland cement should be greater than 2. The restriction on the ratio of lime to silicon dioxide [11] is to ensure that the quantity of silicon dioxide is considerably lower than that of lime so that the setting of concrete is not inhibited. All the cement samples investigated satisfied this requirement. The lime-silicon dioxide ratio for cement samples A, B, and C were 3.61, 2.71 and 3.0 respectively. The results also indicated that the higher the ration of (CaO/SiO<sub>2</sub>) of a cement sample the higher the compressive strength of concrete which can be produced from it and the lower the rate of corrosion.

• **Effect of MgO**

The quantity of magnesium oxide (MgO) in ordinary Portland cement should not exceed 5% [2]. All the cement samples satisfied this requirement with 1.76%, 1.04% and 0.57% for cement samples A, B and C respectively. Magnesium oxide contributes to colour of cement and hardness of the resulting concrete. Cement sample A with the highest MgO content of 1.76 % was expected to produce concrete with the highest compressive strength since MgO contributes to hardness of concrete and lowest rate of corrosion. If the quantity of MgO is in excess of 5 percent, cracks will appear in concrete and which may affect the rate of corrosion by generating spots for penetration of chloride ions in concrete.

• **Effect of SO<sub>3</sub>**

The quantity of sulphur trioxide (SO<sub>3</sub>) content in ordinary Portland cement should be less than 3.5 %. All the samples satisfied this requirement.

• **Effect of Chloride Content**

The chloride content in ordinary Portland cement should be less than 0.4%. All the cement samples in this work satisfied this requirement.

• **Effect of Al<sub>2</sub>O<sub>3</sub>**

Aluminium oxide (Al<sub>2</sub>O<sub>3</sub>) aids the quick setting of cement paste. Cement sample B contained the highest quantity of 8.09 % of Al<sub>2</sub>O<sub>3</sub> resulting in the fastest initial set of the cement paste



- **Effect of Fe<sub>2</sub>O<sub>3</sub>**

Iron oxide (Fe<sub>2</sub>O<sub>3</sub>) contributes to cement colour and helps in the fusion of the different ingredients. The Fe<sub>2</sub>O<sub>3</sub> contents for the different cement samples are 2.32, 3.48 and 1.4493 for cement samples A, B, and C respectively as shown in Table 5.

- h) **Effect of Residues**

British standards consider Na<sub>2</sub>O, K<sub>2</sub>O, TiO<sub>2</sub> and P<sub>2</sub>O<sub>5</sub> in ordinary Portland cement as residues and limit the sum of all of them to 5%. All the cement samples investigated satisfied this requirement with cement samples A, B and C having total residue contents of 0.55, 2.2 and 1.96% respectively. If in excess of 5% efflorescence and unsightly cracking will occur.

- **CONCLUSION**

The following conclusions have been reached from the outcome of this work:

i) The rate of corrosion is affected by the compressive strength of concrete which depends on the chemical properties of cement exhibited in the brand of cement with properties of the other concrete matrix material remaining the same. From the results of this research the different cement brands however had varying chemical properties. The brand with the highest lime (CaO), silicon dioxide (SiO<sub>2</sub>) and Magnesium oxide content in cement had the highest compressive strength of concrete and the lowest rate of corrosion.

ii) Electrochemistry is a feasible method to evaluate the rate of corrosion of a steel bar embedded in concrete under accelerated corrosion.

iii) Based on the results of statistical analysis, predicted values of splitting tensile strength were not significantly different from the experimental values for the sample of cast for experiments for all the models.

### References

- 1) [ Munnell, A. (2008). How Does Public Infrastructure Affect Regional Economic Performance? New England Economic Review. Federal Reserve Bank of Boston: 11-32.
- 2) KS EAS 18. Cement Standard - Part 1: Composition, Specifications and Conformity Criteria. KEBS, Kenya. 2001.
- 3) Li, C. Q., Melchers, R. E. & Zheng, J. J. (2006) An analytical model for corrosion-induced crack width in reinforced concrete structures. ACI Structural Journal, 103(4), pp. 479-487.
- 4) Alonso, C., Andrade, C. & Gonzalez, J. A. (1988) Relation between resistivity and corrosion rate of reinforcements in carbonated mortar made with several cement types. Cement and Concrete Research, 18(5), pp. 687- 698.
- 5) [5]Azad, A. K., Ahmad, S. & Al-Gohi, B. H. A. (2010) Flexural strength of corroded reinforced concrete beams. Magazine of Concrete Research, 62(6), pp. 405-414.
- 6) Otieno, M. B., Beushausen, H.-D. & Alexander, M G. (2010) Corrosion propagation in reinforced concrete structures - state of the art review and way forward. Proceedings of the 6th international conference on Concrete under severe conditions - Environment and loading, CONSEC'10. June 7th -9th 2010, Merida, Yucatan, Mexico.
- 7) Yalcyn, H. & Ergun, M. (1996). The prediction of corrosion rates of reinforcing steels in concrete. Cement and Concrete Research, 26(10), pp. 1593-1599.
- 8) Kenya Bureau of Standards (2005) KS EAS 18-1:2001-Cement Part 1: Composition, Specification and Conformity Criteria for Common Cements. Kenya Bureau of Standards, Nairobi
- 9) Koteng, D.O. (2013) Concrete Use for Sustainable Development. The 20th Engineers International Conference, Kisumu, 8-10 May 2013, 1-19.
- 10) Kumbhar, P.D. and Murnal, P.B. (2012) Assessment of Suitability of Existing Mix Design Methods of Normal Concrete for Designing High Performance Concrete. International Journal of Civil and Structural Engineering, 3, 158-167.
- 11) [BS 12, Specification for Portland cement (BSI Publications, London, 1996).

### Authors

**First Author** – Philip Mogire, Doctor of Philosophy in Civil Engineering Candidate, Department of Civil and Construction Engineering, University of Nairobi, Kenya, [philosiemo@yahoo.com](mailto:philosiemo@yahoo.com).

**Second Author** – Dr. Silvester Abuodha, Senior Lecturer, Department of Civil and Construction Engineering, University of Nairobi, Kenya, [sochieng@yahoo.com](mailto:sochieng@yahoo.com).

**Third Author** – Dr. John Mwero, Lecturer, Department of Civil and Construction Engineering, University of Nairobi, Kenya, [johnmwero1@gmail.com](mailto:johnmwero1@gmail.com).

**Fourth Author** – Prof. Geoffrey Mang'uriu, Professor, Department of Civil, Construction and Environmental Engineering, Jomo Kenyatta University of Agriculture & Technology, [gmanguriu@yahoo.co.uk](mailto:gmanguriu@yahoo.co.uk)

**Correspondence Author** – Philip Mogire, [philosiemo@yahoo.com](mailto:philosiemo@yahoo.com), +254734967989.

# The effect of Selected Cement Brands in Kenya on the Critical Penetration Depth of Rust in Reinforced Concrete Water Conveyancing Structures

Philip Mogire<sup>1,a,\*</sup>, Silvester Abuodha<sup>2,b</sup>, John Mwero<sup>3,c</sup> and Geoffrey Mang'uriu<sup>4,d</sup>

<sup>1,2,3</sup>Department of Civil and Construction Engineering,  
University of Nairobi, Kenya

<sup>4</sup>Department of Civil, Construction and Environmental Engineering,  
Jomo Kenyatta University of Agriculture & Technology  
P.O. Box 62000-00200, Nairobi, KENYA

<sup>a</sup>philosiemo@yahoo.com, <sup>b</sup>sochieng@yahoo.com, <sup>c</sup>johnmwero1@gmail.com, <sup>d</sup>gmanguriu@yahoo.co.uk

DOI: 10.29322/IJSRP.8.11.2018.p8333

<http://dx.doi.org/10.29322/IJSRP.8.11.2018.p8333>

**Abstract-** As the world economies shift to support the United Nations sustainable development goals, new cement manufactures have entered into the Kenyan market producing brands of ordinary Portland Cement meeting the minimum requirement of the Kenya Bureau of Standards. The variant parameter in this brands is the chemical composition of the cement Brands. The aim of this research was to establish the relationship between the cement Brand and the Critical penetration depth of rust and their role in the durability of the reinforced concrete structures.

To achieve the desired objective three cement brands out of six brands manufactured in Kenya; CemX, CemY and Cem Z of ordinary Portland cement with compressive strength 42.5N/mm<sup>2</sup> were sourced from a wholesaler for the study. Other concrete constituent materials; fine and coarse aggregates and steel were obtained from the local Kenyan market. This research was conducted at the University of Nairobi Structures/ Concrete laboratory and the State Department of Infrastructure in the Ministry of Transport, Infrastructure, Housing and Urban Development of the Government of Kenya.

The physical and chemical properties of the materials were investigated for compliance to relevant applicable British and Kenyan standards and if they met the acceptable criteria. Concrete of characteristic strength of 25N/mm<sup>2</sup> derived from the DOE method was used. Concrete materials were batched by weight and mixed by a lab electric pan concrete mixer in batches of 0.009 m<sup>3</sup>. The concrete batches were tested for consistency by the slump and compaction factor tests. For each brand of cement 9 cubes of 150mm x 150mm x 150mm for compression test, 9 cylinders of 150mm x 300mm for tensile strength and 9 cylinders of 150mm x 300mm for accelerated corrosion test were cast. After 24 hours the cast specimens were demolded and immersed in curing tanks for 27 days.

Specimens for compression and tensile test were tested at 7, 14 and 28 days while the specimens for accelerated corrosion were immersed in a 3.5% industrial sodium chloride solution under 6V. The accelerated corrosion specimens were monitored for onset of cracks and stopped when the cracks were 0.1mm in width. From the results in the research, the different Kenyan selected cement brands linearly correlate with the critical penetration depth of rust and the rate of corrosion for the evolution of 0.1mm crack width and this is attributed to their chemical composition.

**Index Terms-** Cement Brands, accelerated corrosion test, Critical penetration depth of Rust.

## 1. INTRODUCTION

For the medium term (2018-2022) of vision 2030, the Republic of Kenya defined four items referred to The Big Four Agenda aimed at accelerating economic growth, focusing on manufacturing, food security and nutrition, and providing universal health coverage and affordable housing. The big four agenda is anchored in Vision 2030 of Kenya and form a commitment in achieving part of the 17 UN Sustainable Development Goals of Vision 2030 for a better and sustainable world. Reinforced concrete Water conveyancing structures play a significant role in the Big Four Agenda and defining the service life is crucial in Kenya's economic sustainability.

Steel is thermodynamically unstable under normal atmospheric conditions and will release energy and revert back to its natural state of iron oxide(rust) and this process is called corrosion. For corrosion to occur in reinforced concrete; the rebar must be at different energy levels, the concrete must act as an electrolyte, and the rebar must act as a metallic connection.

At high pH (12- 13) reinforced concrete is in an alkaline state and thin oxide layer forms on the steel and prevents metal atoms from dissolving forming a passive film [1]. This passive film reduces the corrosion rate to an insignificant level without which the steel would corrode at rates at least 1,000 times higher [2]

Corrosion in reinforced concrete has a significant effect in the service life of structures and is caused by electrochemical reactions with contaminants. The presence of rust on reinforcement bars and appearance of cracks parallel to the reinforcement bars symbolize the presence of corrosion in reinforced concrete. Carbonation inducing a generalized attack and the presence of chlorides inducing a localized attack are the main causes of electrochemical corrosion in reinforced concrete as shown in Figure 1[2].

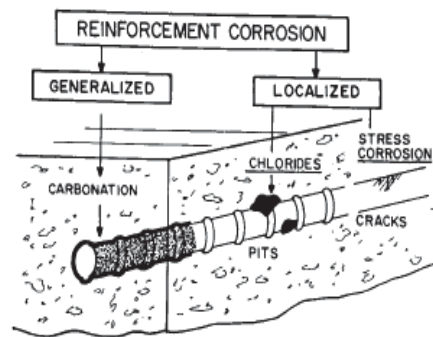


**Figure 1: Types and morphology of the corrosion in concrete: generalized (carbonation), localized (chlorides)[2]**

### Carbonation

In this process atmospheric carbon dioxide diffuses to the steel concrete interface and reacts with the calcium and alkaline hydroxides and cement as shown in equation 1 and 2, lowering the pore solution pH value at the rebar concrete interface to below 9 thus initiating corrosion.



Carbonation does not occur if the concrete is water-saturated or in very dry conditions because moisture is required to form carbonic acid which attacks the  $\text{Ca(OH)}_2$  and diffusion of  $\text{CO}_2$  through water is very slow. Carbonation is very slow and generally follows the square root time law shown in equation 3.

$$x = K\text{CO}_2 t^{0.5} \quad 3)$$

Where

x = carbonation depth after time t

$K(\text{CO}_2)$  = carbonation coefficient/factor for a given concrete

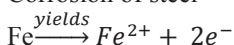
### Chloride attack

The chloride ions may be present in the concrete originating from its constituent materials but the most common source is from outside due to the structure being in an aggressive environment with chloride ion species. Surface chlorides diffuse to the rebar concrete interface and induces local disruption of steel passive layer through the reactions of equation 4 -6 leading into formation of pits on the reinforcement bars.

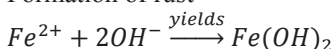
Decomposition of the passivity layer



Corrosion of steel



Formation of rust



The electrochemical reactions take place in the limited volume of aqueous solution present in the pores of the concrete and steel interface. This process results in loss of mass and cross sectional area of steel resulting in reduced load carrying capacity and structural failure. The internal stresses generated by rust which is of a lower density and thus bulkier than the parent steel leads to formation of cover cracking to account for more space required to accommodate the rust. Other effects include reduction of steel-concrete interface bond stains on the concrete bars surface, delamination and spalling. Previous studies, using various analytical and microscopy techniques,

have shown that corrosion products forms in the cement paste adjacent to a corroding rebar [e.g. 3, 4, 5, 6, 7]. The corrosion products continually get deposited at the steel and concrete interface generating stresses that cause progressive deterioration [8]. Chlorides ingress through the net of pores is one of the most common reasons that cause corrosion in reinforcements when these are located in an aggressive environment or when in the mixture such ions are incorporated. Chloride ions are capable of causing localized corrosion therefore leading to a premature and unexpected failure of the structures [9].

## 2. CHLORIDE PENETRATION INTO CONCRETE

In water conveyancing reinforced concrete structures chloride ions are either bound, adsorbed or dissolved in water that is retained in the pores, which forms the pore solution. The total chlorides (combined free and bound) content do not give a realistic indication of the risk of corrosion to the reinforcement but an assessment of the long-term risk to structures exposed to chlorides.

Chlorides from the aggressive external environment penetrate into the interconnected pores or capillary pores, as well as micro and macro-cracks in concrete by convection and the chloride ions diffuse further into the saturated pore system. The concentration gradients of the free chlorides control the process of diffusion. Chloride ions that are harmful to the reinforcing steel are those which are dissolved or are free, but due to the balances that occur, it is possible that chloride ions which are adsorbed, be incorporated into the solution and become hazardous [10][11].

When free chloride ions penetrate the pore system of the concrete structure, some of the ions are fixed to solid concrete structure. The transient chemical reaction affects the flow of free ions in the pore solution. Considering a water conveyancing structure as submerged, the primary chloride transport mechanism is diffusion. The critical penetration depth of rust is shown in figure 2.

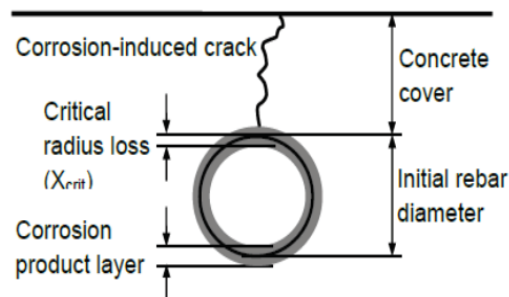


Figure 2: Critical penetration depth of rust of critical radius loss  $X_{crit}$ [12]

## 3.0 METHODOLOGY

This research was conducted at the University of Nairobi Structures/ Concrete laboratory where the physical properties of the materials, sample preparation and testing were done. The chemical properties of the materials were done at State Department of Infrastructure in the Ministry of Transport, Infrastructure, Housing and Urban Development of the Government of Kenya.

### 3.1 Concrete samples

In the constituent materials for test samples, three series of specimens were prepared with a variation in the selected brand of cement; cement brand X, Y, Z of Ordinary Portland cement ( $42.5\text{N/mm}^2$ ), all commercially available in Kenya and manufactured in accordance to KS EAS 18-1: 2001[13], an adoption of the European Norm EN 197 cement standards. Other materials used were, clean river sand, and 20mm maximum size coarse aggregate potable water and 10mm reinforcement bar.

#### 3.1.1 Cement

The chemical composition of each brand of cement used was tested in accordance with KS EAS 18-1: 2001. Three Brands of Cement used in the research were sourced from one wholesaler for three different manufacturers. The cement brands used are denoted CemX, CemY and CemZ in the subsequent parts of this research.

#### 3.1.2. Reinforcement bars

Reinforcing ribbed steel bars used had a tensile strength of strength  $500\text{N/mm}^2$  cut to length and sourced from a local manufacturer. The reinforcing ribbed steel bars were 27 pieces of 10mm diameter and 400 mm long with 120mm wire brushed to remove the mill scale and sprayed with zinc coat in the Lab. The bars were kept in the lab covered with a dry cloth and kept free of moisture until just before concrete placement. Any visible corrosion product was removed by wire brushing prior to placing the bars in the moulds during casting. A single bar was placed at the geometrical centre of the moulds with 120 mm protruding from the concrete cast surface as shown in figure 3.1

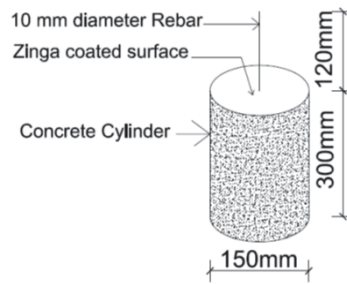


Figure 3.1 Detail of embedded ribbed bar in concrete

### 3.1.3 Other concrete materials

Table 1 shows description and source of other materials of concrete used in the research.

**Table 3.1. Details of materials used in the research**

SN	Description	Source	Remark
1.	Fine aggregates	Stockpile vender sourced from Machakos River	This was washed and oven dried before use.
2.	Coarse aggregates	Kenya builders quarry	5-20mm quarry graded
3.	Mixing water	Tap water in the Lab	

## 3.2. Experimentation

### 3.2.1. Concrete Composition

A mix was designed to meet the requirements of strength, water-cement ratio and cement content for concrete water conveyancing structures. The target strength was 25N/mm<sup>2</sup>. The concrete was batched by weights using the building research establishment (BRE) mix design concrete mix. The mix design is shown in Table 3.2.

**Table 3.2 Basic mix design**

Material	Coarse aggregates	Fine aggregates	Ordinary Portland Cement	Total Free water
Quantity	1300 kg/m <sup>3</sup>	650kg/m <sup>3</sup>	450 kg/m <sup>3</sup>	450 litres/m <sup>3</sup>

Nine specimens per cement brand were cast in a cylindrical mould, 300mm long and 150mm diameter. After casting, the specimens were kept in laboratory conditions (23 °C) for 24 hours. Subsequently, the specimens were de-moulded and stored in a curing tank for 27 days.

### 3.2.2 Exposure

After curing the test specimens were dried for 24 hours in laboratory conditions and then subjected to accelerated corrosion in a tank containing 3.5 % NaCl at room temperature as shown in figure 3.2.



Figure 3.2 Samples of the concrete cylinders in accelerated corrosion set up.

### 3.2.3 Open circuit potential measurements (OCP)

Monitoring of the electrochemical potential was performed by immersing a stainless steel electrode as the anode and in the sodium chloride solution and each group of specimens arranged in series in the cathode as shown in figure 3.3. During the experiment the cathodic and anodic current was measured with time and any crack evolution and size monitored. The experiment in each series was stopped when the biggest crack size reached 0.1mm. During the duration of the test, no replacement of the sodium chloride solution was performed.



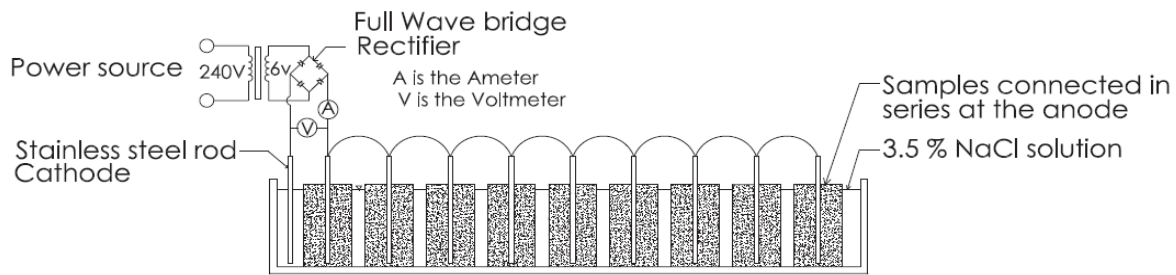


Figure 3.3 Sketch of experimental circuit set up

### 3.3.4 Detection of the onset of corrosion-induced Cracking

Once the specimens were subjected to anodic polarization, the applied current and voltage were monitored on a daily, then weekly basis until corrosion induced cracking appeared on the concrete surface. A detailed optical examination utilizing a graduated optical ruler and lens with 100X-magnification was done on a biweekly basis. The optical examination was required to check for invisible cracks and to accurately measure crack width.

### 3.3.5 Estimation of critical penetration depth of rust ( $X_{crit}$ )

The cracked specimens were demolished to retrieve the reinforcing steel segments for inspection of corrosion morphology and for gravimetric evaluation of mass (see figure 3.4). The extent to which the steel corrosion product was radially transported into surrounding concrete were visually examined. The surface area of corroded carbon steel regions was estimated by the area covered by the steel corrosion product which were confirmed after rust removal.



Figure 3.4 Images of corrosion samples after corrosion.

The steel corrosion product was removed off the surface of reinforcement bar segments in accordance with the procedure of ASTM G1-03 [ASTMG01-2003]. The measured amount of lost steel mass in grams was estimated by subtracting the final weight measured after cleaning from the initial weight. The theoretical mass loss in grams of steel resulting from the applied current was calculated based on Faraday's first law of electrolysis.

$$\Delta m_F = [M \times I \times t / (n \times F)] \quad 7)$$

where  $(M/n \times F)$  is the electrochemical equivalence of the iron substance

M is the molar mass of iron ( $M=55.847 \text{ g/mol}$ ),

n is the effective valence of the iron ions dissolving ( $n=2$ ) and

F is Faraday's constant ( $F=96485 \text{ C/mol}$ ).

I is the applied anodic current in amperes

t is the time in seconds during which the current has been passed through the circuit.

$$\text{Current Efficiency} = \Delta m_G / \Delta m_F \quad 8)$$

The distribution of corrosion along and around the perimeter of carbon steel segments was examined and detailed images taken. The surface of the reinforcement bars was partially corroded therefore the average value of  $X_{crit}$  was estimated by:

$$X_{cr_{eq}} / \mu\text{m} = \frac{\Delta m \cdot 10^4}{\rho \cdot A} \quad 9)$$

Where  $\rho$  is the density of carbon steel (7.858 g/cc)

A is the surface area of the corroded length of the rebar in  $\text{mm}^2$

$\Delta m$  is the change in mass of reinforcement bars in grams

**Rate of corrosion in mm/year**

**Corrosion Rate=  $87.6 \times [w / (D \times A \times T)]$**

10)

where W is the weight loss in milligrams,

D is the density of the material used in g/cc

A is the area of the specimen (cm<sup>2</sup>), and

T is the duration of the test period in hours.

**4.0 RESULTS AND DISCUSSION.**

**4.1.1 Results of Chemical composition of the brands of cement tested.**

The chemical composition in table 4.1 is given in terms of oxides except for the insoluble residue (IR) and Loss of Ignition(LOI).

**Table 4.1 Result of Chemical composition the brands of cement tested.**

SN	Test	Result			KS EAS 18-1: 2001 Requirement
		Cem X	CemY	Cem Z	
1.	CaO%	59.86	59.11	58.82	Sum $\geq$ 50
2.	SiO <sub>2</sub> %	16.56	21.56	19.47	
3.	SO <sub>3</sub> %	2.02	2.78	2.03	$\leq$ 3.5
4.	MgO%	1.76	1.04	0.57	$\leq$ 5
5.	K <sub>2</sub> O%	0.027	0.051	-	
6.	Fe <sub>2</sub> O <sub>3</sub> %	2.32	3.48	1.44	
7.	Al <sub>2</sub> O <sub>3</sub>	7.61	8.09	6.85	3-8
8.	Na <sub>2</sub> O <sub>3</sub> %	0.054	0.018		
9.	LOI%	0.11	0.10	4.75	$\leq$ 5
10.	Cl%	0.012	0.016	0.014	$\leq$ 0.1
11.	IR%	2.20	0.55	1.96	$\leq$ 5

**4.1.2 Effect of Chemical Composition of Cement Samples on the rate of corrosion.**

The different brands however had varying properties attributed to their manufacturing processes and manufacturer.

Some constituent compounds in the cement brands are of varying amounts and are responsible in differences exhibited in the resultant concrete properties.

**a) Effect of Lime (CaO) and silicon dioxide (SiO<sub>2</sub>) on the critical penetration depth of rust and the rate of corrosion**

From table 4.1 there is a notable variation in the amounts of CaO, SiO<sub>2</sub> and Insoluble Residue. CemX has the highest amount of CaO (59.86%), CemY has the highest SiO<sub>2</sub> (21.56%) and CemX has the highest Insoluble residue (2.20%). Both CaO and SiO<sub>2</sub> increases the compressive strength of concrete though SiO<sub>2</sub> has to be limited relative to CaO in order not to negatively affect setting time. The optimum amount of nano-SiO<sub>2</sub> is still unknown because of the fact that the SiO<sub>2</sub> used in different studies are of different types with different particle size, specific surface area and associated production method[14]. In addition, uniform dispersion of SiO<sub>2</sub> in cementitious materials is another issue. The effect of SiO<sub>2</sub> include acting as a filler, nucleation and improving the microstructure and early age compressive strength of the cement. Higher compressive strength depicts a concrete with a more compact matrix and a low ingress rate of chloride ions for the chloride induced corrosion mechanism and hence cement with a higher amount of lime and silicon dioxide will have a smaller critical penetration depth of rust and a low rate of corrosion.

**b) Effect of CaO/SiO<sub>2</sub> on the critical penetration depth of rust and the rate of corrosion**

The ratio of lime (CaO) to silicon dioxide (SiO<sub>2</sub>) contents in ordinary Portland cement should be greater than 2. The restriction on the ratio of lime to silicon dioxide [14] is to ensure that the quantity of silicon dioxide is considerably lower than that of lime so that the setting of concrete is not inhibited and the higher ratio increase the compressive strength and a smaller critical penetration depth of rust and lower corrosion is expected. The lime-silicon dioxide ratio for cement samples X, Y, and Z were 3.61, 2.71 and 3.0 respectively.

**c) Effect of SO<sub>3</sub> on the critical penetration depth of rust and the rate of corrosion**

The amount of SO<sub>3</sub> in all the cement brands were within the acceptable limit. SO<sub>3</sub> controls the setting time of cement to avoid flash set. Kosmatka et al, (1991). Slower setting results in greater compressive strength to the set mass and smaller critical penetration depth and slower rate of corrosion.

**c) Effect of MgO on the critical penetration depth of rust and the rate of corrosion**



The quantity of magnesium oxide (MgO) in ordinary Portland cement should not exceed 5% [10]. All the cement samples satisfied this requirement with 1.76%, 1.04% and 0.57% for cement samples X, Y and Z respectively. Magnesium oxide contributes to the colour of cement and hardness of the resulting concrete. If the quantity of MgO is in excess of 5 percent, cracks will appear in concrete and which may affect the rate of corrosion by generating spots for penetration of chloride ions in concrete.

**d) Effect of Chloride Content on the critical penetration depth of rust and the rate of corrosion**

The chloride content in ordinary Portland cement should be less than 0.4%. All the cement samples in this work satisfied this requirement. Higher amounts of chloride in the cements will contribute to the bound chloride and subsequently to the total amount available for electrochemical reactions in corrosion due to chloride mechanism and subsequently increase the critical penetration depth and the rate of corrosion.

**e). Effect of Al<sub>2</sub>O<sub>3</sub> Content on the critical penetration depth of rust and the rate of corrosion**

The quantity of aluminum oxide in all the brands was within the acceptable limits. An increase in the Al<sub>2</sub>O<sub>3</sub> results in an increase in the time for the initial and final sets and hence an increase in compressive strength resulting in a smaller critical penetration depth and a lower rate of corrosion.

**4.2 Aggregates**

**4.2.1 Properties of aggregates**

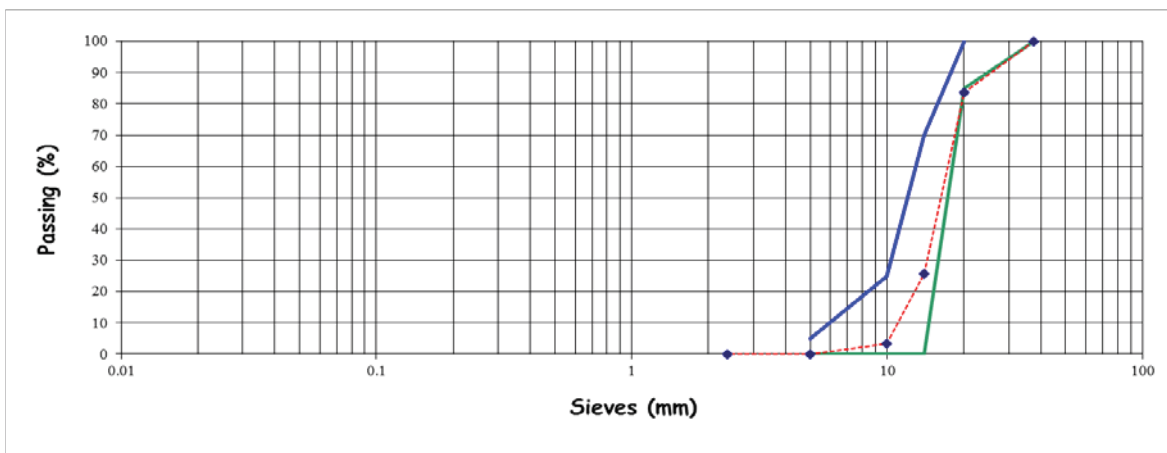
Various tests were carried out on the aggregates to determine their suitability for the research. Water soluble chlorides ions percent were found to be zero in fine aggregates, 0.002 % in coarse aggregates all less than 0.03% acceptable in compliance with BS EN 12620: 2002. Table 4.2 and Table 4.3 show the physical and mechanical properties of the aggregates used while graph 4.1 and graph 4.2 show the gradation of the aggregates.

**Table 4.2: Physical properties of aggregates used in the study**

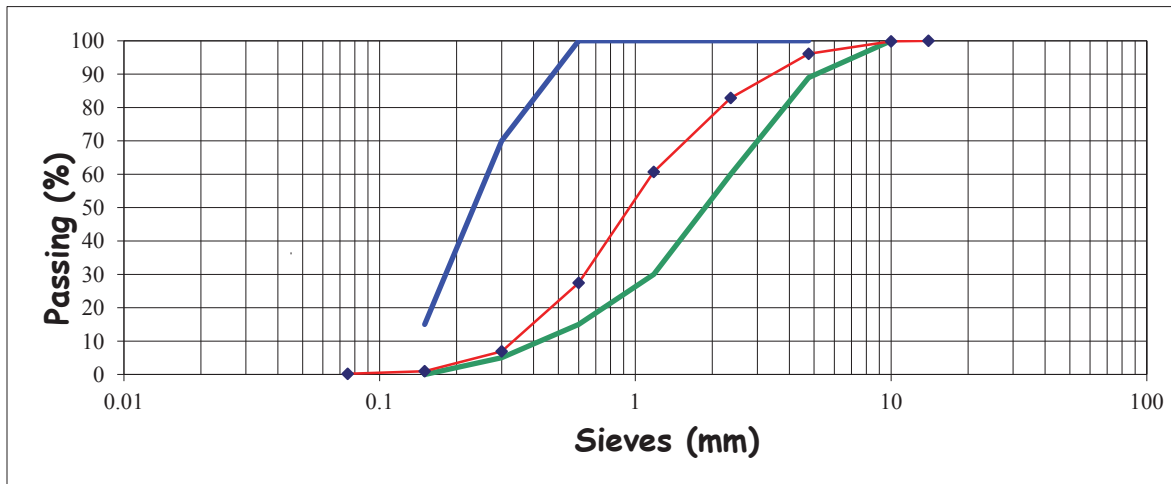
Material	Specific gravity	Absorption %	Silt content %	Max Size
Fine aggregates	2.6	1.8	7.4	4.0
Coarse aggregates	2.6	0.3	0	20.0

**Table 4.3: Mechanical properties carried on coarse aggregates.**

Test	Size of aggregates mm	Crushing value %	Impact Value %	Flakiness index %	Loss Angeles Abrasion Value %
Result	5-20	18	8	35	20



**Graph 4.1 Gradation of Coarse aggregates**



Graph4.2: Gradation of fine aggregates

**4.2.1 Effect of Properties of aggregates on critical penetration depth of rust and the rate of corrosion**

The physical properties, mechanical properties and gradation of aggregates directly affect the compressive strength and fracture energy. Table 4.2 and 4.3 show the physical and mechanical properties of the materials used. Figure 4.1 and 4.2 show the gradation of the aggregates as well graded which results in a compact matrix of the resulting concrete and subsequently an influence in the critical penetration depth of rust and the rate of corrosion. In this research there was no variation in the aggregates used.

**4.3 Hardened properties of concrete**

Table 4.4 shows the compressive strength of the brands of cement used.

**Table 4.4 Results of Average Compressive strength with time**

SN	Cement Brand	Compressive Strength in N/mm <sup>2</sup>		
		7days	14 days	28 days
1.	CemX	25.81	40.28	41.29
2.	CemY	36.379	39.23	44.89
3.	CemZ	34.81	36.26	41.09

**4.3.2 Effect of hardened properties of concrete on the critical radius loss and the rate of corrosion**

From the results of table 4.4, the compressive strength of the concrete reduced with use of cement brand Y, X and Z respectively. This effectively reduces the rate of ingress of chloride ions and the critical penetration depth of rust the rate of corrosion.

**4.4 Accelerated corrosion**

Table 4.5 shows the result of accelerated corrosion while table 4.6 shows the relationship between compressive strength, critical penetration depth of rust and the rate of corrosion.

**Table 4.5 Measurement of Electrode current with time**

Brand of Cement	CemX	CemY	CemZ
Date Cast	30.09.2017	02.10.2017	03.2010.2017
Start of accelerated corrosion	29.10.2017	31.10.2017	01.11.1717
Current at Immersion	Anode	290mA	150mA
	Cathode	269mA	140mA
Current after 30 days	Anode	269mA	140mA
	Cathode	240mA	140mA
Current at 0.1mm crack	Anode	90mA	95mA
	Cathode	98mA	98mA
Duration of crack of 0.1mm	109 days	115 days	106 days
$\Delta m [(M \times I \times t)/(n \times F)]$ ,	246 grams	274grams	226 grams
$\Delta m_{actual}$	1.06grams	0.649grams	1.15grams
Average surface area	1100mm <sup>2</sup>	786 mm <sup>2</sup>	1162mm <sup>2</sup>

corroded,(A)			
Theoretical Critical radius loss Xcrit.	28mm	44mm	25mm
Actual Critical radius loss Xcrit.	0.12mm	0.105mm	0.13mm
Rate of corrosion mm/yr	0.41	0.36	0.43

**Table 4.6 Relationship between the compressive strength, actual critical radius loss and the rate of corrosion**

SN	Cement Brand	Compressive Strength in N/mm <sup>2</sup>			Actual critical radius loss(mm)	Rate of Corrosion(mm/yr)
		7days	14 days	28 days		
1.	Cem X	25.81	40.28	41.29	0.12	0.41
2.	Cem Y	36.379	39.23	44.89	0.105	0.36
3.	Cem Z	34.81	36.26	41.09	0.13	0.43

From tables 4.5 and 4.6 the following can be noted that samples with the highest compressive strength, took the longest period for a crack of 0.1mm to be reached in accelerated corrosion, the lowest critical penetration radius and rate of corrosion and the converse is also true. This results also confirm the trend expected from the chemical compounds in the Cem X, Cem Y and Cem Z. In higher compressive strengths the capillary pore spaces are smaller and successfully reduce the rate of ingress of surface chloride to the rebar/concrete interface. Thus, the diffusion of chloride ions will drop sharply with increased strength and exposure time reducing the critical penetration depth and the rate of corrosion.

### 5. CONCLUSION

This research investigated the effect of selected cement brands in Kenya on the critical penetration depth of rust and the rate of corrosion. The chemical composition of the brands of cement show a marked variation in chemical composition whose effect in compression strength linearly correlate with the critical penetration depth of rust and the rate of corrosion. From the results, for achieving a crack width of 0.1mm in the same accelerated corrosion setup, there is a linear variation in the critical penetration depth of rust and the rate of corrosion for the selected brand of cement.

### REFERENCES

- [1] P.Ghods, O.B. Isgor, F. Bensebaa, D. Kingston, "Angle-resolved XPS study of carbon steel passivity and chloride-induced depassivation in simulated concrete pore solution," Corros. Sci. 2012, 58, 159–167.
- [2] ACI Committee 222, "Protection of Metals in Concrete Against Corrosion," ACI 222R-01, American Concrete Institute, Farmington Hills, Michigan, 2001.
- [3] A.K. Aligizaki, M.R. de Rooij, D.D. Macdonald, "Analysis of iron oxides accumulating at the interface between aggregates and cement paste," Cem. Concr. Res., 30 (2000) 1941-1945.
- [4] G.S. Duffó, W. Morris, I. Raspini, C. Saragovi, "A study of steel rebars embedded in concrete during 65 years," Corros. Sci., 46 (2004) 2143-2157.
- [5] O. Poupard, V.L'Hostis, S. Catinaud, I. Petre-Lazar, "Corrosion damage prognosis of a reinforced concrete beam after 40 years natural exposure in marine environment," Cem. Concr. Res., 36 (2006) 504-520.
- [6] T.D. Marcotte, C.M. Hansson, "Corrosion products that form on steel within cement paste," Mater Struct., 40 (2007) 325-340.
- [7] S. Caré, Q.T. Nguyen, V. L'Hostis, Y. Berthaud, "Mechanical properties of the rust layer induced by impressed current method in reinforced mortar," Cem. Concr. Res., 38 (2008) 1079-1091.
- [8] F.P. Glasser, K.K. Sagoe-Crentsil, "Steel in concrete: Part II Electron microscopy analysis," Mag. Concr. Res., 41 (1989) 213-220.
- [9] W. Aperador, R. Mejía de Gutiérrez, D.M. Bastidas, "Steel corrosion behaviour in carbonated alkali-activated slag concrete," Corrosion Science, vol. 51, 2009.
- [10] W. Aperador, R. Vera, A.M. Carvajal, "Evaluation of the cathodic protection applied to steel embedded in the ASS using the finite element method" International Journal of Electrochemical Science, 7(2012)12870. 5
- [11] E. Busba and A. Sagüés, "Critical Localized Corrosion Penetration of Steel Reinforcement for Concrete Cover Cracking," NACE International's Annual Conference and Exposition, CORROSION, 201
- [12] R. Montoya, W. Aperador, D.M. Bastidas, "Steel corrosion behaviour in carbonated alkali-activated slag concrete," Corrosion Science, 51(2009)2857
- [13] Kenya Bureau of Standards, KS EAS 18-1:2001-Cement Part 1:Composition, Specification and Conformity Criteria for Common Cements. Kenya Bureau of Standards, Nairobi, 2005.
- [14] BS 12, "Specification for Portland cement," BSI Publications, London, 1996.

### AUTHORS

**First Author** – Mogire Philip, PhD Student, Department of Civil and Construction Engineering, University of Nairobi, Kenya, philosiemo@yahoo.com

**Second Author** – Prof. Silvester Abuodha, Associate Professor, Department of Civil and Construction Engineering,

University of Nairobi, Kenya, sochieng@yahoo.com

**Third Author** – Dr. John Mwero, Lecturer, Department of Civil and Construction Engineering, University of Nairobi, Kenya, johnmwero1@gmail.com.

**Fourth Author** – Prof. Geoffrey Mang'uriu, Professor, Department of Civil, Construction and Environmental Engineering, Jomo Kenyatta University of Agriculture & Technology, gmanguriu@yahoo.co.uk

**Correspondence Author** – Mogire Philip, philosiemo@yahoo.com, +254 734 967 989

# A Corrosion Model for prediction of Service Life of Reinforced Concrete water structures.

Philip Mogire<sup>1,a,\*</sup>, John Mwero<sup>2,b</sup>, Silvester Abwodha<sup>3,c</sup> and Geoffrey Mang'uriu<sup>4,d</sup>

<sup>1,2,3</sup>Department of Civil and Construction Engineering,  
University of Nairobi, Kenya

<sup>4</sup>Department of Civil, Construction and Environmental Engineering,  
Jomo Kenyatta University of Agriculture & Technology  
P.O. Box 62000-00200, Nairobi, KENYA

<sup>a</sup>philosiemo@yahoo.com, <sup>b</sup>johnmwero1@gmail.com, <sup>c</sup>sochieng@yahoo.com, <sup>d</sup>gmanguriu@yahoo.co.uk  
\*corresponding author

DOI: 10.29322/IJSRP.10.02.2020.p98104  
<http://dx.doi.org/10.29322/IJSRP.10.02.2020.p98104>

**Abstract-** As the world economies endeavor to support the United Nations sustainable development goals, new technologies are evolving for efficient design and manufacture of civil engineering products. Researchers have up scaled their effort to develop techniques to monitor the performance of civil engineering structures within their service life for optimum return from investment. The aim of this research was to develop a service life model to for prediction of the service life of reinforced concrete water conveyancing structures.

To achieve the desired objective, steel samples were cast in concrete of characteristic strength of 25N/mm<sup>2</sup>, 9 cylinders each of 150mm diameter x 300mm long, 130mm diameter x 300mm long and 100mm diameter x 300mm long respectively in concrete characteristic strength 25N/mm<sup>2</sup>, 30N/mm<sup>2</sup> and 35N/mm<sup>2</sup> for accelerated corrosion test were cast. After 24 hours the cast specimens were demolded and immersed in curing tanks for 27 days and then immersed in a 3.5% industrial sodium chloride solution under 6V. The accelerated corrosion specimens were monitored for onset of cracks and stopped when the cracks were 0.2mm in width.

The physical and chemical properties of the materials were investigated for compliance to relevant applicable British and Kenyan standards for conformity to acceptable criteria. The concrete materials were batched by weight and mixed by a lab electric pan concrete mixer in batches of 0.009 m<sup>3</sup>. The concrete batches were tested for consistency by the slump and compaction factor tests.

From the results a model that takes account of the cover to the rebar, the rebar size and the compressive strength properties of concrete and steel/concrete interface was developed.

The model developed here is for water structures and shows that the time to corrosion cracking of the cover concrete in a chloride contaminated concrete structure is a function of reinforcement cover, corrosion rate and critical mass of the corrosion products. The times to cracking predicted by the model are in good agreement with the observed times to cracking based on this research

**Index Terms-** Accelerated corrosion, water structures, Corrosion model.

## 1. INTRODUCTION

Building on the millennium development goals, in a transformative, inclusive, comprehensive and integrated agenda 2030, the 17 Sustainable Development Goals (SDGs) for Sustainable Development were adopted in September 2015 by 193 countries [1]. The SDGs address humanitarian and environmental problems including poverty, education, health, biodiversity, and climate change (United Nations, 2016). Attention has turned to designing and implementing policies to achieve The SDGs by the designated completion year of 2030. Kenya, among many governments in the developing world have encouraged developing of small hydropower projects to increase power capacity which in turn will accelerate achievement of the 17 SDGs. Each of the small hydropower projects has a reinforced concrete conveyance or diversion structure that require assessment of their performance within their service life. Research in the deterioration models for reinforced concrete water structures is key in their sustainable performance.

Deterioration of reinforced concrete due to corrosion which results from carbonation or from chloride ingress plays a significant role in reduction of the design service life of reinforced concrete water structures and has attracted researchers of various disciplines during the past three decades [2]. Metals store heat as potential energy during their production and release this energy during the corrosion process after reacting with the favorable corrosive environment. These will tend to lose their energy by reverting to compounds more or less similar to their original states, for example the starting material for iron and steel making and the corrosion product rust has the same chemical composition (Fe<sub>2</sub>O<sub>3</sub>). The energy stored during melting and released during corrosion supplies the driving potential for the corrosion process to take place [3], therefore corrosion occurs when at least two metals (or two locations of the reinforcing bar) is at different energy levels. In reinforced concrete the concrete acts as an electrolyte while the rebar act as a metallic connection [4]. At a

pH of 12- 13, reinforced concrete is in an alkaline state and a thin oxide layer forms on the steel and prevents metal atoms from dissolving forming a passive film [5]. The passive film reduces the corrosion rate to an insignificant level without which the steel would corrode at rates at least 1,000 times higher [6].

The presence of rust on reinforcement bars and appearance of cracks parallel to the reinforcement bars is an indication of the presence of corrosion in reinforced concrete structures. Carbonation inducing a generalized attack and the presence of chlorides inducing a localized attack are the main causes of electrochemical corrosion in reinforced concrete as shown in Figure 1[4]. Carbonation induced corrosion commonly occurs in relatively dry environments where sufficient carbon oxide to diffuse into the cover concrete is possible. In chloride containing environments, the chloride ingress is usually faster than the carbonation process, and it is more likely to be the predominant cause of deterioration in reinforced concrete water structures by degrading the resistance of the structure to service loads.

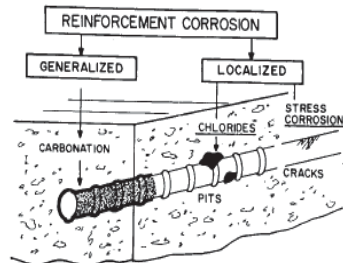


**Figure 1: Types and morphology of the corrosion in concrete: generalized (carbonation), localized (chlorides) [4]**

When reinforcement corrosion becomes visibly detected, deterioration has already occurred and it may be too late to take any corrective or protection measures. This makes the reinforced concrete service life prediction models very critical for any sustainable structure. The permeability of the concrete, nature and force of cracks, and the cover thickness have an incredible role on the start and progression of corrosion.

Various corrosion models have been proposed and can broadly be categorized into either empirical [7], analytical [8-10] or numerical [11-12]. Molina et al. [11] used a smeared crack model for the finite element analysis of cover cracking due to reinforcement corrosion. In their model they presumed corrosion of steel to take a linear variation of the material properties from those of steel to those of rust. Due to lack of information they also assumed that the mechanical properties of rust nearly resemble that of water which is one of the main constituents of rust. Their analysis was based on the experiments of Andrade et al. [13] where the thickness of the concrete cover was 1.25 and 1.9 times the reinforcement diameter.

An empirical equation for predicting the time to cover cracking without reference to the evolution of the damage zone was suggested by Morinaga [14]. In his empirical equation; the time to cover cracking as a function of the corrosion rate, concrete cover thickness and reinforcing diameter was accounted. In close scrutiny of Monariga's results shows that the cover cracking predicted by Morinaga's model is much shorter than the experimentally observed values[15], [16].

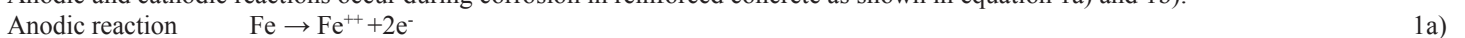
Further investigations in this field have revealed that the consideration of the appropriate mechanical behavior of corrosion products strongly affects the predicted results [17]. Lundgren [18], in an effort to study rebar pull-out, presented a reasonable way to model the effect of corrosion on the bond between the corroded reinforcement and concrete. Lundgren employed finite element analysis and assumed that rust behaves like granular materials, in accordance with the experimental tests of Andrade et al. [19]. Lundgren pointed out that the model could predict the decrease of the bond when splitting of the concrete occurs. It was emphasized that axisymmetric analysis appears to be a satisfactory level of modeling when a study of concrete cover cracking due to uniform corrosion is of concern. However, three dimensional models should be used if localized corrosion is to be studied.

Bhargava et al. [20],[21] presented a mathematical model to predict the time to concrete cover cracking and weight loss of reinforcing bars. However, they assumed that the mechanical properties of corrosion products are the same as those of steel, though reasonably good agreement was obtained between experimental results and the analytical predictions. They showed that tensile strength, initial tangent modulus of concrete, annual mean corrosion rate, and modulus of elasticity of the reinforcement and corrosion significantly influence the predicted time to cover cracking.

In this study a mathematical model is formulated to determine the corrosion rate in water conveyancing structures. This model takes into consideration of the serviceability limiting condition of the crack width of water structures.

## **2. CORROSION INDUCED REINFORCED CONCRETE CRACKING MODEL FOR A WATER CONVEYANCING STRUCTURE**

Anodic and cathodic reactions occur during corrosion in reinforced concrete as shown in equation 1a) and 1b):



Initially, the rate of corrosion will depend on the chloride concentration and the rate of the anodic reaction. Shortly thereafter, as the corrosion becomes more severe and the rust layers build up, the corrosion rate will be controlled by the cathodic reaction and the availability of oxygen at the cathode. The structure of the pit and corrosion products depends on the aqueous phase of the pore solution, rebar type, and pressure adjacent to the bar. Generally, the composition of the expansive corrosion products may be expressed as shown in equation 2:



Corrosion product  $\rightarrow \{a.Fe(OH)_2 + b.Fe(OH)_3 + c.H_2O\}$  [22] 2)  
 where  $a, b$  and  $c$  are variables that depend on the alkalinity of the pore water solution of the concrete, the oxygen supply, and the moisture content.

During progression of corrosion of reinforcement bars in reinforced concrete, the oxidation products increase in volume. The corrosion products take up more volume than the virgin steel rebar and therefore, are inclined to deteriorate the concrete by producing tensile stresses as well as microcracks nearby the rebar. The expansion ratio of the oxide to the original rebar volume depends on the specific type of oxide formed [23]. Depending on the oxidation level, the volume increase due to rebar corrosion is around 2.0 to 6.5 times the original rebar volume [22]. The production of rust may follow a linear or parabolic law depending on the rust properties [24]. When corrosion of reinforcement develops significantly, the corrosive products expand continuously and generate internal pressure to the concrete surface around the steel bar. The continuous process of reinforcement corrosion affects structural serviceability by cracking, spalling the concrete cover and also decreasing the load-bearing capacity thus endangering the structural safety. The physical effects of corrosion include loss of steel area, loss of bond strength between steel reinforcing bars and concrete and reduction of concrete composite strength due to cracking. In this research, a service life model is developed utilizing the results of accelerated corrosion.

A considerable research has been undertaken on corrosion of reinforced concrete. On experimental work on corrosion induced cracking in reinforced concrete, the corrosion process is usually accelerated by various means so that concrete cracking can be achieved in a relatively short time [15]. Due to carbonation or in the presence of chlorides, corrosion is initiated by the breakdown of a 'passive layer'. The composition, pore structure and cover of concrete play a big role in corrosion initiation period as well as rate of corrosion. The rate of corrosion is often modeled using Faraday's law. The pH driven corrosion reaction rate is current density dependent. The resulting mass loss to oxidation for a constant current time interval according to Faraday's law is:

$$\Delta W = (ITA) / (ZF) \quad [25] \quad 3)$$

Where  $\Delta W$  = weight loss (grams)

$I$  = corrosion current (amp)

$T$  = time (sec)

$A$  = atomic weight of iron (56g)

$Z$  = valency of the metal (2)

$F$  = Faraday constant (96500 Amp-sec).

By inserting the specific values of  $A, Z,$  and  $F$  into eq. (3), the rebar mass conversion as a function of time and corrosion current is:

$$\Delta W = 25It \quad 4)$$

Where,  $I$  = corrosion current (amp)

$t$  = time (days).

$$\text{Corrosion Rate (mm/yr)} = 87.6 \times [w / (D \times A \times T)] \quad [26] \quad 5)$$

where  $W$  is the weight loss in milligrams,

$D$  is the density of the corroding reinforcement in  $g/cm^3$

$A$  is the surface area of the specimen subjected to corrosion in  $(cm^2)$ , and

$T$  is the duration of the test period in hours.

### 3.0 Methodology

This study was conducted at the University of Nairobi Concrete and Materials lab where the physical properties of the materials, sample preparation and testing were done. The chemical properties of the ordinary Portland cement and chloride content was done at the State Department of Infrastructure in the Ministry of Transport, Infrastructure, Housing and Urban Development of the Government of Kenya.

#### 3.1 Concrete samples

The constituent materials for preparing test samples consisted of Ordinary Portland cement ( $42.5N/mm^2$ ), clean river sand, 20mm maximum size coarse aggregate and potable water.

##### 3.1.1 Cement

The chemical composition of the cement used in this research was tested. Available cements in Kenya are manufactured in accordance to KS EAS 18-1: 2001, an adoption of the European Norm EN 197 cement standards [27]. The cements locally available are produced for specific uses [28]. The Cement used for this research was ordinary Portland cement type 42.5N sourced from one wholesaler.

##### 3.1.2. Other concrete constituents

Table 1 shows the description and source of other constituents of concrete used in the research.

**Table 1. Details of materials used in the research**

SN	Description	Source	Remark
1.	Fine aggregates	Stockpile vender sourced from Machakos River	This was washed and oven dried before use.
2	Coarse aggregates	Kenya builders quarry	5-20mm uniformly graded at source
3.	10mm ribbed bars	Local manufacturer	Factory cut to 400mm
4.	Mixing water	Potable water in the Lab	

##### 3.2.2. Concrete Mix Design

With a characteristic strength of  $25\text{N/mm}^2$ , the concrete used was designed in accordance with the British Department of environment (DoE) method [29-30].

### 3.2.3 Test on hardened concrete

#### Compressive strength and split tensile strength

The compressive strength of concrete was investigated at 7, 14 and 28 days using a digital Universal Testing Machine shown in figure 2a), with a loading capacity of 2000 KN in accordance to BS EN 12390-3:2009 while the split tensile strength was done using a hydraulic Universal Testing machine as shown in figure 1b) and c).



Figure 2:a) Compression testing machine used in the research, b) and c) Failure mode during split tensile test

### 3.2.4 Accelerated Corrosion

#### 3.2.4.1 Materials and Specimens

This was done through an impressed corrosion test using the procedure below;

- i) 10mm diameter x 400mm long ribbed bars were polished with abrasive papers.
- ii) 120 mm of the surface length of each bar were sprayed with a zinc rich coating and left to naturally dry.
- iii) The mixed concrete (in two batches) was poured into 9 cylindrical samples of 150mm diameter and 300mm long, 130mm diameter and 300mm long, 100mm diameter and 300mm long each with a 10mm diameter rebar
- iv) The specimens were mechanically vibrated for 60s. After 24 hours, the cylindrical concrete specimens were demolded and cured for 27 days.
- vi) The test specimens were dried for 24 hours and then subjected to accelerated corrosion by storing them in a tank containing 3.5 % NaCl at room temperature and an impressed voltage of 6volts applied through a DC power supply regulator. The top and bottom surfaces of the concrete specimens were also sealed with Zinc rich coating so as to allow chloride ingress from the sides to simulate the corrosion of a section of a typical structural member in a water conveyancing structure.

#### 3.2.4.2 Testing Methodology

The accelerated corrosion set up is shown in Figure 3. The rebars projecting were connected in series to the anode and the stainless steel rod was connected to the negative terminal (cathode). The test specimens were subjected to a constant voltage of 6 V applied to the system using a DC power supply regulator. The variation in development of corrosion current was monitored at regular intervals using a high impedance multimeter and the average for the corrosion period taken for calculation of the average mass loss.

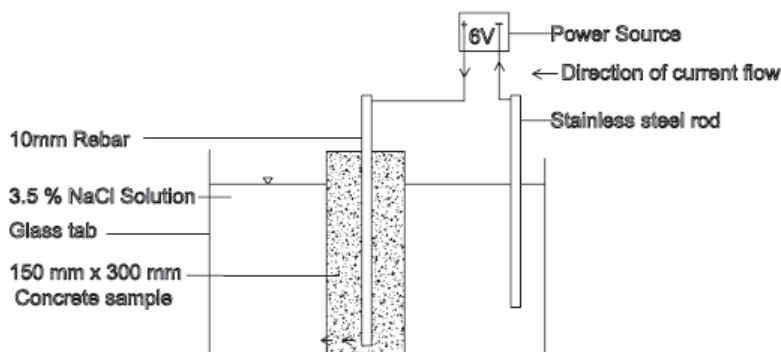
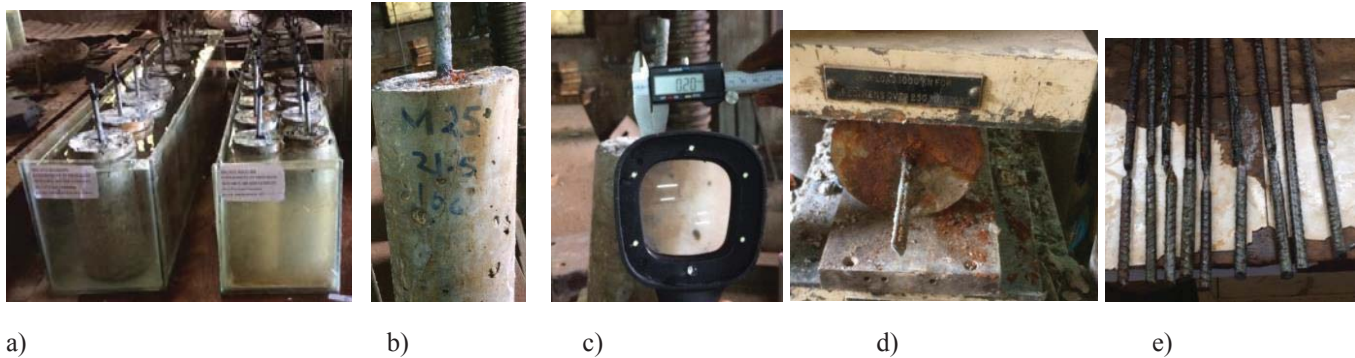


Figure 3:a) Schematic drawing of accelerated corrosion set up, b) Photo of the samples during experimentation

The appearances of first visible cracking were detected by visual observation using a magnification glass with power of x1000. The data collected for crack propagation provided the timing of first cracking and the subsequent time-dependent increase in crack width. After testing, the weight loss of bars due to corrosion were studied by cleaning, drying and weighing the reinforcement bars according to the



gravimetric weight loss method as specified by Standard Practice for Preparing, Cleaning, and Evaluating Corrosion Test Specimens (ASTM G1 – 90). Figure 4 shows samples during experimentation and measurement. The weight loss corresponded closely to that expected from current density ( $i_{corr}$ ) measurements.



**Figure 4: a) Samples during experimentation b) sample with 0.2mm longitudinal crack c) crack measurement d) recovering the corroded steel and e) cleaned rebar's for gravimetric weight loss measurement.**

### 3.3 Results of the material properties

#### i) Properties of aggregates

Various tests were carried out on the aggregates to determine their suitability for the research. Water soluble chlorides ions percent were found to be zero in fine aggregates, 0.002 % in coarse aggregates all less than 0.03% acceptable in compliance with BS EN 12620:2002.

**Table 2: Physical properties of aggregates used in the study**

Material	Specific gravity	Absorption %	Silt content %	Max Size
Fine aggregates	2.6	1.8	7.4	4.0
Coarse aggregates	2.6	0.3	0	20.0

**Table 3: Mechanical properties carried on coarse aggregates.**

Test	Size of aggregates mm	Crushing value %	Impact Value %	Flakiness index %	Loss Angeles Abrasion Value %
Result	5-20	18	8	35	20

#### ii) Chemical Properties of Cement used in the research

Table 4 shows results of the chemical composition of the cement used in the research. All the constituents of cement oxides were within the acceptable limits.

**Table 4 Result of Chemical composition the Cement used.**

SN	Test	Result of the sample	KS EAS 18-1: 2001 Requirement
1.	CaO%	59.11	Sum $\geq 50$
2.	SiO <sub>2</sub> %	21.56	
3.	SO <sub>3</sub> %	2.78	$\leq 3.5$
4.	MgO%	1.04	$\leq 5$
5.	K <sub>2</sub> O%	0.051	
6.	Fe <sub>2</sub> O <sub>3</sub> %	3.48	
7.	Al <sub>2</sub> O <sub>3</sub>	8.09	3-8
8.	Na <sub>2</sub> O <sub>3</sub> %	0.018	
9.	LOI%	0.10	$\leq 5$
10.	Cl%	0.016	$\leq 0.1$
11.	IR%	0.55	$\leq 5$

#### a) Effect of sum of lime (CaO) and silicon dioxide (SiO<sub>2</sub>) corrosion

The sum of lime (CaO) and silicon dioxide (SiO<sub>2</sub>) in the chemical analysis of ordinary Portland cement sample was 80.67%  $\geq 50\%$  within the acceptable limit [31]. This is consistent with the known fact that both CaO and SiO<sub>2</sub> give strength to concrete though SiO<sub>2</sub> has to be limited relative to CaO in order not to negatively affect setting time. The rate of corrosion is related to the strength of a concrete

sample while reduced setting time minimizes plastic shrinkage cracking and hence the rate of corrosion.

### b) Effect of CaO/SiO<sub>2</sub> on corrosion

The ratio of lime (CaO) to silicon dioxide (SiO<sub>2</sub>) contents in ordinary Portland cement should be greater than 2. The restriction on the ratio of lime to silicon dioxide [29] is to ensure that the quantity of silicon dioxide is considerably lower than that of lime so that the setting of concrete is not inhibited minimizing plastic shrinkage cracking.

### c) Effect of MgO on corrosion

The quantity of magnesium oxide (MgO) in ordinary Portland cement should not exceed 5% [32]. If the quantity of MgO is in excess of 5 percent, cracks will appear in concrete and which may affect the rate of corrosion by generating spots for penetration of chloride ions in concrete.

### d) Effect of SO<sub>3</sub> on corrosion

The quantity of sulphur trioxide (SO<sub>3</sub>) content in ordinary Portland cement was less than 3.5 % as required. SO<sub>3</sub> reduces the rate of transpassive layer dissolution inhibiting the onset of corrosion.

### e) Effect of Chloride Content on corrosion

The chloride content in ordinary Portland cement was less than 0.4% as required. Chloride ions in aqueous solution destroys the passivation film of rebars in the process of competing with hydrogen and oxygen ions in the adsorption process, thus leading to the occurrence of pitting corrosion, hole corrosion and crevice corrosion.

### f) Effect of Al<sub>2</sub>O<sub>3</sub> on corrosion

Aluminium oxide (Al<sub>2</sub>O<sub>3</sub>) reacts with free lime in concrete to form CaAl<sub>2</sub>Si<sub>3</sub>O<sub>12</sub>. which reduces the permeability of chloride and improving the corrosion resistance property of embedded steel in concrete. Above 8% the Al<sub>2</sub>O<sub>3</sub> will be in an active condition reducing the corrosion resistance.

### g) Effect of Fe<sub>2</sub>O<sub>3</sub> on corrosion

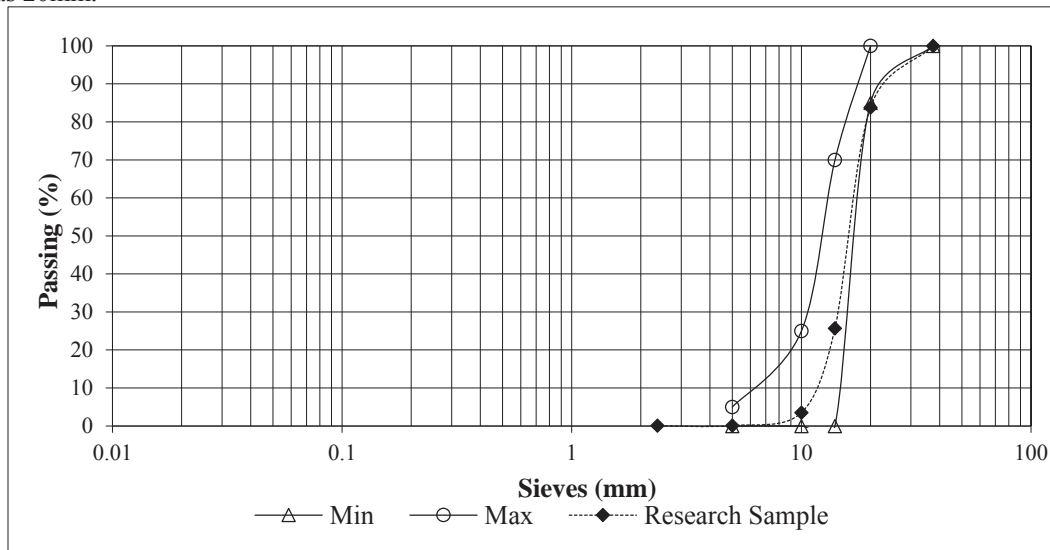
Iron oxide (Fe<sub>2</sub>O<sub>3</sub>) contributes to cement colour and helps in the fusion of the different ingredients. Fe<sub>2</sub>O<sub>3</sub> forms the passivation film reducing the oxygen diffusion rate, which, in turn, reduces the **corrosion** rate.

### h) Effect of Residues on corrosion

British standards consider Na<sub>2</sub>O, K<sub>2</sub>O, TiO<sub>2</sub> and P<sub>2</sub>O<sub>5</sub> in ordinary Portland cement as residues and limit the sum of all of them to 5%. If in excess of 5% efflorescence and unsightly cracking will occur aggravating corrosion.

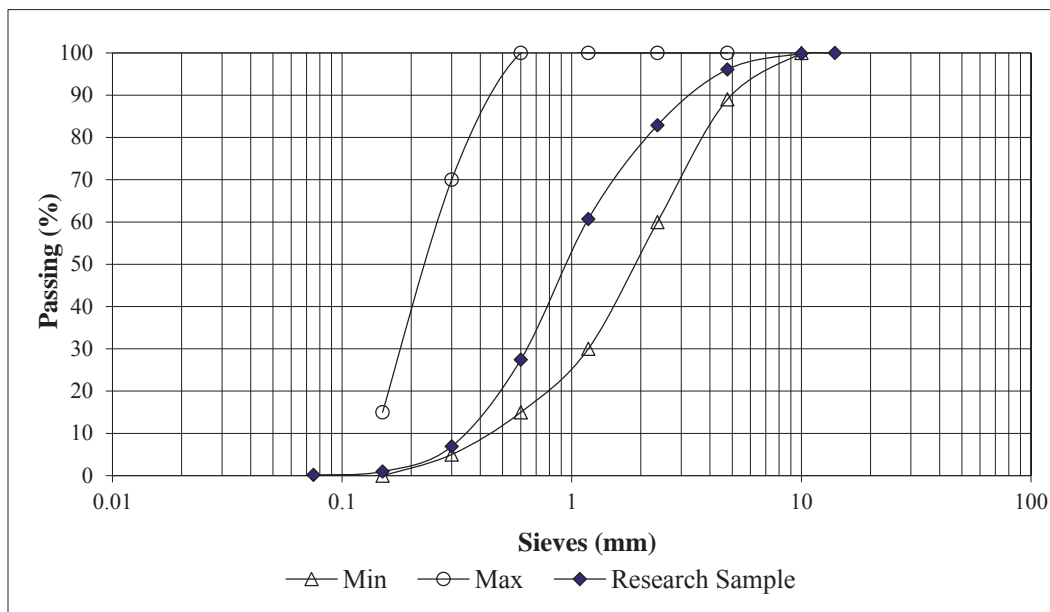
### iii) Gradation of Coarse and Fine aggregates

Particle size distribution analysis on a representative sample as shown on graph 1 of the coarse aggregates for the work was carried out to obtain the proportions by weight of the different sizes of coarse aggregates present. The sample is well graded with a maximum aggregate size was 20mm.



Graph 1 Gradation of Coarse aggregates

Particle size distribution analysis as shown on graph 1 on a representative sample of the fine aggregates for the research was carried out to obtain the proportions by weight of the different sizes of fine particles present according to BS 812-103 and BS 882. The proportions were expressed as percentages by weight passing various sieve sizes conforming to BS 410. As shown in graph 1 the coarse aggregates were well graded and expected to give a well interlocked composite concrete mix.



**Graph 2: Gradation of fine aggregates**

**iv) Results of hardened concrete**

**Table 4: Comparative study of results of hardened concrete for Concrete of characteristic strength 25 N/mm<sup>2</sup>**

Compressive strength (N/mm <sup>2</sup> ) at 28 days	Split tensile strength in N/mm <sup>2</sup>					
	Measured Value	Lavanya & Jegan (2015) $f_{t1}=0.249f_{ck}^{0.772}$	ACI Committee 318(2014) $f_{t2}=0.56f_{ck}^{0.5}$	Anoglu et al (2006) $f_{t3}=0.387f_{ck}^{0.63}$	CEB-FIB (1991) $f_{t4}=0.3f_{ck}^{0.66}$	Gardner (1990) $f_{t5}=0.33f_{ck}^{0.667}$
44.89	4.38	4.70	3.75	4.25	3.70	4.17
53.87	5.26	5.41	4.11	4.77	4.17	4.71
62.85	6.13	6.09	4.44	5.26	4.61	5.22

The comparative results of table 2 show that the split tensile results measured is within the published results of other published authors.

**3.4 Results from Accelerated Corrosion Tests**

From equation 4 and 5

$\Delta W = 25It$  (gms) for calculated mass loss.

Where, I = corrosion current (amp) averages measured during accelerated corrosion (4.0, 2.4 and 2.0 milliamperes measured for concrete characteristic strength 35N/mm<sup>2</sup>, 30N/mm<sup>2</sup> and 25N/mm<sup>2</sup> respectively).

t = time (days).

**Corrosion Rate(mm/yr) = 87.6 x [w/(D x A x T)]**

where W is the weight loss in milligrams measured as an average from corroded samples.

D is the density of the rebar used, g/cc, =7.8

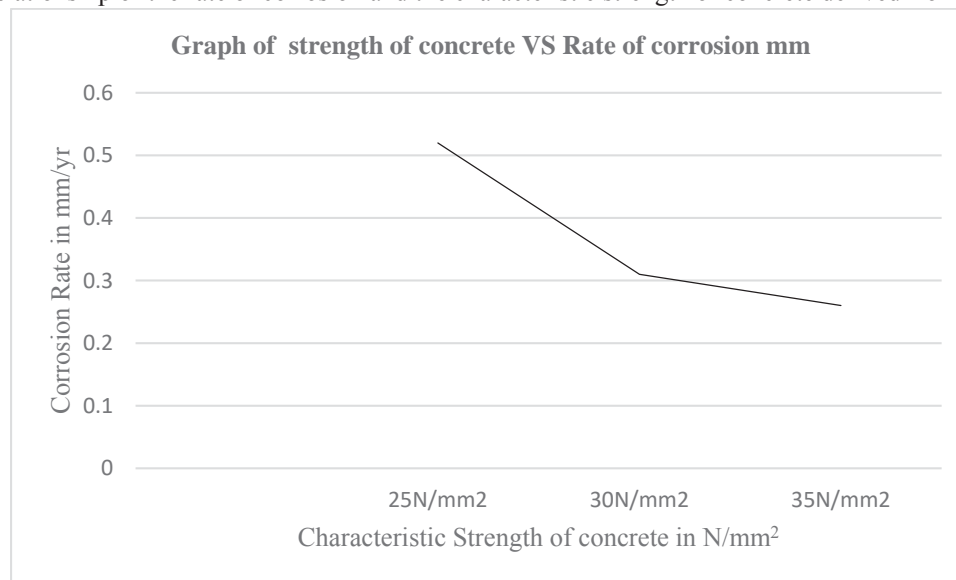
A is the surface area of the specimen subjected to corrosion (cm<sup>2</sup>), and =91.11

T is the duration of the test period in hours.

**Table 5: The rate of corrosion of rebar from samples from different diameter samples and strengths**

Concrete characteristic strength	Sample series	Rate of corrosion in mm/yr						
		Average mass of steel sample before corrosion (gms)	Average mass of steel sample after corrosion (gms)	Loss in weight (gms)measured	Loss in weight (gms) Calculated	Duration in days	Rate of corrosion mm/yr (measured)	Rate of corrosion mm/yr (calculated)
25N/mm <sup>2</sup>	150mm diameter	371	360.4	10.6	10.7	107	0.51	0.51
	130mm diameter	371	362.3	8.7	8.7	86	0.52	0.52
	100mm diameter	371	363.2	7.8	7.6	76	0.53	0.52
30N/mm <sup>2</sup>	150mm diameter	371	361.5	9.5	9.4	156	0.31	0.31
	130mm diameter	371	362.4	8.6	8.5	142	0.31	0.31
	100mm diameter	371	363.4	7.6	7.6	127	0.31	0.31
35N/mm <sup>2</sup>	150mm diameter	371	361.6	9.4	9.3	186	0.26	0.26
	130mm diameter	371	362.4	8.6	8.6	172	0.26	0.26
	100mm diameter	371	363.1	7.9	7.9	158	0.26	0.26

Graph 3 shows the Relationship of the rate of corrosion and the characteristic strength of concrete derived from table 5.



**Graph 3: Relationship of the rate of corrosion vs the rate of corrosion**

From table 5 and graph 3, it can be observed that the rate of corrosion is affected by the characteristic strength and this is attributed to the rate at which the aggressive chloride ions took to reach the rebar to enhance the onset of corrosion. It took a longest period for samples of characteristic 35N/mm<sup>2</sup> to corrode and result to a crack width of 0.2mm while samples with characteristic strength 25 N/mm<sup>2</sup> exhibited the shortest time. It can also be observed that concrete cover affects the duration of corrosion within the same characteristic strength of concrete but the rate of corrosion remains the same and this is because concrete of the same characteristic strength has the same electrical resistance.

### 3.4.1 Crack Initiation ( $t_1$ )

This is the first visible crack, which was observed through a magnifying glass ( $\times 1000$ ) and this period of time ( $t_1$ ) can be referred to as time to crack initiation.  $t_1$  depends on concrete tensile strength ( $f_t$ ). The model developed by Liu & Weyers (1996) reasonably predicts the time to first cracking although the predicted times are under-estimated (approximately 11%) when compared to results obtained from accelerated corrosion testing.

The time to crack initiation by Liu & Weyers (1996) model is the time when stresses resulting from the expansion of corrosion products exceed the tensile strength of concrete. The critical amount of corrosion products needed to cause first cracking consists of two parts:

- (i) the amount of corrosion products required to fill the total porous zone around the steel/concrete interface; and
- (ii) the amount of corrosion products then needed to generate the critical tensile stresses.

The time to cracking is influenced by corrosion rate, cover, bar spacing, concrete quality, and material properties. Therefore, the model proposed by Liu & Weyers (1996) was assumed herein as suitable for estimating the time to first cracking.

### 3.4.2 Crack Propagation ( $t_2$ )

Cracks first observed at the concrete surface through the magnifying glass were very small (width of less than 0.2mm) with lengths varying from 30mm to 300mm. Cracks width and length then increased in an inhomogeneous manner until they extended and joined together to create continuous corrosion-induced longitudinal cracking when the crack width was 0.2mm when the experiment stopped.

## 4.0 DETERIORATION MODEL

### i) Model development

Consider the schematic drawing shown in figure 5 for this research.

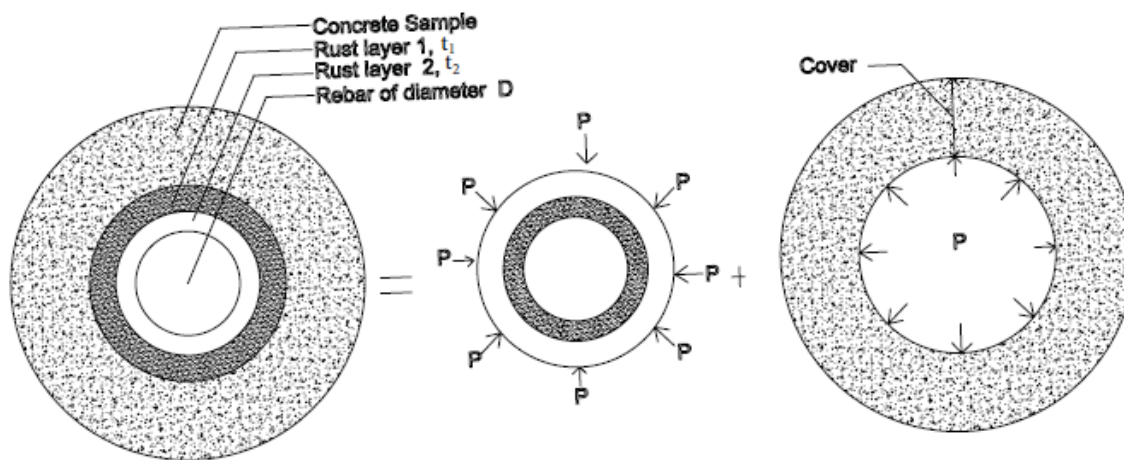


**Figure 5 Schematic drawing of expansive pressure on surrounding concrete due to accumulation of rust products**

Layer 2 is a transition zone between cement paste and aggregate and is influenced by the water/cement ratio, degree of consolidation and hydration, aggregate sizes and steel reinforcement. The weight of materials in this zone denoted as  $M_p$  can be expressed as,

$$M_p = \rho_{\text{rust}} V_p \tag{6}$$

where

$\rho_{\text{rust}}$  is the density of corrosion products and

$V_p$  is the total volume of interconnected pores around layer 2 of thickness  $t_1$ .

A steel bar having diameter  $D$  will increase its diameter to  $D+2t_1$ , when the mass of the amount of corrosion products reaches  $M_p$ . For a 300mm length of steel bar, since  $t_1 \ll D$ ,  $M_p$  can be estimated from equation 6,

$$M_p = 0.3\pi\rho_{\text{rust}} D t_1 \tag{7}$$

It can be seen that  $M_p$  is related to the size of the reinforcement, density of rust products and property of steel/concrete interface.

### ii) Estimation of $M_{\text{crit}}$

The critical amount of rust products to initiate a crack consists of two parts,  $M_p$ , the amount of corrosion products to fill the total interconnected pores around the steel/concrete interface (layer 2), and  $M_s$ , the amount of corrosion products that generate the critical tensile stresses, of 300mm length of steel bar, the value  $M_s$  can be estimated from equation 5,

$$\begin{aligned}
 M_s &= 0.3\pi\rho_{rust} [(t_1+t_2)(D+t_1+t_2)] \\
 &= 0.3\pi\rho_{rust} [D+(M_{st}/\rho_{st})] \\
 &= 0.3\rho_{rust} [\pi(t_1+t_2)D+(M_{st}/\rho_{st})]
 \end{aligned}
 \tag{8}$$

Where  $\rho_{rust}$ : the density of corrosion products

$\rho_{st}$ : the density of steel

$t_1$ : the thickness of the area around the steel/concrete interface and is the radial displacement under pressure

$t_2$ : the thickness of the corrosion products to generate the tensile stresses

$D$ : the diameter of the steel reinforcement

$M_{st}$ : mass loss of the rebar

Based on the theory of elasticity by Timoshenko and Goodier (1970) and Ugural (1986) and modelling the reinforced concrete as a thick wall cylinder under internal pressure  $P$ . The pressure  $P$  at concrete/rust products interface can be expressed as:

$$P = \frac{2E_{ef}t_2}{(D+2t_1)\left(\frac{b^2+a^2}{b^2-a^2}+v_c\right)}
 \tag{9}$$

where  $v_c$  is Poisson's ratio of the concrete,

$E_{ef}$  is an effective elastic modulus of the concrete

$a$  is the inner radius  $=(D+2t_1)/2$

$b$  is the outer radius  $= [C+(D+2t_1)/2]$ ,  $C$  is the cover in which

$E_{ef} = Ec/(1+jcr) = 1.16$

$Ec$  is elastic modulus of the concrete  $= 0.45\sqrt{fc} = 3.015$  and

$jcr$  is the creep coefficient of the concrete  $= 1.6$ .

$t_2$  is the thickness of the concrete under pressure

The thickness of concrete causing pressure is the thickness of corrosion products generating the pressure on the concrete.

At failure and considering that cracking first occurred over the reinforcement (the observed corrosion cracks were located along the thickness of the samples from the steel rebars to the edge of the sample and then longitudinally), the minimum stress required to cause cracking of the cover concrete equals the tensile strength of concrete,

$$P = \frac{2Cf_t}{D+2t_1}
 \tag{10}$$

where  $C$  is the cover depth of concrete

$f_t$  is the tensile strength of concrete.

From equations 6 and 7,  $t_2$  may be expressed as,

$$t_2 = \frac{cf_t}{E_{ef}} \left( \frac{a^2+b^2}{b^2-a^2} + v_c \right)
 \tag{11}$$

Therefore, the critical amount of corrosion products needed to induce cracking of the cover concrete can be estimated from equations 5 and 8,

$$M_{crit} = \rho_{rust} \left( 0.3\pi \left[ \frac{cf_t}{E_{ef}} \left( \frac{a^2+b^2}{b^2-a^2} + v_c \right) + t_1 \right] D + \frac{M_{st}}{\rho_{st}} \right)
 \tag{12}$$

From equation 9, the critical amount of corrosion products needed to induce cracking of the cover concrete is dependent on the tensile strength of concrete, cover depth, elastic modulus of concrete and properties of steel/concrete interface.

### iii) Growth of Rust Products

As the rust layer grows thicker, the ionic diffusion distance increases, and the rate of rust production decreases because the diffusion is inversely proportional to the oxide thickness. The rate of rust production can be written as follows,

$$\frac{dM_{rust}}{dt} = \frac{k_p}{M_{rust}}
 \tag{13}$$

where  $M_{rust}$  is amount of rust products (kg),

$t$  is corrosion time (years) and

$k_p$  is the rate of rust production and is related to the rate of rebar loss, which may be expressed in terms of corrosion rate,

$$k_p = 2.59 \times 10^{-6} (1/\alpha) \pi D i_{cor}
 \tag{14}$$

where  $\alpha$  is the ratio of the molecular weight of rust to that of iron,

$D$  is the steel diameter (cm.) and

$i_{cor}$  is the annual mean corrosion rate ( $\mu A/cm^2$ ).



Integrating equation 10, the growth of rust products can be obtained,

$$M_{rust}^2 = 2 \int_0^t 2.59 \times 10^{-6} (1/\alpha) \pi D i_{cor} dt \tag{15}$$

After calculating the corrosion rate from experimental data, the amount of rust products for a certain period of corrosion can be estimated.

**iv) Time to Cracking**

When the amount of corrosion products reaches the critical amount of rust products, the internal expansion stress will exceed the tensile strength of concrete and cause the cracking of the cover concrete. According to equation 11, for a constant corrosion rate, the time to cracking,  $t_{cr}$  can be given as follows:

$$t_{cr} = M_{crit}^2 / 2 [2.59 \times 10^{-6} (1/\alpha) \pi D i_{cor}] \tag{16}$$

where  $M_{crit}$  is the critical amount of corrosion products in kilograms. Since corrosion rate is a function of corrosion time as presented in equation 11, using the numerical method, the time to cracking can be also calculated from equation 16.

Table 6 Based on calculated critical amount of rust products is obtained from equation 12 and the times to cracking is obtained from equation 16. The results are summarized in Table 6. As it can be seen from the table in column 5 and 6, the measured times to cracking are within the predicted values by the model.

**Table 6: Parametric study of predicted and observed times to cracking of the research and the model**

Concrete characteristic strength	Sample series	Rebar diameter(mm)	Cover depth(mm)	Measured corrosion rate mm/year	Time in years Model predicted*	Time in years Measured
25N/mm <sup>2</sup>	100mm diameter x 300mm high	10	140	0.51	0.153-0.319	0.215
	130mm diameter x 300mm high	10	120	0.52	0.186-0.389	0.243
	150mm diameter x 300mm high	10	90	0.53	0.272-0.566	0.302
30N/mm <sup>2</sup>	100mm diameter x 300mm high	10	140	0.31	0.239-0.498	0.441
	130mm diameter x 300mm high	10	120	0.31	0.306-0.638	0.401
	150mm diameter x 300mm high	10	90	0.31	0.374-0.778	0.359
35N/mm <sup>2</sup>	100mm diameter x 300mm high	10	140	0.26	0.285-0.594	0.525
	130mm diameter x 300mm high	10	120	0.26	0.365-0.761	0.486
	150mm diameter x 300mm high	10	90	0.26	0.436-0.908	0.430

\*The model predicted times to cracking were calculated taking  $\alpha_1$  value of 1.8 for (FeO) and 3.75 for (Fe(OH)<sub>2</sub>) for corrosion products. [33]

From Table 6, it can be observed that the measured times to cracking are within the model predicted time.

## 5.0 Conclusions

The following conclusions can be made from this research:

1. The model proposed shows that amount of corrosion products to fill the total interconnected pores around the rebar/concrete interface (Mp) and the amount of corrosion products to generate the critical tensile stress (Ms) constitute the critical mass of corrosion products (M<sub>crit</sub>) to induce cracking of the concrete cover. The critical mass of corrosion products is influenced by the type of corrosion products, the cover to the rebar, the rebar size and the compressive strength of concrete and steel/concrete interface.
2. The time to corrosion model developed here, that is for a maximum crack width of 0.2mm as a specified limit of water structures shows that the time to corrosion cracking of the cover concrete in a chloride contaminated concrete structure is a function of reinforcement cover, concrete compressive strength, corrosion rate and critical mass of the corrosion products. The times to cracking predicted by the model are in good agreement with the observed times to cracking based on this research

## REFERENCES

- [1] United Nations (2015). "Transforming our world: the 2030 Agenda for Sustainable Development," Available from [www.un.org/ga/search/view\\_doc.asp?symbol=A/RES/70/1&Lang=E](http://www.un.org/ga/search/view_doc.asp?symbol=A/RES/70/1&Lang=E).
- [2] Hossein M. S., Keivan K., Alireza Hashemian A., (2010). *A model for the evolution of concrete deterioration due to reinforcement corrosion*. Mathematical and Computer Modelling 52: 1403-1422
- [3] Palanisamy G., (2019). "Corrosion Inhibitors," IntechOpen, DOI: 10.5772/intechopen.80542.
- [4] Mogire P.O., Abwodha S., Mweru J.N., Mangurui G.N., (2018), "The effect of Selected Cement Brands in Kenya on the Critical Penetration Depth of Rust in Reinforced Concrete Water Conveyancing Structures," International Journal of Scientific and Research Publications, 11: 2250-3153.
- [5] Ghods P., Isgor O.B., Bensebaa F., Kingston D., (2012). "Angle-resolved XPS study of carbon steel passivity and chloride-induced depassivation in simulated concrete pore solution," Corros. Sci. 58:159-167.
- [6] ACI Committee 222, "Protection of Metals in Concrete Against Corrosion," ACI 222R-01, American Concrete Institute, Farmington Hills, Michigan, 2001.
- [7] Alonso C, Andrade C, Rodriguez J, Diez J.M., (1998), "Factors controlling cracking of concrete affected by reinforcement corrosion," Mater and Struct 31: 435-441.
- [8] Bazant Z.P., (1979), "Physical model for steel corrosion in concrete sea structures – Application," J Struct Div 105(6): 1155-1166.
- [9] Liu Y, Weyers RE (1998), "Modeling the time-to-corrosion cracking in chloride contaminated reinforced concrete structures," ACI Mater J 95(6): 675-681.
- [10] Li C.Q., Melchers R.E, Zheng J.J., (2006), "Analytical model for corrosion-induced crack width in reinforced concrete structures," ACI Struct J 103(4): 479-487.
- [11] Molina F. J, Alonso C, Andrade C., (1993), "Cover cracking as a function of rebar corrosion: Part 2 – Numerical model," Mater and Struct 26: 532-548.
- [12] Du Y.G., Chan A.H.C., Clark L.A., (2006), "Finite element analysis of the effects of radial expansion of corroded reinforcement," Comp and Struct 84: 917-929.
- [13] Andrade, C., Alonso, C. and Molina, F. J. "Cover cracking as a function of bar corrosion: Part I—Experimental test," Mater. Struct. 26 (1993) 453-464.
- [14] Morinaga S. (1989). "Prediction of Service Lives of Reinforced Concrete Buildings based on Rate of Corrosion of Reinforcing Steel," Special report of the Institute of Technology, Japan, Skimiza Corporation.
- [15] Liu Y., Weyers R.E., (1998). "Modelling the time to corrosion in cracking in chloride contaminated reinforced concrete structures," ACI Mat. J. 95:675-681.
- [16] Bhargava K., Ghosh A.K., Mori Y., Ramanujam S. (2006). "Model for cover cracking due to rebar corrosion in RC structures," Eng. Struct., 28:1093-1109
- [17] Kiani K. (2002). "Study of reinforcement corrosion in RC structures via reproducing kernel particle method," M.Sc. Thesis. Tehran, Sharif University of Technology.
- [18] Andrade C. Alonso C., Molina F.J. (1993). "Cover cracking as a function of rebar corrosion: part 1-experimental test," Mater. Struct., 26:453-464.
- [19] Lundgren K. (2002). "Modeling the effect of corrosion on bond in reinforced concrete," Mag. Concr. Res., 54:165-173.
- [20] Bhargava K., Ghosh A.K., Mori Y., Ramanujam S. (2006). "Analytical model for time to cover cracking in RC structures due to rebar corrosion," Nucl. Eng. Des., 236: 1123-1139.
- [22] Bhargava K., Ghosh A.K., Mori Y., Ramanujam S. (2005). "Modeling of time to corrosion-induced cover cracking in reinforced concrete structures," Cem. Concr. Res., 35: 2203-2218.
- [23] P Mehta P.K., Monteiro P.J.M. (1997). "Concrete Microstructure, Properties and Materials," Indian Concrete Institute, Chennai, India.
- [24] Liu Y., (1996). "Modeling the time to corrosion cracking of the cover concrete in chloride contaminated reinforced concrete structures," Ph.D. Thesis, Blacksburg, Virginia Polytechnic Institute and State University, 1996.
- [25] Muhammad H.R., Khatun S., Uddin S.K.M., Nayeem M.A. (2010). "Effect of Strength and Covering on Concrete Corrosion," European Journal of Scientific Research, 4 (2010) 492-499
- [26] Visalakshi T. (2014). "Corrosion assessment in rebars of reinforced concrete structures using equivalent parameters extracted from piezo-patches," A PhD thesis in Civil engineering in India Institute of Technology, Delhi.
- [27] Kenya Bureau of Standards, KS EAS 18-1:2001-Cement Part 1: Composition, Specification and Conformity Criteria for Common Cements. Kenya Bureau of Standards, Nairobi, 2005.
- [28] Kumbhar, P.D. and Murnal, P.B. (2012), "Assessment of Suitability of Existing Mix Design Methods of Normal Concrete for Designing High Performance Concrete," International Journal of Civil and Structural Engineering, 3:158-167.
- [39] Neville M. (1996). "Properties of Concrete," Pitman Publishing Company, London, UK.
- [30] Neville A.M., Brooks J.J. (2012). "Concrete Technology," Longman, London, UK.
- [31] BS 12, "Specification for Portland cement," BSI Publications, London, 1996.
- [32] Aperador W., Vera R., Carvajal A.M., (2012). "Evaluation of the cathodic protection applied to steel embedded in the ASS using the finite element method" International Journal of Electrochemical Science, 7(2012)12870. 5
- [33] Bhargava, K., Ghosh, A. K., Mori, Y., Ramanujam, S. (2005). "Modeling of time to corrosion-induced cover cracking in reinforced concrete structures." Cement and Concrete Research, 35: 2203-2218.



AUTHORS

**First Author** – Mogire Philip, PhD Student, Department of Civil and Construction Engineering, University of Nairobi, Kenya, philosiemo@yahoo.com

**Second Author** – Dr. John Mwero, Senior Lecturer, Department of Civil and Construction Engineering, University of Nairobi, Kenya, johnmwero1@gmail.com.

**Third Author** – Prof. Silvester Abuodha, Associate Professor, Department of Civil and Construction Engineering, University of Nairobi, Kenya, sochieng@yahoo.com

**Fourth Author** – Prof. Geoffrey Mang'uriu, Professor, Department of Civil, Construction and Environmental Engineering, Jomo Kenyatta University of Agriculture & Technology, gmanguriu@yahoo.co.uk

**Correspondence Author** – Mogire Philip , philosiemo@yahoo.com, +254 734 967 989

# Effect of Selected Commercially Available Corrosion Inhibitors in Kenya on Bond Strength of Reinforced Concrete.

Philip Mogire<sup>1\*</sup>, Silvester Abuodha<sup>2</sup>, John Mwero<sup>3</sup>, Geoffrey Mang'uriu<sup>4</sup>

Department of Civil and Construction Engineering,  
University of Nairobi, Kenya<sup>1,2,3</sup>

Department of Civil, Construction and Environmental Engineering,  
Jomo Kenyatta University of Agriculture & Technology, Nairobi, Kenya<sup>4</sup>

Corresponding author: 1\*



**ABSTRACT**— Corrosion of reinforced concrete water structures generates tensile stress within the concrete and reinforcement interface influencing the service life of structures. This research investigated the influence of selected commercially available corrosion inhibitors in Kenya in combination of selected brands of ordinary Portland cement on the bond behavior of reinforced concrete members. To achieve the desired objective, samples in concrete of characteristic strength of 25N/mm<sup>2</sup>, 9 cylinders each of 150mm diameter x 300mm long each for four corrosion inhibitors and one control experiment were cast with an embedded rebar of 10mm diameter and 110mm long. For each series 9 cubes of 150mm x 150mm and 9 cylinders of 150mm diameter x 300mm long were cast for compressive strength and split tensile strength test respectively. After 24 hours the cast specimens were demolded and immersed in curing tanks for 27 days and tested for bond strength. The physical and chemical properties of the materials were investigated for compliance to relevant applicable British and Kenyan standards for conformity to acceptable criteria. The concrete materials were batched by weight and mixed by a lab electric pan concrete mixer in batches of 0.009 m<sup>3</sup>. The concrete batches were tested for consistency by the slump and compaction factor tests. The result show that bond strength increased with all selected corrosion inhibitors in combination with each respective cement brand. A bond strength model that correlated significantly with Orangun et al and Stanish et al model has been proposed.

**KEYWORDS:** Reinforced concrete, Bond strength, Corrosion inhibitors

## 1. INTRODUCTION

Reinforced concrete is among the materials widely used in construction of water conveyance structures. Steel as a constituent material in reinforced concrete provides tensile strength while concrete, an alkalinity material provides a physical barrier, that protects the steel from corrosion. The alkalinity of the concrete with pH values of about 12 to 14 [1], provides the conditions for the formation of a passive film protecting the steel reinforcement from corrosion [2]. The protection provided by the concrete is not sufficient because the concrete is porous thus allowing the penetration of aggressive agents, such as chloride ions that lead to the corrosion of the reinforcement that subsequently affects the bond strength. The ultimate limit state design of reinforced concrete is based on the fundamental assumption that there exists an effective bond linking concrete and steel when the structural element is loaded and the behavior of the composite material depends on this bond. The strength capacity of concrete and steel is directly related with their bond strength. For a reinforced concrete member to exhibit its full design strength there must be no slipping between concrete and the steel reinforcement. The reinforcing steel must resist the tension force, and the change in

tension force in the bar is transmitted to the concrete by the bond stress. The essence of bonding in reinforced concrete member is the mechanical interlocking between concrete and reinforcement as well as the deformity characteristic in the longitudinal and transverse ribs of the reinforcement [3]. The bond of reinforcing bars to the surrounding concrete influences the behavior of reinforced concrete structures in many ways [4]. It is a major factor for the maximum load carrying capacity of reinforced concrete elements since it affects the anchorage of bars and the strength of lap slices. The deformation capacity of the reinforced concrete elements, and hence the redistribution capacity in statically indeterminate structures, is directly influenced by the bond. Consequently, a fundamental issue for reinforced concrete structures is the bond between the reinforcing bars and the concrete [5]. One drawback in reinforced concrete bond research is the absence of a generalized method for determining bond strength [6]. This leads comparisons between various researches and test results on bond difficult. Most investigators have used pull-out tests that are commonly adopted in reinforced concrete bond studies [7–10]. Use of corrosion inhibitors is among the strategies available to control reinforced concrete deterioration due to corrosion and hence the service life of the structures. The efficiency of commercially available corrosion inhibitors in Kenya varies hence the need to identify their effect on bond strength and other concrete properties. This research presents the effect of selected corrosion inhibitors commercially available in Kenya on bond strength of reinforced concrete. The validity, accuracy, and efficiency of the proposed results are established by comparing the results of the present study with the works of other researchers. The results of the analysis presented in this research indicate that all the selected corrosion inhibitors increased the bond strength of reinforced concrete.

## **2. BACKGROUND**

When reinforcing steel corrodes a decrease in load-carrying capacity of reinforced concrete components occurs through decrease of the cross-sectional area of the steel bars as the effect of corrosion increases, and the severity of reinforcement corrosion can have a significant effect on flexural strength, deformational behavior, ductility and bond. The effect of corrosion on the bond at the interface of the steel rebar and the concrete is affected and consequently the composite action of reinforced concrete. The expansive nature of the corrosion products that build up at the interface exerts a radial pressure on the surrounding concrete, which leads to cracking and spalling. Spalling will reduce the bond by removing the concrete cover, which in turn will reduce the confinement of the steel rebar and expose the concrete to further corrosion activity. Corrosion also causes the ribs on the rebar to deteriorate, which changes the surface area of the bar and decreases bond strength. According to Shetty et al (2011) [11] bond strength is attributed to chemical adhesion of the concrete to the steel, friction at the bar-concrete interface from mill-scale, rust and other surface irregularities, bearing against the rib faces and shear acting along a cylindrical concrete surface between adjacent ribs. The chemical adhesion results from the weak bonds between the steel and the hardened hydrated cement paste of the concrete, which is lost when the applied load on the steel bar is increased. Once the embedded bar begins to slip, the friction contributes to the bond strength at the concrete-steel interface. Bond strength is primarily derived from the bearing and mechanical interlock of the ribs on the surface of the steel bar with the concrete. Owing to the angle of the ribs, a horizontal force develops between the concrete and the rib face angle, which exerts bursting forces that tend to split the concrete. The thickness of the concrete cover and the confinement of the reinforcement now limit the magnitude of the failure load. Chung et al (2004) [12] found that the level of corrosion had a significant impact on the flexural crack pattern of reinforced concrete slabs subjected to four-point loading. From their study, the reinforced concrete slabs that were tested at lower corrosion levels displayed more flexural cracks than the slabs subjected to severe corrosion. Although a greater number of cracks formed at low levels of corrosion, the cracks were distributed along the length of the slab with small crack widths and sufficient warning of impending failure. At higher corrosion levels a smaller amount of localized cracks was produced

that had much larger crack widths and propagated at a rapid pace. Thus, it can be said that a loss in bond due to corrosion will result in wider, more localized cracks, which makes the concrete more susceptible to moisture ingress and increases the rate of deterioration of the structure. Various researchers have proposed various empirical equations to calculate bond strength as a function of corrosion level. Stanish et al (1999) [13] derived equation 1 by normalizing the estimated bond strength by the square root of the 28-day compressive strength,  $f'_c$ , and performing a linear regression analysis with the available data points. When no corrosion is present, their relation corresponds to the estimated value of 0.66 given by ACI 408.1R-90. This equation indicates that there is no increase in bond strength at low corrosion levels and any corrosion would immediately result in a decrease in bond strength.

$$\frac{u_b}{\sqrt{f'_c}} = 0.77 - 0.027C_0 \quad 1)$$

Where

$u_b$  is bond strength in  $N/mm^2$

$f'_c$  is the concrete cylinder strength (assumed to be  $0.8 \cdot f_{cu}$ ) in  $N/mm^2$

$f_{cu}$  is the concrete compressive cube strength in  $N/mm^2$

Cabrera (1996) [13] derived equation 2 for normal Portland cement concrete and only applies to corrosion levels greater than approximately 0.9%.

$$u_b = 23.478 - 1.313C_0 \quad 2)$$

Lee *et al* (2002) [15] proposed equation 3 and 4 by expressing bond properties of reinforcement as a function of corrosion percentage. Neither of these equations makes provision for the fact that bond strength seems to increase at low corrosion levels (for less than 2% reduction in reinforcing bar mass).

$$u_b = 5.21e^{-0.0561C_0} \text{ for } C_0 \geq C_c \quad 3)$$

$$u_b = 0.34f_{cu} - 1.93 \text{ for } C_0 \geq C_c \quad 4)$$

where

$C_0$  is corrosion percentage

$C_c$  is corrosion percentage at cracking.

Orangunet al. [16] proposed the following formula for bond strength:

$$\tau_u = 0.083045 \sqrt{f'_c} \left[ 1.2 + 3 \left( \frac{c}{d_b} \right) + 50 \left( \frac{d_b}{L_D} \right) \right] \quad 5)$$

Where  $\tau_u$  is the bond strength in  $N/mm^2$

$c$  is the minimum concrete cover in mm

$f'_c$  is the cylinder compressive strength of concrete in  $N/mm^2$

$d_b$  is the bar diameter in mm and

$l_d$  is the development length in mm

This research is aimed at establishing whether a selected available commercial corrosion inhibitors will have a detrimental effect on bond strength and hence the service life of reinforced concrete water conveyancing structures.

### 3. Methodology

This research was conducted at the University of Nairobi Concrete and Materials lab where the physical properties of the materials, sample preparation and testing was done. The chemical properties of the ordinary Portland cement and chloride content was done in State Department of Infrastructure in the Ministry of Transport, Infrastructure, Housing and Urban Development of the Government of Kenya.

#### 3.1 Concrete samples

The constituent materials for preparing test samples consisted of Ordinary Portland cement (42.5N/mm<sup>2</sup>), clean river sand, and 20mm maximum size coarse aggregate and portable water.

### 3.1.1 Cement

The chemical composition of the cement used in this research was tested. Available cements in Kenya are manufactured in accordance to KS EAS 18-1: 2001, an adoption of the European Norm EN 197 cement standards [16]. The cements locally available are produced for specific uses [17]. The Cement used for this research was ordinary Portland cement type 42.5N sourced from one wholesaler.

### 3.1.2. Other concrete materials

Table 1 shows the description and source of other materials of concrete used in the research.

**Table 1.** Details of materials used in the research

SN	Description	Source	Remark
1.	Fine aggregates	Stockpile vender sourced from Machakos River	This was washed and oven dried before use.
2	Coarse aggregates	Kenya builders quarry	5-20mm uniformly graded at the source
3.	10mm ribbed bars	Local manufacturer	Factory cut to 400mm
4.	Mixing water	Portable water in the Lab	

### 3.2.2. Concrete Mix Design

The concrete used for this works was of characteristic strength of 25N/mm<sup>2</sup> designed in accordance with the DOE method [18-19].

### 3.2.3 Test on hardened concrete

To access the effect of selected corrosion inhibitors of the properties of concrete, a minimum of three specimens were cast for testing at a time for any test and the average value obtained by testing the specimens considered. A total number of 135 cubes of size 150mm for compressive strength test, 135 cylinders of 150mm diameter and 300mm long for split tensile strength test, 135 numbers of 150mm diameter and 300mm long concrete cylinders with centrally placed steel rod of diameter 10 mm and length 1010mm for bond strength. Table 2 shows the details of the specimens cast for each test.

**Table 2:** Number of specimen's cast

Identification	Cubes for compression test	Cylinders for split tensile test	Cylinders for bond strength
Control Concrete	27	27	27
Fly ash concrete	27	27	27
Concrete with Inhibitor X	27	27	27
Concrete with Inhibitor Y	27	27	27
Concrete with Inhibitor Z	27	27	27

Inhibitor X is an admixture with 2-dimethylaminoethanol, inhibitor Y is a 30% by mass calcium nitrite [Ca(NO<sub>2</sub>)<sub>2</sub>] based while inhibitor Z is 30% by mass calcium nitrate [Ca(NO<sub>3</sub>)<sub>2</sub>] based.

### 3.2.4 Testing Methodology for bond strength

Before pouring the concrete in the moulds of pull out test, the internal surfaces of these moulds were oiled and the sides tightly secured. The length of 10mm diameter reinforcing steel bars was 1010 mm factory cut. Fresh concrete was mixed by a concrete pan mixer and poured into the mould in five layers and vibrated by a vibrating table in 60 seconds. After 24 hours, the moulds were removed and the concrete specimens cured in a water tank for 27 days. Three brands of cement were used and concrete cubes and cylinders for each brand of cement were cast in 9 samples, and the compressive strength, split tensile strength and pull out strength was tested at 7, 14 and 27 days. All the tests listed below were conducted;

- a) Tests on fresh concrete
  - i) Slump test
  - ii) Compaction Factor test
- b) Strength tests
  - i) Compressive strength test
  - ii) Split tensile strength test
  - iii) Bond strength test

### 3.2.5 Testing of samples

- a) Compression test

The compressive strength of concrete was investigated at 7, 14 and 27 days using a digital Universal Testing Machine with a loading capacity of 2000 KN shown in figure 3.1 in accordance to BS EN 12390-3:2009.



**Figure 3.1:** a) Digital compression machine during cube testing for compressive strength and b) a sample during compression testing

- b) Split tensile test

A hydraulic Universal Testing machine as shown in figure 3.2 a) and b) was used to test the cylinders for tensile strength.



**Figure 3.2:** Sample during split tensile test

- c) Pull-out testing

A manually operated hydraulic pump with a load cell of 100 kN connected to the load detector shown in figure 3.3 was used to perform the bond tests. The load was applied with a rate of 2 kN/sec and distributed on the specimen surface by a square steel plate with size of 20 cm and a hole at the center. All



the specimens were tested at age of 28 days.



a)

Sample confining apparatus

b) Tensile load detection equipment

c) Current Transformer

**Figure 3.3 a)- c) Pull out Testing equipment used in the research**

### 3.2.6 Bond stress calculation

Bond stress is calculated as average stress between the reinforcing bar and the surrounding concrete along the embedded length of the bar. In general, the bond stress corresponding to the maximum pull out load can be regarded as the bond strength or the ultimate bond. The criterion of ultimate bond strength is characterized by its clear definition and simplicity in bond strength interpretation. For uniform bond, the bond stress  $S$  can be expressed as:

$$S = \frac{P_{\max}}{\pi \times L \times d} \quad 5)$$

Where  $P_{\max}$  = maximum pull out load

$d$  = diameter of the bar

$L$  = Embedded bar length

## 4.0 Results of the material properties

### 4.1 Properties of aggregates

Various tests were carried out on the aggregates to determine their suitability for the research. Water soluble chloride ions percent were found to be zero in fine aggregates, 0.002 % in coarse aggregates all less than 0.03% acceptable in compliance with BS EN 12620: 2002. Chloride ions are the most aggressive and widest spread corrosive ion since it contributes to corrosion of steel reinforcement [19] by destroying the passivity condition when they are adsorbed. Limiting the water soluble chloride ions in the concrete constituents reduces the total amount of free chloride ions responsible for steel reinforcement corrosion [20].

**Table 3:** Physical properties of aggregates used in the study

Material	Specific gravity	Water Absorption %	Silt content %	Max Size
Fine aggregates	2.6	1.8	7.4	4.0
Coarse aggregates	2.6	0.3	0	20.0

The specific gravity of all the aggregates are within the limits of 2.4 – 3.0 stated in literature [21-24] and they influence the mix design of the concrete. The water absorption of the fine aggregates is within the limits of 1% – 3% stated in literature and British Standards [25-28] and therefore a low water absorption hence suitable for concrete works. The very low water absorption in the coarse aggregates need was taken

into consideration in the mix design. ASTM C117[29] give an allowable limit of 10% for silt and clay content in fine aggregates for concrete production while BS 882 give a limit of 4% [30]. As a thumb rule according to [31], the total amount of deleterious materials in aggregates should not exceed 5%. The silt content in the fine aggregate was more than the allowable percentage of silt content, it was washed and oven dried before use.

**Table 4:** Mechanical properties carried on coarse aggregates.

Test	Size of aggregates mm	Crushing value %	Impact Value %	Flakiness index %	Loss Angeles Abrasion Value %
Result	5-20	18	8	35	20

The mechanical properties of aggregates depend on the properties of the parent rock. The Aggregates Impact Value gives a measure of resistance to load 30% as value stated in literature and British Standards [32-33] and specified in [34]. The Aggregate Crushing Value provides resistance of the aggregates to the applied loads and for this research it was within the acceptable limit of 30% for wearing courses.

#### 4.2 Chemical Properties of selected OPC Brands in Kenya used for the research

Table 5 shows the results of the chemical analysis of the ordinary cement brands used in this research

**Table 5** Result of Chemical composition the Cement used.

SN	Test	Result			KS EAS 18-1: 2001 Requirement
		Cem A	Cem B	Cem C	
1.	CaO%	59.86	59.11	58.82	Sum $\geq$ 50
2.	SiO <sub>2</sub> %	16.56	21.56	19.47	
3.	SO <sub>3</sub> %	2.02	2.78	2.03	$\leq$ 3.5
4.	MgO%	1.76	1.04	0.57	$\leq$ 5
5.	K <sub>2</sub> O%	0.027	0.051	-	
6.	Fe <sub>2</sub> O <sub>3</sub> %	2.32	3.48	1.44	
7.	Al <sub>2</sub> O <sub>3</sub>	7.61	8.09	6.85	3-8
8.	Na <sub>2</sub> O <sub>3</sub> %	0.054	0.018		
9.	LOI%	0.11	0.10	4.75	$\leq$ 5
10.	Cl%	0.012	0.016	0.014	$\leq$ 0.1
11.	IR%	2.20	0.55	1.96	$\leq$ 5

##### a) *Effect of sum of lime (CaO) and silicon dioxide (SiO<sub>2</sub>) on bond strength*

From table 5 there is a notable variation in the amounts of CaO, SiO<sub>2</sub> and Insoluble Residue. Cem A has the highest amount of CaO (59.86%), Cem B has the highest SiO<sub>2</sub> (21.56%) and Cem A has the highest Insoluble residue (2.20%). The sum of lime (CaO) and silicon dioxide (SiO<sub>2</sub>) obtained in the chemical analysis of ordinary Portland cement should not be less than 50% [35]. All cement samples used for this work satisfied this requirement. Cement sample B has a CaO + SiO<sub>2</sub> value of 80.67 % and produced the highest compressive strength of 44.89 N/mm<sup>2</sup>. This is consistent with the known fact that both CaO and SiO<sub>2</sub> give compressive strength and hence bond strength to concrete though SiO<sub>2</sub> has to be limited relative to CaO in order not to negatively affect setting time.

##### b) *Effect of CaO/SiO<sub>2</sub> on bond strength.*



The ratio of lime (CaO) to silicon dioxide (SiO<sub>2</sub>) contents in ordinary Portland cement should be greater than 2. The restriction on the ratio of lime to silicon dioxide [35] is to ensure that the quantity of silicon dioxide is considerably lower than that of lime so that the setting of concrete is not inhibited. All the cement samples investigated satisfied this requirement. The lime-silicon dioxide ratio for cement samples A, B, and C were 3.61, 2.71 and 3.0 respectively. The results also indicated that the higher the ratio of (CaO/SiO<sub>2</sub>) of a cement sample the higher the compressive strength of concrete which can be produced from it and the higher the bond strength.

**c) *Effect of MgO on bond strength.***

The quantity of magnesium oxide (MgO) in ordinary Portland cement should not exceed 5% [34]. All the cement samples satisfied this requirement with 1.76%, 1.04% and 0.57% for cement samples A, B and C respectively. Magnesium oxide contributes to colour of cement and hardness of the resulting concrete. Cement sample A with the highest MgO content of 1.76 % was expected to produce concrete with the highest compressive strength since MgO contributes to hardness of concrete and highest bond strength. If the quantity of MgO is in excess of 5 percent, cracks will appear in concrete and which may reduce the bond strength by reducing the effective length.

**d) *Effect of SO<sub>3</sub> on bond strength***

The quantity of sulphur trioxide (SO<sub>3</sub>) content in ordinary Portland cement should be less than 3.5 %. All the samples satisfied this requirement.

**e) *Effect of Chloride Content on bond strength***

The chloride content in ordinary Portland cement should be less than 0.4%. All the cement samples in this work satisfied this requirement.

**f) *Effect of Al<sub>2</sub>O<sub>3</sub>***

Aluminium oxide (Al<sub>2</sub>O<sub>3</sub>) aids the quick setting of cement paste. Cement sample B contained the highest quantity of 8.09 % of Al<sub>2</sub>O<sub>3</sub> resulting in the fastest initial set of the cement paste

**g) *Effect of Fe<sub>2</sub>O<sub>3</sub>***

Iron oxide (Fe<sub>2</sub>O<sub>3</sub>) contributes to cement colour and helps in the fusion of the different ingredients. The Fe<sub>2</sub>O<sub>3</sub> contents for the different cement samples are 2.32, 3.48 and 1.4493 for cement samples A, B, and C respectively as shown in Table 5.

**h) *Effect of Residues***

British standards consider Na<sub>2</sub>O, K<sub>2</sub>O, TiO<sub>2</sub> and P<sub>2</sub>O<sub>5</sub> in ordinary Portland cement as residues and limit the sum of all of them to 5%. All the cement samples investigated satisfied this requirement with cement samples A, B and C having total residue contents of 0.55, 2.2 and 1.96% respectively. If in excess of 5% efflorescence and unsightly cracking will occur and reduce the bond strength.

### **4.3 Composition of corrosion inhibitors used in the research**

**a) *Inhibitor Y and Inhibitor Z***

Both inhibitors are anodic and were in liquid form but inhibitor Y was a calcium nitrite [Ca(NO<sub>2</sub>)<sub>2</sub>] based while inhibitor Z was calcium nitrate [Ca(NO<sub>3</sub>)<sub>2</sub>] based. The two inhibitors increase the compressive strength of concrete with no susceptibility to alkali-aggregate reaction (AAR) [35]. The inhibitors act as accelerators of cement hydration and as a passivating inhibitor due to their oxidizing properties, which

stabilize the passive film [35].

**b) Fly Ash**

Table 6 shows the result of the chemical analysis of fly ash that was used in this study. Fly ash acts as an inhibitor by reducing permeability and increasing chloride resistance. From the chemical analysis result the % by volume of CaO in the fly ash used is 5.64% which is less than 8% composition by volume and this is fly ash class F as per ASTM C618. Also the sum of SiO<sub>2</sub>, Al<sub>2</sub>O<sub>3</sub> and Fe<sub>2</sub>O<sub>3</sub> by composition in the sample is 71.21% which is greater than 70% as required by ASTM C618 standard for class F fly ash. The fly ash was used in the concrete mix by replacing ordinary Portland cement by 25%. This percentage has the capacity of controlling damaging alkali-silica reaction (ASR) in concrete and the effect has been ascribed to the reduced concentration of alkali hydroxides in the pore solution.

**Table 6** shows the chemical analysis of the fly ash used

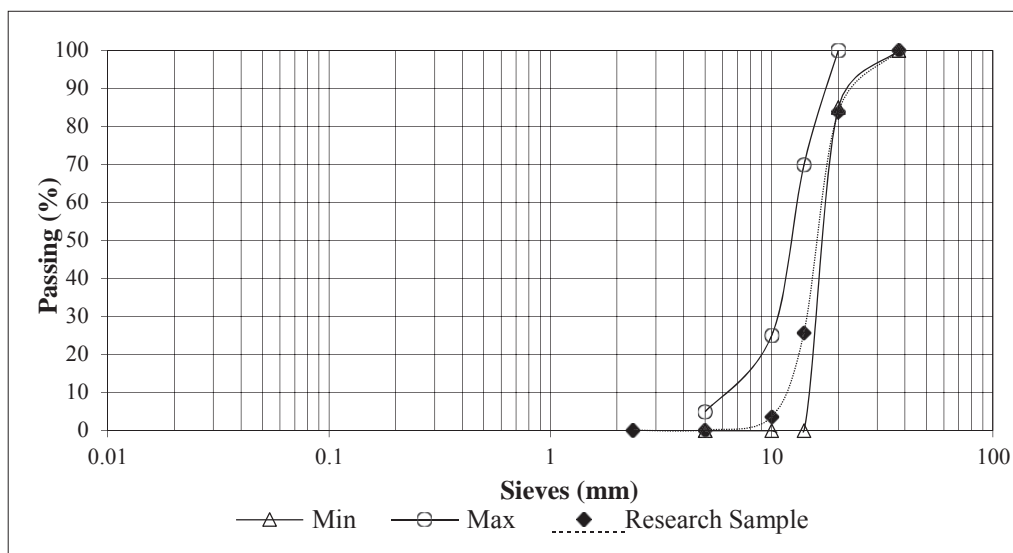
<b>Parameter</b>	<b>Result</b>	<b>Test Standard</b>
SiO <sub>3</sub>	47.18 %	ASTM C618
Al <sub>2</sub> O <sub>3</sub>	19.87%	
Fe <sub>2</sub> O <sub>3</sub>	10.61%	
UBC	0.99%	
Na <sub>2</sub> O	0.86%	
Fineness(Residue on 45 Micron)	8.69%	
Moisture content	0.07%	
MgO	3.79%	
Cl	0.047%	
Bulk Density	1.03 Gm/cc	
TiO <sub>2</sub>	1.01	
CaO	5.64	
K <sub>2</sub> O	1.17	
P <sub>2</sub> O <sub>5</sub>	0.243	

**c) Inhibitor X**

Is an Amino alcohols based corrosion inhibitor in liquid form?

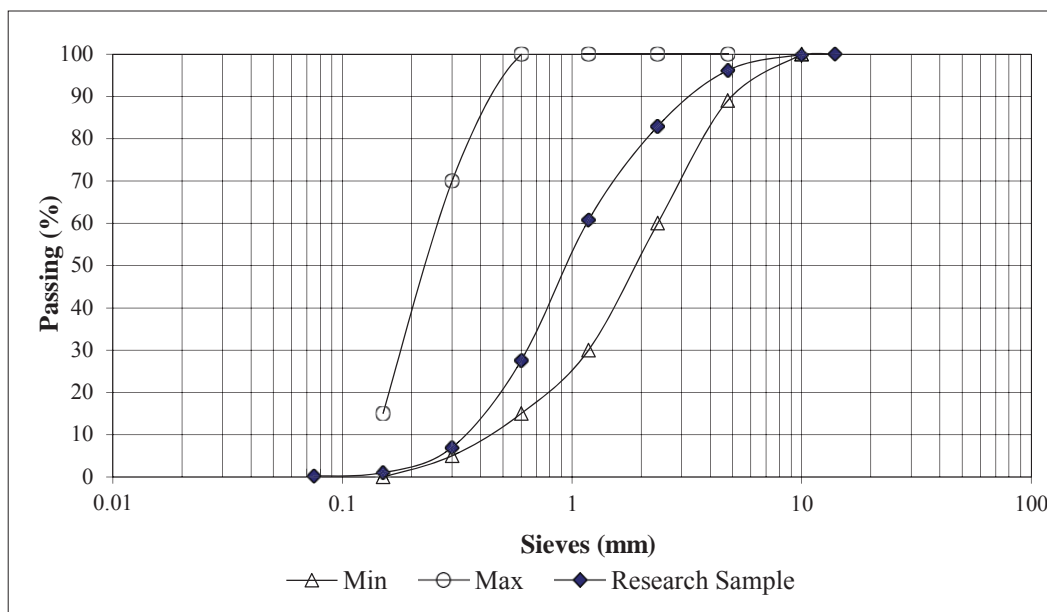
**4.4 Gradation of Coarse and Fine aggregates**

Particle size distribution analysis on a representative sample as shown on graph 1 of the course aggregates for the work was carried out to obtain the proportions by weight of the different sizes of coarse aggregates present. The sample is well graded with a maximum aggregate size was 20mm.



**Graph 1** Gradation of Coarse aggregates

Particle size distribution analysis as shown on graph 2 on a representative sample of the fine aggregates for the research was carried out to obtain the proportions by weight of the different sizes of fine particles present according to BS 812-103 and BS 882. The proportions were expressed as percentages by weight passing various sieve sizes conforming to BS 410. As shown in graph 1 the coarse aggregates were well graded and expected to give a well interlocked composite concrete mix.



**Graph 2:** Gradation of fine aggregates

**4.5 Results of fresh concrete tests**

Table 7 shows the result of fresh concrete tests

**Table 7** Results of fresh concrete test

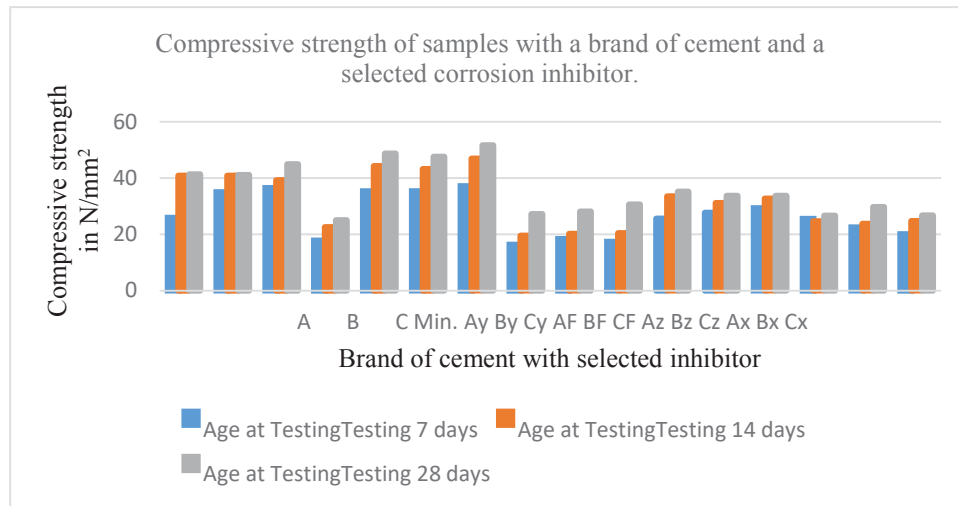
Mix with and without inhibitor	Cement Type	w/c ratio	Slump(mm)	Compaction Factor
--------------------------------	-------------	-----------	-----------	-------------------

Control-No inhibitor	A	0.5	73.3	0.97
	B	0.5	68	0.96
	C	0.5	93	0.95
Inhibitor Y	A	0.5	60	0.95
	B	0.5	63	0.93
	C	0.5	64	0.94
Fly Ash	A	0.5	55	0.93
	B	0.5	40	0.94
	C	0.5	45	0.97
Inhibitor Z	A	0.5	66	0.95
	B	0.5	65	0.95
	C	0.5	66	0.92
Inhibitor X	A	0.5	60	0.96
	B	0.5	65	0.95
	C	0.5	64	0.96

From the results of table 7, at the same water cement ratio fly ash had the lowest slump with all cement brands and thus a reduced workability. Fly ash has spherical shaped particles that act as miniature ball bearings within the concrete mix and require less water for a lubricant effect.

#### 4.6 Results of hardened concrete

Bar chart 1-3 shows comparative relationship of the hardened properties of concrete with selected inhibitors.



**Bar Chart 1** Compressive strength in N/mm<sup>2</sup> of samples with a brand of cement and a selected corrosion inhibitor at 7,14 and 28 days

From bar chart 1, it can be noted that the corrosion inhibitor with 30% calcium nitrite in combination with selected cement brands had the highest increase in compressive strength while all the other inhibitors. The corrosion inhibitors influence in the compressive strength of concrete is most likely caused by their reaction with water and cement during the reaction of cement hydration. The compressive strength of concrete has an influence on the bond strength and their relationship is critical in bond strength modelling.

Graph 4 shows the failure mode during split tensile testing while bar chart 2 shows the relationship between the split tensile strength and the corrosion inhibitor in combination with a selected brand of cement.

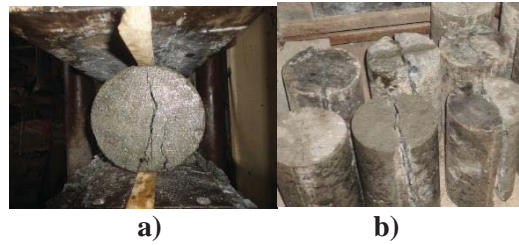
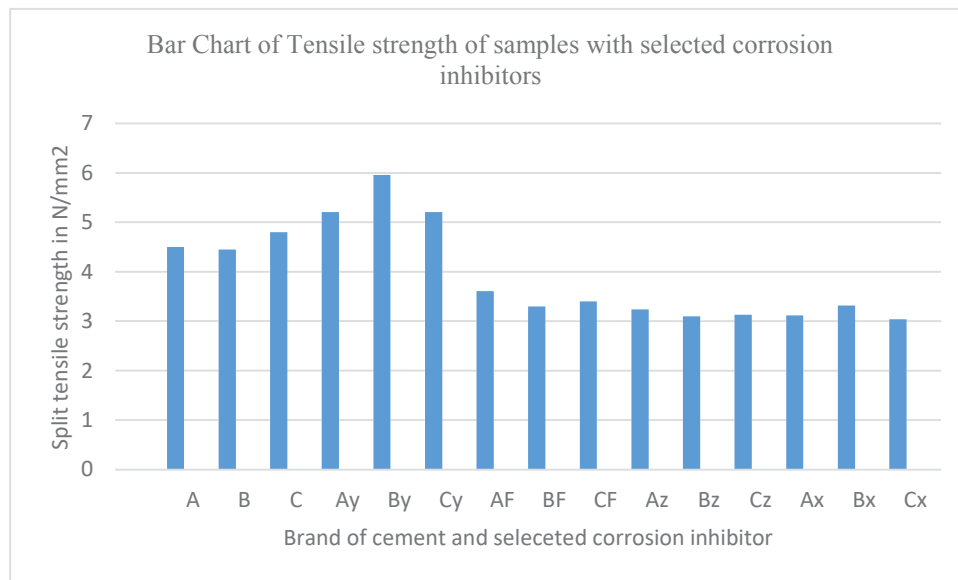
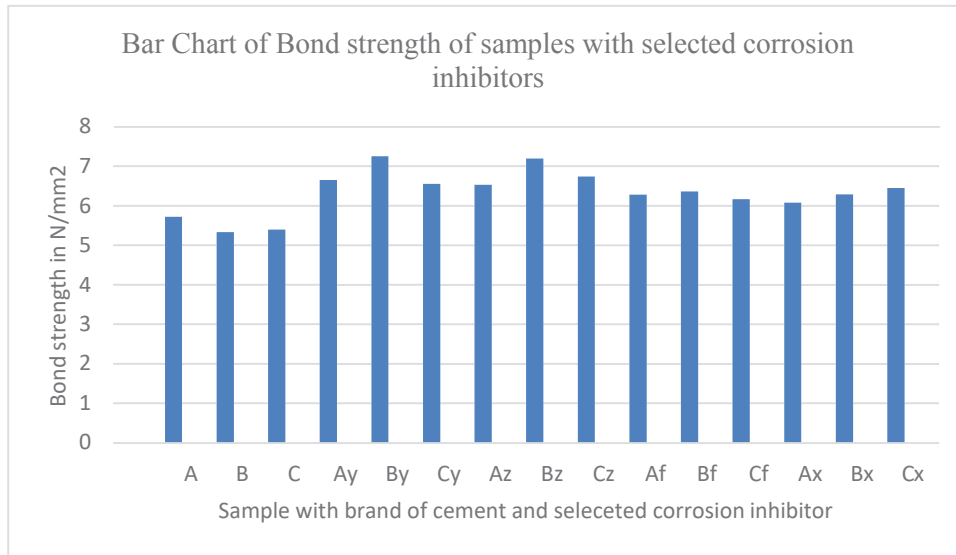


**Figure 4:** a) and b) Failure mode of the samples during split tensile test.



**Bar Chart 2:** Split tensile strength in N/mm<sup>2</sup> for samples with a brand of cement and a selected corrosion inhibitor

From bar chart 2, it can be noted that the corrosion inhibitor with 30% calcium nitrite in combination with selected cement brands had an increased split tensile strength and the converse is true for all the other corrosion inhibitors. The corrosion inhibitors influence in the split tensile strength of concrete is most likely caused by their reaction with water and cement during the reaction of cement hydration. The split tensile strength result correlation with results of existing models gives a view of the expected bond strength results.



**Bar Chart 3:** Bond strength for samples with a brand of cement and a selected corrosion inhibitor

From bar chart 3, all corrosion inhibitors in combination with the respective cement brand selected increased the bond strength with use of inhibitor x giving the lowest result. The corrosion inhibitors increase in bond strength of concrete is most likely caused by their reaction with water and cement during the reaction of cement hydration thus affecting the compressive strength. Most bond strength models have based their result on compressive strength and hence the need for a parametric study of the result of this research with the models of other authors.

#### 4.7 Parametric study of the results

Table 8 gives a comparative result of the split tensile strength from works of other authors

**Table 8:** Comparative study of results of hardened concrete.

Selected inhibitor	Cement Brand	Bond strength	Compressive strength (N/mm²) at 28 days( $f_{ck}$ )	Split tensile strength in N/mm²						
				Measure Value	Lavanya & Jegan (2015) $f_{t1}=0.249f_{ck}^{0.772}$	ACI Committee 318(2014) $f_{t2}=0.56f_{ck}^{0.5}$	Anoglu et al (2006) $f_{t3}=0.387f_{ck}^{0.63}$	CEB-FIB (1991) $f_{t4}=0.3f_{ck}^{0.6}$	Gardner (1990) $f_{t5}=0.33f_{ck}^{0.66}$	
No Inhibitor	Cem A	5.72	41.29	4.50	4.40	3.60	4.03	3.50	3.95	
	Cem B	5.33	41.09	4.45	4.39	3.59	4.02	3.48	3.93	
	Cem C	5.40	44.89	4.80	4.70	3.75	4.25	3.69	4.17	
Inhibitor Y	Cem A	6.65	48.7	5.21	5.00	3.91	4.48	3.90	4.40	
	Cem B	7.25	47.5	5.96	4.90	3.86	4.41	3.83	4.33	
	Cem C	6.56	51.6	5.21	5.23	4.02	4.64	4.05	4.58	
Inhibitor Z	Cem A	6.53	35.2	3.61	3.89	3.32	3.65	3.15	3.55	
	Cem B	7.20	33.7	3.30	3.76	3.25	3.55	3.06	3.45	
	Cem C	6.74	33.69	3.40	3.76	3.25	3.55	3.06	3.45	
Fly Ash	Cem A	6.28	27.27	3.24	3.20	2.92	6.65	2.66	3.00	

	Cem B	6.36	28.13	3.10	3.27	2.97	3.17	2.71	3.06
	Cem C	6.17	30.6	3.13	2.94	3.10	3.34	2.87	3.23
Inhibitor X	Cem A	6.08	26.6	3.12	3.13	2.89	3.06	2.62	2.94
	Cem B	6.29	29.7	3.32	3.41	3.05	3.28	2.81	3.17
	Cem C	6.45	26.7	3.04	3.14	2.89	3.06	2.62	2.95

**Table 9** Correlations of Result of Split tensile strength of this work with results of other authors.

		This work	Lavanya & Jegan(2015)	ACI Committee 318(2014)	Anoglu et al(2006)	CEB-FIB(1991)	Gardner(1990)
This work	Pearson Correlation	1	.945**	.947**	.369	.948**	.948**
	Sig. (2-tailed)		.000	.000	.176	.000	.000
Lavanya & Jegan(2015)	Pearson Correlation	.945**	1	.982**	.330	.983**	.983**
	Sig. (2-tailed)	.000		.000	.230	.000	.000
ACI Committee 318(2014)	Pearson Correlation	.947**	.982**	1	.302	1.000**	1.000**
	Sig. (2-tailed)	.000	.000		.274	.000	.000
Anoglu et al(2006)	Pearson Correlation	.369	.330	.302	1	.308	.310
	Sig. (2-tailed)	.176	.230	.274		.264	.261
CEB-FIB(1991)	Pearson Correlation	.948**	.983**	1.000**	.308	1	1.000**
	Sig. (2-tailed)	.000	.000	.000	.264		.000
Gardner (1990)	Pearson Correlation	.948**	.983**	1.000**	.310	1.000**	1
	Sig. (2-tailed)	.000	.000	.000	.261	.000	

\*\* . Correlation is significant at the 0.01 level (2-tailed).

From table 8 and 9

- It can be observed that other than their primary role of corrosion inhibiting, all the inhibitors improved the bond strength of the reinforced concrete.
- The split tensile strength results of this work significantly correlate with results of other authors. Table 10 shows a parametric study of bond stress result of this work with result of other authors.

**Table 10:** Parametric study of bond strength of this work with other authors.

Selected inhibitor	Cement Brand	Bond Strength (N/mm <sup>2</sup> )	Orangun et al(Eq.5)	Bond Strength(N/mm <sup>2</sup> ) Stanish <i>et al</i> (1999) $u_b=[0.77 - 0.027C_o]\sqrt{0.8f_{cu}}$
No Inhibitor	Cem A	5.72	3.20	4.43
	Cem B	5.33	3.19	4.41
	Cem C	5.40	3.34	4.61
Inhibitor Y	Cem A	6.65	3.45	4.81
	Cem B	7.25	3.43	4.75
	Cem C	6.56	3.56	4.94
Inhibitor	Cem A	6.53	2.95	4.09





Z	Cem B	7.20	2.89	4.00
	Cem C	6.74	2.89	4.00
Fly Ash	Cem A	6.28	2.60	3.60
	Cem B	6.36	2.64	3.65
	Cem C	6.17	2.76	3.81
Inhibitor X	Cem A	6.08	2.66	3.55
	Cem B	6.29	2.72	3.75
	Cem C	6.45	2.57	3.55

Table 11 shows statistical correlation of the bond strength results.

**Table 11** Correlations of results of this work with results of other researche

		This work	Orangun et al	Stanish <i>et al</i>
This work	Pearson Correlation	1	.000	.012
	Sig. (2-tailed)		.999	.967
	N	15	15	15
Orangun et al	Pearson Correlation	.000	1	.998**
	Sig. (2-tailed)	.999		.000
	N	15	15	15
Stanish <i>et al</i>	Pearson Correlation	.012	.998**	1
	Sig. (2-tailed)	.967	.000	
	N	15	15	15

\*\* . Correlation is significant at the 0.01 level (2-tailed)

From results of table 11, the results of this work have no significant correlation with the results of Orangun et al and Stanish et al and hence the need to propose a model that will significantly correlate this works results the existing models.

#### 4.8 Proposed Bond strength Model

Table 12 shows tests between bond stress results of this work and those of Orangun et al and Stanish et al

<b>Table 12</b> Tests of Between-Subjects Effects of this research and those of Orangun et al and Stanish <i>et al</i>							
Source	Dependent Variable	Type III Sum of Squares	df	Mean Square	F	Sig.	
Corrected Model	This work	.000a	0	.	.	.	
	Orangun et al	.000b	0	.	.	.	
	Stanish <i>et al</i>	.000a	0	.	.	.	
Intercept	This work	601.793	1	601.793	1954.346	.000	
	Orangun et al	134.102	1	134.102	1141.984	.000	
	Stanish <i>et al</i>	255.854	1	255.854	1063.524	.000	
Error	This work	4.311	14	.308			
	Orangun et al	1.644	14	.117			
	Stanish <i>et al</i>	3.368	14	.241			
Total	This work	606.104	15				

	Orangun et al	135.746	15
	Stanish <i>et al</i>	259.222	15
Corrected	This work	4.311	14
Total			
	Orangun et al	1.644	14
	Stanish <i>et al</i>	3.368	14
a R Squared = .000 (Adjusted R Squared = .000)			
b R Squared = .000 (Adjusted R Squared = .000)			

From the table 12 and bond strength results of this work its proposed to correct the works of Orangun et al for the selected corrosion inhibitors with a new model in equation 6;

$$\tau_u = 0.136526 \sqrt{f'_c} \left[ 1.2 + 3 \left( \frac{c}{d_b} \right) + 50 \left( \frac{d_b}{L_d} \right) \right] \quad (6)$$

Where  $\tau_u$  is the bond strength in N/mm<sup>2</sup>

C is the minimum concrete cover in mm

$f'_c$  is the cylinder compressive strength of concrete in N/mm<sup>2</sup>

$d_b$  is the bar diameter in mm and

$L_d$  is the development length in mm

Table 13 shows the correlation of the proposed bond strength model from this research and the bond strength model of Orangun et al and Stanish et al

**Table 13** Correlations of bond strength results of this work with the proposed model and Stanish et al bond strength model

		This work	Stanish <i>et al</i>	Proposed Model
This work	Pearson	1	.012	.008
	Correlation			
	Sig. (2-tailed)		.967	.979
	N	15	15	15
Stanish <i>et al</i>	Pearson	.012	1	1.000**
	Correlation			
	Sig. (2-tailed)	.967		.000
	N	15	15	15
Proposed Model	Pearson	.008	1.000**	1
	Correlation			
	Sig. (2-tailed)	.979	.000	
	N	15	15	15

\*\* Correlation is significant at the 0.01 level (2-tailed).

From table 13, the proposed model strongly correlates with the results of this work and the model of Stanish et al and is applicable to the selected corrosion inhibitors for reinforced concrete of characteristic strength 25N/mm<sup>2</sup>.

## 5. Conclusions

From the results of this research, the following conclusions can be drawn;

- At the selected dosages of the selected corrosion inhibitors in combination with all respective brands of cement increased the bond strength of reinforced concrete increased.
- The bond strength results of this research do not significantly correlate with the models of Orangun et al and Stanish et al.
- A new proposed bond strength model (a modifying the model of Orangun et al) significantly correlates with the results of this research and the Stanish et al bond strength model.

## 6. References

- [1] Mogire P. O, Abwodha S., Mwero J.N and Manguriu G.N.(2018), "The effect of Selected Cement Brands in Kenya on the Critical Penetration Depth of Rust in Reinforced Concrete Water Conveyancing Structures," *International Journal of Scientific and Research Publications*, 8(11), 2250-3153.
- [2] Hossein M.S., Keivan K. and Alireza H. (2010), "A model for the evolution of concrete deterioration due to reinforcement corrosion", *Mathematical and Computer Modelling*, 52 (9) 1403-1422.
- [3] De Groot A.K., Kusters G.M.A and Monnier T. (1981), "Numerical modeling of bond-slip behavior", *Concrete Mechanics*, 26(1B), 6-38.
- [4] FIP, "Bond of reinforcement in concrete: state-of-art report," *Fib Bulletin No. 10*, CEB-FIP, Lausanne, Switzerland, 2000.
- [5] CEB-FIP, *Structural Concrete—Textbook on Behaviour, Design and Performance*, Updated Knowledge of the CEB-FIP Model Code 1990, vol. 1, Sprint-Druck, Stuttgart, Germany, 1999.
- [6] Sungnam H. and Sun-Kyu P. (2012), "Uniaxial Bond Stress-Slip Relationship of Reinforcing Bars in Concrete", *Advances in Materials Science and Engineering*.
- [7] Dai J., Ueda T. and Y. Sato Y. (2006), "Unified analytical approaches for determining shear bond characteristics of FRP-concrete interfaces through pullout tests," *Journal of Advanced Concrete Technology*, 4(1), 133–145.
- [8] Eligehausen R., Popov E.P., and Bertero V.V.(1983), "Local Bond stress-slip relationships of deformed bars under generalized excitations," Report UCB/EERC-83/23, University of California, Berkeley, Calif, USA.
- [9] Fantilli A.P. and Vallini P. (2007), "A cohesive interface model for the pullout of inclined steel fibers in cementitious matrixes," *Journal of Advanced Concrete Technology*, 5(2), 247–258.
- [10] Oh B.H and Kim S.H. (2007), "Realistic models for local bond stress-slip of reinforced concrete under repeated loading," *Journal of Structural Engineering*, 133(2), 216–224.
- [11] Kearsley E.P. and Joyce A (2014), "Effect of corrosion products on bond strength and flexural behaviour of reinforced concrete slabs", *J. S. Afr. Inst. Civ. Eng.*, 56(2), 21-29.
- [12] Chung L., Cho S.H., Kim J.H.J. and Yi S.T.(2004), "Correction factor suggestion for ACI development length provisions based on flexural testing of RC slabs with various levels of corroded reinforcing bars", *Engineering Structures*, 26(8), 1013-1026.

- [13] Stanish K., Hooton R.D. and Pantazopoulou, S.J.(1999), “Corrosion effects on bond strength in reinforced concrete”, *ACI Structural Journal*, 96(6), 915-21.
- [14] Cabrera J.G. (1996), “Deterioration of concrete due to reinforcement steel corrosion”, *Cement and Concrete Composites*, 18(1), 47-59.
- [15] Lee H. S, Noguchi T. and Tomosawa F. (2002), “Evaluation of the bond properties between concrete and reinforcement as a function of the degree of reinforcement corrosion”, *Cement and Concrete Research*, 32(8): 1313-1318.
- [16] Orangun C.O., Jirsa I.O., Breen J.E.(1977), “A re-evaluation of test data on development length and splices”, *ACI J.* 74(3)
- [17] Kenya Bureau of Standards, KS EAS 18-1:2001(2005), “Cement Part 1: Composition, Specification and Conformity Criteria for Common Cements”, Kenya Bureau of Standards, Nairobi.
- [18] Neville M. (1996). “Properties of Concrete,” Pitman Publishing Company,” London, UK.
- [19] Barberon F., Bouny V.B., Zanni H., Bresson B., Caillerie J.B., Malosse L. and Zehong G.(2005), “Interactions between chloride and cement-paste materials”, *Magn. Reson. Imag.*, 23, 267-272.
- [20] Tutti K., (1982), “Corrosion of Steel in Concrete”, Swedish Cement and Concrete Research Institute, Stockholm, Sweden.
- [21] Neville A.M., Brooks J.J. (2012), “Concrete Technology,” Longman, London, UK.
- [22] Obi L. (2017), “Evaluation of the Effects of Coarse Aggregate Sizes on Concrete Quality”, *European Journal of Engineering Research and Science*, 2(1).
- [23] Neville A. M. (2011). *Properties of Concrete*, 5th edition. Pearson Education Limited.
- [24] Arumugam, B. (2014), “Effect of Specific Gravity on Aggregate Varies the Weight of Concrete Cube”, *International Journal of Civil Engineering*, 1(3), 1-9.
- [25] British Standard Institutes, BS EN 1097-6:2000, Tests for mechanical and physical properties of aggregates. Determination of particle density and water absorption, British Standard Institution, London.
- [26] British Standard Institutes, BS 882:1992, Specification for aggregates from natural sources for concrete.
- [27] British Standard Institutes, BS 8007:1987, Code of practice for the design of concrete structures for retaining aqueous liquids.
- [28] Zerdi A.T. (2014), “Strength Exhibition of M25 Grade Concrete with Limestone Quarry Dust Utilization for Fine Aggregates”, *Global Journal of Research Analysis International* 5(1), 2016 No.3.

[29] ASTM C117, "Standard Test Method for Materials finer than 75-um (No. 200) sieve in mineral aggregates by washing." American Society for Testing and Materials, 1995.

[30] BS 882; - Specification for aggregates from natural sources for concrete. British Standards Institute, London United Kingdom, 1992.

[31] ASTM C40, (2004), "Standard Test Method for effect of organic impurities in fine aggregates on strength of mortar," American Society for Testing and Materials ASTM International.

[32] Neville A. M. and Brooks J.J. (2010). Concrete Technology, 2nd edition. Prentice Hall.

[33] BS 12, Specification for Portland cement (BSI Publications, London, 1996).

[34] KS EAS 18. Cement Standard - Part 1: Composition, Specifications and Conformity Criteria. KEBS, Kenya. 2001.

[35] Østnor T.A. and Justnes H. (2011), "Anodic corrosion inhibitors against chloride induced corrosion of concrete rebars", *Advances in Applied Ceramics*, 110(3), 131-136.



This work is licensed under a Creative Commons Attribution Non-Commercial 4.0 International License.

# A Corrosion Model for Prediction of the Service Life of Reinforced Concrete Water Conveyancing Structures.O

Philip Mogire<sup>1\*</sup>, Silvester Abuodha<sup>2</sup>, John Mwero<sup>3</sup>, Geoffrey Mang'uriu<sup>4</sup>,

Department of Civil and Construction Engineering, University of Nairobi, Kenya<sup>1,2,3</sup>

Department of Civil, Construction and Environmental Engineering Jomo Kenyatta University of Agriculture & Technology, Nairobi, Kenya<sup>4</sup>

Corresponding author: 1\*



**ABSTRACT**— With increased competing demands of sustainable and green structures to support the United Nations sustainable development goals, new technologies are evolving for efficient design and manufacture and construction of civil and environmental engineering products. Researchers have up scaled their effort to develop techniques to monitor the performance of civil engineering structures within their service life for optimum return from investment. The aim of this research was to develop a corrosion model for prediction of the service life of reinforced concrete water conveyancing structures. To achieve the desired objective, steel samples were cast in 9 cylinders each of 150mm diameter x 300mm long, 130mm diameter x 300mm long and 100mm diameter x 300mm long in concrete of characteristic strength 25/mm<sup>2</sup>, 30N/mm<sup>2</sup> and 35N/mm<sup>2</sup> respectively. After 24 hours the cast specimens were demolded and immersed in curing tanks for 28 days and then immersed in a 3.5% industrial sodium chloride solution under 6V. The accelerated corrosion specimens were monitored for onset of cracks and stopped when the cracks were 0.2mm in width. The physical and chemical properties of the materials were investigated for compliance with relevant and applicable British and Kenyan standards for conformity to acceptable criteria. The concrete materials were batched by weight and mixed by a lab electric pan concrete mixer in batches of 0.009 m<sup>3</sup>. The concrete batches were tested for consistency by the slump and compaction factor tests. The applicability of existing models for critical corrosion depth for cover cracking was assessed. The corrosion current density of existing models was evaluated using results of this work and a model was proposed that matched with the experimental data reasonably well. Further, a corrosion service life prediction model that takes account of the cover to the rebar, the compressive strength and split tensile properties of concrete has proposed. The service life model developed here is for reinforced concrete water conveyancing structures subjected to chloride contamination. The model defines a criterion for corrosion initiation period, crack propagation period to 0.05mm width and propagation period from 0.05mm to 0.2mm. The results of the analysis of the present model significantly correlate well with experimental work and results of other researchers.

**KEYWORDS:** Service Life model, Corrosion, Reinforced Concrete.

## 1. INTRODUCTION

Among the materials used for construction of water conveyance structures is reinforced concrete due to its excellent performance and overall advantages. Corrosion of steel reinforcement has been recognized as a primary factor contributing to the deterioration of concrete structures [1,2]. Deterioration due to reinforcement corrosion leads to a decrease in durability of reinforced concrete structures resulting in a sharp reduction in their service lifespan and high maintenance costs [3]. The corrosion of steel reinforcement in concrete is an electrochemical process that causes the dissolution of iron to form a complex mixture of iron oxides,

hydroxides and hydrated oxides that evolves according to the prevailing local environment [4,5]. Corrosion products have specific volumes ranging from about two to six times that of the iron consumed [6] depending on the degree of oxidation. The main corrosion-induced damage mechanisms in reinforced concrete structures is shown by;

- a decrease in the rebar cross-sectional area,
- a possible loss of steel load capacity [7,8]
- loss of flexural stiffness [9,10]
- cracking and spalling of the concrete cover [11,12]
- loss of bond along the steel/concrete interface [8].

Although most of the research on chloride-induced corrosion has been on chloride ingress into concrete, there has been an increasing effort in recent years to quantify the progressive damage in reinforced concrete due to the advancement of steel reinforcement corrosion [13-15]. The new effort is of great relevance in the structural assessment of deteriorated reinforced concrete water conveyancing structures with corroded reinforcement, and it must be included in estimations of the service life. Extensive analytical, numerical and experimental studies have been devoted to cracking of the concrete cover due to reinforcement corrosion. To speed up the corrosion process in the experiments, impressed current is adopted [16,17]. This provides corrosion of reinforcing steel bars, where the whole surface of the bar corrodes. Another method used to accelerate corrosion is immersing reinforced concrete samples in a chloride rich solution and connecting the reinforcing bar to cathode element through a particular voltage [18]. While in the beginning some pits on the reinforcement bar do occur, general corrosion is dominant at later stages [19]. Due to time constraints, concrete cracking due to natural chloride induced corrosion is rarely studied [20]. External chloride penetration leads to pitting corrosion, which creates non-uniform pressure around the bar. This could potentially lead to faster cover cracking than uniform corrosion. Analytical or numerical models based on the thick-walled cylinder theory; and numerical models based on finite elements or similar methods have also been devoted to studying the reinforced concrete corrosion phenomenon. Analytical and numerical models based on the thick-walled cylinder theory, with different levels of sophistication, have been used by a number of authors (e.g. [21,23]. The rate of corrosion is usually not constant but evolves due to the corrosion process itself and due to climate variations. Therefore, a representative, or average, value of the corrosion rate, ( $V_{corr}$ ), first has to be determined [24]. The rate of corrosion ( $V_{corr}$ ) in reinforced concrete can be represented by the volumetric loss of the reinforcement bars by unit of surface area and unit time and can be obtained from equation 1 or 2[25].

$$V_{corr} \text{ (mm/y)} = 0.0116 i_{corr} \text{ (\mu A/cm}^2\text{)} \text{ for uniform corrosion current} \quad 1)$$

or

$$V_{corr} \text{ (mm/y)} = 0.0116 I_{corr} \text{ (\mu A/cm}^2\text{)} \text{ for non-uniform corrosion current} \quad 2)$$

Where  $i_{corr}$  is the uniform corrosion current density?

$I_{corr}$  is the non-uniform corrosion current density?

Due to the impossibility of direct visual observation of the morphology of corrosion,  $I_{corr}$  is the most feasible expression of the corrosion current when measuring in concrete [25] and therefore equation 2 is preferred. For getting accurate rates of corrosion, it's essential that the values of the corrosion current density are obtained in order to accurately predict the service lifespan of the reinforced concrete structures [26].  $I_{corr}$  is usually obtained through electrochemical measurement in an experiments [27,28]. The shortcomings of the electromechanical determination of  $I_{corr}$  include;



- $I_{\text{corr}}$  is measured on the whole exposed area of the steel reinforcement; however, the corrosion is localized in a small zone.
- The measured  $I_{\text{corr}}$  value is significantly affected by the galvanic current flowing between the corroding and passive zones on the steel surface [29].

Due to the shortcomings of the electromechanical technique to measure  $I_{\text{corr}}$ , there is need to develop an accurate criterion for its measurement. The rate of reinforcement corrosion can also be calculated from the weight loss method in equation 3.

$$V_{\text{corr}} (\text{mm/y}) = 87.6 \times (W / DAT) [30] \quad 3)$$

Where

W = weight loss of the reinforcement bar in milligrams

D = Reinforcement bar density in  $\text{g/cm}^3$

A = Surface area of the sample exposed to corrosion in  $\text{cm}^2$

T = time of exposure of the reinforcement bar in hours

This research presents a service life model for reinforced concrete water conveyancing structures. The validity, accuracy, and efficiency of the proposed model is established by comparing the model results with experimental work and works of other researchers. The results of the analysis of the present model significantly correlate well with experimental work and results of other researchers.

## 2. BACKGROUND OF CORROSION KINEMATICS

The electrochemical process that underlies corrosion of steel reinforcement in concrete involves two chemical reactions. The anodic reaction is iron oxidation, described by equation 4. Iron ions ( $\text{Fe}^{2+}$ ) dissolve into the pore solution with electrons left inside the steel bar. These electrons are consumed by a cathodic reaction, i.e., an oxygen reduction producing hydroxides according to equation 5.

Anodic reaction:



Cathodic reaction



Both the anodic and cathodic reactions occur along the surface of the steel electrode. Additionally, an ionic current of hydroxide ions flows through the surrounding electrolyte from the cathodic to the anodic areas, balanced by an electric current through the steel, as shown in Fig. 2.1[31]. The anode hydroxide ions and  $\text{Fe}^{2+}$  ions form ferrous hydroxide, the primary corrosion product, which undergoes further oxidation, becoming black rust or brown rust depending on the amount of oxygen available.



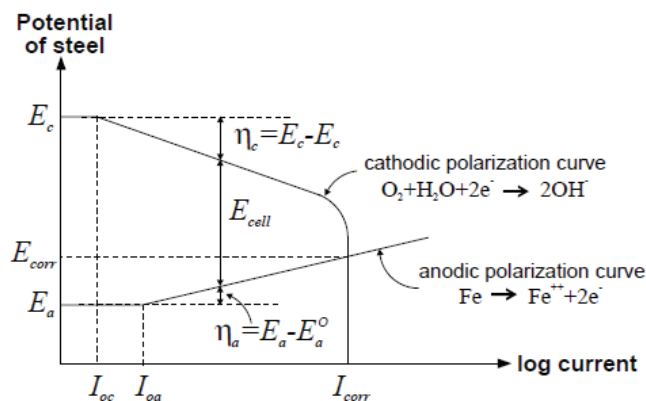


**Figure 2.1** Evans diagram for the anodic and cathodic processes taking place on the reinforcing steel surface. [31]

**2.1 Reinforcement corrosion**

Assuming an electric charge and isotropic conductivity, the electric potential distribution between the anodic and cathodic polarization curve is described by Laplace’s Equation 6 whose solution can only be derived with prescribed geometries and boundary conditions.;

$$\nabla^2 E = 0 \tag{6}$$

Where  $\nabla^2$  is the Hamilton operator

E is the Electric potential

The current density at any location of the steel surface can also be determined by Ohm’s law from Equation 7.

$$i_{corr} = \frac{1}{\rho_{el}} \frac{\partial E}{\partial n} \tag{7}$$

Where  $\rho_{el}$  is the concrete resistivity

n is the direction normal to the steel surface.

Taking into account the effects of activation and concentration polarization according to Butler-Volmer kinetics, the surface boundaries can be described by the Tafel Equations 8 and 9.

The kinetics of oxidation of iron are given by:

$$i_a = i_{oa} e^{2.3(E_a - E_{oa})/\beta_a} \tag{8}$$

The kinetics of oxygen reduction are given by:

$$i_c = \frac{C}{C_o} i_{oc} e^{2.3(E_{oc} - E_c)/\beta_c} \tag{9}$$

Where

$i_a$  = Current density of the iron oxidation reaction ( $\mu A/cm^2$ )

$i_{oa}$  = Exchange current density for iron dissolution ( $\mu A/cm^2$ )

$E_a$  = Potential at the concrete pore solution immediately next to the steel surface(V)

$E_{oa}$  = Equilibrium potential of the anodic reaction (V)

$\beta_a$  = Activation tafel slope for the anodic reaction (V)

$i_c$  = Current density of the oxygen reduction reaction ( $\mu A/cm^2$ )

$i_{oc}$  = Exchange current density for cathodic reaction ( $\mu A/cm^2$ )

$E_{oc}$  = equilibrium potential of the cathodic half-cell reaction, taken as the standard electrode potential, i.e., 0.160 V vs. SCE

$E_c$  = potential at the concrete pore solution immediately next to the steel surface(V)

$\beta_c$  = Activation tafel slope for the Cathodic reaction (V)

$C_o$  = dissolved oxygen concentration at the external concrete surface (kg/m<sup>3</sup> of solution)

$C$  = dissolved oxygen concentration at the steel surface (kg/m<sup>3</sup> of solution)

It has been observed that  $\beta_a$  increases over time when chloride ions are present in the concrete, from 0.338 V at 1 day to 0.480 V at 90 days while  $\beta_c$  decreases over time from 0.309–0.394V over the same period and condition. [32].

The reinforcing steel is freely corroding when the polarization taking place at the anode and the cathode is enough to make their polarization curves meet as illustrated in Fig.2.2. At this point, the corrosion system develops a new equilibrium corrosion potential  $E_{corr}$  and corrosion current  $I_{corr}$ . The intersection of the two electrode polarization curves represents conditions at which the anodic and cathodic currents are equal (but opposite in polarity) and no net current flows across the steel/concrete interface, i.e.,

$$I_{corr} = i_a \times A_a = i_c \times A_c \quad (10)$$

where  $A_a$  and  $A_c$  denote the surface areas where the anodic and cathodic reactions take place, respectively. By substituting Eqs. 8 and 9 into Equation 10 an estimate of the equilibrium corrosion potential can be obtained from equation 11:

$$E_{corr} = \frac{1}{\beta_a + \beta_c} \left[ \frac{\beta_a \beta_c}{2.3} \ln \left( \frac{i_{oc}}{i_{oa}} \frac{C}{C_o} \frac{A_c}{A_a} \right) + \beta_c E_{oa} + \beta_a E_{oc} \right] \quad (11)$$

Taking into account the effects of resistivity and oxygen diffusion, and assuming a relative humidity of 75 % and temperature of 20°C, Vu and Stewart [33] developed an empirical model which gives the corrosion current density at the start of the propagation period (at time  $t_1$ ) as a function of water cement ratio and cover thickness:

$$i_{corr}(t_1) = 37.8(1 - w/c)^{-1.64} / d \quad (\mu A/cm^2) \quad (12)$$

where  $w/c$  is the water cement ratio obtained from the Bolomey's formula and  $d$  is the cover thickness (mm).

For  $t < 1$  year

$$i_{corr}(t_2) = \left[ i_{corr}(t_1) (1 + t_2)^{-\frac{1}{3}} \right] / d \quad (\mu A/cm^2) \quad (13)$$

Inserting equation 12 into Equation 13 gives:

$$i_{corr}(t_2) = \left[ 37.8 (1 - w/c)^{-1.64} (1 + t_2)^{-\frac{1}{3}} \right] / d \quad (\mu A/cm^2) \quad (14)$$

For  $t > 1$  year

$$i_{corr}(t_2) = [i_{corr}(t_1) 0.85 t_2^{-0.29}] / d \quad (15)$$

Inserting Equation 12 into 15 gives

$$i_{corr}(t_2) = [32.13 (1 - w/c)^{-1.64} t_2^{-0.29}] / d \quad (16)$$

Li 2004a [34] proposed a corrosion density model in equation 17,

$$i_{corr} = 0.3682 \ln(t) + 1.1305 \quad (17)$$

Where  $i_{corr}$  is the corrosion current density ( $\mu m/cm^2$ ) and  $t$  is the time (years) from corrosion initiation.

The corrosion model was established from the experimental data and the influence of the corrosion duration was considered. This model cannot rationally reflect the corrosion process of the reinforcement bar in chloride induced corrosion affected reinforced concrete structures as other factors influencing the corrosion rate are ignored.

## 2.2 Service life design

The Tuutti's model [35] is widely accepted as the conceptual model for the deterioration of structures (Fig.2.2). As a function of time, the model distinguishes an initiation time followed by a propagation time and shows the respective limit states in the two periods.

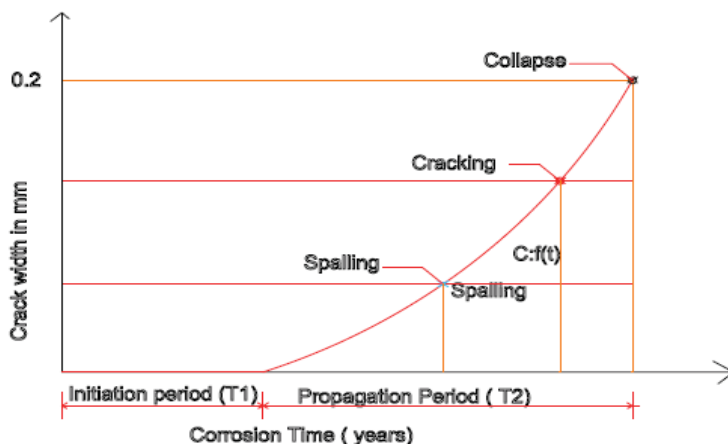


**Figure 2.2:** Graph of Service life design limit states for water structures

From the graph in figure 2.3

$$T_{cr} = T_1 + T_2$$

18)

### 2.2.1 Initiation time $T_1$

The time needed for first cracking of the concrete cover as a result of the expansive forces exerted by the corrosion products mainly depends on the tensile strength of the concrete ( $f_t$ ), the type of corrosion, the rate of corrosion and the concrete cover-to-rebar diameter ratio  $c/d$  which define the critical penetration depth.

Rasheeduzzafar et al. [36] found that the ratio of concrete cover to bar diameter was a better predictor for critical corrosion loss than either parameter alone.

Based on experimental studies, Rodriguez et al. [15] proposed Equation 19 for evaluating the attack penetration  $x_{crit}$  corresponding to crack initiation:

$$x_{crit} = 83.8 + 7.4 \frac{c}{d} - 22.6 f'_t \quad (\mu\text{m}) \quad 19)$$

where

$x_{crit}$  is the attack penetration or the decrease in the reinforcing bar radius ( $\mu\text{m}$ ),

$c/d$  is the cover/diameter ratio and

$f'_t$  is the concrete tensile strength  $\text{N}/\text{mm}^2$ .

From Equation 19 the critical penetration depth increases with cover depth and decreases with increasing reinforcement diameter, which is as reported in most experimental investigations. However, as the resistance of the concrete to cracking is strain-limited and not strength-limited the concrete tensile strength may not be the main parameter controlling the crack initiation. Moreover, in the relationship the unit is not correct, indicating that the tensile strength should be replaced or combined with other mechanical concrete parameters [37].

Xu and Shayan [38] considered the combination of concrete cover and its embedded steel as a thick-wall concrete cylinder which surrounds the embedded steel, and the expansion of corroded steel exerting an internal pressure to the concrete cylinder. They derived Equation 20 for the attack penetration depth  $x_{crit}$ .

$$x_{crit} = \frac{f_t(c+d)(1+\nu)}{E_{eff}d\beta} \quad 20)$$

Where,

$x_{crit}$  = Corrosion loss at crack initiation ( $\mu\text{m}$ )

C = Concrete cover (mm)

$d$  = bar diameter(mm)

$f_t$  = Concrete tensile strength (N/mm<sup>2</sup>)

$\nu$  =concrete poison's ratio

$\beta$  = Relative volume change due to conversion of steel to rust =  $(\Delta V/V)$

$E_{eff}$  =effective elastic modulus= $E/(1+\phi)$  (N/mm<sup>2</sup>)

$E$  =Elastic modulus (N/mm<sup>2</sup>)

$\phi$  = concrete creep coefficient

From their model, the predicted critical corrosion loss was found four or greater as much as the calculated values based on the measured corrosion rates from Linear Polarization Resistance (LPR) test in their research. This is because in calculating corrosion loss from the LPR test, it is assumed that the whole surface area subjected to corrosion is corroding. This is not true for non-uniform corrosion and therefore the calculated corrosion loss from LPR tests should be modified based on the actual corroded area of the embedded steel to present the real values.

Torres and Sagues [39] studied the effects of localized corrosion and derived Equation 21 which relates the length of corroded steel and cover-bar diameter ratio to the critical corrosion loss.

$$x_{crit} = 11.0 \frac{c}{d} \left( \frac{c}{l} + 1 \right)^2 \quad (21)$$

Where

$x_{crit}$  = Corrosion loss at crack initiation( $\mu\text{m}$ )

$C$  = Concrete cover (mm)

$d$  = bar diameter(mm)

$l$  = length of exposed steel (mm)

Other factors including the tensile strength that may contribute to the critical penetration depth were not taken into account in Equation 21. The initiation corrosion period is evaluated from Equation 22:

$$T_1(\text{years}) = \frac{x_{crit}(\text{mm})}{V_{corr} \left( \frac{\text{mm}}{\text{year}} \right)} \quad (22)$$

### 2.2.2 Propagation time $T_2$

The corrosion propagation period ( $T_2$ ) is the time necessary for sufficient corrosion to occur to cause unacceptable damage to the reinforced concrete structures, e.g. cover cracking. The length of this period depends on the definition of an acceptable limit state [40]. This level of damage will vary depending on the requirements of the use of the structure. Assuming a particular damage limit state, the propagation period depends principally on the corrosion rate. The limit state may be described in terms of parameters that define the propagation period including loss of steel cross sectional area [41] and loss of steel/concrete bond [42]. Once the corrosion rate ( $V_{corr}$ ) is quantified, the effect of any variable that alters it during propagation period [43], such as inhibitors or the presence of moisture in chloride-bearing concrete, can be studied, the condition of a real structure can be assessed, and the propagation period [44] quantified by integrating the value over time. Based on theoretical physical models for corrosion of steel in concrete exposed to seawater, Bazant et al. [45] proposed a numerical model shown in Equation 23 for reinforcement corrosion in concrete, to assess the time to corrosion that may lead to splitting of cover concrete.

$$T_2 = \rho_{corr} \frac{d\Delta d}{p j_r} \quad (23)$$

Where

$T_2$  = propagation period (years).

$\rho_{corr}$  =Combined density factor for steel and rust (kg/m<sup>3</sup>)

$d$  =diameter of rebar(mm)

$\Delta d$  = increase in diameter of rebar due to rust formation(cm)

P = perimeter of rebar(mm)

$j_r$  = instantaneous corrosion rate of rust (g/m<sup>2</sup>s)

The instantaneous corrosion rate of rust can be calculated from Equation 24;

$$j_r = \frac{W}{F} i_{corr} \quad (24)$$

Where

W=equivalent weight of steel (g)

F= Faradays constant(C)

$i_{corr}$  =Corrosion current density ( $\mu\text{A}/\text{cm}^2$ )

From Bezan't's numerical model, the corrosion rate is the most significant parameter in determining the time to cracking of the cover concrete. This model has never been experimentally validated.

Liu and Weyers [18] derived a model that includes the time required for corrosion products to fill an assumed porous zone at the steel/concrete interfaces before creating an internal pressure on the surrounding concrete. In their model (Equation 25), the time from corrosion initiation to cover cracking,  $t_{crack}$ , is given as a function of the critical amount of rust product needed to induce cracking of the concrete cover,  $M_{crit}$ , and the corrosion rate,  $k_p$ :

$$T_{crack} = \frac{M_{crit}^2}{2k_p} \quad (25)$$

Where  $M_{crit}$  is modelled as Equation 26;

$$M_{crit} = \rho_{rust} \left( \pi \left[ \frac{Cf_t}{E_{ef}} \left( \frac{a^2+b^2}{b^2-a^2} + v_c \right) + t_1 \right] d + \frac{M_{st}}{\rho_{st}} \right)$$

(26)

$v_c$  is Poisson's ratio of the concrete,

$E_{ef}$  = an effective elastic modulus of the concrete;  $E_{ef} = E_c/(1+\varphi)$

$E_c$  = elastic modulus of the concrete (N/mm<sup>2</sup>)

a = the inner radius [(d+2t<sub>1</sub>)/2] (mm)

b = the outer radius [C+(d+2t<sub>1</sub>)/2] (mm)

C = the concrete cover (mm)

$E_c$  = elastic modulus of the concrete

$\varphi$  = the creep coefficient of the concrete

t<sub>1</sub> = is the thickness of the concrete under pressure(mm)

d = original diameter of steel (mm)

$f_t$  = Split tensile strength(N/mm<sup>2</sup>)

Equation 27 shows Liu and Weyers expression of the rate of rust production,  $k_p$ :

$$k_p = 0.098 \times 10^{-4} (1/\alpha) \pi d i_{corr} \quad (27)$$

where:

0.098 = numerical coefficient to fit experimental data

$\alpha$  = relation between atomic weight of iron (55.8) and the molecular weight of the rust product; e.g  $\alpha = 0.523$  if the corrosion product is Fe(OH)<sub>3</sub>

d = diameter of the steel bar (mm)

$i_{corr}$  = annual mean corrosion rate ( $\mu\text{A}/\text{cm}^2$ )

Inserting Equation 26 and 27 into Equation 25;

$$T_{crit} = \left[ \rho_{rust} \left( \pi \left[ \frac{cf_t}{E_{ef}} \left( \frac{a^2+b^2}{b^2-a^2} + v_c \right) + t_1 \right] d + \frac{M_{st}}{\rho_{st}} \right) \right]^2 \frac{5.846\alpha}{di_{corr}} \quad (28)$$

For a given crack width (w)[18],Equation 29 can be used to evaluate the rebar radius decrease

$$w = 0.05 + \beta[x - x_{crit}], [0 \leq w \leq 1.0mm] \quad (29)$$

Where

w=characteristic crack width(mm)

x=rebar radius decrease(mm)

$x_{crit}$ =critical penetration depth (mm)

$\beta$ = Coefficient which depends on the position of the bar ( $\beta= 0.01$  for top cast bars and 0.0125 for bottom cast bars)

In Liu-Weyers model the rate of steel mass loss caused by corrosion was assumed to decrease with time in which the coefficients used were obtained by fitting experimental data. The thickness of the pore band around the steel/concrete interface( $t_1$ ) was assumed as 12.5  $\mu\text{m}$  in the validation of their model. In good quality concretes the thickness of the concrete under pressure( $t_1$ ) is not a distinct band, the reported thickness varies, but is typically in the range of 15-50  $\mu\text{m}$  [46-48]. The sensitivity of this parameter has not been studied. The model has not been verified against concrete structures under field exposure where chloride ions diffuse into the concrete. From Liu-Weyers model,  $T_2$  can be found by subtracting  $T_1$  from  $T_{crack}$ .

Based on field and laboratory data, Morinaga [49] suggested Equation 30 for predicting the time to cracking. He assumed that cracking of concrete will first occur when there is a certain quantity of corrosion products forming on the reinforcement.

$$T_2 = \frac{Q_{cr}}{j_r} \quad (30)$$

$$Q_{cr} = 0.602d \left( 1 + \frac{2c}{d} \right)^{0.85} \quad (31)$$

Where

$Q_{cr}$  =amount of corrosion in concrete cracks( $\text{g}/\text{cm}^2$ )

c = concrete cover thickness(mm)

According to Equation 30 the time to cracking is a function of the corrosion rate, concrete cover depth and reinforcing diameter. This model does not include any effect of mechanical concrete properties and it is difficult to identify the limitations of its validity.

Wang and Zhao [50] recommended a stage technique for utilizing limited component examination to focus the thickness of the corrosion product comparing to the time term when the surface concrete cracks. Their model is described in Equations 32-34;

$$T_2 = \frac{H}{p_r} \quad (32)$$

and

$$\frac{\Delta}{H} = 0.33 \left( \frac{d}{c} \right)^{0.565} f_{cu}^{1.436} \quad (33)$$

$$p_r = \frac{W}{F\rho_{st}} i_{corr} \quad (34)$$

Where

W = equivalent weight of steel (kg)

$f_{cu}$  = cube strength of concrete( $\text{kN}/\text{cm}^2$ )

$\Delta$  = thickness of corrosion product (cm)

H= no of cracks in the cover

$\rho_{st}$  =density of steel( $\text{kg}/\text{m}^3$ )



$i_{\text{corr}}$  is the average corrosion rate ( $\mu\text{A}/\text{cm}^2$ ),

Wang and Zhao empirical model assumed that the corrosion products will fill the steel/ concrete interface and develop an expansive pressure or tensile stress on the cover concrete, which will crack when the exerted tensile stress from the expansive corrosion product exceeds the tensile strength of the concrete. This model is applicable when field and laboratory data for corrosion current density is available.

### 2.2.3 Service life of reinforced concrete water conveyancing structures

The end of service life of this research is limited by the maximum crack width allowed for water structures. In reference to BS 8007 cracks less than 0.2 mm in width will self-heal if the cracked concrete element is in contact with water that is not flowing or exerting a pressure.

**Figure 2.3** [51] the relationship of the crack width and the wall thickness –water retaining height ration by

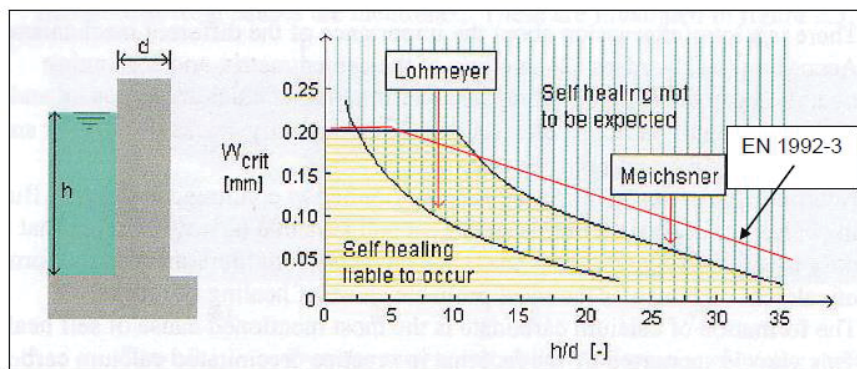


**Figure 2.3:** Self-healing of cracks to Jones [51]

From the graph in Figure 2.3 the Eurocode has  $h/d$  ratios higher than those by Lohmeyer and Meichsner for crack widths less than about 0.17 mm. This shows that that for a given water height,  $h/d$ , and section thickness,  $h$ , EN1992-3 predicts that self-healing of cracks will occur at a larger crack width limit for crack widths less than 0.17 mm for a given hydraulic ratio. In this research due to consideration of water structures, a limit crack width of 0.2mm will be considered for low pressure reinforced concrete water structures. A number of modelling efforts have also been devoted to define the corrosion initiation and propagation periods but none has distinctively defined the periods for water conveyancing structures. The present work addresses two important aspects regarding the service life of reinforced concrete water conveyancing structures. The parameters for the initiation and propagation period are defined and the periods calculated. From the results a parametric study is done and a new proposed model for the service life of water conveyancing structures is defined.

### 3.Methodology

This study was conducted at the University of Nairobi Concrete and Materials Lab where the physical properties of the materials, sample preparation and testing were done. The chemical properties of the ordinary Portland cement and chloride content was done at the State Department of Infrastructure in the Ministry of Transport, Infrastructure, Housing and Urban Development of the Government of Kenya.

#### 3.1 Concrete samples

The constituent materials for preparing test samples consisted of Ordinary Portland cement ( $42.5\text{N}/\text{mm}^2$ ), clean river sand, 20mm maximum size coarse aggregate and potable water.

### 3.1.1 Cement

The chemical composition of the cement used in this research was tested. Available cements in Kenya are manufactured in accordance to KS EAS 18-1: 2001, an adoption of the European Norm EN 197 cement standards [52]. The cements locally available are produced for specific uses [53]. The Cement used for this research was sourced from one wholesaler.

### 3.1.2. Other concrete constituents

Table 3.1 shows the description and source of other constituents of concrete used in the research.

**Table 3.1. Details of materials used in the research**

SN	Description	Source	Remark
1.	Fine aggregates	Stockpile vender sourced from Machakos River	This was washed and oven dried before use.
2	Coarse aggregates	Kenya builders quarry	5-20mm uniformly graded at source
3.	10mm ribbed bars	Local manufacturer	Factory cut to 400mm
4.	Mixing water	Potable water in the Lab	
4.	Mixing water	Potable water in the Lab	

### 3.2 Concrete Mix Design

With a characteristic strength of 25N/mm<sup>2</sup>, 30N/mm<sup>2</sup> and 35N/mm<sup>2</sup> the concrete used was designed in accordance with the British Department of environment (DoE) method [54-55].

### 3.3 Accelerated Corrosion

#### 3.3.1 Materials and Specimens

This was done through an impressed corrosion test using the procedure below;

- i) 10mm diameter x 400mm long ribbed bars were polished with abrasive papers.
- ii) 120 mm of the surface length of each bar were sprayed with a zinc rich coating and left to naturally dry.
- iii) The mixed concrete was poured into 9 cylindrical samples of 150mm diameter and 300mm long, 130mm diameter and 300mm long, 100mm diameter and 300mm long each with a 10mm diameter rebar
- iv) The specimens were mechanically vibrated for 60s. After 24 hours, the cylindrical concrete specimens were demolded and cured for 28 days.
- vi) The test specimens were dried for 24 hours and then subjected to accelerated corrosion by storing them in a tank containing 3.5 % NaCl at room temperature and an impressed voltage of 6Volts applied through a DC power supply regulator. The top and bottom surfaces of the concrete specimens were also sealed with Zinc



rich coating so as to allow only chloride ingress from the sides to simulate the corrosion of a section of a typical structural member in a water conveyancing structure.

### 3.3.2 Testing Methodology

The accelerated corrosion set up is shown in Fig.3.1. The rebars projecting were connected in series to the anode and the stainless steel rod was connected to the negative terminal (cathode). The test specimens were subjected to a constant voltage of 6 V applied to the system using a DC power supply regulator. The variation in development of corrosion current was monitored at regular intervals using a high impedance multimeter and the average for the corrosion period taken for calculation of the average mass loss.

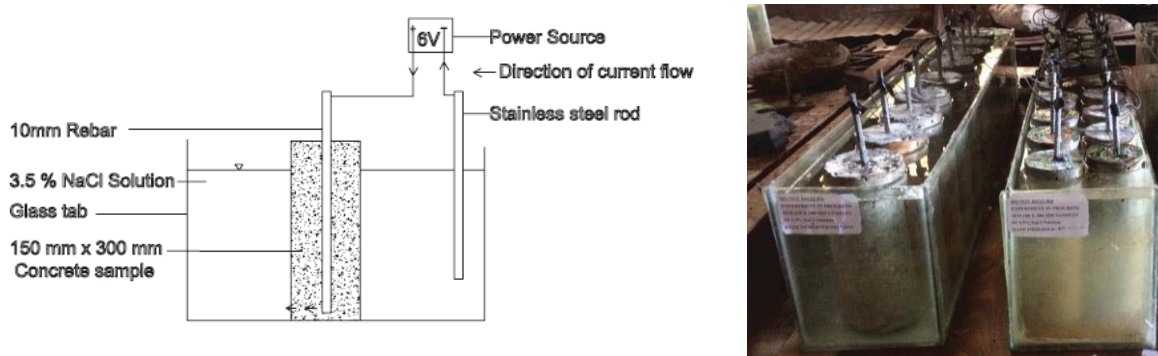


**Figure 3.1:** a) Schematic drawing of accelerated corrosion set up, b) Photo of the samples during experimentation

The appearances of first visible cracking were detected by visual observation using a magnification glass with power of x1000. The data collected for crack propagation provided the timing of first cracking and the subsequent time-dependent increase in crack width. After testing, the weight loss of bars due to corrosion were studied by cleaning, drying and weighing the reinforcement bars according to the gravimetric weight loss method as specified by Standard Practice for Preparing, Cleaning, and Evaluating Corrosion Test Specimens (ASTM G1 – 90). Fig.3.2 shows samples during experimentation and measurement.

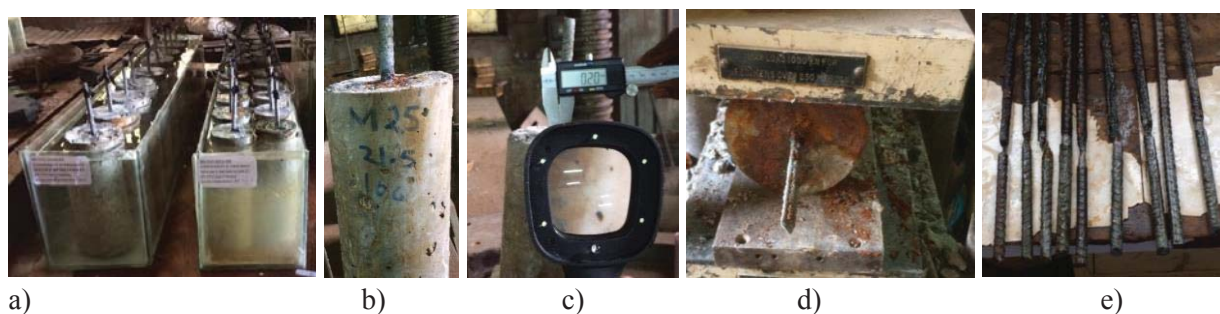


**Figure 3.2:** a) Samples during experimentation b) sample with 0.2mm longitudinal crack c) crack measurement d) recovering the corroded steel and e) cleaned rebar's for gravimetric weight loss measurement.

### 3.4 Results of the material properties

#### i) Properties of aggregates

Various tests were carried out on the aggregates to determine their suitability for the research. Water soluble chlorides ions percentage were found to be zero in fine aggregates, 0.002 % in coarse aggregates all less than

0.03% acceptable in compliance with BS EN 12620: 2002. Table 3.2 shows the physical properties of the aggregates used in the study.

**Table 3.2:** Physical properties of aggregates used in the study

Material	Specific gravity	Absorption %	Silt content %	Maximum Size
Fine aggregates	2.6	1.8	7.4	4.0
Coarse aggregates	2.6	0.3	0	20.0

The specific gravity of all the aggregates are within the limits of 2.4 – 3.0 stated in literature [56,57] and they influence the mix design of the concrete. The water absorption of the fine aggregates is within the limits of 1% – 3% stated in the literature and British Standards [58-62] and therefore a low water absorption and hence suitable for concrete works. The very low water absorption in the coarse aggregates need was taken into consideration in the mix design. ASTM C117[63] gives an allowable limit of 10% for silt and clay content in fine aggregates for concrete production while BS 882 give a limit of 4% [64]. As a thumb rule according to [65], the total amount of deleterious materials in aggregates should not exceed 5%. The silt content in the fine aggregate was more than the allowable percentage of silt content, it was washed and oven dried before use. Table 3.3 shows the mechanical properties of the coarse aggregates used in the study.

**Table 3.3:** Mechanical properties carried on coarse aggregates.

Test	Size of aggregates mm	Crushing value %	Impact value %	Flakiness index %	Loss on Abrasion Value %
Result	5-20	18	8	35	20

The mechanical properties of aggregates cannot be improved but depend on the properties of the parent rock. The Aggregates Impact Value is less than 30% value stated in literature and British Standards [65] and specified in [66]. It therefore follows that Aggregates Impact Value of all the aggregates tested are very suitable for concreting works. The Aggregate Crushing Value is less than 35% value allowed for concreting works as stated in the literature [67].

ii) Chemical Properties of Cement used in the research

Table 3.4 shows results of the chemical composition of the cement used in the research. All the constituents of cement oxides were within the acceptable limits.

**Table 3.4** Result of Chemical composition the Cement used.

SN	Test	Result of the sample	KS EAS 18-1: 2001 Requirement
1.	CaO%	59.11	Sum $\geq$ 50
2.	SiO <sub>2</sub> %	21.56	
3.	SO <sub>3</sub> %	2.78	$\leq$ 3.5
4.	MgO%	1.04	$\leq$ 5
5.	K <sub>2</sub> O%	0.051	
6.	Fe <sub>2</sub> O <sub>3</sub> %	3.48	
7.	Al <sub>2</sub> O <sub>3</sub>	8.09	3-8
8.	Na <sub>2</sub> O <sub>3</sub> %	0.018	
9.	LOI%	0.10	$\leq$ 5
10.	Cl%	0.016	$\leq$ 0.1
11.	IR%	0.55	$\leq$ 5

**a) Effect of sum of lime (CaO) and silicon dioxide (SiO<sub>2</sub>) corrosion**

The sum of lime (CaO) and silicon dioxide (SiO<sub>2</sub>) in the chemical analysis of ordinary Portland cement sample was 80.67%  $\geq$  50% within the acceptable limit [66]. This is consistent with the known fact that both CaO and SiO<sub>2</sub> give strength to concrete though SiO<sub>2</sub> has to be limited relative to CaO in order not to negatively affect setting time. The rate of corrosion is related to the strength of a concrete sample while reduced setting time minimizes plastic shrinkage cracking and hence the rate of corrosion.

**b) Effect of CaO/SiO<sub>2</sub> on corrosion**

The ratio of lime (CaO) to silicon dioxide (SiO<sub>2</sub>) contents in ordinary Portland cement should be greater than 2. The restriction on the ratio of lime to silicon dioxide [66] is to ensure that the quantity of silicon dioxide is considerably lower than that of lime so that the setting of concrete is not inhibited minimizing plastic shrinkage cracking and hence limiting corrosion.

**c) Effect of MgO on corrosion**

The quantity of magnesium oxide (MgO) in ordinary Portland cement should not exceed 5% [66]. If the quantity of MgO is in excess of 5 percent, cracks will appear in concrete and which may affect the rate of corrosion by generating spots for penetration of chloride ions in concrete.

**d) Effect of SO<sub>3</sub> on corrosion**

The quantity of sulphur trioxide (SO<sub>3</sub>) content in ordinary Portland cement was less than 3.5 % as required. SO<sub>3</sub> reduces the rate of the passive layer dissolution inhibiting the onset of corrosion.

**e) Effect of Chloride Content on corrosion**

The chloride content in ordinary Portland cement was less than 0.4% as required. Chloride ions in aqueous solution destroys the passivation film of rebars in the process of competing with hydrogen and oxygen ions in the adsorption process, thus leading to the occurrence of pitting corrosion, hole corrosion and crevice corrosion.

**f) Effect of Al<sub>2</sub>O<sub>3</sub> on corrosion**

Aluminium oxide ( $Al_2O_3$ ) reacts with free lime in concrete to form  $CaAl_2Si_3O_{12}$ . which reduces the permeability of chloride and improving the corrosion resistance property of embedded steel in concrete. Above 8% the  $Al_2O_3$  will be in an active condition reducing the corrosion resistance.

**g) Effect of  $Fe_2O_3$  on corrosion**

Iron oxide ( $Fe_2O_3$ ) contributes to cement colour and helps in the fusion of the different ingredients.  $Fe_2O_3$  forms the passivation film reducing the oxygen diffusion rate, which, in turn, reduces the **corrosion** rate.

**h) Effect of Residues on corrosion**

British standards consider  $Na_2O$ ,  $K_2O$ ,  $TiO_2$  and  $P_2O_5$  in ordinary Portland cement as residues and limit the sum of all of them to 5%. If in excess of 5% efflorescence and unsightly cracking will occur aggravating corrosion.

**iii) Gradation of Coarse and Fine aggregates**

Particle size distribution analysis on a representative sample shown on Fig.3.3 for the course aggregates for the work was carried out to obtain the proportions by weight of the different sizes of coarse aggregates present. The sample is well graded with a maximum aggregate size was 20mm.

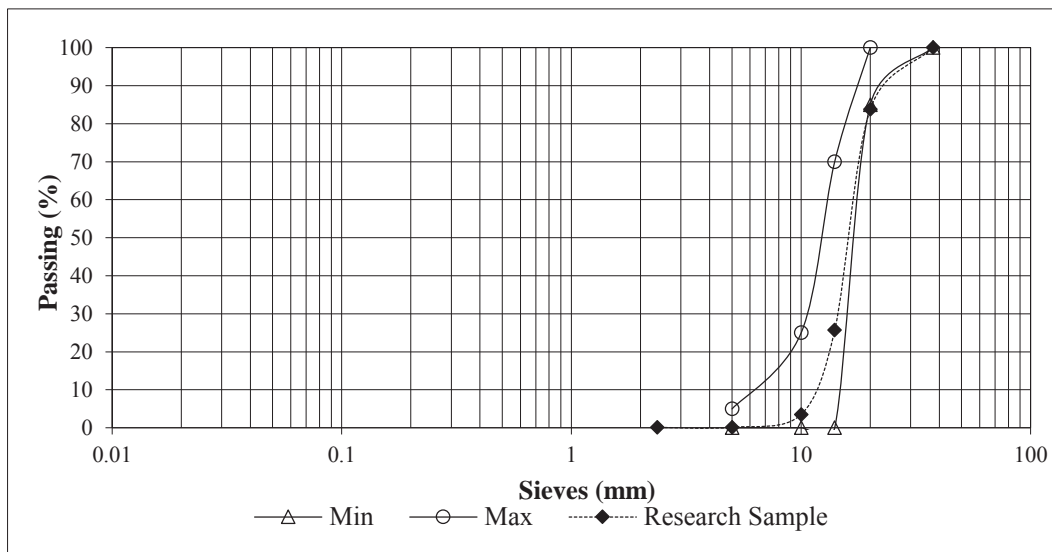


**Figure 3.3:** Graph 1 Gradation of Coarse aggregates

Particle size distribution analysis as shown on Fig.3.4 on a representative sample of the fine aggregates for the research was carried out to obtain the proportions by weight of the different sizes of fine particles present according to BS 812-103 and BS 882. The proportions were expressed as percentages by weight passing various sieve sizes conforming to BS 410. As shown on the graph of Fig.3.4, the coarse aggregates were well graded and expected to give a well interlocked composite concrete mix.

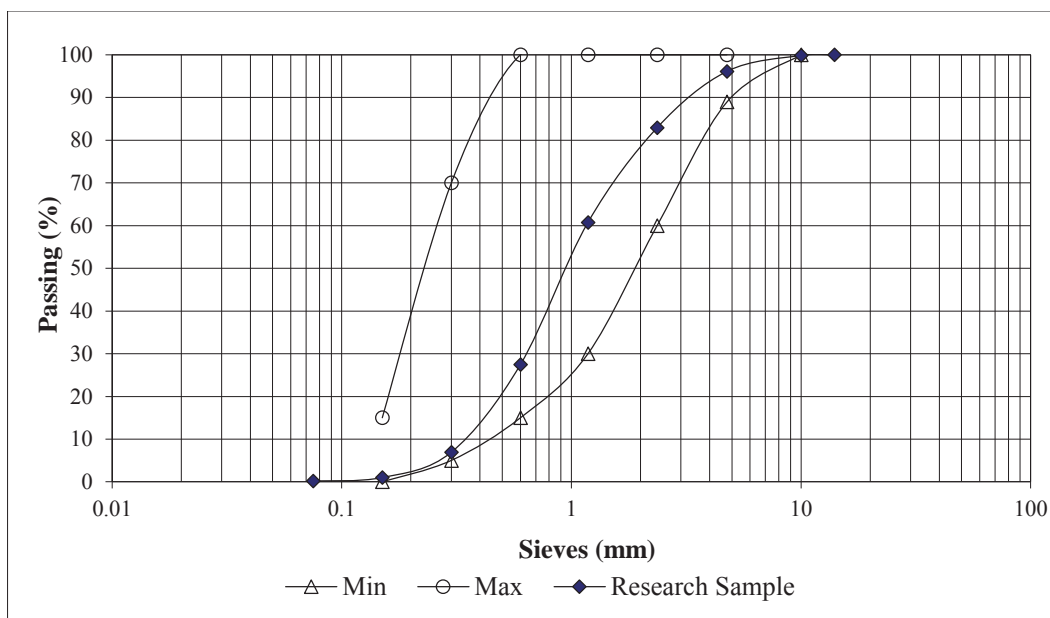


Figure 3.4: Graph of gradation of fine aggregates

iv) Results of hardened concrete

Table 3.5 shows a parametric study of the results of hardened concrete while Table 3.6 show a statistical analysis of the split tensile test result.

Table 3.5: Comparative study of results of hardened concrete of this work (laboratory) with models of other researchers.

Compressive Strength (average observed values) (N/mm <sup>2</sup> ) at 28 days	Split tensile strength in N/mm <sup>2</sup>					
	Average observed value	Lavanya & Jegan (2015) $f_{t1}=0.249f_{ck}^{0.772}$	ACI Committee 318(2014) $f_{t2}=0.56f_{ck}^{0.5}$	Anoglu et al (2006) $f_{t3}=0.387f_{ck}^{0.63}$	CEB-FIB (1991) $f_{t4}=0.3f_{ck}^{0.66}$	Gardner (1990) $f_{t5}=0.33f_{ck}^{0.667}$
44.89	4.38	4.70	3.75	4.25	3.70	4.17
53.87	5.26	5.41	4.11	4.77	4.17	4.71
62.85	6.13	6.09	4.44	5.26	4.61	5.22

Table 3.6: Statistical analysis of the results of this work (laboratory) and the output of models of other researchers.

	The ratios of split tensile strength of this work and the existing models				
	Mean	Standard deviation	Maximum	Minimum	Maximum-Minimum
This work	5.2567	0.87500	6.13	4.38	1.75
Lavanya & Jegan (2015)	5.4000	0.69505	6.09	4.70	1.39
ACI Committee 318(2014)	4.1000	0.34511	4.44	3.75	0.69
Anoglu et al (2006)	4.7600	0.50507	5.26	4.25	1.01
CEB-FIB (1991)	4.1600	0.45508	4.61	3.70	0.91
Gardner (1990)	4.7000	0.52507	5.22	4.17	1.05

The comparative results of Table 5 and 6 show that the output of laboratory work of this study shows a good agreement with published work of other authors. The split tensile strength is important because it a function of the initiation time utilized in this work hence its accuracy validation.

v) The critical penetration depth

The critical penetration depth is essential in calculating the initiation time of corrosion. Table 3.7 shows the parametric study of the critical penetration depth from Equations,19,20 and 21.

**Table 3.7** Parametric study of the critical penetration depth by different models

Sample Identity Characteristic strength and cover	Compressive strength( $f_{cu}$ ) (N/mm <sup>2</sup> )	Tensile strength( $f_t$ ) (N/mm <sup>2</sup> )	Critical penetration depth mm		
			Rodriguez et al.	Torres-Acosta & Sagues	Xu and Shayan
25 70mm N/mm <sup>2</sup> 60mm	44.89	4.38	0.0366	0.1190	0.8817
45mm			0.0292	0.0961	0.7714
30 70mm N/mm <sup>2</sup> 60mm			0.0181	0.0661	0.6061
30 70mm N/mm <sup>2</sup> 60mm	53.87	5.26	0.0167	0.119	0.9946
45mm			0.0093	0.0961	0.8703
35 70mm N/mm <sup>2</sup> 60mm			-0.0018	0.0661	0.6838
35 70mm N/mm <sup>2</sup> 60mm	62.85	6.13	-0.0029	0.1190	1.125
45mm			-0.010	0.0961	0.9844
			-0.0214	0.0661	0.7735

From the results of Table 3.7, it can be noted that in all the models the critical penetration depth decreases with decrease in concrete cover. This is due to less resistance of samples with smaller covers for the same tensile strength. The Torres-Acosta and Sagues model has no variation in the strength of concrete. It is also noted that in the Rodriguez et al. model, the critical penetration depth tends to below zero for concrete strength of 30N/mm<sup>2</sup> and 35N/mm<sup>2</sup>. This is due to non-consideration of the mechanical properties which affect the resistance of the concrete to cracking. The Xu and Shayan model considers the variants considered in this work and has been adopted in calculation of the initial corrosion period.

### 3.5 Results from Accelerated Corrosion Tests

#### 3.5.1 Results from this work and from other researchers.

For this work Equation 3 was used to calculate the rate of corrosion (mm/year) inserted in equation 2 for the current density from the measured time for evolution of the maximum of the crack width of 0.2mm. The values shown in Table 3.8 were used to determine the equilibrium potential in Equation 11.

**Table 3.8: Adopted values for determination of equilibrium potential( $E_{corr}$ )**

Parameter	Value	Reference source
$C(t = 0)$	0.005kg/m <sup>3</sup>	Bařzant, 1979a
$C_o(t = 0)$	8.576 x 10 <sup>3</sup> kg/m <sup>3</sup>	[67]
$E_{oa}$	-3V	Applied Voltage
$i_{oa}$	3.75 x 10 <sup>-4</sup> µA/cm <sup>2</sup>	Kranc, S., and Sag'u'es, A. [68]
$i_{oc}$	1.25 x 10 <sup>-5</sup> µA/cm <sup>2</sup>	
$E_{oc}$	3 V	Applied voltage

$\beta_a$	0.57 V	Calculated for an equivalent corrosion period
$\beta_c$	0.42 V	
$E_{corr}$	-1.52 V	From equation 11
$i_a$	14.71 $\mu\text{A}/\text{cm}^2$	From equation 8
$V_{corr}$	0.1705 mm/year	

$T_1$  is calculated from Equation 22 by converting to an equivalent rate of corrosion subsequently and subtracting from the duration of the test samples for propagation period applied in Vu and Stewart [33] and Li(2004a) [34] shown in table 3.8. Table 3.9 shows the critical penetration depth and current density for different samples.

$$T_1(\text{years}) = \frac{x_{crit}(\text{mm})}{0.0116I_{corr}\alpha(\mu\text{A}/\text{cm}^2)} \quad \text{and } T_2 = \text{Total corrosion time} - T_1$$

**Table 3.9:** The critical penetration depth and current density of samples tested.

Sample Identity	Cover (mm)	Mass of steel sample (gms)		Loss in weight (gms) measured	Critical penetration depth $X_{crit}$ (mm)	Duration in days		Corrosion current density ( $\mu\text{A}/\text{cm}^2$ )			
		before corrosion	after corrosion			$T_1$	$T_2$	This work	Vu and Stewart (2000)	Li(2004a)	
25 N/mm <sup>2</sup>	150mm diameter	70	371	360.4	10.6	0.8817	19	88	0.691	1.86	0.606
	130mm diameter	60	371	362.3	8.7	0.7714	16	70	0.729	2.204	0.520
	100mm diameter	45	371	363.2	7.8	0.6061	14	62	0.766	2.204	0.473
30 N/mm <sup>2</sup>	150mm diameter	70	371	361.5	9.5	0.9946	21	135	0.388	1.419	0.766
	130mm diameter	60	371	362.4	8.6	0.8703	19	123	0.303	1.674	0.729
	100mm diameter	45	371	363.4	7.6	0.6838	15	112	0.312	2.243	0.691
35 N/mm <sup>2</sup>	150mm diameter	70	371	361.6	9.4	1.125	24	162	0.237	1.164	0.833
	130mm diameter	60	371	362.4	8.6	0.9844	21	151	0.237	1.637	0.804
	100mm diameter	45	371	363.1	7.9	0.7735	17	141	0.227	1.836	0.785

**Fig.3.5** shows the relationship between corrosion current density against reinforcement cover and propagation period from Table 3.9.



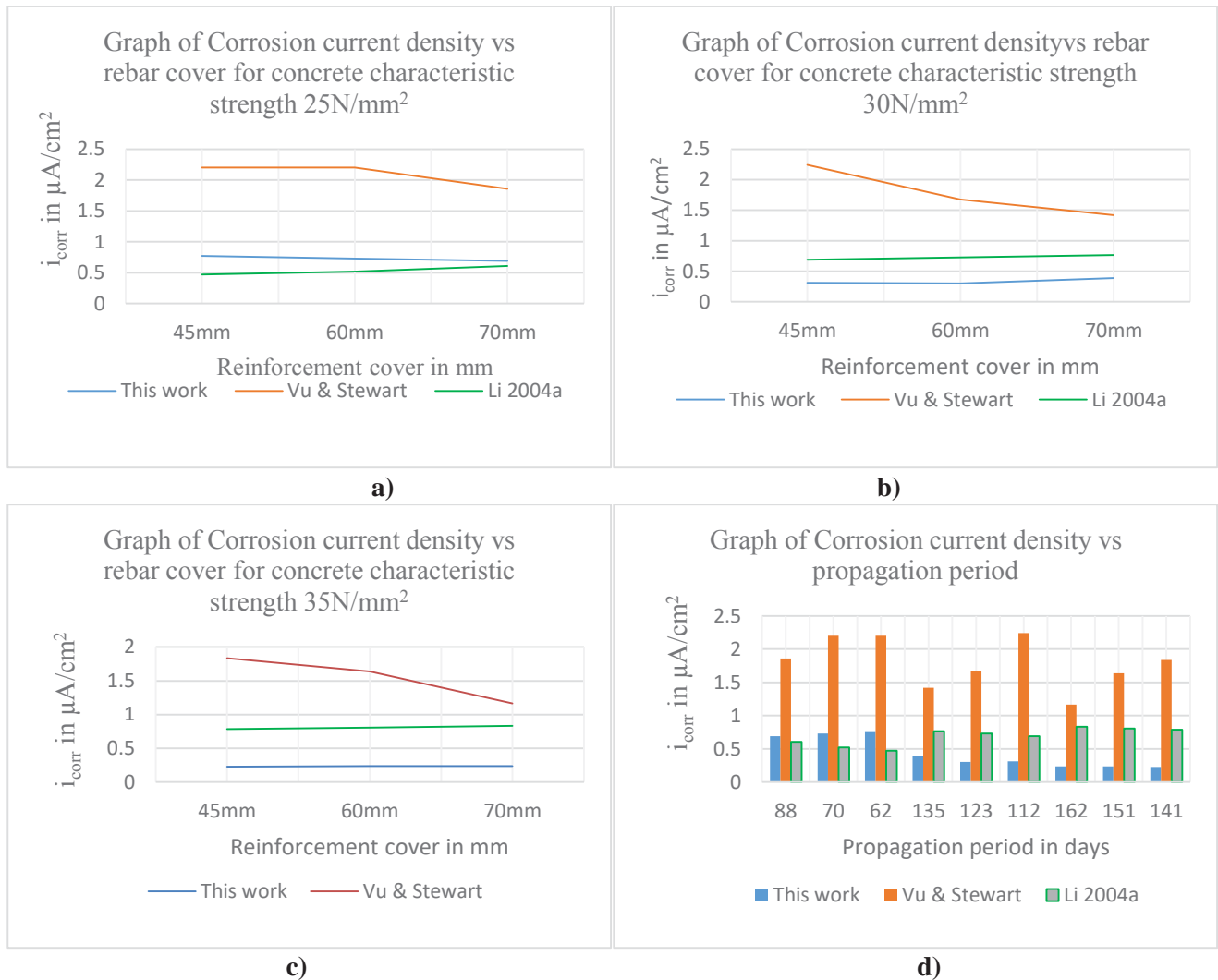


**Figure 3.5:** a)-c) Graph of Current density vs reinforcement cover for 25N/mm<sup>2</sup>, 30N/mm<sup>2</sup> and 35N/mm<sup>2</sup> and d) propagation period

From Fig. 3.5 graph a)-c), it is noted that the corrosion current density generally decreased with an increase in reinforcement cover in this work and the Vu and Stewart model in all concrete strengths considered. Corrosion current density depends on physical, electromechanical and mechanical processes where the cover thickness plays an important role. In the Li 2004a model the corrosion current density increases with an increase in concrete cover within the same concrete strength but remains constant for the same cover in different strengths. The Li 2004a model considers only the corrosion duration and neglects any other factor. From Fig. 3.5 d), it can be noted that the corrosion current density decreased with increase in propagation period in this study and in the Vu and Stewart. As the current density increases the rust expansion over the bar increases with a decrease in propagation period.

Fig. 3.6 shows the relationship between the critical penetration depth and the corrosion current density of this work and selected models.



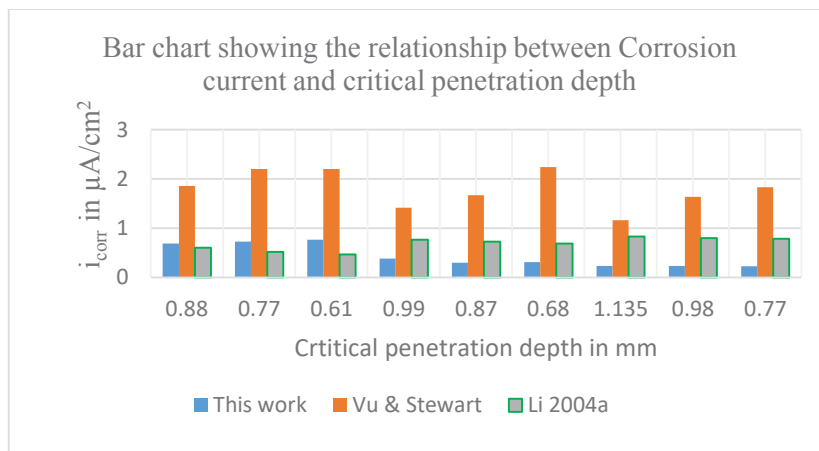


**Figure 3.6:** Relationship between the critical penetration depth and the corrosion current density of this work and selected models.

From Fig.3.6, the corrosion current density by Vu and Stewart is more than twice the results of this work. This is because not all factors affecting the corrosion rate are considered. In the Li 2004a model the corrosion current density decreases with decrease in critical penetration depth contrary to the results of this work. This model considers the corrosion period as the only factor influencing the corrosion current density, the influence of more factors may influence the results.

Fig.3.7 shows the relationship between corrosion current density and reinforcement mass loss for a crack width of 0.2mm

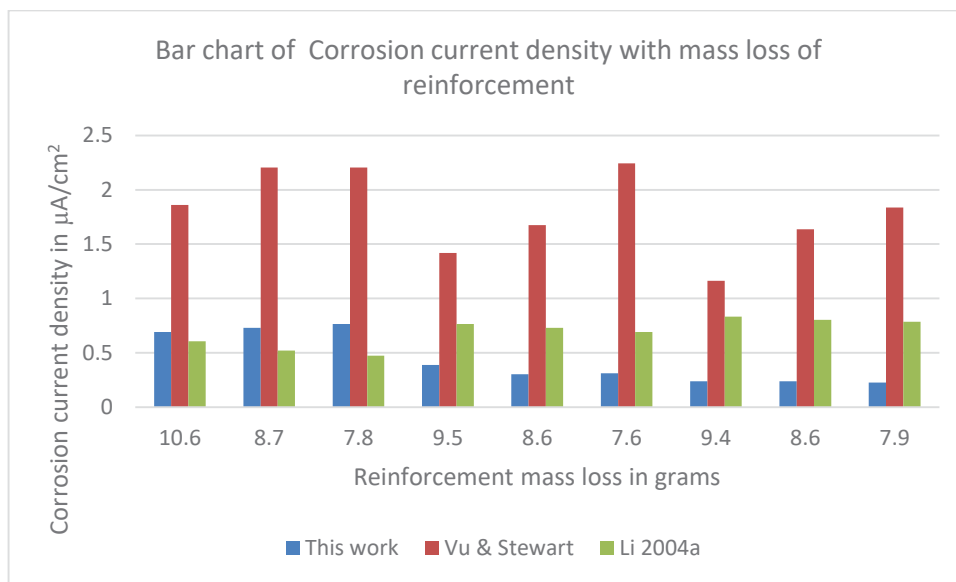


**Figure 3.7** Relationship between corrosion current density and reinforcement mass loss for a crack width of 0.2mm

From Fig.3.7, the corrosion current density by Vu and Stewart increases with decrease in reinforcement mass loss and is contrary to the results of this work and the Li 2004a model. Other than the corrosion period, the water cement ratio and the concrete cover, the mechanical properties of the concrete may influence the rate of corrosion current density and reinforcement mass loss.

The correlation of the result of this work and those of the Vu and Stewart (2000) model have been used for generation of the proposed current density model for the propagation period for this study.

**3.5.2 Statistical relationship of the result of this work and those of Vu and Stewart (2000).**

Table 9 shows the correlation of the result of this work and those of Vu and Stewart (2000)

**Table 3.9:** Correlations of the results of this work and those of Vu and Stewart

		This work	Vu & Stewart
Kendall's	This work	Correlation Coefficient 1.000	0.400
		Sig. (2-tailed) 0.000	0.140
	Vu	&Correlation Coefficient 0.400	1.000
	Stewart	Sig. (2-tailed) 0.140	0.000
Spearman's rho	This work	Correlation Coefficient 1.000	0.546
		Sig. (2-tailed) 0.000	0.128
	Vu	&Correlation Coefficient 0.546	1.000
	stewart	Sig. (2-tailed) 0.128	0.000

From Table 3.9, the result of this work has no significantly correlation with the results of Vu and Stewart model. A modified Vu and Stewart model is proposed for this work.

**3.5.3 Proposed model for this work**

Fig.3.8 shows a Graph for the relationship between this work and the Vu and Stewart model.

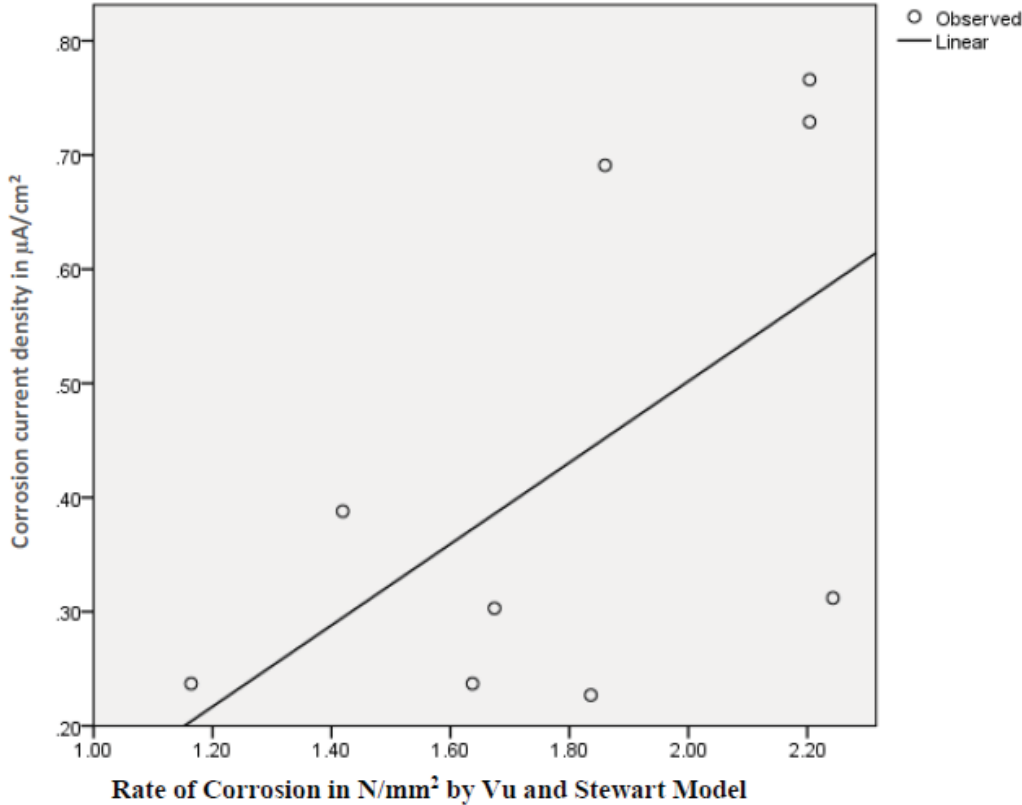


**Figure 3.8:** Relationship of the results of this work and those of Vu and Stewart (2000)

From Fig.3.8, a coefficient of 0.356, standard error of 0.028, Table 3.10 shows the statistical comparison between the output of this work, the Vu and Stewart (2000) and the proposed model.

**Table 3.10:** Statistical Relationship between the results of this work, the Vu model and the proposed model

	Mean	Std	Std. Error	Sig. (2-tailed)	95% Confidence Interval	
	difference		Mean		Lower	Upper
This work	0.4322	0.22855	0.07618	0.010	0.2565	0.6079
Vu and Stewart	1.8046	0.37408	0.12469	0.001	1.5170	2.0921
Proposed model	0.6411	0.13299	0.04433	0.001	0.5389	0.7433

From table 3.10, the proposed model output for this work compares well with the output of this research and therefore the corrosion current density can be obtained from equation 34:

$$i_{corr}(t_2) = \left[ 13.46 (1 - w/c)^{-1.64} (1 + t_2)^{-\frac{1}{3}} \right] / d \quad (\mu\text{A}/\text{cm}^2) \quad (34)$$

### 3.5.3 Proposed service Life model of reinforced concrete water conveyancing structures

#### a) Crack Initiation Period ( $T_1$ ) and propagation ( $T_2$ )

This is the time to first visible crack and is obtained from Equation 35;

$$T_1 = \left( \frac{f_t(c+d)(1+\nu)}{E_{eff}d\beta} \right) \times 10^{-3} \times \left( 0.0116 I_{corr} \left( \frac{\mu\text{A}}{\text{cm}^2} \right) \right)^{-1} (\text{years}) \quad (35)$$

The propagation period from experimental work was obtained from total period for 0.2mm crack evolution minus crack initiation period( $T_1$ ).

#### b) Crack propagation Period ( $T_2$ )

Equation 36 is proposed for calculation of  $T_2$  in days and compared with the experimental results and models of others researches as shown in table 3.11.

$$T_2 = \left[ \rho_{rust} \left( L \pi \left[ \frac{Cf_t}{E_{eff}} \left( \frac{a^2+b^2}{b^2-a^2} + \nu_c \right) + t_1 \right] d + \frac{M_{st}}{\rho_{st}} \right) \right]^2 \frac{4.9691\alpha}{di_{corr}} + \left[ \left( \frac{\omega-0.05}{\beta} + x_{crit} \right) \frac{f_t}{0.07192i_{corr}k} \right] \quad (36)$$

$T_2$  can be defined into two levels;

$$T_2 = T_{p1} + T_{p2}$$

$$T_{p1} = \left[ \rho_{rust} \left( L \pi \left[ \frac{Cf_t}{E_{eff}} \left( \frac{a^2+b^2}{b^2-a^2} + \nu_c \right) + t_1 \right] d + \frac{M_{st}}{\rho_{st}} \right) \right]^2 \frac{5.846\alpha}{di_{corr}} \quad (37)$$

$$T_{p2} = \left[ \left( \frac{\omega-0.05}{\beta} + x_{crit} \right) \frac{f_t}{0.07192i_{corr}k} \right] \quad (38)$$

Where

L =reinforcement length exposed to corrosion(cm)

C= Concrete cover in cm

$\omega$  =characteristic crack width taken as 0.2mm

$x_{crit}$ =critical penetration depth (mm)

$\beta$ = Coefficient taken as 0.01125

$t_1$  =0.002 cm

$\rho_{rust} = 3.6 \text{ g}/\text{cm}^3$

$\nu_c$  = Concrete poison's ratio taken as 0.2

$E_{eff}$  =effective elastic modulus= $E/(1+\phi)$  (N/mm<sup>2</sup>)

E =Elastic modulus (N/mm<sup>2</sup>)

$\phi$  = concrete creep coefficient

k = Current density factor taken as 10.

$f_t$  = Concrete tensile strength (N/mm<sup>2</sup>)

$\alpha$  = relation between atomic weight of iron (55.8) and the molecular weight of the rust product taken as 0.523.

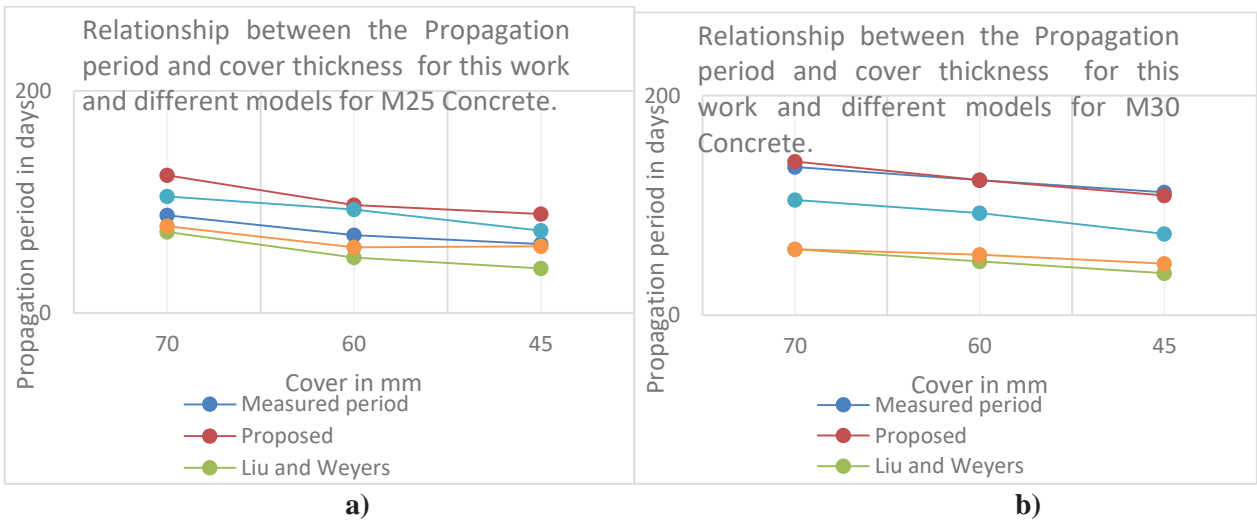
a = the inner radius [(d+2t<sub>1</sub>)/2] (cm)

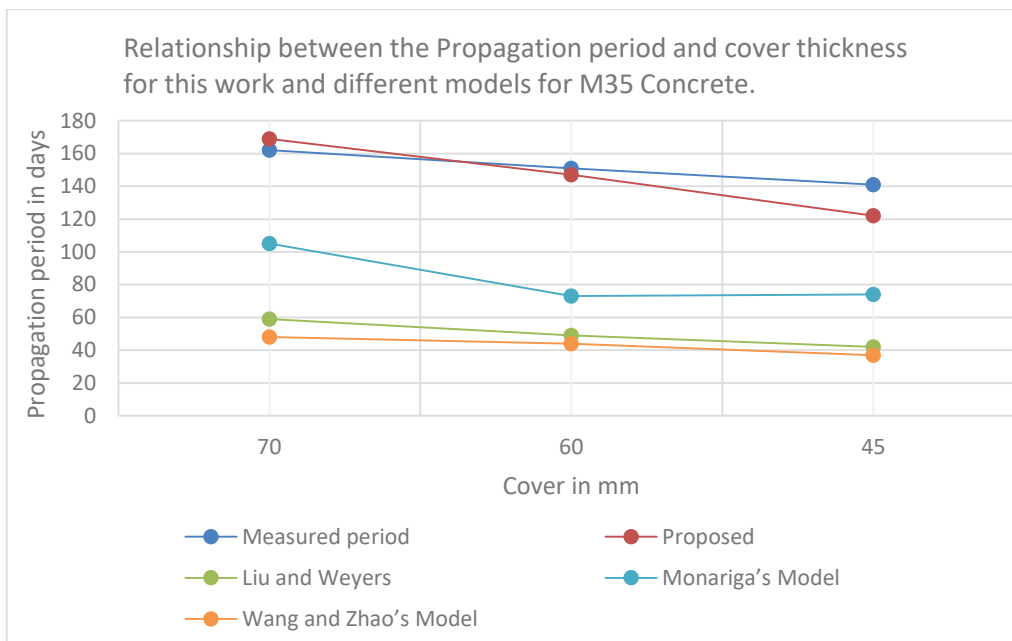
b = the outer radius [C+(d+2t<sub>1</sub>)/2] (cm)

**Table 3.11** shows a parametric study of the propagation period of experimental work with a proposed model and models of other researchers.

Sample Identity		Reinforcement cover in mm	Mass loss of steel sample after corrosion (gms)	T <sub>2</sub> days				
				Measured period	Proposed Model	Liu and Weyers Model	Monariga's Model	Wang and Zhao's Model
25 N/mm <sup>2</sup>	150mm diameter	70	10.6	88	124	73	105	78
	130mm diameter	60	8.7	70	97	50	93	59
	100mm diameter	45	7.8	62	89	40	74	60
30 N/mm <sup>2</sup>	150mm diameter	70	9.5	135	140	60	105	60
	130mm diameter	60	8.6	123	123	49	93	55
	100mm diameter	45	7.6	112	109	38	74	47
35 N/mm <sup>2</sup>	150mm diameter	70	9.4	162	169	59	105	48
	130mm diameter	60	8.6	151	147	49	73	44
	100mm diameter	45	7.9	141	122	42	74	37

Figure 3.8 shows the relationship between the reinforcement cover and the propagation period results of this work, the proposed model and the results of other models as shown in Table 3.11.





c)

**Figure 3.8:** Graph a)-c) Relationship between the reinforcement cover and the propagation period results of this work, the proposed model and the results of other models as shown in table 3.11

From Table 3.11 and Figure 3.8, the propagation period reduced with reduction of concrete cover and strength in the study results and all models considered. This is because it takes a shorter period for chloride ions to percolate from the surface to the reinforcement bar in a smaller cover and the contrary is true for larger covers. In stronger concrete samples, the voids are more compressed reducing the rate of percolation of the aggressive chloride ions responsible for corrosion. The proposed model has a high correlation with the results of this work comparable to the other models considered. This is because after crack initiation considered approximately 0.05mm, the models have not

**3.5.4 Application and limitation of the proposed model.**

Figure 3.9 shows the procedure to estimate the corrosion points of initiation and propagation points for service life prediction.

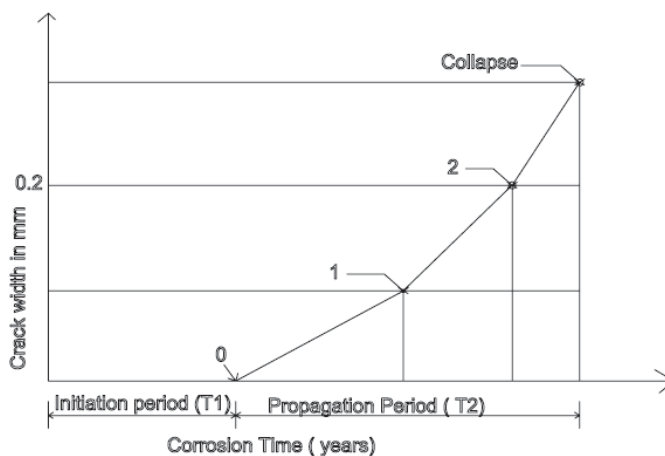


**Figure 3.9:** Corrosion initiation and propagation points.

Point 0: is the initiation period calculated from Equation 35 and is associated with loss of the passivation layer.

Point 1: is the propagation period calculated using  $T_{p1}$  and is related to crack width of approximately 0.5mm.

Point 2: is the propagation period calculated using  $T_{p2}$  and is related to crack expansion for maximum acceptable width.

This model is limited for use for water conveyancing structures.

#### 4.0 Conclusion

From the results of this research, the following conclusions can be drawn;

- The rate of corrosion is affected by the compressive strength, split tensile strength and reinforcement cover.
- Li(2004a) model does not correlate with the results of this work and those of Vu and Stewart (2000) model.
- A service life model for water conveyancing structures has been proposed taking account of the initiation and propagation period.

#### 5. References

- [1] Bolzoni, F., Coppola, L., Goidanich, S., Lazzari, L., Ormellese, M., and Pedferri, M. P. (2004), "Corrosion inhibitors in reinforced concrete structures," Part 1: Preventative technique. Corrosion Engineering, Science and Technology, 39(3), 219-228.
- [2] Lee, S. K., Krauss, P. D., and Virmani, Y. P. (2005), "Resisting corrosion," Public Roads, 68(6), 58-63.
- [3] Xu J., Jiang L. and Wang Q. (2009), "Finite element model of reinforcement corrosion in concrete," Water Science and Engineering, 2(2), 71-78.
- [4] Talbot D., Talbot J. (1998), "Corrosion Science and Technology," CRC Press, London.
- [5] Bertolini L., Elsener B., Pedferri P. and Polder R. (2004), "Corrosion of Steel in Concrete," Wiley.
- [6] ACI Committee 222(2005), Protection of metals in concrete against corrosion, ACI 222R-01, ACI Manual of Concrete Practice.
- [7] Torres-Acosta, A. A., Navarro-Gutierrez, S. and Teran-Guillen. (2007), "Residual flexure capacity of corroded reinforced concrete beams," Engineering Structures, 29, 1145–1152.
- [8] Zhang, R., Castel, A. and Francois, R. (2009), "Serviceability limit state criteria based on steel–concrete bond loss for corroded reinforced concrete in chloride environment," Materials and Structures.
- [9] Torres-Acosta, A. A., Fabela-Gallegos, M. J., Munoz-Noval, A., Vazques-Vega, D. and Hernandez-Jimenez, J. R. (2004), "Influence of corrosion on the structural stiffness of reinforced concrete beams," Corrosion. 60(9): 862-872.
- [10] Malumbela, G., Alexander, M. and Moyo, P. (2009b), "Steel corrosion of RC structures under sustained service loads – a critical review," Engineering Structures. 31: 2518-2525.

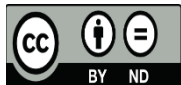
- [11] Liu Y. and Weyers, R.E. (1998), "Modeling the Time-to-Corrosion Cracking in Chloride Contaminated Reinforced Concrete Structures," *ACI Materials Journal*. 95(6): 675-681.
- [12] El Maaddaway, T. and Soudki K. (2007), "A model for prediction of time from corrosion initiation to corrosion Cracking," *Cement and Concrete Composites*. 29(3): 168-175.
- [13] Andrade, C., and Alonso, C. (1996a), "Durability design based on models for corrosion rates," In H. Jennings, J. Kropp, and K. Scrivener (Eds.), *The Modelling of Microstructure and Its Potential for Studying Transport Properties and Durability* (pp. 473–492). The Netherlands: Kluwer Academic Publishers.
- [14] Andrade, C., and Alonso, C. (1996b), "Progress on design and residual life calculation with regard to rebar corrosion of reinforced concrete," In N. Berke, E. Escalante, C. Nmai, and D. Whiting (Eds.), *Techniques to Assess the Corrosion Activity of Steel Reinforced Concrete Structures*, ASTM STP 1276 (pp. 23–40).
- [15] Rodriguez, J., Ortega, L., Casal, J., and Diez, J. (1996), "Corrosion of reinforcement and service life of concrete structures," In C. Sjöström (Ed.), *Durability of Building Materials and Components*, 7 (1), 117–126.
- [16] Tran, K., Nakamura, H., Kawamura, K., Kunieda, M. (2011), "Analysis of crack propagation due to rebar corrosion using RBSM," *Cement Concrete Comp*, 33:906-17.
- [17] Toongoenthong, K., Maekawa, K. (2005), "Simulation of coupled corrosive product formation, migration into crack and propagation in reinforced concrete," *J Adv Concr Technol*, 3(2):253-65.
- [18] Liu, Y., Weyers, R.E. (1998), "Modeling the time-to-corrosion cracking in chloride contaminated reinforced concrete structures," *ACI Mater J*, 95(6):675-80.
- [19] Luković, M., Pacheco, J., Schlangen, E. (2013), "Cracking of the concrete cover due to reinforcement corrosion: A two-dimensional lattice model study," *Construction and Building Materials*, 44:626–638.
- [20] Wong, H., Zhao, Y.X., Karimi, A.R., Buenfeld, N.R., Jin, W.L. (2010), "On the penetration of corrosion products from reinforcing steel into concrete due to chloride-induced corrosion," *Corros Sci*, 52:2469-80.
- [21] Martín-Peréz B. (1999), "Service life modelling of R.C. highway structures exposed to chlorides," Toronto: University of Toronto.
- [22] Balafas, I., Burgoyne, C.J. (2011), "Modeling the structural effects of rust in concrete cover," *J Eng Mech-ASCE*, 137(3):175-85.
- [23] Pantazopoulou, S., Papoulia, K.D. (2001), "Modeling cover-cracking due to reinforcement corrosion in RC structures," *J Eng Mech-ASCE*, 27(4):342-51.
- [24] Duracrete (2000), "Probabilistic Performance based Durability Design of Concrete Structures," The European Union–Brite EuRam III, BE95-1347/R17, CUR, Gouda, The Netherlands.

- [25] RILEM TC 154-EMC (2003), "Electrochemical Techniques for Measuring Metallic Corrosion," *Materials and Structures / Matériaux et Constructions*, 37, 623-643.
- [26] Ahmad S. (2003), "Reinforcement corrosion in concrete structures, its monitoring and service life prediction: A Review," *Cement and Concrete Composites*, 25(4-5), 459-471.
- [27] Montemor, M. F., Simoes, A. M. P., and Salta, M. M. (2000), "Effect of fly ash on concrete reinforcement corrosion studied by EIS," *Cement and Concrete Composites*, 22(3), 175-185.
- [28] Sathiyarayanan, S., Natarajan, P., Saravanan, K., Srinivasan, S., and Venkatachari, G. (2006), "Corrosion monitoring of steel in concrete by galvanostatic pulse technique," *Cement and Concrete Composites*, 28(7), 630-637.
- [29] Andrade, C., and Alonso, C. (2004), "Test methods for on-site corrosion rate measurement of steel reinforcement in concrete by means of the polarization resistance method," *Materials and Structures*, 37(9), 623-643.
- [30] Nikunj N. S. Vanpariya K. (2019), "Evaluation of corrosion rate in steel reinforcement of RCC," *International Research Journal of Engineering and Technology*, 6(11), 1030-1034.
- [31] RILEM TC 154-EMC (2003), "Electrochemical Techniques for Measuring Metallic Corrosion' *Materials and Structures / Matériaux et Constructions*," 36, 461-471
- [32] Yalcyn, H., and Ergun, M. (1996), "The prediction of corrosion rates of reinforcing steels in Concrete," *Cement and Concrete Research*, 26(10), 1593-1599.
- [33] Vu, K.A.T. & Stewart, M.G. (2000), "Structural reliability of concrete bridges including improved chloride-induced corrosion models," *Structural Safety*, 22(4), 313-333.
- [34] Li, C.Q. (2004a), "Reliability based service life prediction of corrosion affected concrete structures," *Journal of Structural Engineering* 130(10), 1570-1577.
- [35] Tuutti, K. 1982, *Corrosion of Steel in Concrete*, Swedish Cement and Concrete Research Institute, Fo 4.82, Stockholm.
- [36] Rasheeduzzafar, Dakhil, F. H., Bader, M. A., & Mukarram Khan, M. (1992). "Performance of Corrosion-Resisting Steels in Chloride-Bearing Concrete," *ACI Materials Journal*, Vol. 89, No. 5, pp. 439-448.
- [37] State of the art- Modelling of reinforcement corrosion in concrete. Coin Project Report 7 - 2008
- [38] Shayan, A., Xu, A. (2016), "Relationship between Reinforcing Bar Corrosion and Concrete Cracking," *Aci Materials Journal* 113(1).
- [39] Torres-Acosta, A. A., & Sagues, A. A. (2004). "Concrete Cracking by Localized Steel Corrosion--Geometric Effects," *ACI Materials Journal*, 101(6), 501-507



- [40] El Hajj, Peter. (2015). Probabilistic Modelling of Multiphase Degradations for Maintenance Optimization of Infrastructures in Civil Engineering. Thesis for: Doctor of Philosophy in Civil Engineering
- [41] Teplý B., Vorechovská, D.)2012), “Limit states, reliability and modelling,”*Journal of Advanced Concrete Technology*, 10(11).
- [42] Andrade., Alonso, C. (1996), “Corrosion rate monitoring in the laboratory and on-site,” *Construction and Building Materials*, 10(5), 315-328
- [43] Andrade, C., Sanchez, J, Fulla, J., Rebolledo, N., Tavaré, S. F. (2012) On-site corrosion rate measurements:3D simulation and representative values. *Mater Corros* 63(12):1154–1164
- [44] Andrade, C. (2017), “Reliability analysis of corrosion onset: initiation limit state,” *J Struct Integr Maint* 2(4):200–208
- [45] Bazant, Z. (1979b). Physical model for steel corrosion in concrete sea structures—application. *Journal of the Structural Division*, 105(ST6), 1155–1166.
- [46] Scrivener, K.L., Crumbie, A.K., Laugesen, P. (2000), “The interfacial transition zone (ITZ) between cement paste and aggregate in concrete,” *Interface Sci.*,12(4):411-21.
- [47] Shane, J.D., Mason, T.O., Jennings, H.M., Garboczi, E.J., Bentz, D.P. (2000), “Effect of the interfacial transition zone on the conductivity of portland cement mortars,” *J Am Ceram Soc.*,83(5):1137-44.
- [48] Yang, C.C. (2005), “Effect of the percolated interfacial transition zone on the chloride migration coefficient of cement-based materials,” *Mater Chem Phys.*,91(2-3):538-44.
- [49] Morinaga,S. (1989), “Prediction of Service Lives of Reinforced Concrete Buildings Based on Rate of Corrosion of Reinforcing Steel,” Special report of the institute of Technology, Japan, Skimiza Corporation.
- [50] Wang, X.M., Zhao, H.Y., 1993. The residual service life prediction of RC structures. In: Nagataki, S. (Ed.), *Durability of Building Materials and Components*, 6, 1107–1114.
- [51] Jones A. (2008) Eurocode 2 – Design of concrete structures: Part 3. Liquid-retaining and Containment Structures. Dissemination of information workshop, Brussels February 2008.
- [52] Kenya Bureau of Standards,KS EAS 18-1:2001-Cement Part 1:Composition, Specification and Conformity Criteria for Common Cements. Kenya Bureau of Standards, Nairobi,2005.
- [53] Kumbhar, P.D. and Murnal, P.B. (2012), “Assessment of Suitability of Existing Mix Design Methods of Normal Concrete for Designing High Performance Concrete,” *International Journal of Civil and Structural Engineering*, 3,158-167.
- [54] Neville M. (1996). “Properties of Concrete,” Pitman Publishing Company,” London, UK.
- [55] Neville A.M., Brooks J.J. (2012). “Concrete Technology,” Longman, London, UK.

- [56] Shetty M. S. Concrete Technology Theory and Practice S. Chand & Company Ltd. Ram Nagar, New Delhi.
- [57] Neville A. M. (2011), Properties of Concrete, 5th edition. Pearson Education Limited.
- [58] Arum gam, B. (2014), “Effect of Specific Gravity on Aggregate Varies the Weight of Concrete Cube,” International Journal of Civil Engineering, 1(3),1-9.
- [59] British Standard Institutes, BS EN 1097-6:2000, Tests for mechanical and physical properties of aggregates. Determination of particle density and water absorption, British Standard Institution, London
- [60] British Standard Institutes, BS 882:1992, Specification for aggregates from natural sources for concrete
- [61] British Standard Institutes, BS 8007:1987, Code of practice for the design of concrete structures for retaining aqueous liquids
- [62] Zerdi A.T. (2014). Strength Exhibition of M25 Grade Concrete with Limestone Quarry Dust Utilization for Fine Aggregates, Global Journal of Research Analysis International,5(1).
- [63] ASTM C117, "Standard Test Method for Materials finer than 75-um (No. 200) sieve in mineral aggregates by washing." American Society for Testing and Materials, 1995.
- [64] BS 882; - Specification for aggregates from natural sources for concrete. British Standards Institute, London United Kingdom, 1992.
- [65] ASTM C40, "Standard Test Method for effect of organic impurities in fine aggregates on strength of mortar," American Society for Testing and Materials ASTM International, 2004.
- [66] KS EAS 18. Cement Standard - Part 1: Composition, Specifications and Conformity Criteria. KEBS, Kenya. 2001.
- [67] Bažant, Z. (1979b),” Physical model for steel corrosion in concrete sea structures application,” Journal of the Structural Division, 105(ST6), 1155–1166.
- [68] Kranc, S., and Sag˘ues, A. (1994), “Computation of reinforcing steel corrosion distribution in concrete marine bridge substructures,” Corrosion, 50(1), 50–61.



This work is licensed under a Creative Commons Attribution Non-Commercial 4.0 International License.



## Correlation of tensile strength and corrosion initiation period of reinforced concrete

Philip Mogire, John Mwero, Silvester Abuodha & Geoffrey Mang'uriu |

To cite this article: Philip Mogire, John Mwero, Silvester Abuodha & Geoffrey Mang'uriu | (2021) Correlation of tensile strength and corrosion initiation period of reinforced concrete, Cogent Engineering, 8:1, 1999039, DOI: [10.1080/23311916.2021.1999039](https://doi.org/10.1080/23311916.2021.1999039)

To link to this article: <https://doi.org/10.1080/23311916.2021.1999039>



© 2021 The Author(s). This open access article is distributed under a Creative Commons Attribution (CC-BY) 4.0 license.

---



Published online: 17 Nov 2021.

---



Submit your article to this journal [↗](#)

---



View related articles [↗](#)

---



View Crossmark data [↗](#)

---



## CIVIL & ENVIRONMENTAL ENGINEERING | RESEARCH ARTICLE

# Correlation of tensile strength and corrosion initiation period of reinforced concrete

Philip Mogire<sup>1\*</sup>, John Mwero<sup>2</sup>, Silvester Abuodha<sup>2</sup> and Geoffrey Mang'uriu<sup>2</sup>

Received: 25 May 2021

Accepted: 10 October 2021

\*Corresponding author: Philip Mogire, Department of Civil and Construction Engineering, University of Nairobi, Nairobi, Kenya  
E-mail: [philosiem@yahoo.com](mailto:philosiem@yahoo.com)

Reviewing editor: Sanjay Kumar Shukla, School of Engineering, Edith Cowan University, Perth, Australia

Additional information is available at the end of the article

**Abstract:** Service life of reinforced concrete constitutes initiation and propagation period. Tensile strength is among the mechanical hardened properties of concrete that influence the corrosion initiation. This research work examines the relationship between split tensile strength and corrosion initiation period of reinforced concrete. The physical and chemical properties of the materials were investigated for compliance for use in reinforced concrete. Concrete of three classes M25, M30 and M35 was cast. For each class, 9 specimens for compression and split tensile strength respectively were prepared and tested at 7, 14 and 28 days. A model for tensile strength was proposed and compared with other models. A parametric study of the critical penetration depth, -a component of the corrosion initiation period, was done using published models. From the results of the study, the proposed and published tensile strength models compare well. It was also noted that the critical penetration depth increases with an increase in tensile strength. The corrosion initiation period linearly increases with the split tensile strength. The tensile strength of concrete can be considered as an input parameter in the initiation period in corrosion service life models.



Philip Mogire

### ABOUT THE AUTHORS

Philip Mogire holds a B.Sc.(Civil) and M.Sc.in Civil Engineering (Structural). Currently, he is pursuing a PhD in Civil Engineering at the University of Nairobi, Kenya. He worked as a design engineer for small hydropower projects for three years. He has published several papers in international Journals. He is currently a Projects Engineer in Small Hydro Power projects at VS Hydro (K) Ltd and a Sessional Assistant Lecturer in Structural Engineering at the Technical University of Kenya. His research interests include service life modeling for concrete structures, application of nanotechnology in concrete materials and smart concrete structures.

John Mwero is a Senior Lecturer in the department of Civil and Construction Engineering at the University of Nairobi.

Silvester Abuodha is an Associate Professor in the department of Civil and Construction Engineering at the University of Nairobi.

Geoffrey Mang'uriu is a Professor of Civil Engineering in the department of Civil, Construction and Environmental Engineering at Jomo Kenyatta University of Agriculture and Technology.

### PUBLIC INTEREST STATEMENT

Currently, there is an increased construction of water infrastructure projects for supply of clean energy, consumption or irrigation in developing countries. These projects constitute reinforced concrete components as conveyancing, traffic support or housing structures. The performance of the structures at any age within their lifespan should be able to be defined for optimal performance and scheduled rehabilitations. Most codes of practice define a design life but not a structural behavior at a specific age. Corrosion initiation is affected by the hardened properties of concrete. While there is a huge investment in constructing the projects, the risks associated with accidents from their performance are high. It is against this background that the researchers investigated the relationship between the tensile strength and corrosion initiation of reinforced concrete. The results of this study confirmed a relationship between tensile strength and corrosion initiation period of reinforced concrete. The outcome of this research will help engineers in modeling the service life of reinforced concrete water structures.

**Subjects:** Materials Science; Civil, Environmental and Geotechnical Engineering; Design

**Keywords:** Tensile strength; critical penetration depth; corrosion initiation period

### 1. Introduction

Understanding degradation due to corrosion of reinforced concrete water structures is crucial in modelling service life. In a service environment, carbonation and chloride ingress (aggressive agents) will occur until steel corrosion initiates (Huang & Goodwin, 2019) and these are the most relevant damaging mechanisms in reinforced concrete structures (Šmilauer et al., 2013). Carbonation induces a generalized corrosion while the presence of chloride ions in the surroundings of the steel provokes localized corrosion (Yihui et al., 2014). During service life, corrosion of reinforcement can be divided into initiation and propagation phase described as shown in Figure 1 (Mogire et al., 2020).

The initiation period ( $t_i$ ) is the time taken by the aggressive agents to reach the reinforcement or passivate the steel. Estimation of corrosion initiation period in RC structures is crucial for minimizing both maintenance costs and failure risks (Nguyen et al., 2017). As part of the design life, if a certain amount of steel deterioration until unacceptable degree of corrosion is reached is considered, then the propagation ( $t_p$ ) period is part of the service life ( $t_i$ ) formulated as:

$$t_i = t_i + t_p \tag{1}$$

Many achievements on corrosion initiation models due to chloride ingress by diffusion have been reported (Arteaga et al., 2011; Khan et al., 2017; Šmilauer et al., 2017). The corrosion starts when the concentration of chlorides exceeds a critical value in the place of reinforcement restricted to:

$$C(x, t) = C_s \left[ 1 - \operatorname{erf} \left( \frac{x}{2\sqrt{D_m(t)f(w)t}} \right) \right] \tag{2}$$

where  $C_s$  is the chloride content at surface [ $\text{kg}/\text{m}^3$ ],  $D_m(t)$  is the mean (averaged) diffusion coefficient at time  $t$  [ $\text{m}^2/\text{s}$ ],  $x$  is the distance from the surface in [m] and  $f(w)$  introduces acceleration by cracking (equals to one for a crack-free concrete).  $C_s$  and  $C(x, t)$  can be related to a concrete volume or to a binder mass.

The initiation period is influenced by the mechanical properties of concrete and environmental factors. Reinforcement cover depth and porosity are the two main concrete actors. Cover plays a role because carbonation and chloride ingress are diffusion processes whose rate of

**Figure 1.** Initiation and propagation phase (Mogire et al., 2020).

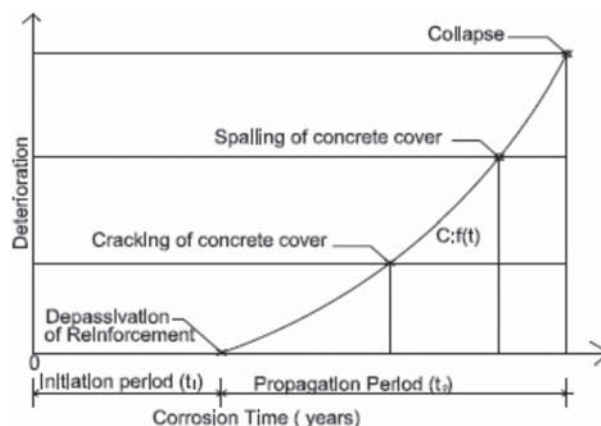
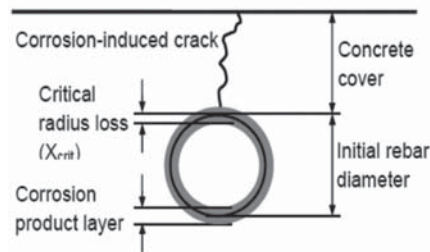


**Figure 2.** Critical penetration depth or the critical radius loss ( $X_{crit}$ ) (Mogire et al., 2018).



development is a power function of time. Environmental actions are responsible for the lack of durability of reinforcement as they are the source of temperature cycles, water supply through rain and snow or as a conveyance system, carbonation and chlorides.

During propagation period, the corrosion rate for chlorides depends on the corrosion current density ( $i_{corr}$ ) is determined based on Faraday's law (DuraCrete, 2000; Rodriguez et al., 1996) as:

$$\frac{dx_{corr}}{dt} = 0.0116i_{corr}(t) \quad (3)$$

Where  $\frac{dx}{dt}$  is the average corrosion rate in the radial direction [ $\mu\text{m}/\text{year}$ ],  $i_{corr}$  is corrosion current density [ $\mu\text{A}/\text{cm}^2$ ] and  $t$  is calculated time after the end of initiation period [years].

By integration of Equation (3),

$$x_{corr} = \int_{t_{ini}}^t 0.0116i_{corr}(t)R_{corr}dt \quad (4)$$

where  $x_{corr}$  is the total amount of corroded steel in radial direction [mm] and  $R_{corr}$  is parameter, which depends on the type of corrosion [-]. For uniform corrosion (carbonation)  $R_{corr} = 1$ , corrosion (chlorides)  $R_{corr} = <4; 5.5>$  according to (Darmawan & Stewart, 2007). From Equation (4):

$$t_{ini} = \frac{29t - 2500x_{corr}}{29i_{corr}R_{corr}} \quad (5)$$

Andrade et al. (2010) have developed Equation (6) for calculating corrosion-induced crack widths of the concrete cover in natural environments based on experimental test results. This equation establishes a relationship between the crack width at any time in corrosion progression with original radius loss.

$$w = k \left( \frac{x_{corr}}{C/\phi} \right) \quad (6)$$

where  $w$  is the crack width (mm),  $c$  is the reinforcement cover (mm),  $\phi$  is the original diameter of the bar (mm),  $x_{corr}$  is the radius loss (mm) and  $k$  is a factor the value of which is derived from experimental results, taken as 9.5.

Vu and Stewart (RILEM TC 154-EMC, 2003) developed an empirical model which gives the corrosion current density at the start of the propagation period (at time  $t_1$ ) as a function of water cement ratio and cover thickness as shown in Equation (7):

$$i_{corr}(t_1) = 37.8(1 - w/c)^{-1.64}/d(\mu\text{A}/\text{cm}^2) \quad (7)$$

Where  $w/c$  is the water cement ratio obtained from the Bolomey's formula is the cover thickness (mm).

Substituting Equation (6) into 5 and  $t = 0$  for the start of the propagation period, the initiation period can be obtained from Equation (8).

$$t_{ini} = \left| \frac{2500x_{corr}}{29i_{corr(t_1)}R_{corr}} \right| \tag{8}$$

The critical penetration depth ( $x_{crit}$ ) is the amount of radius loss of reinforcement during corrosion that initiates a longitudinal crack on the surface of reinforced concrete as shown in Figure 2. (Mogire et al., 2018)

Substituting  $x_{crit} = x_{corr}$  for corrosion initiation period in Equation (7):

$$t_{ini} = \left| \frac{2500x_{crit.}}{29i_{corr(t_1)}R_{corr}} \right| \tag{9}$$

None of the published literature shows the effect of the split tensile strength of concrete on corrosion initiation. This paper presents the results of the study to establish a correlation between the initiation period and the split tensile strength of concrete.

## 2. Materials and method

This research was conducted at the University of Nairobi Structures/ Concrete laboratory where the physical properties of the materials, sample preparation and testing were done. The chemical properties of the materials were done at State Department of Infrastructure in the Ministry of Transport, Infrastructure, Housing and Urban Development of the Government of Kenya.

### 2.1. Concrete samples

In the constituent materials for test samples, three series of specimens were prepared with a variation in the concrete characteristic strength. Ordinary Portland cement, clean river sand, 20 mm maximum size coarse aggregate and potable water.

### 2.2. Experimentation

#### 2.2.1. Concrete composition

The concrete used for this study was of characteristic strength as shown in Table 1 designed according to the Department of Environment's Design (DOE) method (Ejiogu et al., 2020; Sharma, 2020).

Using the mix proportions in Table 1, fresh concrete was prepared by using an electric mixing pan, poured into the moulds in five layers and vibrated by a vibrating table for 60 seconds. A slump test was carried out to BS EN 12350-2 for each batch of concrete. After 24 hours, the moulds were removed and the concrete specimens cured at normal room temperature in a water tank for 27 days.

**Table 1. Basic mix proportions**

Characteristic Strength(N/mm <sup>2</sup> )	Coarse aggregates Kg/m <sup>3</sup>	Fine aggregates Kg/m <sup>3</sup>	Ordinary Portland Cement Kg/m <sup>3</sup>	Total Free water Kg/m <sup>3</sup>
M25	1190	650	450	225
M30	1069	638	450	225
M35	1075	631	469	225

**Table 2. Physical and mechanical properties of aggregates**

Material	Specific gravity	Water Absorption %	Silt content %	Crushing Value %	Impact Value %	Los Angeles Abrasion value %	Max. Size
FA	2.6	1.8	7.4	18	8	20	4.0
CA	2.6	0.3	0	-	-	-	20.0
Limit	-	-	-	<45	<45	30	



**Figure 3. Gradation of Coarse aggregates.**

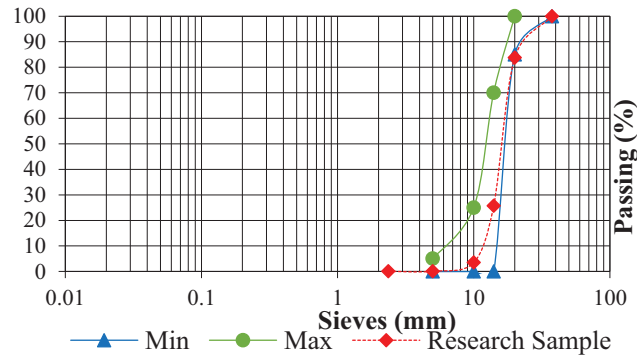
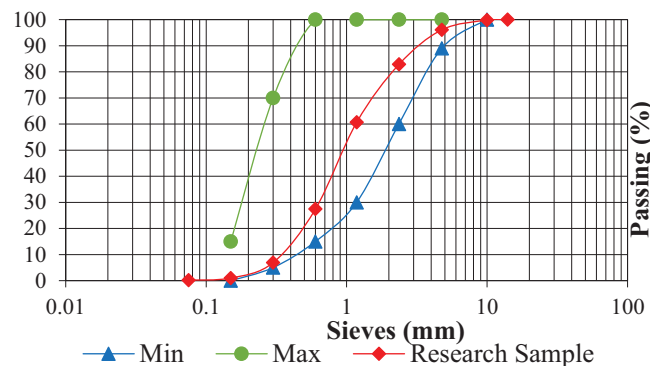


**Figure 4. Gradation of fine aggregates.**



### 2.2.2. Test method for hardened concrete properties

150 mm cube, cylinders with a diameter of 150 mm\* 300 mm long, cylinders of diameter 150 mm \* 1200 mm and 150 mm \*100 mm long in line with BS EN 12390-1:2012 (2012) and BS EN 12390-5 (2009) concrete specimen specifications for compressive strength and tensile strength. A total number of 27 cubes and 27 cylinder specimens for tensile strength prepared, cured and tested according to the methods stipulated in BS EN 12390-2 (2019) [16], BS EN 12390-6 (2009) for 7,14 and 28 days' compressive strength and tensile strength. Each sample for compressive strength was subjected to loading until failure using an automated electronic testing machine which conforms to BS EN 12390-4 (2019). A Universal testing machine(UTM) maximum load of 2000 kN was used to test the cylinders for tensile strength.

### 2.2.3. Material properties

Water-soluble chloride ions were found to be zero in fine aggregates, 0.002% in coarse aggregates. The percentage of chloride is less than the maximum limit of 0.03% as per BS EN 12620 (2002) and therefore acceptable for use. Chlorides below the acceptable threshold ensures that total bound chlorides which may contribute to corrosion is minimized. Table 2 shows the physical and mechanical properties of the aggregates used in this study.

As seen in Table 2, the specific gravity of all the aggregates is within the limits of 2.4–3.0 conforming to BS EN 1097-6:2013 (2013) and they influence the mix design of the concrete. The optimal concrete strength is attained when the specific gravity of coarse aggregates is higher than that of water and lower than that of cement. The water absorption of the fine aggregates is within the limits of 1%–3% in BS EN 1097-6:2013 (2013)] implying a low water absorption hence suitable for concrete works. The low water absorption in the coarse aggregates was taken into consideration in the mix design.

**Table 3. Chemical composition of the cement used in the study**

TEST RESULT OF CEMENT IN % COMPOSITION TO KS EAS 18-1: 2017											
	<b>CaO</b>	<b>SiO<sub>2</sub></b>	<b>SO<sub>3</sub></b>	<b>MgO</b>	<b>K<sub>2</sub>O</b>	<b>Fe<sub>2</sub>O<sub>3</sub></b>	<b>Al<sub>2</sub>O<sub>3</sub></b>	<b>Na<sub>2</sub>O<sub>3</sub></b>	<b>LOI</b>	<b>Cl</b>	<b>IR</b>
	59.11	21.56	2.78	1.04	0.051	3.48	8.09	0.018	0.10	0.016	0.55
REQUIREMENT	SUM ≥ 50	-	≤ 3.5	≤ 5	-	-	3-8	-	≤ 5	≤ 0.1	≤ 5

Figure 5. Slump for each characteristic strength of concrete in the study.

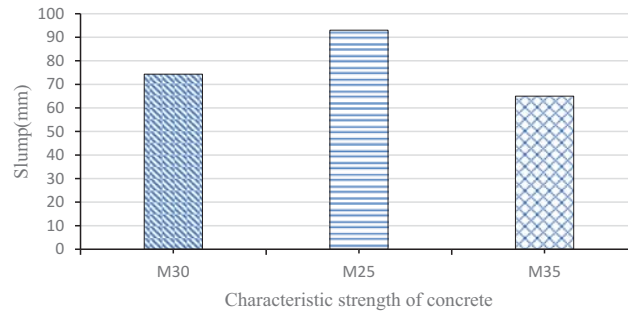
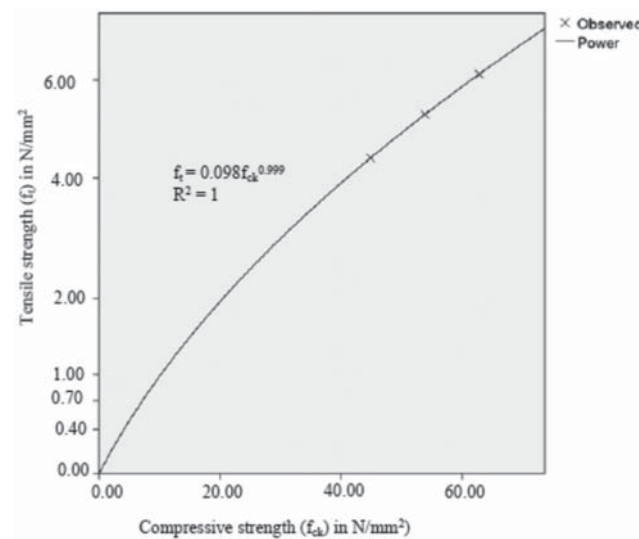


Figure 6. Relationship of split tensile strength and compressive strength from the study.



BS EN 12620:2013(2013) give an upper limit of 3% for non-harmful fines. The silt content in the fine aggregate was more than the allowable percentage of silt content, it was washed and oven dried before use. The Aggregates Impact Value is less than 30% specified in KS EAS 18-1: 2017 (2017). It therefore follows that Aggregates Impact Value of all the aggregates tested are very suitable for concreting works.

The particle size distribution analysis on a representative sample as shown in Figure 3 of the coarse aggregates for the work was carried out to obtain the proportions by weight of the different sizes of coarse aggregates present. The sample is well graded with a maximum aggregate size was 20 mm.

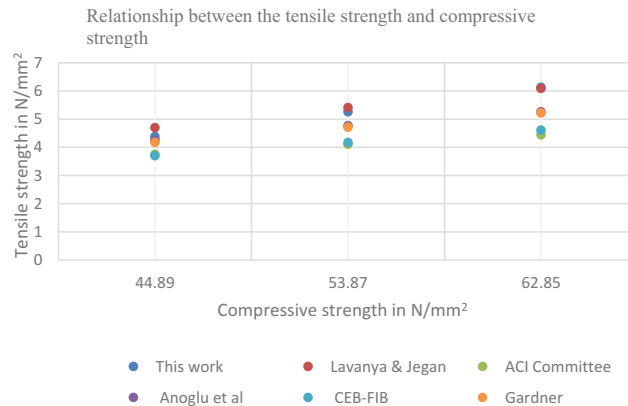
Particle size distribution analysis as shown in Figure 3 on a representative sample of the coarse aggregates for the research was carried out to obtain the proportions by weight of the different sizes of fine particles present according to BS EN 933-1 (2012). The proportions were expressed as percentages by weight passing various sieve sizes conforming to BS 410. The sample is well graded with a maximum aggregate size of 20 mm. From the gradation curve, a portion of the sample falls within the gradation limits. Workability can be achieved with such aggregates without greater fines. This sample is expected to give a sample of high tensile strength and increased corrosion initiation period.

Figure 4 shows the grading of the fine aggregates used in the study. They were well graded and expected to give a well-interlocked composite concrete mix.

**Table 4. Results of hardened properties of the study**

Strength Class (N/mm <sup>2</sup> )	Compressive strength (N/mm <sup>2</sup> ) at 28 days( $f_{ck}$ )	Split tensile strength in N/mm <sup>2</sup>					
		This work $f_t = 0.098f_{ck}^{0.999}$	Lavanya and Jegan (2015) $f_t = 0.249f_{ck}^{0.772}$	ACI Standard (2014) $f_t = 0.56f_c k^{0.5}$	Arıoglu et al. (2006) $f_t = 0.387f_c k^{0.63}$	CEB-FIP Model Code for Concrete Structures (1990) $f_t = 0.3f_{ck}^{0.66}$	Gardner (1990) $f_t = 0.33f_{ck}^{0.667}$
25	44.89	4.38	4.70	3.75	4.25	3.70	4.17
30	53.87	5.26	5.41	4.11	4.77	4.17	4.71
35	62.85	6.13	6.09	4.44	5.26	4.61	5.22

**Figure 7. Relationship of split tensile strength and compressive strength from the study.**



From the gradation curve of Figure 4, the sample falls within the gradation limits. This minimizes the volume of the cement paste while increasing tensile strength and corrosion initiation period. This gradation is important as the quantity passing the 600 micron was used in the respective mix design of the study.

Table 3 shows the chemical properties of the selected Cem 1 cement used in the study.

From Table 3, the sum of calcium oxide (CaO) and silicon dioxide (SiO<sub>2</sub>) is 80.67% and is greater than 50% as per KS EAS 18-1:2017. Increased sum of CaO and SiO<sub>2</sub> increases compressive strength and subsequently, tensile strength and corrosion initiation. Similarly, an increase in insoluble residue reduces compressive strength. The ratio (CaO)/(SiO<sub>2</sub>) contents in Cem 1 cement should be greater than 2. The restriction is to ensure that the setting of concrete is not inhibited. The ratio of (CaO/SiO<sub>2</sub>) in interaction with insoluble residue of cement influences the compressive strength.

The quantity of magnesium oxide (MgO) in Cem 1 cement should not exceed 5% (Sharma, 2020). The cement samples satisfied this requirement with 1.04%. MgO contributes to the colour of cement and hardness of the resulting concrete. If the quantity of MgO is more than 5%, cracks will appear in concrete, which may reduce the bond strength by reducing the effective length. Cracks may subsequently increase and accelerate the ingress of aggressive agents that may initiate corrosion.

The chloride content in ordinary Portland cement should be less than 0.4%. The cement in this study satisfied this requirement. Chloride content limits ensure a reduced amount available to aggravate corrosion initiation. Na<sub>2</sub>O, K<sub>2</sub>O, TiO<sub>2</sub> and P<sub>2</sub>O<sub>5</sub> in Cem 1 are considered residues and their sum is limited to 5% (Sharma, 2020). If these values are more than 5%, efflorescence and unsightly cracking will occur, thus reducing the tensile strength.

### 3. Results and discussion

#### 3.1. Results of fresh concrete

The result for the slump test of the fresh concrete is shown in Figure 5. The slumps obtained are in the medium range (65–93 mm).

From Figure 5, M25 had the highest slump while M35 had the lowest slump. Workability increases with increase in slump and this reduces the resulting strength on concrete. This result suggests that tensile strength and corrosion initiation period will decrease with characteristic strength of concrete.

**Table 5. Critical penetration depth for the samples**

Sample Identity	Characteristic strength and cover	Compressive strength( $f_{cu}$ ) (N/mm <sup>2</sup> )	Tensile strength( $f_t$ ) (N/mm <sup>2</sup> )	Critical penetration depth mm		
				Aperador et al. (2009)	Torres-Acosta and Sagüés (2004)	Shayan and Xu (2016)
25 N/mm <sup>2</sup>	70 mm	44.89	4.38	0.0366	0.1190	0.133
	60 mm			0.0292	0.0961	0.115
	45 mm			0.0181	0.0661	0.089
30 N/mm <sup>2</sup>	70 mm	53.87	5.26	0.0167	0.119	0.161
	60 mm			0.0093	0.0961	0.140
	45 mm			-0.0018	0.0661	0.107
35 N/mm <sup>2</sup>	70 mm	62.85	6.13	-0.0029	0.1190	0.187
	60 mm			-0.010	0.0961	0.162
	45 mm			-0.0214	0.0661	0.125

**Table 6. Relationship between cover, crack width and critical penetration depth**

Specimen characteristic strength and reinforcement cover		Crack width Equ.6(mm)	Shayan and Xu (2016) (mm) $x_{crit} = \frac{f_t(c+d)(1+v)}{E_{eff}d\beta}$
25 N/mm <sup>2</sup>	70 mm	0.181	0.133
	60 mm	0.182	0.115
	45 mm	0.188	0.089
30 N/mm <sup>2</sup>	70 mm	0.218	0.161
	60 mm	0.222	0.140
	45 mm	0.225	0.107
35 N/mm <sup>2</sup>	70 mm	0.254	0.187
	60 mm	0.257	0.162
	45 mm	0.264	0.125

**Table 7. Result of corrosion initiation period( $t_1$ )**

Cube strength (N/mm <sup>2</sup> )	Tensile strength (N/mm <sup>2</sup> )	$x_{crit}$ (mm)	$I_{curr}(t_1)$ ( $\mu$ A/cm <sup>2</sup> )	$t_1$ (Years)
41.29	4.38	0.133	0.992	2.3
53.87	5.26	0.161	0.925	3.0
62.85	6.13	0.187	0.905	3.56

### 3.2. Results of hardened properties of concrete

Figure 6 shows a relationship between the compressive and tensile strength of concrete used in this study. The strengths are the averages of the concrete of characteristic strength 25 N/mm<sup>2</sup>, 30 N/mm<sup>2</sup> and 35 N/mm<sup>2</sup> respectively.

The relationship of the tensile and compressive strength from Figure 6 forms a proposed model equation as one of the outputs of this work used to compare with other published models shown in Table 4. The coefficient of determination ( $R^2 = 1$ ) is very high. This implies that the 100% of the variability of tensile strength is accounted by the regression model. This result suggests that the developed model is adequate to explain the data. The proposed tensile strength model was used to establish a relationship with the corrosion initiation period of reinforced concrete.

Table 4 shows the results of compressive and split tensile strength of this study and the output of published models.

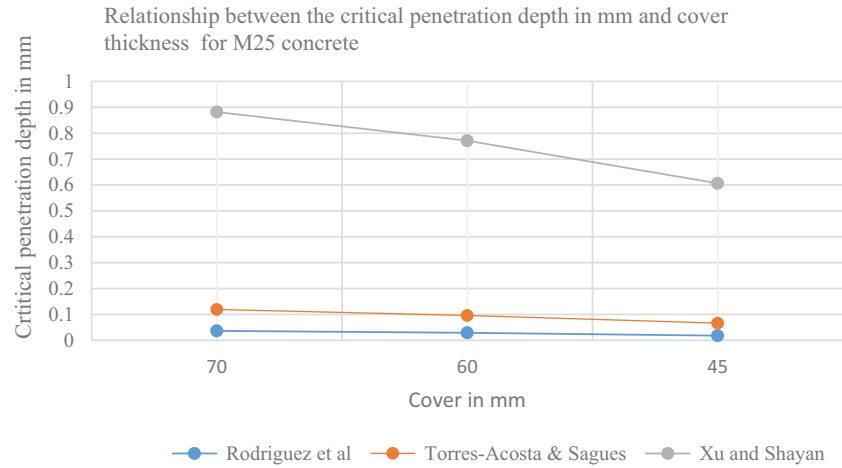
Figure 7 shows a relationship between split tensile strength and compressive strength as reflected in Table 4.

From Figure 7, it can be noted that the tensile strength of this study generally compares well with the output of other authors but closely relate to the Lavanya and Jegan model, hence reliable in its application.

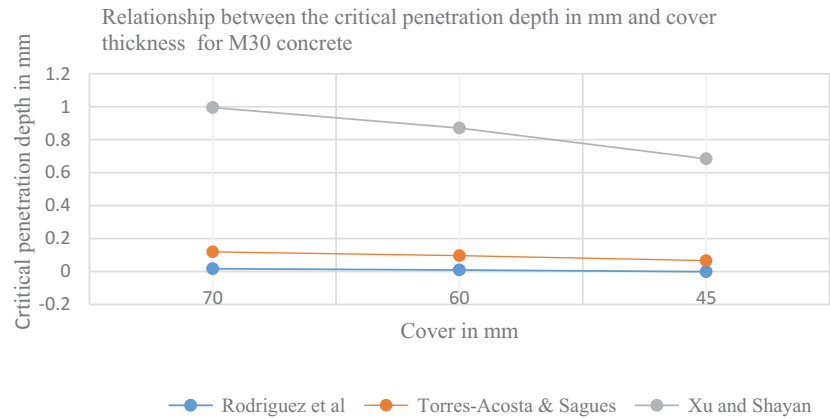
### 3.3. Critical penetration depth

Table 5 shows the critical penetration depth of the samples for this study for a reinforcement bar of 10 mm.

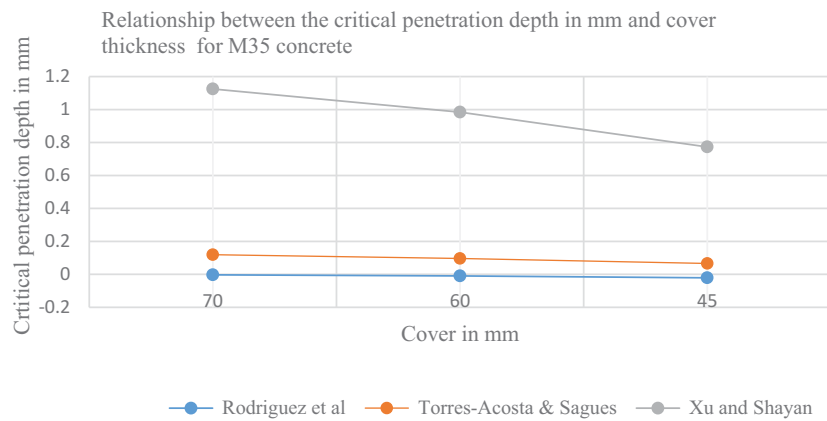
**Figure 8. Relationship between the critical penetration depth and concrete cover thickness for (a)M25, (b) M30 and M35 by various authors.**



a)



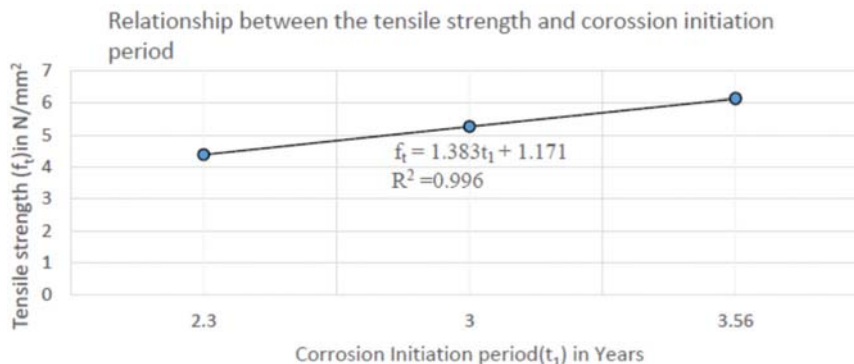
b)



c)



**Figure 9. Relationship between tensile strength and corrosion initiation period.**



From Table 5, Figure 8(a-c) was drawn showing a relationship between the critical penetration depth and concrete cover thickness of selected strength by various authors.

From the results of Table 5 and Figure 8, it can be noted that in all the models the critical penetration depth decreased with decrease in concrete cover. The Torres-Acosta and Sagues model has no variation in the strength of concrete. It is also noted that in the Rodriguez et al. model, the critical penetration depth tends to below zero for concrete strength of 30 N/mm<sup>2</sup> and 35 N/mm<sup>2</sup>. This is due to non-consideration of the mechanical properties which affect the resistance of the concrete to cracking. The Xu and Shayan model for critical penetration depth considers the variables considered in this work and has been adopted in calculation of the corrosion initiation period.

Table 6 shows a relation between reinforcement cover, crack width and critical penetration depth for a 10 mm bar diameter.

From Table 6, it can be noted that the crack width increases with a reduction of concrete cover. Similarly, the critical penetration depth decreases with increase in crack width. Crack evolution and expansion on the surface of a specimen is due to stresses resulting from increase in corrosion products. More corrosion products are required to cause a surface crack in concrete with a larger reinforcement cover and the converse also is true. Similarly, there is an increase in the critical penetration depth with increase in concrete characteristic strength and this is due to increase in tensile strength resisting the expansive pressure of the corrosion products.

### 3.4. Corrosion initiation period

Table 7 shows the corrosion initiation period and critical penetration depth from Equation (9) the Xu and Shayan mode (Shayan & Xu, 2016).

Figure 9 shows a relationship between tensile strength and initiation period derived from Table 7.

From Figure 9 the corrosion initiation period increases linearly with increase in tensile strength of concrete with a coefficient of determination of 0.996. This implies that the 99.6% of the variability of tensile strength is accounted by the regression model. This result suggests that the developed model is adequate to explain the data. The crack initiation period is affected by the tensile properties of concrete after depassivation of the reinforcement in concrete.

## 4. Conclusion

A study of the relationship between the split tensile strength for M25, M30 and M35 concrete and corrosion initiation period has been done in this study. Corrosion initiation period increased with

split tensile strength of concrete. A derived linear polynomial model as a function of corrosion initiation period is adequate to account for the variability in the tensile strength data. Based on the test results the following conclusions can be drawn;

- (a) Corrosion initiation period is longer with increased concrete cover/reinforcement thickness.
- (b) Corrosion initiation period increases linearly with increase of the tensile strength and this relationship can be incorporated in service life models of reinforced concrete.

#### Funding

The authors received no direct funding for this research.

#### Author details

Philip Mogire<sup>1</sup>  
E-mail: [philosiemmo@yahoo.com](mailto:philosiemmo@yahoo.com)  
John Mwero<sup>2</sup>  
Silvester Abuodha<sup>2</sup>  
Geoffrey Mang'uriu<sup>2</sup>

<sup>1</sup> Department of Civil and Construction Engineering, University of Nairobi, Nairobi, Kenya.

<sup>2</sup> Department of Civil, Construction and Environmental Engineering, Jomo Kenyatta University of Agriculture & Technology, Nairobi, Kenya.

#### Disclosure statement

No potential conflict of interest was reported by the author(s).

#### Citation information

Cite this article as: Correlation of tensile strength and corrosion initiation period of reinforced concrete, Philip Mogire, John Mwero, Silvester Abuodha & Geoffrey Mang'uriu, *Cogent Engineering* (2021), 8: 1999039.

#### References

- ACI Standard. (2014). Building code requirements for structural concrete (ACI 318-14). 720-730.
- Andrade, C., Muñoz, A., & Torres-Acosta, A. (2010). Relation between crack width and corrosion degree in corroding elements exposed to the natural atmosphere. *Proceedings, Fracture Mechanics of Concrete and concrete structures*, Seoul, Korea: Korea Concrete Institute.
- Aperador, W., Mejia de Getierrez, R., & Bastidas, D. M. (2009). Steel corrosion behaviour in carbonated alkali-activated slag concrete. *Corrosion Science*, 51(9), 2027-2033. <https://doi.org/10.1016/j.corsci.2009.05.033>
- Arteaga, E. B., Chateauneuf, A., Silva, M. S., Bressolette, P., & Schoefs, F. (2011). A comprehensive probabilistic model of chloride ingress in unsaturated concrete. *Engineering Structures*, Elsevier, 33(3).
- Arıoglu, N., Girgin, Z. C., & Arıoglu, E. (2006). Evaluation of ratio between splitting tensile strength and compressive strength for concretes up to 120 MPa and its application in strength criterion. *ACI Material Journal*, 18.
- BS EN 1097-6:2013. (2013). Tests for mechanical and physical properties of aggregates. Determination of particle density and water absorption.
- BS EN 12390-1:2012. (2012). Testing hardened concrete: Shape, dimensions and other requirements for specimens and moulds.
- BS EN 12390-4. (2019). Compressive strength, specification for testing machines.
- BS EN 12390-6 (2009). Testing hardened concrete: Tensile splitting strength of test specimens.
- BS EN 12620:2013. (2013). Aggregates for concrete.
- BS EN 933-1. (2012). Tests for geometrical properties of aggregates - Part 1: Determination of particle size distribution - Sieving method.
- BS EN 12620. (2002). *Aggregates for concrete*.
- BS EN 12390-5. (2009). *Testing hardened concrete part 5: Flexural strength of specimens*.
- BS EN 12390-2. (2019). *Testing hardened concrete part 2: Making and curing specimen for strength tests*.
- CEB-FIP Model Code for Concrete Structures. (1990). Evaluation of the time dependent behaviour of concrete. *Bulletin d'Information No. 199, Comite European Du Béton/Fédération Internationale De la Précontrainte, Lausanne, 1991, 201(11), 184.* <https://www.icvirtuallibrary.com/doi/Abs/10.1680/ceb-fibmc1990.35430>
- Darmawan, M. S., & Stewart, M. G. (2007). Effect of pitting corrosion on capacity of prestressing wires. *Magazine of Concrete Research*, 59(2), 131-139. <https://doi.org/10.1680/mac.2007.59.2.131>
- DuraCrete. (2000). *Probabilistic performance based durability design of concrete structures*. The European Union-Brite EuRam III.
- Ejiogu, I. K., Mamza, P. A. P., Nkeonye, P. O., & Yaro, S. A. (2020). Comparison of ACI, IS and DOE methods of concrete mix design. *NJE*, 27(1), 68-83.
- Gardner, N. J. (1990). Effect of temperature on the early-age properties of type I, type III, and type I/ fly ash concretes. *ACI Materials Journal*, 87(1), 68-78. <https://concrete.org/publications/internationalconcreteabstractsportal/m/detail/id/2381>
- Huang, I.-W., & Goodwin, F. (2019). *Modeling the corrosion related service life of existing concrete structures. Proceedings of the Corrosion 2019*, Nashville, Tennessee, USA: NACE International.
- Khan, M. U., Ahmad, S., & Al-Gahtani, H. J. (2017). Chloride-induced corrosion of steel in concrete: An overview on chloride diffusion and prediction of corrosion initiation time. *International Journal of Corrosion*, 2017, 1-9. <https://doi.org/10.1155/2017/5819202>
- KS EAS 18-1: 2017. (2017). Cement-part 1: Composition, specification and conformity criteria for common cements.
- Lavanya, G., & Jegan, J. (2015). Evaluation of relationship between split tensile strength and compressive strength for geopolymer concrete of varying grades and molarity. *International Journal of Applied Engineering Research*, 10(15), 35523-35527.
- Mogire, P., Mwero, J., Abuodha, S., & Manguriu, G. (2018). The effect of selected cement brands in Kenya on the critical penetration depth of rust in reinforced concrete water conveying structures. *International Journal of Scientific and Research Publications*, 8(11), 8333. <https://doi.org/10.29322/ijsrp.8.11.2028.p8333>
- Mogire, P., Mwero, J., Abuodha, S., & Manguriu, G. (2020). A corrosion model for prediction of service life of reinforced concrete water structures. *International Journal of Scientific and Research Publications (IJSRP)*, 10(2), p98104. <https://doi.org/10.29322/IJSRP.10.02.2020.p98104>
- Nguyen, P. T., Arteaga, E. B., Amiri, O., & Soueidy, C. (2017). An efficient chloride ingress model for long-term lifetime assessment of reinforced

- concrete structures under realistic climate and exposure conditions. *International Journal of Concrete Structures and Materials*, 11(2), 199–213. <https://doi.org/10.1007/s40069-017-0185-8>
- RILEM TC 154-EMC. (2003). Electrochemical techniques for measuring metallic corrosion. *Materials and Structures/Matériaux Et Constructions*, 36, 461–471. <https://doi.org/10.1617/13718>
- Rodríguez, J., Ortega, L. M., Casal, J., & Diez, J. M. (1996). Corrosion of reinforcement and service life of concrete structures. In *Proc. Of Int. Conf. On Durability of Building Materials and Components*, 1, 117–126. <https://www.researchgate.net/publication/285739202>
- Sharma, M.(2020).Seismic potential parameter of concrete gravity dam. *Conference: Recent trend in Civil Engineering*. <https://doi.org/10.13140/RG.2.2.28803.45600>
- Šmilauer, V., Hájková, K., Jendele, L., & Červenka, J. (2017). Durability assessment of reinforced concrete structures due to chloride ingress up and beyond induction period. In *the 39th IABSE Symposium – Engineering the Future*. September 21–23, Vancouver, Canada: IABSE/vancouver.
- Shayan, A., & Xu, A. (2016). Relationship between reinforcing bar corrosion and concrete cracking. *Aci Materials Journal*, 113(1), 3–12. <https://doi.org/10.14359/51688460>
- Smilauer, V., Jendele, L., & Cervenka, J. (2013). Prediction of carbonation and chloride ingress in cracked concrete structures. In *the proceedings of the Fourteenth International Conference on Civil, Structural and Environmental Engineering Computing*, Civil-Comp Press, Stirlingshire, UK, Paper 215. <https://doi.org/10.4203/ccp.102.215>
- Torres-Acosta, A., & Sagüés, A. (2004). Concrete cracking by localized steel corrosion - geometric effects. *ACI Materials Journal*, 101(6), 501–507. <https://www.concrete.org/publications/acimaterialsjournal.aspx>
- Yihui, Z., Gencturk, B., Kaspar, W., & Arezou, A. (2014). Carbonation-induced and chloride-induced corrosion in reinforced concrete structures. *Journal of Materials in Civil Engineering*, 27(9). [https://doi.org/10.1061/\(ASCE\)MT.1943-5533.0001209](https://doi.org/10.1061/(ASCE)MT.1943-5533.0001209)



© 2021 The Author(s). This open access article is distributed under a Creative Commons Attribution (CC-BY) 4.0 license.

You are free to:

Share — copy and redistribute the material in any medium or format.

Adapt — remix, transform, and build upon the material for any purpose, even commercially.

The licensor cannot revoke these freedoms as long as you follow the license terms.

Under the following terms:

Attribution — You must give appropriate credit, provide a link to the license, and indicate if changes were made.

You may do so in any reasonable manner, but not in any way that suggests the licensor endorses you or your use.

No additional restrictions

You may not apply legal terms or technological measures that legally restrict others from doing anything the license permits.



**Cogent Engineering (ISSN: 2331-1916) is published by Cogent OA, part of Taylor & Francis Group.**

**Publishing with Cogent OA ensures:**

- Immediate, universal access to your article on publication
- High visibility and discoverability via the Cogent OA website as well as Taylor & Francis Online
- Download and citation statistics for your article
- Rapid online publication
- Input from, and dialog with, expert editors and editorial boards
- Retention of full copyright of your article
- Guaranteed legacy preservation of your article
- Discounts and waivers for authors in developing regions

**Submit your manuscript to a Cogent OA journal at [www.CogentOA.com](http://www.CogentOA.com)**



# The Relationship between Bond Strength and Critical Penetration Depth of Rust in Reinforced Concrete Structures

Philip Mogire<sup>1</sup>, John Mwero<sup>1</sup>, Silvester Abuodha<sup>1</sup> & Geoffrey Mang'uriu<sup>2</sup>

<sup>1</sup> Department of Civil and Construction Engineering, University of Nairobi, 30197-00100, Nairobi, Kenya

<sup>2</sup> Department of Civil, Construction and Environmental Engineering, Jomo Kenyatta University of Agriculture and Technology, 62000-00100, Nairobi, Kenya

Correspondence: Philip Mogire, Department of Civil and Construction Engineering, University of Nairobi, 30197,00100, Nairobi, Kenya. E-mail: philosiemo@yahoo.com

Received: October 27, 2021

Accepted: November 15, 2021

Online Published: November 30, 2021

## Abstract

Bond strength and critical penetration depth of rust are major factors that affect the service life of reinforced concrete structures. This research endeavored to establish a relationship between the bond strength and critical penetration depth of rust for reinforced concrete structures. There are 7 brands of Cem 1 cement in Kenya available for use in concrete structures. To achieve the desired objective, three Cem 1 cement brands (Cem A, B and C), fine aggregates, coarse aggregates and steel were obtained from the local Kenyan market. The chemical and physical properties of the materials were investigated. For a selected design strength of 25N/mm<sup>2</sup>, concrete materials were batched by weight and mixed by an electric pan mixer. For each brand of cement 9 cubes of size 150mm \* 150mm \* 150mm for a compression test, 9 cylinders of 150mm \* 300mm for tensile strength and 9 cylinders of 150mm \* 300mm for bond strength were cast. After 24 hours, the cast specimens were demoulded and immersed in curing tanks for 27 days. Specimens for compression, split tensile and bond strength were tested at 7, 14 and 28 days. From the results, it was observed that the chemical composition of Cem 1 brands in the Kenyan market vary, which affects the hardening properties of concrete. A model for the critical penetration depth of rust in reinforced concrete was proposed by establishing a correlation between the split tensile and bond strength and substituting it in the Xu and Shayan model. The proposed and published models compared well. From the proposed model, a relationship between the critical penetration depth and bond strength was established. It was noted that the critical penetration depth increased with an increase in the bond strength of reinforced concrete. The results of this research are expected to contribute to the modeling of the service life of reinforced concrete structures.

**Keywords:** bond strength, cement brands, critical penetration depth

## 1. Introduction

The Kenyan Presidency (2018-2022) defined four pillars (manufacturing, affordable housing, universal health coverage and food security) for better implementation of its strategies. Cement as a construction material has a direct or indirect effect on the sustainability of the defined pillars and consequently the realization of the United Nations Sustainable Development Goals. There are 7 Cem 1 brands in Kenya manufactured by different manufacturers to cope up with the demand in the region. The brands differ in chemical composition that may affect the properties of hardened concrete, including local bond stress, split tensile and compressive strength.

The local bond stress slip behavior of reinforced concrete is a fundamental property required for the analysis and design of concrete structures at both serviceability and ultimate limit state (Sturm & Visintin, 2018). The bond behavior of reinforced concrete structures is an interaction between reinforcing steel and concrete. It enables the transfer and compatibility of deformation between the reinforcing steel bar and the surrounding concrete (Zhao & Lin, 2018). The bond properties have little, if any, effect on tension-stiffening but a major effect on crack parameters; spacing and width (Sturm, Visintin, & Oehlers, 2021), depth, frequency and healing (Shaikh, 2018) aggravating the ingress of corrosion agents, thus affecting serviceability (Sturm, Visintin, & Oehlers, 2017). These agents, on a critical scale, will destroy the passive film on the reinforcement, after which corrosion will be initiated (Chen, Berrocal, & Lofgren, 2020).

Time required for concrete cover cracking is used as a service life indicator in the assessment of deterioration of corrosion-affected reinforced concrete structures (Baji & Shi, 2020). Corrosion progression is time related and many studies have been conducted to evaluate the corrosion penetration depth (radius loss) (Chen et al., 2020). The critical penetration depth ( $X_{crit}$ ) is the amount of reinforcement radius loss required to cause a crack on the surface (Mogire, Abuodha, Mwero, & Mang'uriu, 2018). There has been an attempt to develop models for calculating the critical penetration depth of rust in reinforced concrete structures.

Torres-Acosta and Sagiúés, Xu and Shayan (Hajkovaá, Smilauera, Jendeleband, & Cervenkab, 2018, Alonso, Andrade, Rodrigues, & Diez, 1998) developed models for the critical penetration depth of rust based on experiments. The results of these models give different outputs due to different component parameters.

The input parameters in the critical penetration depth of rust can be acquired by experiments or artificial intelligence (AI) based techniques. Within the various AI-based techniques, artificial neural networks (ANNs) and adaptive neurofuzzy inference system (ANFIS) are the most commonly used methods.

ANN method was also applied for the prediction of compressive strength for different types of concrete, such as high-strength concrete (Sobhani, Najimi, Pourkhorshidi, & Parhizkar, 2010) and no-slump concrete (Nguyen & Dinh, 2020). Nguyen and Dinh applied the ANFIS method to estimate the 28-day compressive strength of concrete (Armaghani, Hatzigeorgiou, Karamani, Skentou, Zoumpoulaki, & Asteris, 2019). In a recent study, Armaghani et al. applied an ANN method to predict the shear strength of the concrete beam. To the best of the authors' knowledge, there has been no available research to apply the AI-based models for predicting the critical penetration depth of rust or bond strength of reinforced concrete. Accordingly, in this study, for a characteristic compressive strength of 25N/mm<sup>2</sup>, a series of 3 Cem 1 brands was used to prepare concrete for split tensile, compressive and bond strength. A relationship between the split tensile and bond strength has been established, which is incorporated in a proposed model for the critical penetration depth of rust.

This research proposes a model for critical penetration depth of rust by establishing a relationship between the split and bond strength of reinforced concrete and substituting it in the Xu and Shayan model. A relationship between the proposed critical penetration depth of rust and bond strength of reinforced concrete has been established. A parametric study of the critical penetration depth of rust has been done and the proposed model is compared with the published research.

This study proposes that the critical penetration depth of rust increases with an increase in bond strength. A relationship established between the critical penetration depth of rust and bond strength can be applied in calculating the corrosion initiation period in reinforced concrete structures.

## 2. Method

The study was conducted at the University of Nairobi Concrete and Materials Lab, where the physical properties of the materials were identified and the sample preparation and testing were done. The chemical properties of the selected Cem 1 brands were identified in the State Department of Infrastructure in the Ministry of Transport, Infrastructure, Housing and Urban Development of the Government of Kenya.

### 2.1 Cement, Aggregates and Water for the Study

Available Cem 1 brands of cement in Kenya are manufactured in accordance with KS EAS 18-1(2017). The cements were sourced from a local wholesaler and were randomly selected. Table 1 shows the sources of the fine aggregate(FA), coarse aggregates(CA) reinforcing steel bar and water used in this study.

Table 1. Details of material for this study

SN	Description	Source	Remark
1.	Fine aggregates	Machakos River	
2.	Coarse aggregates	Kenya Builders quarry	5-20mm graded at source
3.	10mm ribbed bars	Local Manufacturer	Factory cut to 1010mm length
4.	Mixing water	lab	Portable

### 2.2 Test for Mechanical Properties of Aggregates

Table 2 shows the reference standard used for the procedure of testing aggregates the physical and mechanical properties of aggregates.

Table 2. Testing procedure for physical and mechanical properties of aggregates

Test	Standard for test procedure
Specific gravity	ASTM C128
Water absorption	BS 812-2:1995
Silt content	ASTM C142-97
Crushing value	BS EN 1097-2
Impact value	BS EN 1097-2
Flakiness index	BS/EN 933-3
Los Angeles abrasion value	BS/EN 1097-2

### 2.3 Mix Design

The concrete used for this study was of characteristic strength 25 N/mm<sup>2</sup> designed according to the Department of Environment's Design (DOE) method (Ejiogu et al., 2020) and constituted the proportions shown in Table 3.

Table 3. Mix proportions of materials for this study

Cem1 (kg/m <sup>3</sup> )	FA (kg/m <sup>3</sup> )	CA (kg/m <sup>3</sup> )	Water (kg/m <sup>3</sup> )
450	650	1190	225

Using the mix proportions, fresh concrete was prepared by using an electric mixing pan, poured into the moulds in five layers and vibrated by a vibrating table for 60 seconds. A slump test was carried out for each batch of concrete. After 24 hours, the moulds were removed and the concrete specimens cured at normal room temperature in a water tank for 27 days.

### 2.4 Size, Power, and Precision

Cubes of size 150mm\*150mm\*150mm, cylinders with a diameter of 150mm\* 300mm long, cylinders of diameter 150mm \* 30mm long with 10mm diameter \*1010mm long reinforcing ribbed steel bar centrally placed in line with BS 12390-1 (2012), BS EN 12390-5 (2009) and ACI 318 -08 specifications were employed to produce concrete specimens for compressive strength, tensile strength and bond strength. A total number of 27 cubes, 27 cylinder specimens for tensile strength and 27 cylinders for bond strength were prepared, cured and tested according to the methods stipulated in BS EN 12390-2 (2019), BS EN 12390-6 (2009), [20] for 7,14 and 28 days' compressive strength, tensile and bond strength. Each sample for compressive strength was subjected to loading until failure using an automated electronic testing machine, which conforms to BS EN 12390-4 (2019). A universal testing machine (UTM) maximum load of 2000 kN was used to test the cylinders for tensile strength.

The bond strength study was carried out through a pull out test in which a manually operated hydraulic pump with a load cell of 100 kN was used. The load was applied at a rate of 2 kN/sec and distributed on the specimen surface by a 200mm square steel plate with a hole at the center system. The setup of the pull out test is shown in Figure 1.



(a) Sample confining apparatus (b) Tensile load detection equipment

Figure 1. (a)- (b) Pull out Testing equipment during sample testing (Source: Author)

Bond stress ( $S$ ) in MPa was calculated as average stress between the reinforcing bar and the surrounding concrete along the embedded length of the bar from Equation 1.

$$S = \frac{P_{\max}}{\pi d_b L_d} \quad (1)$$

Where  $P_{\max}$  was the maximum pullout load(N),  $d_b$  was diameter of the bar(mm) and  $L_d$  was the embedded bar length(mm).

### 2.5 The Critical Penetration Depth of Rust

From the results of the split tensile and bond strength, a relationship was established and substituted in Equation 4 for a proposed model for critical penetration depth of rust. Other parameters adopted in the proposed model are shown in Table 4

Table 4. Parameters values for the proposed model

c(mm)	d(mm)	$f_t$ (MPa)	$\nu$	$\beta$	E(MPa)	$\phi$
70	10	variable	0.2	2.2	30	2

The results of the proposed and published models were compared. Further, a relationship between the critical penetration depth and bond strength was established.

## 3. Results and Discussions

Physical and mechanical tests on aggregates were carried out to determine their suitability for use in the study.

### 3.1 Results and Discussion of Material Properties

Water soluble chlorides ions in fine aggregates were found to be zero percent and 0.002 % in coarse aggregates. The percentage of chloride is less than the maximum limit of 0.03% as per BS EN 12620(2002) and therefore acceptable for use. High water soluble chlorides in the aggregates may aggravate the threshold available in concrete and contribute to corrosion. Table 5 shows the physical properties of the aggregates used in this study.

Table 5. Physical properties of aggregates used in the study

Material	Specific gravity	% Water Absorption	% Silt content	Max. Size(mm)
FA	2.6	1.8	7.4	4.0
CA	2.6	0.3	0	20.0

As seen in Table 5, the specific gravity of all the aggregates is within the limits of 2.4 – 3.0 conforming to BS EN 1097-6:2013 and they influence the mix design of the concrete. The optimal concrete strength is attained when the



specific gravity of coarse aggregates is higher than that of water and lower than that of cement. The water absorption of the fine aggregates is within the limits of 1% – 3% in BS EN 1097-6(2013) implying a low water absorption hence being suitable for concrete works. The low water absorption in the coarse aggregates was taken into consideration in the mix design.

ASTM C117 - 17 gives an allowable limit of 10% for silt and clay content in fine aggregates for concrete production, while BS EN 12620(2013) gives an upper limit of 3% for non-harmful fines. The silt content in the fine aggregate was more than the allowable percentage of silt content; it was washed and oven-dried before use. Table 6 shows the mechanical properties of the coarse aggregates used in this study.

Table 6. Mechanical properties of coarse aggregates

Test	Result	Limit
Crushing value %	18	<45
Impact Value %	8	<45
Loss Angeles Abrasion Value %	20	30

The mechanical properties of aggregates cannot be improved but depend on the properties of the parent rock. The Aggregates Impact Value is less than 30% specified in KS EAS 18-1(2017). It, therefore, follows that the Aggregates Impact Value of all the aggregates tested were very suitable for concreting works.

The particle size distribution analysis on a representative sample, as shown in Fig.2 of the coarse aggregates for the work, was carried out to obtain the proportions by weight of the different sizes of coarse aggregates present. The sample is well graded with a maximum aggregate size of 20mm. From the gradation curve, a reasonable portion falls within the gradation limits. Reasonable workability can be achieved with such aggregates without greater fines.

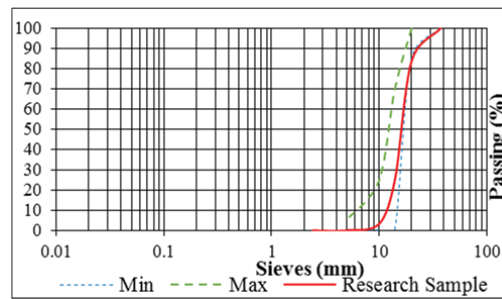


Figure 2. Gradation of Coarse aggregates

Particle size distribution analysis, as shown in Figure 3, on a representative sample of the fine aggregates for the research was carried out to obtain the proportions by weight of the different sizes of fine particles present according to BS EN 933-1(2012). The proportions were expressed as percentages by weight passing various sieve sizes conforming to BS 410. As shown in Figure 3, the fine aggregates were well graded and expected to give a well interlocked composite concrete mix.



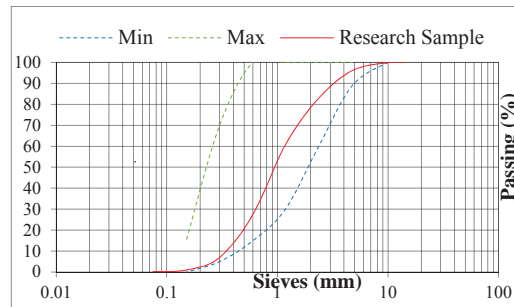


Figure 3. Gradation of fine aggregates

Table 7 shows the chemical properties of the selected Cem 1 brands in Kenya used in this study.

Table 7. Chemical composition of the cement used in the study

Test	Result			KS EAS 18-1: 2017
	Cem A	Cem B	Cem C	Requirement
CaO%	59.86	59.11	58.82	Sum $\geq$ 50
SiO <sub>2</sub> %	16.56	21.56	19.47	
SO <sub>3</sub> %	2.02	2.78	2.03	$\leq$ 3.5
MgO%	1.76	1.04	0.57	$\leq$ 5
K <sub>2</sub> O%	0.027	0.051	-	
Fe <sub>2</sub> O <sub>3</sub> %	2.32	3.48	1.44	
Al <sub>2</sub> O <sub>3</sub>	7.61	8.09	6.85	3-8
Na <sub>2</sub> O <sub>3</sub> %	0.054	0.018		
LOI%	0.11	0.10	4.75	$\leq$ 5
Cl%	0.012	0.016	0.014	$\leq$ 0.1
IR%	2.20	0.55	1.96	$\leq$ 5

From Table 7, Cem A has the highest amount of lime(CaO) (59.86%) and Insoluble residue (2.20%), Cem B has the highest Silicon dioxide (SiO<sub>2</sub>) (21.56%). The increased sum of (CaO) and (SiO<sub>2</sub>) increases compressive strength and subsequently, bond strength and critical penetration depth should not be less than 50%. Similarly, an increase in insoluble residue reduces compressive strength. All cement samples used for this work satisfied this requirement of KS EAS 18-1(2017). Cement sample B has a CaO + SiO<sub>2</sub> value of 80.67 % and produced the highest compressive strength of concrete (44.89 N/mm<sup>2</sup>). SiO<sub>2</sub> has to be limited relative to CaO in order not to negatively affect setting time.

The ratio (CaO)/(SiO<sub>2</sub>) contents in Cem 1 cement should be greater than 2. The restriction is to ensure that the setting of concrete is not inhibited. All the cement samples investigated fulfilled this requirement. The ratio of CaO/SiO<sub>2</sub> in interaction with an insoluble residue of cement influences the compressive strength.

The quantity of magnesium oxide (MgO) in Cem 1 cement should not exceed 5%. All the cement samples satisfied this requirement with 1.76%, 1.04% and 0.57% for cement samples A, B and C, respectively. MgO contributes to the colour of cement and hardness of the resulting concrete. If the quantity of MgO is more than 5%, cracks will appear in concrete, which may reduce the bond strength by reducing the effective length. Cracks may subsequently increase and accelerate the critical penetration depth.

The chloride content in ordinary Portland cement should be less than 0.4%. All the cement samples in this work satisfied this requirement. Chloride content limits ensure a reduced amount available to aggravate corrosion, which in turn reduces bond strength.

Na<sub>2</sub>O, K<sub>2</sub>O, TiO<sub>2</sub> and P<sub>2</sub>O<sub>5</sub> in Cem 1 are considered residues and their sum is limited to 5%(Sharma,2020). All the cement samples investigated fulfilled this requirement, with cement samples A, B and C having total residue contents of 0.55, 2.2 and 1.96%, respectively. If these values are more than 5%, efflorescence and unsightly cracking will occur, thus reducing the bond strength.

### 3.2 Results of Fresh Concrete Test

The result for the slump test of the fresh concrete is shown in Figure 4. The slumps obtained are in the medium range (68-93mm).

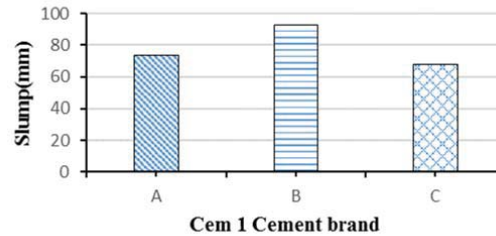


Figure 4. Slump from Cem 1 brands of cement

From Figure 4, concrete with Cem B brand of cement had the highest slump while C had the lowest slump. Workability increases with an increase in a slump and this reduces the resulting strength on concrete.

### 3.3 Results of Hardened Concrete

Table 8 shows the compressive, split tensile and bond strength results.

Table 8. Results of properties of hardened concrete

Cem 1 brand	Compressive strength (N/mm <sup>2</sup> )	Tensile strength (N/mm <sup>2</sup> )	Bond strength (N/mm <sup>2</sup> )
A	41.29	4.5	4.42
B	41.09	4.45	4.33
C	44.89	4.48	4.4

From Table 8, Figures 5, 6 and 7 are drawn to show the relationship of the hardened properties of concrete for a selected brand of cement. Fig. 5 shows a bar chart of a comparative relationship of the hardened properties of concrete with a selected Cem 1 brand.

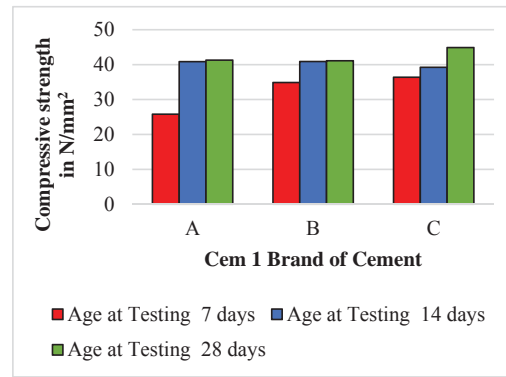


Figure 5. Bar chart of Compressive strength for selected Cem 1 Cement brand

From Figure 5, it can be noted that a choice of a brand of Cem 1 cement influences the compressive strength. As expected, Cem C with the highest CaO/SiO<sub>2</sub> ratio in interaction with insoluble residue had the highest compressive strength. A high compressive strength increases bond strength and affects the critical penetration depth. This result is also in line with those from Fig.3, as increase in slumps causes reduced strength, durability and permeability of concrete. The test was carried out after 27 days of curing.

Figure 6 shows a bar chart of the relationship of split tensile strength and a selected Cem 1 brand of cement as shown in Table 8.

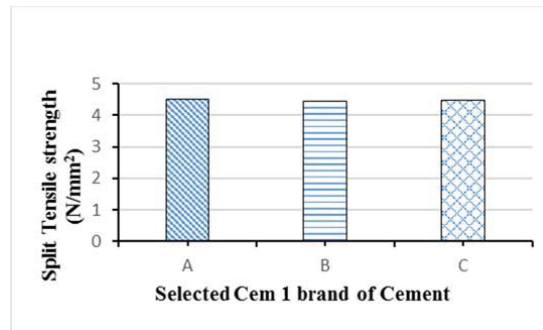


Figure 6. Bar Chart showing the relationship of split tensile strength of concrete with selected Cem 1 brands of cement.

From Figure 6, it can be shown that concrete with Cem C has the highest split tensile strength. Cem C has the highest CaO/SiO<sub>2</sub> ratio in combination with insoluble residue and increases the compressive strength and subsequently the split tensile strength. Figure 7 shows a relationship between bond strength and a brand of Cem 1 cement.

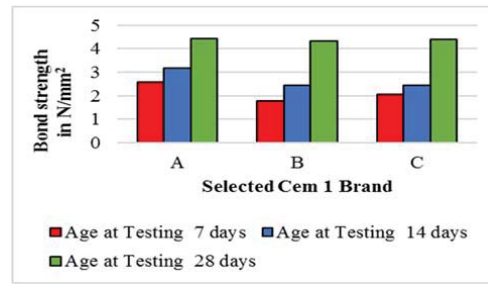


Figure 7. Relationship of bond strength and selected Cem 1 cement brand

From Figure 7, a selected Cem 1 cement brand influenced the bond strength of the reinforced concrete samples. Samples with Cem B brand of cement had the lowest chemical constituents that affect compressive strength and subsequently had the lowest bond strength as expected.

Based on the results shown in Figure 7, the choice of Cem 1 brand of cement significantly affects the bond strength and subsequently the service life of the respective structures.

Table 9 shows a statistical relationship between split tensile and bond strength in a linear regression statistical model with a 96.2 % coefficient of determination.

Table 9. Statistical relationship between tensile and bond strength

R Square	F	Sig	Constant	b1
0.962	25.21	0.124	2.187	0.522

From Table 9, Equation 2 is proposed for this study.

$$f_t = 2.187 + 0.522f_b \quad (2)$$

Where  $f_b$  is the bond strength (MPa).

#### 3.4 Result of the Critical Penetration Test

This section discusses and analyses the published models for evaluating the critical penetration depth of rust. It also compares them with the proposed model. Torres-Acosta and Sagüés (Hajikova et al., 2018) proposed Equation 3 when corrosion is localized to a short length.

$$X_{crit}/mm \approx 0.011 \left(\frac{c}{d}\right) \left(\frac{c}{L} + 1\right) \quad (3)$$

Where C is the cover depth(mm) of concrete, d is diameter(mm) of the reinforcement and L (mm) is the uniformly corroding segment length.

Their application cannot be extrapolated to include intersections of the rebar with preexisting cracks and does not take into account the tensile properties of concrete.

Alonso et al. (1998) showed that the corrosion loss required to generate the first visible crack is linearly proportional to the cover-rebar diameter ratio (c/d) in Equation 4.

$$x_{crit} = 7.53 + 9.32 \frac{c}{d} \quad (4)$$

Where  $x_{crit}$  is corrosion loss at crack initiation in  $\mu\text{m}$ , c is concrete cover in mm and d is bar diameter in mm.

Equation 4 was derived on the assumption that general corrosion in steel will cause the concrete to crack, and in cases when corrosion is limited to small locations, such as when corrosion occurs at damaged sites of epoxy-coated bars, it cannot predict the critical corrosion loss.

Xu and Shayan (2016) considered the combination of concrete cover and its embedded steel as a thick-wall concrete cylinder which surrounds the embedded steel. The expansion of corroded steel exerted an internal pressure on the concrete cylinder. They derived Equation 5 for the attack penetration depth.

$$x_{crit} = \frac{f_c c(c+d)(1+v)}{E_{eff} d \beta} \quad (5)$$

Where  $x_{crit}$  is the attack penetration or the decrease in the reinforcing bar radius ( $\mu\text{m}$ ),  $c$  is the concrete cover (mm),  $d$  is the bar diameter (mm),  $v$  is concrete poisson's ratio,  $\beta$  is the relative volume change ( $\Delta V/V_{steel}$ ) due to conversion of steel to rust, is the effective elastic modulus (MPa) equal to  $E/(1+\varphi)$ ,  $E$  is the elastic modulus(MPa) and  $\varphi$  is the creep coefficient of concrete.

From their model, the predicted critical corrosion loss was found to be four times or greater as much as the calculated values based on the measured corrosion rates from Linear Polarization Resistance (LPR) test in their research. This is because in calculating corrosion loss from the LPR test, it is assumed that the whole surface area subjected to corrosion is corroding. This is not true for non-uniform corrosion and, therefore, the calculated corrosion loss from LPR tests should be modified based on the actual corroded area of the embedded steel to present the real values.

Substituting Equation 2 into Equation 5 for the tensile strength results to Equation 6 for a proposed model for the critical penetration depth of rust.

$$x_{crit} = \frac{c(c+d)(1+v)(2.187+0.522f_b)}{E_{eff} d \beta} \quad (6)$$

Table 10 shows a comparative study of the output of this work and published research for critical penetration depth of rust.

Table 10. Relationship of the proposed and published work for critical penetration depth of rust

Bond strength(MPa)	Critical penetration depth of rust in mm			
	This work	Xu and Shayan(2016)	Alonso et al(1998)	Acosta et al
4.33	0.136	0.136	0.0728	0.096
4.4	0.137	0.137	0.0728	0.096
4.42	0.137	0.137	0.0728	0.096

From Table 10, it can be shown that the proposed and published models compares well.

Figure 8 shows the relationship between the critical penetration depth of rust from the proposed model and the bond strength of reinforced concrete

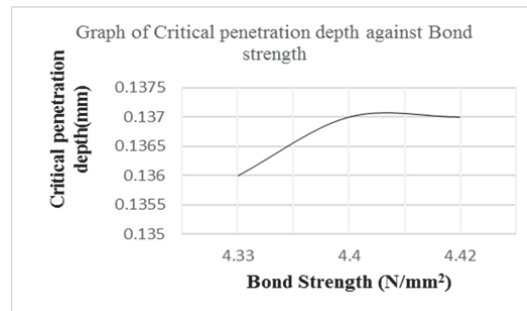


Figure 8. Relationship between critical penetration depth and bond strength of reinforced concrete

From Figure 8, it can be shown that the critical penetration depth increases with an increase in bond strength. The use of a selected cem 1 brand of cement affects compressive, split tensile and bond strength, as shown in Figures 5, 6 and 7. This shows that the concrete properties that affect bond strength, including compressive strength and split tensile strength, will affect critical penetration depth. The magnitude of these hardened properties of concrete continue to increase with an increase in the curing period beyond 27 days because of continuous hydration of cement. The increment is significantly small to alter the output of this work.

#### 4. Conclusion

A study of selected Cem 1 brands of cement intended for structural applications has been done in this research. The variation in the chemical composition of the selected brands affects the compressive, split tensile, bond strength and critical penetration depth. According to the analyses and experiments of hardened properties of the tested samples, it was found that available Cem 1 brands of cement in the Kenyan market vary in chemical composition, and this affects the hardened properties of concrete.

It can also be deduced that the critical penetration depth of rust in reinforced concrete increases with an increase in bond strength, and this is attributed to all the factors that affect the split tensile strength, which subsequently affects both properties. The relationship between the critical penetration depth of rust and the bond strength established in this study can be used in the calculation of the initiation period of the service life of reinforced concrete structures. The results obtained are applicable to reinforced concrete of characteristic strength 25N/mm<sup>2</sup>. Further study of the relationship between split tensile and bond strength in higher characteristic strength is proposed.

#### Nomenclature

$a_1$	parameter = $7.44e^{-5}$	m
$a_2$	parameter = $7.30e^{-6}$	m
$a_3$	parameter = $-1.74e^{-5}$	m/MPa
$A_f$	fractional corroding area relative to that of the entire rebar	mm <sup>2</sup>
$c$	concrete cover	mm
$C$	concrete cover	m
$d$	bar diameter	mm
$d_{ini}$	initial bar diameter	m
$E$	elastic modulus	Nmm <sup>-2</sup>
$E_{eff}$	effective elastic modulus = $E/(1+\phi)$	Nmm <sup>-2</sup>
$f_t$	concrete tensile strength	MPa
$fb$	concrete bond strength	MPa
$f_{t, ch}$	the characteristic splitting tensile strength of concrete	MPa
$L$	length of uniformly corroding segment	mm
$L_f$	fractional corroding length relative to the entire bar	mm
$x_{crit}$	critical radius loss	$\mu\text{m}$
$\beta$	relative volume change due to conversion of steel to rust = $(\Delta V/V)$	
$\phi$	concrete creep coefficient	
$v$	concrete poison's ratio	

#### Conflict of Interests

The authors declare that there is no conflict of interests regarding the publication of this paper.

#### References

- ACI 318-08. *Building Code Requirements for Structural Concrete and Commentary*. American Concrete Institute, U.S.A.
- Alonso, C., Andrade, J., Rodrigues, & Diez, J. M. (1998). Factors Controlling Cracking of Concrete Affected by Reinforcement Corrosion. *Materials and Structures*, 31(211), 435-441. <https://doi.org/10.1007/BF02480466>

- Armaghani, D. J., Hatzigeorgiou G. D., Karamani, C., Skentou, A., Zoumpoulaki, I., & Asteris, P. G. (2019). Soft computing-based techniques for concrete beams shear strength. *Procedia Structural Integrity*, 17, 924-933. <https://doi.org/10.1016/j.prostr.2019.08.123>
- ASTM C117 – 17. *Standard Test Method for Materials Finer than 75- $\mu$ m (No. 200)*. Sieve in Mineral Aggregates by washing. ASTM International. U.S.A. <https://www.astm.org/Standards/C117>.
- Baji, H., Yang, & Shi, W. (2020). A Probabilistic Model for Time to Cover Cracking Due to Corrosion. *Structural Concrete*, 21, 12. <https://doi.org/10.1002/suco.201900341>
- British Standard Institute. (2009). *BS EN 12390-6:2009: Testing hardened concrete: Tensile splitting strength of test specimen*. BSI
- British Standard Institute. (2012). *BS EN 933-1:2012: Tests for geometrical properties of aggregates - Part 1: Determination of particle size distribution - Sieving method, Tests for mechanical and physical properties of aggregates*. BSI.
- British Standard Institute. (2013). *BS EN 1097-6:2013: Determination of particle density and water absorption*. BSI
- British Standard Institute. (2013). *BS EN 12620:2013: Aggregates for concrete*. BSI.
- British Standard Institute. (2019). *BS EN 12390-3:2019: Testing hardened concrete: Shape, dimensions and other requirements for specimens and moulds, Testing hardened concrete - Part 3: Compressive strength of test specimens*. BSI.
- British Standard Institute. (2019). *BS EN 12390-4:2019: Compressive strength, Specification for testing machines*. BSI.
- Chen, E., Berrocal, C. G., Löfgren, I., & Lundgren, K. (2020). Correlation between concrete cracks and corrosion characteristics of steel reinforcement in pre-cracked plain and fibre-reinforced concrete beams. *Mater Struct.*, 53, 33. <https://doi.org/10.1617/s11527-020-01466-z>
- Ejiogu I. K., Mamza, P. A. P., Nkeonye, P. O., & Yaro, S. S. (2020). Comparison of ACI, IS and DOE methods of concrete mix design, *NJE*, 27(1), 68-83.
- Hájková, K., Šmilauera, V., Jendeleband, L., & Červenka, J. (2018). Prediction of reinforcement corrosion due to chloride ingress and its effects on serviceability. *Engineering Structures*, 174, 768-777. <https://doi.org/10.1016/j.engstruct.2018.08.006>
- Kenya Standard. (2017). *KS EAS 18-1:2017: Cement-Part 1: Composition, specification and conformity criteria for common cements*. KS.
- Mishra, A. K., Kumar, R., & Aithal, S. (2020). Economic Operation of Cement: A Case of Gautam Buddha Airport Upgrading Component Project. *International Journal of Applied Engineering and Management*, 4(2). <https://doi.org/10.5281/zenodo.4108233>
- Mogire, P., Abuodha, S., Mweru, J., & Mang'uriu, G. (2018). The effect of Selected Cement Brands in Kenya on the Critical Penetration Depth of Rust in Reinforced Concrete Water Conveyancing Structures. *International Journal of Scientific and Research Publications*, 8(11), 8333. <https://doi.org/10.29322/IJSRP.8.11.2018.p8333>
- Nguyen, T. T., & Dinh, K. (2020). An artificial intelligence approach for concrete hardened property estimation. *Journal of Science and Technology in Civil Engineering*, 14(2), 40-52. [https://doi.org/10.31814/stce.nuce2020-14\(2\)-04](https://doi.org/10.31814/stce.nuce2020-14(2)-04)
- Shaikh, F. U. A. (2018). Effect of Cracking on Corrosion of Steel in Concrete. *Int. J. Concr Struct Mater*, 12. <https://doi.org/10.1186/s40069-018-0234-y>.
- Sharma, M. (2020). Seismic potential parameter of concrete gravity dam. *Conference: Recent trend in Civil Engineering*. <https://doi.org/10.13140/RG.2.2.28803.45600>
- Sobhani, J., Najimi, M., Pourkhorshidi, R. A., & Parhizkar, T. (2010). Prediction of the compressive strength of no-slump concrete: a comparative study of regression, neural network and anfis models. *Construction and Building Materials*, 24(5), 709-718. <https://doi.org/10.1016/j.conbuildmat.2009.10.037>
- Sturm, A. B., & Visintin, P. (2018). Local bond slip behavior of steel reinforcing bars embedded in ultra-high performance fibre reinforced concrete. *Structural Concrete*. <https://doi.org/10.1002/suco.201700149>

- Sturm, A. B., Visintin, P., & Oehlers, D. J. (2017). Time-dependent serviceability behavior of reinforced concrete beams: Partial interaction tension stiffening mechanics. *Structural Concrete*, 19(5), 33. <https://doi.org/10.1617/s11527-020-01466-z>
- Sturm, A. B., Visintin, P., & Oehlers, D. J. (2021). Mechanics of Shear Failure in Fiber-Reinforced Concrete Beams. *Journal of Structural Engineering*, 147, 3. [https://doi.org/10.1061/\(ASCE\)ST.1943-541X.0002934](https://doi.org/10.1061/(ASCE)ST.1943-541X.0002934)
- Xu, A., & Shayan, A. (2016). Relationship between Reinforcing Bar Corrosion and Concrete Cracking. *Aci Materials Journal*, 113(1). <https://doi.org/10.14359/51688460>
- Zhao, Y., & Lin, H. (2018). The bond Behaviour between Concrete and Corroded Reinforcement: State of the Art, in 2018. *Sixth International Conference on Durability of Concrete Structures*, University of Leeds, United Kingdom.

### Copyrights

Copyright for this article is retained by the author(s), with first publication rights granted to the journal.

This is an open-access article distributed under the terms and conditions of the Creative Commons Attribution license (<http://creativecommons.org/licenses/by/4.0/>).